Lecture Notes in Electrical Engineering 731

Electronic Navigation Research Institute *Editor*

Air Traffic Management and Systems IV

Selected Papers of the 6th ENRI International Workshop on ATM/CNS (EIWAC2019)

Springer

Lecture Notes in Electrical Engineering

Volume 731

The book series *Lecture Notes in Electrical Engineering* (LNEE) publishes the latest developments in Electrical Engineering - quickly, informally and in high quality. While original research reported in proceedings and monographs has traditionally formed the core of LNEE, we also encourage authors to submit books devoted to supporting student education and professional training in the various fields and applications areas of electrical engineering. The series cover classical and emerging topics concerning:

- Communication Engineering, Information Theory and Networks
- Electronics Engineering and Microelectronics
- Signal, Image and Speech Processing
- Wireless and Mobile Communication
- Circuits and Systems
- Energy Systems, Power Electronics and Electrical Machines
- Electro-optical Engineering
- Instrumentation Engineering
- Avionics Engineering
- Control Systems
- Internet-of-Things and Cybersecurity
- Biomedical Devices, MEMS and NEMS

For general information about this book series, comments or suggestions, please contact leontina.dicecco@springer.com.

To submit a proposal or request further information, please contact the Publishing Editor in your country:

China

Jasmine Dou, Editor (jasmine.dou@springer.com)

India, Japan, Rest of Asia

Swati Meherishi, Editorial Director (Swati.Meherishi@springer.com)

Southeast Asia, Australia, New Zealand

Ramesh Nath Premnath, Editor (ramesh.premnath@springernature.com)

USA, Canada:

Michael Luby, Senior Editor (michael.luby@springer.com)

All other Countries:

Leontina Di Cecco, Senior Editor (leontina.dicecco@springer.com)

**** This series is indexed by EI Compendex and Scopus databases. ****

More information about this series at http://www.springer.com/series/7818

Electronic Navigation Research Institute
Editor

Air Traffic Management and Systems IV

Selected Papers of the 6th ENRI International Workshop on ATM/CNS (EIWAC2019)

Springer

Editor
Electronic Navigation Research Institute
Chofu, Tokyo, Japan

ISSN 1876-1100 ISSN 1876-1119 (electronic)
Lecture Notes in Electrical Engineering
ISBN 978-981-33-4668-0 ISBN 978-981-33-4669-7 (eBook)
https://doi.org/10.1007/978-981-33-4669-7

This Springer imprint is published by the registered company Springer Nature Singapore Pte Ltd.
The registered company address is: 152 Beach Road, #21-01/04 Gateway East, Singapore 189721, Singapore

Committee Members' List

EIWAC2019 Technical Program Committee

Chair of EIWAC2019 Technical Program Committee and Editor in Chief

Tadashi Koga, Electronic Navigation Research Institute (ENRI), Japan

EIWAC2019 Technical Program Committee Members

Dirk Kuegler, Deutsches Zentrum für Luft- und Raumfahrt, (DLR), Germany
Jean-Marc Loscos, Direction des Services de la navigation aérienne (DSNA/DTI), France
Naoki Matayoshi, Japan Aerospace Exploration Agency (JAXA), Japan
Noboru Takeichi, Tokyo Metropolitan University, Japan
Sonosuke Fukushima, ENRI, Japan
Takeyasu Sakai, ENRI, Japan
William C. Johnson, National Aeronautics and Space Administration (NASA), USA

Secretaries

Naoki Kanada, ENRI, Japan
Navinda Kithmal Wickramasinghe, ENRI, Japan

Preface

This is the fourth book compiled by the Electronic Navigation Research Institute (ENRI) after one of its workshops. ENRI is a national laboratory in Japan that specializes in air traffic management (ATM) and communication, navigation, and surveillance (CNS) for aviation. Since 2009, it has organized biannual international workshops under the title "ENRI International Workshop on ATM/CNS (EIWAC)." The aim of the EIWACs is to contribute to the development of civil aviation by facilitating the exchange and sharing of up-to-date information about ATM and CNS. The sixth workshop, EIWAC2019, was held in October 2019 in Tokyo. The main theme of EIWAC2019 was "Exploring Ideas for World Aviation Challenges." It has been a great honor for ENRI to provide opportunities to discuss future aviation in the presence of key players from international organizations, civil aviation authorities, aviation industries, and academic institutions from all over the world.

This book has been published to share the essence of EIWAC2019 with people all over the world involved in ATM/CNS R&D. It comprises five parts. Part One gives an overview of EIWAC2019 and summaries of the keynote and special speeches. Parts Two, Three, Four, and Five consist of selected academic papers presented at EIWAC2019. Parts Two, Three, and Four discuss research related to ATM, and Part Five discusses research related to CNS.

Each chapter consists of papers that have passed through two stages of selection. First, the technical program committee (TPC) conducted on-site evaluations with the help of professionals and experts who participated in EIWAC2019. They objectively evaluated the quality of the presentations and manuscripts. The ones that received high scores were nominated as candidate papers. Then in the second stage, the candidate papers went through a process of review by professionals and experts. Multiple anonymous reviewers reviewed and judged the quality of each one.

I believe that the book offers readers novel ideas and wonderful discoveries and that it will further encourage R&D activities in the field of ATM/CNS.

Finally, I would like to express my deep gratitude to all the EIWAC2019 TPC members, editors, and reviewers who voluntarily gave us their support during the selection, review, and compilation processes. The TPC members have been listed separately in the book, and special gratitude has been expressed to them.

Tokyo, Japan T. Koga

Contents

Introduction

Introduction to the Sixth ENRI International Workshop on ATM/CNS (EIWAC2019)

S. Ozeki, Y. Fukuda, S. Fukushima, T. Koga, T. Sakai, E. Itoh, and N. K. Wickramasinghe

Abstract This chapter provides an overview of the sixth ENRI International Workshop on ATM/CNS (EIWAC2019), together with summaries of presentations in keynote sessions and special speeches. It also explains the Electronic Navigation Research Institute's approach to organizing EIWAC. EIWAC2019 was held in Nakano, Tokyo, from October 29 to 31, 2019. In the workshop, various aspects of air traffic management (ATM) and its enablers in the fields of communication, navigation, and surveillance (CNS) were discussed.

Keywords Global Air Safety Plan · Global Air Navigation Plan · ATM · CNS · UTM · Standardization

1 Introduction

The Electronic Navigation Research Institute (ENRI) is part of the National Institute of Maritime, Port, and Aviation Technology (MPAT). MPAT was established in 2016 by uniting research institutes affiliated with Japan's Ministry of Land Infrastructure, Transport, and Tourism (MLIT). ENRI has been conducting research and developing and testing electronic navigation systems for almost half a century. It is now the only institute in Japan specializing in air traffic management (ATM) and communication, navigation, and surveillance (CNS) for aviation.

Air traffic is increasing steadily all around the world. Mitigation of congestion and reduction of environmental impact while maintaining safety and efficiency have been common interests for the whole world for the last decade. Demand for increased air traffic capacity, efficiency, and safety has been particularly strong in the Asia-Pacific region because Asia has the fastest-growing rate of air traffic. ENRI is therefore conducting R&D in order to respond to this demand, and provides timely solutions through improved national, regional, and global aviation systems.

S. Ozeki · Y. Fukuda · S. Fukushima · T. Koga (✉) · T. Sakai · E. Itoh · N. K. Wickramasinghe
Electronic Navigation Research Institute (ENRI), 7-42-23, Jindaiji-Higashi-Machi, Chofu, Tokyo 182-0012, Japan
e-mail: koga@mpat.go.jp

Air Traffic Management and Systems IV, Lecture Notes in Electrical Engineering 731,
https://doi.org/10.1007/978-981-33-4669-7_1

In addition to its R&D activities, ENRI is now expected to contribute to harmonization and standardization regarding the current and emerging ATM/CNS technologies and operations, which will lead to fully harmonized global aviation systems with modern performance-based technologies and procedures. However, it is not necessarily easy for the aviation community in the Asia-Pacific region to share comprehensive information on the latest ATM/CNS technologies and operations. This is because there are different local traffic policies and ATM/CNS capabilities.

In view of this, ENRI decided to organize an international workshop to discuss ATM/CNS technologies and operations, mainly for the Asia-Pacific region, but also for the rest of the world as well. This workshop was named "ENRI International Workshop on ATM/CNS (EIWAC)." The first workshop was held in 2009. Since then, EIWAC has been held biannually, and the latest one (EIWAC2019) was held in October 2019 in Tokyo.

The purpose of publishing this book is to share selected topics presented and discussed in EIWAC2019. This chapter first gives an overview of the EIWACs, presenting the speaker, title, and a summary of each speech in the plenary session. Selected papers from the technical sessions are provided in Chaps. 2, 3, 4 and 5.

2 Overview of the EIWACs

ENRI would like to thank the members of the EIWAC Technical Program Committee (EIWAC-TPC) for their tremendous contributions to making the workshop more attractive to potential participants. Members from other organizations offered comments to help improve EIWAC by including viewpoints from outside ENRI.

EIWAC has sessions for keynote speakers, and other sessions for technical discussions on operations and R&D as well. The keynote sessions of EIWAC are held to share strategic updates among participants and are scheduled to take place on the first day in most cases. The technical sessions offer participants opportunities to review operational facts and the progress of R&D with reference to updates from the keynote sessions.

Table 1 presents a brief summary of the 1st to 3rd EIWACs, and Table 2 summarizes the 4th to 6th. The workshop started in 2009 as a two-day event and was later expanded to include one more day for technical sessions, to accommodate more presentations. It continues to grow as international participants offer more presentations and side meetings [1–6].

One of the advisors to ENRI suggested that outstanding papers for EIWAC should be made more visible to more researchers and students in the aviation community, in order to encourage the next generation. ENRI responded to this comment in 2012 by engaging an editorial team to compose the first book, "Air Traffic Management Systems," collecting selected papers from EIWAC2013 [7]. This was followed up with "Air Traffic Management Systems—II" from EIWAC2015 [8], and "Air Traffic Management Systems—III" from EIWAC2017 [9]. These books were published by Springer Japan in 2014, 2017, and 2019, respectively.

Table 1 Summary of the EIWAC series (2009, 2010, 2013)

Meeting #	1st	2nd	3rd
Name	EIWAC2009	EIWAC2010	EIWAC2013
Dates	March 5–6, 2009	November 10–12, 2010	February 19–21, 2013
Venue	Ohtemachi Sankei Plaza, Ohtemachi, Tokyo	Akihabara Convention Hall, Akihabara, Tokyo	Odaiba Miraikan Hall, Odaiba, Tokyo
Theme	Towards future ATM/CNS	Safety, efficiency and environment	Drafting future sky
Keynote speakers	4	7	9
Panel session	N/A	"Future of automation in ATM," six panelists	"Future ATM: centralized, de-centralized or best mixed," four panelists
Other sessions			Poster, tutorial
Technical sessions	6	19	17
Presentations	22, incl. 9 from Japan	45, incl. 12 from Japan	46, incl. 13 from Japan
Participants	480	550	539
On 1st day	N/A	N/A	238
Non-Japanese	20	60	80
Countries	7	14	13

3 Keynote Speeches

This section gives a summary of the keynote speeches in EIWAC2019. EIWAC2019 had seven keynote speeches on day one.

3.1 Stephen P. Creamer, "Exploring Ideas for World Aviation Challenges"

Mr. Creamer is the director of the Air Navigation Bureau (ANB) of the International Civil Aviation Organization (ICAO). His presentation was about the latest activities of the ANB and digital transformation perspectives. ICAO works toward the vision of achieving sustainable growth of the global civil aviation system. The ANB's areas of focus are two of ICAO's five strategic objectives: Aviation Safety and Capacity and Efficiency.

The 40th ICAO Assembly in 2019 endorsed the Global Aviation Safety Plan (GASP) and the Global Air Navigation Plan (GANP) updates. The vision of the GASP is to achieve and maintain the aspirational safety goal of zero fatalities in commercial operations by 2030 and maintain it thereafter. The GASP promotes the

Table 2. Summary of the EIWAC series (2015, 2017, 2019)

Meeting #	4th	5th	6th
Name	EIWAC2015	EIWAC2017	EIWAC2019
Dates	November 17–19, 2015	November 14–16, 2017	October 29–31, 2019
Venue	Ryogoku KFC hall and rooms, Ryogoku, Tokyo	Congres Square Nakano, Nakano, Tokyo	Nakano Central Park conference, Nakano, Tokyo
Theme	Global harmonization for future sky	Drafting future skies	Exploring ideas for world aviation challenges
Keynote speakers	13	5	7
Panel session	N/A	N/A	Digitalization in aviation: a standardization perspective
Other sessions	Poster	Poster, tutorial	Poster, special speech
Technical sessions	18	17	18
Presentations	70, incl. 30 from Japan	71, incl. 25 from Japan	72, incl. 19 from Japan
Participants	744	630	861
On 1st day	259	205	268
Non-Japanese	174	180	257
Countries	17	13	19

implementation of safety management and a risk-based approach. A series of six goals in the GASP support the overall aspirational safety goal. These goals call for states to implement effective safety oversight systems and state safety programs. The GANP requested ICAO to take action to evolve toward a performance-driven, strategic planning environment that interacts with regional development and implementation programs. The sixth edition of the GANP is organized into a multilayer structure. The four-layer structure facilitates decision-making by providing stable strategic direction for the evolution of the air navigation system.

Frontier technologies provide innovative solutions and tools to the air transport system, such as automation and unmanned systems, transport electrification, big data, artificial intelligence, machine learning, and digitalization of processes. New technologies incur relatively low development costs, allowing small and medium-sized "start-up" enterprises to be at the forefront of transformation in air transport. New entrants are drones that fly below 400 feet and above high altitudes, and spacecraft under autonomous control. There are challenges in the wake of these technological developments, which calls for an unprecedented design of a balanced environment capable of fostering innovation. Regulatory and policy transparency and enforcement, legal certainty for businesses, cybersecurity, consumer and data protection,

and a fair, environmentally, economically, and socially sustainable development on a global scale will be ensured.

Global traffic density is increasing. The only way to meet this demand is going to be a transformative reliance on exchange of information in the air traffic management (ATM) system. A large number of digital parts are migrating into airplanes. Everything is becoming fundamentally based on digital technology, as seen for example in the evolution of manufacturing technologies, remote towers, the way people move through airports, and the way freight moves through the system. All the parts of the aviation ecosystem are always interacting, so digital transformation is a big deal.

When you make things digital, you make them vulnerable to cyberthreats. If every state puts in place a different infrastructure or a different architecture to respond to these threats, it's going to be really hard to maintain interoperability. We need to find a way to create a system architecture that takes cybersecurity into consideration as a foundational element. The 13th Air Navigation Conference recommended that ICAO establishs a formal project for the urgent and transparent development of a globally harmonized aviation trust framework.

The first ICAO trust framework was set up in 1944 with the establishment of the Chicago Convention. ICAO establishes international standards. Those standards are used by civil aviation authorities to issue certificates. Because they're issued in relation to these standards, other authorities recognize these certificates and trust is established. It's old fashioned and it isn't digital, but it's worked well ever since it started. There are volumes of standards used to regulate licenses, certificates, authorizations, and approvals. We need to develop solutions to accommodate new entrants. Therefore, we need to talk about how to move this out of the paper world and into the digital world.

Within a trust framework, it's a foundational fact that you need to know who is in your network so you know how to secure your network. Digital certificates are extremely efficient and are used all over the world in a form referred to as a public key infrastructure (PKI) system. You could use those commercial parties' mechanisms to distribute digital certificates. All we do is put some other governance on top of it. You need a digital certificate so you can secure your organization, drone, or airplane's communications with the rest of the network. So, whenever your aircraft or air navigation service provider sends or receives a message request, the sender and receiver identify each other and integrity can be validated back with the trust bridge.

For decades, we've been trying to isolate ourselves from the rest of the world with physical isolation. This is just really hard to do now, because no matter how hard you try, your data is going to cross paths with the rest of the world. ICAO can figure out how many addresses we need and how big an address block we we'd have to get. Therefore, ICAO needs to work with the Internet's governing bodies to obtain top-level domain and private address space capacity. These assets could be made "private" and could provide a first layer of logical isolation from the public Internet.

ICAO can facilitate a globally trusted identity, but each stakeholder will have to decide how it should be used in its own system. As threats evolve, new controls will be needed to ensure trust framework entities continue to operate within their roles. ICAO is best positioned to develop a protected and globally harmonized architecture.

In conclusion, Mr. Creamer summarized four points: (1) Focus on staying safe as we introduce change; (2) the pace of change is accelerating because of new entrants; (3) the underlying connectivity challenge has to be handled first; and (4) bringing along regulators and other safety workers to stay abreast of the changes is just as important as the underlying technology.

3.2 Florian Guillermet, "The Digital Transformation of Air Traffic Management: Why and How"

Mr. Guillermet is the executive director of the SESAR Joint Undertaking. Two years ago, at EIWAC2017, he gave a presentation entitled, "Toward a digital aviation infrastructure." At EIWAC2019, his speech started with why the digital transformation of air traffic management is necessary. Then, he discussed how SESAR intends to introduce the digital transformation, some of the solutions for this that SESAR has developed in Europe, and some of the remaining challenges.

He started with why. The world around us is changing very fast. He mentioned three emerging changes. First, environmental protection is becoming an important topic. In Europe, there are strong demands to mitigate the impact of aviation on the environment. Second, air traffic in Europe is expanding year on year. This is bringing with it ever larger numbers of delayed, canceled, rerouted, and rescheduled flights. Third, new technologies such as robotics, data analytics, artificial intelligence, communication, and connectivity are emerging and changing not only our daily lives but also aviation technologies and air traffic management. To accommodate these changes, Europe needs a bold vision that embraces the digital transformation of aviation.

He discussed how digital transformation will be achieved. He introduced many of SESAR's challenges in the presentation, but two key issues here are ATM architecture and automation. The SESAR master plan proposes a new architecture. The new architecture includes not only current airspace but also new airspace operations, such as higher airspace operations and U-space operations. The new architecture has the characteristics of a fully scalable system with strong air-ground integration. Also, the architecture should rely on a digital ecosystem, the elimination of environmental inefficiencies caused by the aviation infrastructure, and ensuring that it offers solutions that will fully exploit the potential offered by next-generation aircraft for cleaner and quieter flight. The second key technology for digital transformation is automation.

The master plan has developed an automation model and roadmap. The automation will mainly come from robotics, not ATM. Automation in ground and airborne locations will have to be applied in a highly safety-critical environment like ATM and aviation. In addition to automation, visualization, connectivity, and data sharing will be key technologies in the aviation and ATM of the future.

In conclusion, Mr. Guillermet highlighted three essential points for succeeding in the digital transformation of air traffic management. First, environmental impact is a huge threat to the full aviation system in Europe. This means the significant challenge of achieving a system where not a single drop of kerosene is wasted in the entire flight, and in the entire system, be it in the air or on the ground. The second point was that adapting the current system that uses old technologies or extending the current technologies will not be sufficient for digital transformation.

People can already see the behavior and performance that the aviation systems need. To continue the aviation success story, it will be necessary to consider not only traffic growth but also other factors like new threats (cyberthreats) and societal challenges. The third point was that we acknowledge somehow that this is something that combines not just innovation and industrial action, but also governmental action. He talked about sovereignty. The things that control the skies of the future will not be the same as the systems we have today. All governments need to invest in those technologies if they want to remain in control of what's flying in the future, because a lot will of it will be done through information management. If they don't control the information, they won't control what's flying in the future.

In addition to these three points, he also gave the audience some vital messages at the end of his presentation. Digital transformation can proceed through bilateral or multilateral cooperation between the various regions. The standardization body plays a key role in this respect, because technology is growing fast and accelerating. The only way we can keep up the pace in terms of the regulatory environment is to link it with industry standards that are performance-based and not focused on technology.

3.3 Christopher Loring, "Moving Innovation to Implementation"

Mr. Loring is the manager of the International Division in the FAA's NextGen Collaboration and Messaging Office. In his presentation, he spoke about the situation and perspectives regarding the FAA's NextGen program on behalf of Ms. Pamela Whitley, the Assistant Administrator for NextGen at the FAA. The Next-Generation Air Transportation System, or NextGen, is the FAA-led modernization of the air transportation system in the United States. The aim is to make flying even safer, more efficient, and more predictable.

Mr. Loring began by reported that they were now at the stage of taking NextGen beyond the R&D and incremental development phase, and moving it into full implementation. Many lessons were learned along the way. For example, there were mismatches between the plans and reality—some of the plans were too aggressive. They also learned that politics played a much larger role than they had thought. While it made sense to develop a plan to close or consolidate certain facilities and equipment based on efficiencies gained through the modernization plans, the political realities did not align with this, and they had to change the plans. The people side is just

as important as technology. This was an important lesson learned—to gain the trust and garner the commitment of multiple partners to work together to develop a global approach to modernization and of stakeholders to achieve everyone's common goals.

At ICAO's 40th assembly, he saw that many countries understand the need to participate in and be interoperable with a global air traffic management modernization plan, and many are just beginning the planning phase for doing so. Some countries have begun their modernization programs, and some are looking to move toward more advanced concepts, like broader PBN implementation, ADS-B or system-wide information management. It is clear that we in the ATM R&D community need to help countries understand where we have been, what lessons we have learned, and where we are going.

Speaking of goals, the culmination of the NextGen programs, processes, and procedures will be the holistic implementation of trajectory-based operations as proposed in the FAA TBO vision for 2025 and beyond, as well as the ICAO Global Air Navigation Plan. Holistic implementation here means giving strategic consideration to the entire airspace system. It does not mean implementing TBO everywhere. TBO will be implemented where it is required based on the strategic needs of the entire national airspace system, not on the tactical needs of individual airports. For TBO to deliver its anticipated performance benefits, all the capabilities and processes integral to it will need to be developed and deployed in a globally harmonized manner.

As TBO is a comprehensive and holistic concept that incorporates almost every aspect of the global aviation ecosystem, a significant amount of research and development still needs to be done. The FAA is working with the user communities through the NextGen advisory committee to determine the best combination of capabilities to use in a given operational environment. Researchers are evaluating whether the application could increase airspace capacity by delegating spacing and sequencing to the flight deck. Airframe and engine improvements, as well as alternative jet fuels currently in operation or in the research phase, may lead to additional emission and energy benefits in the future. Noise reductions will come from airframe and engine improvements, as well as from changes in aircraft operations.

Mr. Loring pointed out that since information management and communications are significant enablers with regard to all of these considerations, cybersecurity is another important area of research. While the threats are many, new areas of research are producing technologies such as resilient self-adaptation and big data analytics that promise solutions to some of the cyberchallenges. Research will also be done into methods for securing the NAS in an environment where the trustworthiness of some systems is unknown.

The FAA is currently working with NASA on a construct for urban air mobility, or UAM. This includes examining the technological, operational, and regulatory issues that need to be amended or developed in order for UAM to grow. The FAA is developing performance-based rules—including definitions and certifications for the aircraft—to ensure safe integration into a very complex airspace and environment. Also, many of the aircraft are involved in long-duration flights, in addition to existing aircraft, several other supersonic and hypersonic aircraft, and balloons. The FAA is working both internally and with ICAO to develop a global framework for these

operations that utilizes autonomy, automation, and the current regulatory construct to assure safety, while maintaining efficiency.

Finally, Mr. Loring again noted that TBO is an evolutionary realization of ICAO's global air traffic management concept. It is clear that the ATM R&D community needs to understand where it has been and where it is going if it is to help with the global implementation of ATM modernization. According to Mr. Loring's presentation, the biggest lesson when it comes to innovation, R&D, and implementation is to work together to gain the trust and garner the commitment of global stakeholders. "We are no longer individual countries implementing our own programs. We are all in this together," he concluded.

3.4 Tohru Kawaharabata, "CARATS Long-Term Vision for Air Traffic Systems—The Challenge for Implementation of Future Technology"

Mr. Kawaharabata is the director general of the air navigation services department of JCAB. He spoke about four topics related to Japan's long-term vision for future air traffic systems, the Collaborative Actions for Renovation of Air Traffic Systems (CARATS).

The first topic was the future trend of air traffic demand. According to a statistical survey by ICAO, the number of departures will rise to approximately 38 million globally, and world passenger traffic, expressed in terms of total scheduled revenue passenger kilometers (RPKs), will grow by 6.7% to reach approximately 8.2 trillion RPKs. International scheduled passenger traffic expressed in terms of RPKs grew by 6.4% in 2018. In particular, the Asia-Pacific is the fastest-growing region, with an increase of 7.3%. How JCAB is going to deal with this traffic growth is the most urgent and crucial issue. Meanwhile, the number of aircraft flying over the Japanese flight information region is also expected to increase by a factor of 1.5 in the next two decades. In order to achieve continued economic growth in Japan and its neighboring countries, a sufficient air traffic control capacity will be required to support the growing demand, as a kind of aviation infrastructure for such a level of economic activity. In addition, Japan is going to host the upcoming Olympic and Paralympic Games Tokyo 2020. Since the Japanese flight information region covers a large part of the Pacific Ocean, JCAB, as a member of the community of air navigation service providers, is in a good position to take various proactive measures to cope with the surge in air traffic demand in this rapidly growing region. JCAB has been providing the air navigation service with high levels of safety, punctuality, and efficiency for many years by keeping itself up-to-date on the most recent ATC services through appropriate budgetary and staffing measures, in order to meet the demand. On the other hand, since this demand will continue to increase, we will have to improve our current air traffic control system so that it can respond correctly to the changing environment, especially future limitations on airspace and the workload of

air traffic controllers. In addition, various new needs have arisen for air traffic control systems, such as the need for improved user convenience and operational efficiency, and for more economical operations.

The second topic was the future of air navigation. Since aircraft fly across national borders, the global approach is an important concept in the aeronautical transport field. Therefore, an aviation infrastructure that supports air navigation services must provide seamless services to international flights. With this background, and considering the necessity of meeting the growing air traffic demand, ICAO has set the basic direction for internationally harmonized ATM for the year 2025 and beyond in the form of the Global Air Navigation Plan (GANP), a long-term vision for modernizing global ATM operations. Based on this vision, a lot of countries have made their own air navigation plans. It is important to take global harmonization into consideration when making such plans. The new GANP also aims to bring the aviation community together to achieve an agile, safe, secure, sustainable, high-performing, and interoperable global air navigation system.

The third topic was the CARATS. For the national level, JCAB, as the Japanese air navigation service provider, created its long-term vision for the CARATS concept in 2010, with the cooperation of all parties concerned. It aims to renovate air traffic systems to meet the growing demand and needs. In order to improve air traffic systems so they meet the growing demand and a variety of other needs, it will be necessary to have collaboration with stakeholders in air navigation. For the CARATS, all stakeholders, including industry, academia, and the government, have joined together and discussed important issues on a collaborative decision-making basis. Meanwhile, they always keep in mind that in order to ensure international interoperability, it is necessary to cooperate closely with the states concerned. Regarding the content of the CARATS, they have set several goals to be achieved in the framework of the CARATS. Also, each measure for achieving these goals has been implemented step by step. In addition, to clarify the outcome of each item contained in the CARATS, more specific measurable targets have been set for each goal, and the degree of progress is checked on a yearly basis to ensure effective implementation of the CARATS measures. In order to achieve those goals, they will have to carry out drastic reforms regarding the conventional concepts of ATM and basic CNS technologies. The CARATS framework provides eight directions for the reforms, with a focus on the transition to trajectory-based operation as one of the major final targets. The measures for these eight reform directions have been developed within the framework of the CARATS, and are categorized into two groups: one is defined as operational improvements, and the other as enablers of technical factors that will help achieve the reforms. Corresponding to these measures, JCAB has developed roadmaps for the implementation of the operational improvements and the enablers. Before putting each measure into practice, they will verify that it is cost-effective and feasible from various points of view. At the implementation stage, they will review the roadmaps and, if necessary, modify them in response to further changes after the decision to implement. In his speech, Mr. Kawaharabata introduced two CARATS measures: RNP-AR (authorization required) procedures and controller–pilot data link communication (CPDLC).

For his final topic, he spoke about the harmonization of standards. The realization of new technology is indispensable for R&D. Besides this, to ensure interoperability at a global level, an integral requirement is to harmonize the standardization activities. JCAB has participated in experimental programs for system-wide information management (SWIM), such as a Mini-Global Demonstration trial undertaken with the cooperation of countries including the US, Canada, Australia, and Singapore, in cooperation with ENRI.

3.5 Naoki Tanaka, "Challenge, Leading to Growth—Corporate Strategy of Japan Airlines"

Japan Airlines (JAL), one of the representative airlines in Japan, serves about 1000 flights per day to more than 44, 000 million customers, using 235 aircraft. A total of 34, 000 employees welcome international passengers at 95 airports worldwide, taking them to more than 400 destinations all over the world in cooperation with code share partners. To meet the growing demand for passenger transport, especially resulting from the strategic targeting of tourism in Japan, JAL is planning to add a further 100 flights in 2020 in the Tokyo metroplex area—which includes Tokyo International (Haneda) and Narita International airports—while achieving ecologically friendly operations. They have drawn up future visions for sustainable growth in aviation: a mid-term management plan for three to five years and long-term goals for ten years. The year 2020 will be a landmark year because of the Olympic Games and the expansion of the Tokyo metroplex airports. Therefore, JAL has set a target phase called "Challenge, Leading to Growth" for preparing for the Olympic year 2020 and contributing to successful growth beyond it.

They have extended their business domain, the full-service carrier business (in which they have 70 years' of continuous history), to provide their worldwide business services more widely in order to achieve sustainable growth. They began introducing the A350 aircraft (which will replace the B777 as their new flagship) in September 2019. Other projects include creating smart airports, which will minimize passengers' waiting times in the airport area. Self-check-in and baggage drops will be increased at airports in the near future. Moving toward further customer convenience, the key is to increase the networks of routes operated in partnership with other airlines in the OneWorld alliance. Furthermore, joint business with American Airlines, Finnair, and Iberia will improve timetables, fares, and airport connections. Beyond the alliance group, collaboration with Hawaiian, China Eastern, China Southern, Alaska, etc. will aim to connect more than 500 destinations all over the world. JAL has created a new LCC airline, ZIPAIR, which flies B787 wide-body aircraft on long and medium-length flight routes to accommodate rapidly growing demand.

Creating new forms of social value is another important key in JAL's future structure. To promote their innovation process, JAL established "Innovation Lab" in 2018. The Lab members actively work to develop their ideas into social value. For example,

they investigate ways to apply artificial intelligence (AI) to increase the value of precious human resources. Developing AI and robotics to assist with checking counters will enable even better customer service. Recording maintenance logs with smartphone applications will support engineers and enhance the safety and efficiency of their work procedures. Virtual reality (VR) will enable crews and mechanics to raise the precision of their training processes. These technologies will bring about innovation that will add an enormous amount of extra quality to customers' journeys and operational matters in the future. JAL continues to pursue sustainable development of the aviation society all around the world.

3.6 Yoshiaki Tsuda, Akira Fukabori, and Kevin Kajitani, "ANA's Endeavor to Connect All 7.5 Billion People on Earth"

All Nippon Airlines (ANA) started their aviation business as a small startup: their original company was "Nippon Helicopter (NH)," which was a small private helicopter company that started operating with only two helicopters. Currently, 43,000 employees work at ANA, and they offer 1200 flights per day using around 300 aircraft. Behind the company's dramatic growth lies a pioneering spirit that has been passed on to younger generations. In 2016, ANA established "Digital Design Lab (DDL)" as an innovation engine for their entire airline group. Their first approach was to create disruptive business models for airlines. One of their ideas is "avatar" technology, which will enable people to travel all over the world virtually.

The DDL has started to work on pioneering the new avatar technology. What this means is physical avatars: physical robotic systems that will enable us to essentially teleport our presence, senses, and consciousness to a remote location, essentially existing in a place that our bodies are not currently in. Why, then, would ANA, an airline that physically transports passengers, pursue robotic avatar technology—and why now? The reason is that people around the world are still not connected physically by long-distance transfer provided by airline transport. According to an estimate by the DDL's Avatar Division, the impact of airline industry transport on the global economy is a mere 6%. They say that, as the industry that has connected the world over the last 100 years, airlines should be at the forefront of this endeavor again.

"ANA is not simply an airplane operator," they say. Airplanes are not what their main core business is about, but simply the tools that they currently use to provide their services. Their ultimate goal as a company is not to operate airplanes, but to bridge the gaps of distance, time, and culture that exist in our world.

Imagine that you work weekdays in Tokyo and get to go home, three hours north of Tokyo, only on the weekends, but can interact with and go home via avatar whenever you like. And when you log in to your avatar, your wife says "Welcome home" and, "Now you're home, I'm going to watch TV or do a hobby." Then your son says,

"Papa, let's run around the house and play together." And when you log out from the avatar, he hugs you before you leave the robot. Your son is two years old, and as you can imagine, a two-year-old cannot sit in front of a video chat for more than 30 s. But because you are physically present, your son is able to recognize that it is Papa, and you are able to interact with and essentially take time to care for him—and that frees up time for your wife.

Just this year, the World Economic Forum announced their top ten emerging technologies for 2019, and ranked at number six was collaborative telepresence, in which ANA's Avatar initiative was listed. So, this avatar movement is real, and they believe that it is just around the corner and is what the future of avatars will be.

3.7 Shigeru Ozeki, "Innovations for Future Aircraft Operation and Standardization"

After introducing ENRI, Mr. Ozeki, the director general of ENRI, presented the reason why digitalization is under discussion for ATM/CNS, with reference to collective intelligence, or intelligence that grows out of a group. Then, innovation and standardization were discussed, including how collective intelligence works for them. This presentation was based on the fact that operation of an aircraft is supported by the collective intelligence that is formed from the pilot, air traffic controllers, airport operators, dispatchers, weather specialists, engineers, inspectors, lawyers, and many others who work on each aspect of aircraft operation.

The first point in the presentation was that digitalization of ATM/CNS will furnish an environment for having better collective intelligence for aircraft operation. Digitalization will make exchanging knowledge easier, even when the contributors to the collective intelligence for flying are distant in space or time. For example, digitalization will provide automated tools to extract information from data, to communicate or share the information, and to manage it and operations on it. Sharing information among experts in various areas will support finding new knowledge or new combinations of knowledge. We need better collective intelligence to achieve innovation and standardization with new knowledge or new combinations of knowledge in order to overcome the restrictions of conventional air traffic management.

The second point in the presentation was that innovation and standardization may help each other regarding exchanging knowledge among the teams working on innovation. The teams working on standardization may become focal points for various kinds of knowledge to build up the collective intelligence for aircraft operation to be standardized. The teams working on innovation may provide knowledge that is new to the standardization teams. Conversely, the innovation teams may be inspired by the discussions in the standardization teams, because the standardization teams will have a broader range of knowledge than the innovation teams in most cases. This is why the presenter invited representatives from the innovation teams to join the standardization teams.

At the end of the presentation, conformity of strategic direction in each layer of activities was discussed, in order to think about a better environment for collective intelligence to fly in. Strategies have a layered structure. For example, there are ICAO strategies, national strategies, project strategies, and so on. A layer may be an environment or resource plan for other layers. If there is no conformity between the directions of each layer, their perspectives will not be focused on a common future. This will mean the directions for collective intelligence in each layer will not fit in with the others and will be hard to import into the other layers. This kind of environment will be hard to work in.

Conformity of strategic directions among the layers will be necessary for a compatible perspective. To achieve this, coordination within each layer and among layers will be important. One recommended method is participation in multi-disciplinary meetings like EIWAC.

4 Panel Discussion

The panel discussion of EIWAC2019 was held on October 29, 2019, on the theme of "Digitalization in Aviation—A Standardization Perspective." Digital transformation was a key spotlight topic in EIWAC2019, and the objective of the panel discussion was to bring together leaders involved in regulatory and standardization activities to share their expertise in facing challenges and developing strategies to consolidate different approaches to achieving this global objective.

Panelists:

- Mr. Stephen P. Creamer (Director of Air Navigation Bureau, ICAO)
- Mr. Christian Schleifer-Heingärtner (Secretary General, EUROCAE)
- Mr. Terry McVenes (President and CEO, RTCA)

Moderators:

- Mr. William C. Johnson (Senior Aircraft Engineer, NASA Langley Research Center)
- Mr. Hajime Yoshimura (Senior Air Talks Officer at JCAB, MLIT)

Mr. Johnson commenced the panel discussion with an overview of its theme and objective. The event included two presentations by Mr. Schleifer-Heingärtner and Mr. McVenes, followed by a discussion that included a Q&A session with the audience.

Mr. Schleifer-Heingärtner's presentation focused on EUROCAE activities on standardization methodologies and its strategies for keeping up the pace of standardizing the new technologies and innovations being introduced into the aviation community. He discussed the workflow for deployment of such technologies and how a regulatory framework is supported and complemented by standards during the process. He emphasized the challenges regarding addressing new-entrant technologies in a timely manner while maintaining the core values of being open, transparent,

and census-driven, without compromising safety. He stressed the fact that a regulatory framework is not always the basis for developing standards. He suggested that the best kind of driven approach is an industry-driven initiative, where the standards-developing organizations can support it with their knowledge and experience in order to move it forward and achieve its objectives in an efficient and effective manner. He also implied that his organization is risk-based, operation-centric and has a performance-based regulatory framework, but doesn't draw any conclusions about whether the standards it defines provide any technical solutions, because the products possess minimum operational performance standards.

Mr. McVenes commenced his presentation with an introduction to RTCA and its role in the world of standardization. RTCA has developed about one-hundred MOPS and more than thirty MASPS since its inception, and these have been referenced by over 100 FAA regulations advisory circulars or technical standard orders and more than fifty ICAO SARPS. He mentioned the commitment of RTCA to bringing industry and government together and working with international partners to develop and increase the efficiency of the air traffic system. He clarified Mr. Schleifer-Heingärtner's remarks by pointing out the importance of collaboration between standards-developing organizations for achieving harmonization as an aviation community. Mr. McVenes noted that using a consensus-based process to develop standards that are not only technically complete but also operationally effective is crucial to ensuring that the new technologies can be integrated into the system through those standards in a much quicker time. RTCA is currently working with FAA to develop MOPS that are scalable in terms of meeting the safety criteria based upon the operation. He stressed the fact that standards-developing organizations must be very adaptable, need to increase their pace, and have to expand their ways of thinking in terms of looking at different aspects of aviation, without compromising on safety in any way. He concluded his presentation by saying that working together with EUROCAE and ICAO is so vital for the industry because the harmonization and interoperability that these organizations must have through its standards is vitally important.

The discussion session was commenced by Mr. Johnson by raising the issue of how the standards-developing organizations are working to close the gap between vehicle manufacturers and standards, given that new entrants in aviation have short lifespans with rapidly evolving technology, while standards might take years to introduce. Mr. Schleifer-Heingärtner noted that these organizations are well aware of the current trend in the aviation markets and the needs of the industry, and supported the strategy of scalable standards mentioned by Mr. McVenes. He also emphasized however that standards must be consensus-driven and ensuring safety is paramount, and that these will require time. Mr. Terry suggested that early engagement with the industry will be important to help bring new technology to the market swiftly. He also said that collaboration between standards-developing organizations will be vital to shortening the cycle time of the standardization process and avoiding unnecessary waste of resources due to lack of communication between these entities.

Mr. Creamer joined the discussion by talking about the safety of air transport and how the standards have helped to create such confidence in users. He said that risks

related to air transport have not been completely eliminated, but are being managed and the management process is built on over a hundred years of experience. He compared examples to show the difficulty of leaping toward a customer-based standardization process and emphasized the potential benefits approving new technologies could bring to users in need, for example, providing the capability to deliver blood to a clinic located 100 km away within a few minutes' time. He was also willing to share the idea that the aviation world is going to see a steady evolution rather than a revolution through digitalization, and the possibility of creating a parallel set of regulatory provisions and mastering its evolution so that new industries can co-exist and operate within traditional air transport. Mr. Creamer confirmed the position of ICAO on the process of regulating standards in a purpose-specific and efficient manner.

Regarding the question raised by Mr. Yoshimura on the possibility of shortcutting any process to speed up the regulatory framework, Mr. McVenes commented that getting a new entrant certified in a timely fashion without compromising safety is quite challenging, and stressed how these organizations have achieved the safety criteria deliberately, step by step and sometimes by using lessons learned through tombstone mentality. Mr. Schleifer-Heingärtner added that regulatory procedures are streamlined and in good order to deliver on time. He also noted a new suggestion developed with the SESAR Joint Undertaking to have a direct link when R&D activities are conducted. He stressed however that these procedures will need lot of coordination and verification before being certified. Mr. Creamer added that if an industry understands how to identify and manage risk, the outcomes will potentially be approved in a regulatory sense in a local environment, but the products must be demonstrated at a local level before being certified for the global market.

One question raised during the Q&A session was the challenges faced by the aviation community due to a performance-based regulatory framework. Mr. Creamer showed how crucial it is to implement a solid functional hazard analysis and risk assessment followed by cataloging and implementing mitigation measures by a regulator, in order to ensure that the right decisions are made for safety management. Another question was from the airline operational domain and concerned the trust framework of ICAO and what it expected from the standards-developing organizations to ensure that users are operating within that framework. The panelists agreed that trust is the key to ensuring interaction between different bodies that could eventually lead to achieving greater heights and overcoming more challenges in the aviation world.

Mr. Johnson concluded the panel discussion by stating that it had demonstrated that there was an important need for aviation operators, users, and manufacturers to work closely with standards-developing organizations to fulfill the demands of both traditional and emerging aviation markets, and that it had also had shown how those operations and markets could evolve together into a common ecosystem while ensuring the safety and efficiency of their systems. The digitalization of aviation holds challenges for everyone, so everyone must work together to enable aviation to undergo its next evolutionary change.

5 Special Speeches

This section summarizes the special speeches given in EIWAC2019. EIWAC2019 included a one-hour speech from EUROCAE on day two, and a speech from DSNA on day three.

5.1 Christian Schleifer-Heingärtner, "Current and Future Aviation Standards—Shaping Global Standards Through Collaboration"

Mr. Schleifer-Heingärtner is the secretary-general of EUROCAE. In his presentation, he introduced the EUROCAE association's current situation, then spoke about its current domains of activity and new activities.

First, he introduced the current situation regarding EUROCAE, which is a standardization body based in the EU: as of 2019, it has 300 members, 40 active working groups, and 2500 experts. EUROCAE has seen a minimum of 10% growth per year for the last six years. Its members are from industry, manufacturers, parts manufacturers, equipment manufacturers, engine manufacturers, aircraft manufacturers, and ground infrastructure manufacturers for ATM sites. Coordination and collaboration with many stakeholders in aviation are important to developing standards. EUROCAE does 50% of its activities jointly with RTCA and 10% with SAE. It is one of the standards-developing organizations recognized by the international standards-developing organization at ICAO. Mr. Schleifer-Heingärtner explained the standard-developing process adopted by EUROCAE. They believe that the development process should be transparent and open to the public.

Second, he introduced EUROCAE's current domains of activity. These are Avionics, Communication, Navigation, Surveillance, ATM Systems, Airports, SWIM, Electric (lightning protection/high-voltage), Security, AIS/MET, RPAS/VTOL&GA, and Miscellaneous (fuel cells, hybrid propulsion, space, ice detection, C-UAS, N-GAP).

Then, he went into detail about some of the working groups. For example, EUROCAE developed the Flight Tracking and Return Link Service in WG-98 Aircraft Emergency Locator Transmitters. An initiative by ICAO called Global Aeronautical Distress and Safety System (GADSS) arose from the disappearance of Malaysian Aircraft 370. GADSS is about tracking or having a position when an aircraft is in distress. One of the GADSS solutions is EUROCAE ED-62. EUROCAE updated the emergency locator transmitter standard, so it is now ED-62B. WG-98 is a good example of a joint activity EUROCAE conducted with RTCA. Mr. Schleifer-Heingärtner also went into detail about the following: WG, WG-100 Remote/Virtual Tower, WG-109 RWIS (Runway Weather Information

Systems), WG-111 A-CDM, WG-105UAS, WG-115 C-UAS, WG-112 VTOL, WG-113 Hybrid Electric Propulsion, WG-72 Aeronautical Systems Security, and WG-114 Artificial Intelligence.

Third, he talked about the following new activities conducted by the technical working program in 2020:

- Digitalization, digital transformation and big data
- AI and blockchains
- Automation and autonomous flying
- Virtualization: virtual centers, virtual towers and augmented reality
- Drones, UAS, RPAS, and UTM
- Counter drone technology
- Urban air mobility and flight taxis (VTOL pilot project)
- Urban CNS and GNSS/ GSM performance in urban areas
- ATFM and civil/military applications
- Health monitoring and predictive maintenance
- Single pilot operations
- Computer vision
- Quantum computing
- Air-to-air connectivity
- Higher airspace operations
- Electronic conspicuity
- ATM data service providers
- Ground-handling
- Environmental activities
- Hybrid electric technologies
- Space travel
- Space-based solutions.

In conclusion, he emphasized the importance of shaping global standards through collaboration. In order to achieve global interoperability, EUROCAE will need participation from all over the world. That contribution will lead to globally applicable standards.

5.2 Patrick Souchu, "Sharing Trajectory Views: The Key Enabler for Trajectory-Based Operations"

Mr. Souchu is the SESAR program director at DSNA (the French Air Navigation Service Provider). The title of his presentation was, "Sharing trajectory views: the key enabler for trajectory-based operations." Current ATM operations have different views of the same trajectory. This is because each stakeholder has different needs, and these views often differ for various reasons. This will not be acceptable if ATM users are to use these trajectories for more advanced capabilities. Stakeholders should

share a common trajectory. Mr. Souchu discussed three steps toward overcoming this problem in Europe.

The first step is flight plan adherence recommendation. In Europe, many flight plans differ from the actual trajectories. In 2017–2018, the EUROCONTROL network manager and service providers issued a recommendation calling for improved flight adherence to flight plans, to not only on the part of the airlines but also of the controllers. This is because if a controller give a direct route, then it will affect many other sectors. The controller may not be aware of the impact on other sectors, especially in terms of congestion. This recommendation was therefore issued and has been implemented through collaboration between airlines and CFSPs, and between airlines and ATCs.

The second step is sharing information on the ground by means of FF-ICE and IOP of flight objects. The ICAO FF-ICE initiative will facilitate the sharing of enhanced flight information in the planning and execution phase. As an instance of this FF-ICE concept in the execution phase in particular, SESAR is currently addressing this sharing of flight information with the notion of flight object interoperability, something that was initially defined in EUROCAE document ED-133. At the ATC level, IOP will improve safety and capacity. It will ensure a constant and consistent view of all traffic flows, even those processed by other flight data processing systems. It will reduce the ATCO workload because of better traffic anticipation. It will allow more enhanced and efficient coordination compared with all the current standards in Europe. It will enable more enhanced and efficient negotiation with downstream units compared to current voice negotiation and will improve the performance of conflict detection and resolution tools. At the ATFM level, it will also contribute to significant improvements in trajectory consistency and trajectory accuracy, and thereby allow us to reduce the uncertainty buffer. It will therefore improve the predictability and performance of the demand and capacity balancing.

The third step is sharing information between the air and ground. One of the first examples of air-ground coordination is the use of a selected flight level, which is transmitted by Mode S enhanced surveillance and already provides large safety benefits. Another example is the downlinking of aircraft's extended projected profiles (called EPPs). EPPs are computed and updated onboard, and transmitted by Automatic Dependency Surveillance Contract (ADSC) using a standard called ATN B2. There are plenty of potential uses for these onboard trajectories, but large safety gains can be expected if they are used to highlight possible discrepancies between the airborne trajectory computed by the FMS and downlinked and ground-based trajectories computed by the flight data processing system.

In conclusion, he pointed out that for various reasons, trajectory views are not always consistent today. This could result in safety issues and inefficiency, and impose serious limitations on moving to trajectory-based operation. However, three steps will lead to sharing of views. The enhanced ground-ground sharing of information via FF-ICE and flight object interoperability and the new air-ground data link capabilities for sharing air and ground trajectories using ATN B2 are almost there. Finally, sharing views will enable trajectory-based operation.

6 Conclusions

The sixth ENRI International Workshop on ATM/CNS (EIWAC2019) was held in October 2019 with the aim of comprehensively sharing information on the latest ATM/CNS technologies and operations among the participants, and seeking potential partners for R&D, standardization and global harmonization activities.

This chapter began with a history and overview of the EIWAC series. It then summarized the topics and opinions presented by the keynote and special speakers, who were from various organizations, among them regulators, standardization bodies, ANSPs, operators, and R&D organizations. The keynote and special speeches showed that the speakers had a common awareness regarding the problems facing current aviation systems. Digitalization and emerging technologies will be key solutions to these problems.

References

1. EIWAC2009 homepage, https://www.enri.go.jp/eiwac/2009/en/index.html
2. EIWAC2010 homepage, https://www.enri.go.jp/eiwac/en_EIWAC2010siryou.html
3. EIWAC2013 homepage, https://www.enri.go.jp/eiwac/en_EIWAC2013siryou.html
4. EIWAC2015 homepage, https://www.enri.go.jp/eiwac/eiwac_2015_eng.html
5. EIWAC2017 homepage, https://www.enri.go.jp/eiwac/eiwac_2017_eng.html
6. EIWAC2019 homepage, https://www.enri.go.jp/eiwac/eiwac_2019_eng.html
7. Electronic Navigation Research Institute, Ed., Air Traffic Management and Systems (Springer, 2014), pp. 3–14
8. Electronic Navigation Research Institute, Ed., Air Traffic Management and Systems II (Springer, 2017), pp. 3–24
9. Electronic Navigation Research Institute, Ed., Air Traffic Management and Systems III (Springer, 2019), pp. 3–15

ATM Performance

Volatility in Air Traffic Management—How Changes in Traffic Patterns Affect Efficiency in Service Provision

T. Standfuss, M. Whittome, and I. Ruiz-Gauna

Abstract Air traffic demand and distribution fluctuates in long-, medium-, and short-term perspective. In order to ensure safe and efficient flight operations, air navigation service providers need to ensure that enough capacity is available for airspace users. For this purpose, reliable traffic forecasts are necessary to avoid capacity shortages or excesses and subsequently costs. However, the provision of air navigation services is hampered by several effects, i.e., unpredictable traffic patterns and trends. Despite awareness of such problem, there is not a common definition or metric yet to measure the so-called 'volatility.' The aim of this paper is twofold: to set out an approach addressing volatility measures for different spatial and periodical scopes, and to show the effects of demand fluctuations on the ATM system from a holistic point of view.

Keywords ATM · ANSP · Performance · Volatility · Fuzzy cognitive mapping

1 Motivation

Due to the growing number of flights and the high cost pressure on airlines, the provision of air navigation services (ANS) has recently drawn increasing attention from both the academic and the policy decision-makers perspectives. A major challenge regarding ANS provision is 'planning under uncertainties' as a result, for example, of a volatile traffic demand in terms of movement numbers and flow patterns, which significantly influence resource planning and allocation. Several factors could cause

T. Standfuss (✉)
Chair of Air Transport Technology and Logistics, Technische Universität Dresden, Institute of Logistics and Aviation, Dresden, Germany
e-mail: thomas.standfuss@tu-dresden.de

M. Whittome
FABEC Functional Airspace Block Europe Central, Langen, Germany
e-mail: matthias.whittome@dfs.de

I. Ruiz-Gauna
Metroeconomica, Bilbao, Spain
e-mail: itziar.ruizgauna@metroeconomica.com

Air Traffic Management and Systems IV, Lecture Notes in Electrical Engineering 731,
https://doi.org/10.1007/978-981-33-4669-7_2

or amplify volatility (i.e., weather phenomena, strikes, geopolitics, airline decisions or unexpected economic downturn [1]).

Volatile traffic affects ANS planning at multiple time-scales and operational levels [2]. Changes in traffic demand and flow patterns have a direct influence on pre-tactical and strategical capacity planning. Since airspace users tend to act more and more on a short-term basis, it seems reasonable to think that volatility has increased over the past years.

Against this backdrop, the paper focuses on two issues. Firstly, it provides a specific definition and derived metrics in order to evaluate volatility in air traffic management (ATM). Secondly, the influence of volatile traffic on ATM performance is analyzed, discussing two potential approaches.

For this purpose, the paper is structured as follows: Sect. 2 deals with the state of the art regarding volatility measurement as well as the underlying approaches published by authors with an operational or academic background. Section 3 introduces volatility definition and metrics, the latter also being applied to several data sets. In Chap. 4, we present the results for volatility on ANSP level and discuss potential effects on costs and resources. We also compare different volatility metrics and check applicability and meaningfulness.

Since there are several operational subdivisions of one ANSP, we calculate volatility scores for sector families in Chap. 5. The influence of volatility on performance is determined in Sect. 6. Key mechanisms within the ATM systems are analyzed by applying fuzzy cognitive mapping. Section 7 finishes with some conclusions and determines a way forward.

2 Current Situation and Literature Review

Volatility is a rather new field of research in the ATM context. The impact of volatility on performance has still neither been investigated by academic studies nor included in official EUROCONTROL benchmarking reports. As a result, volatility of air traffic is not considered in the policy decision-making process (e.g., the performance scheme of the SES Regulations). This may lead to insufficient collection and/or distribution of route charges in terms of an efficient demand-capacity-balancing.

In May 2018, FABEC and the Baltic Functional Airspace Block (Baltic FAB, composed of the countries of Poland and Lithuania) conducted the workshop 'Volatility in Air Traffic and its impact on ATM Performance.' The conference papers dealt primarily with unpredictability and capacity planning under uncertainties from an operational or an academic point of view (e.g., [3, 4]).

EUROCONTROL uses 'traffic variability' as a metric for demand fluctuations, by comparing the peak value with the corresponding average over a given time (e.g., annually) and operational level, e.g., area control center (ACC) [5]. However, the measure proposed by EUROCONTROL has shortcomings: as only the highest and the average numbers are taken into account, volatility during all other 10 months or 50 weeks is neglected. In addition, variability can be called 'seasonality,' since only

the whole year is considered. Trends for 5–10 years for investment cycles or during a week for shift planning purposes are not contemplated.

In summary, the currently available and applied metrics provide a first approach to describe traffic demand fluctuations. Furthermore, spatial and temporal aspects were considered. However, even though it is commonly agreed that volatility has a high impact on performance [2], there is neither a clear definition of the word itself within the ATM context nor are formulas available to quantify traffic demand volatility and its influence on delay and other performance indicators. For all these reasons, a holistic approach is missing which includes interdependencies between factors which cause or are influenced by volatility (cause and effect chain).

The current study aims to close this research gap by defining and comparing valid volatility metrics. The approaches used are applicable to multiple time horizons (long-, medium-, and short-term), and operational levels (ANSP, area control centers, sector families, etc.). Thus, this paper contributes significantly to the understanding of the extent and effects of traffic fluctuations.

3 Volatility Metrics

Volatility is a measure often used in finance, which enables a risk assessment. Approach, applications, and formulas are described comprehensively in [6–9]. In the context of air traffic and ANS provision, we define volatility as the variability of traffic flow along a specific unit within a given time period. In accordance with the financial metrics, traffic volatility σ denotes the (short-term) fluctuation of a time series by its mean or trend [10]. It is measured by the sum of standard deviation of change rates R_i (e.g., of flights) between two or more periods (1). The arithmetic mean is indicated as μ, and n represents the number of observations.

$$\sigma = \sqrt{\frac{1}{n} \times \sum_{i=1}^{n} (R_i - \mu)^2} \tag{1}$$

This metric measure 'historic volatility' and is time-invariant. It summarizes the probability of observing extreme values of traffic demand. The changes might be defined as absolute, relative, or logarithmic terms. Formula (2) represents another alternative to approach volatility, by calculating the standard deviation based on the observed values h (e.g., for flights) in period t (instead of the change rates, $\bar{h}$ stands for the arithmetic mean of h). It is used when samples are considered rather than the whole population.

$$\sigma = \sqrt{\sum_{t=1}^{T} \frac{(h_t - \bar{h})^2}{T - 1}} \tag{2}$$

Noting that the standard deviation is scale-dependent, it might be also worth computing the percentage coefficient of variation (CV), as shown in (3).

$$CV = \frac{100}{\overline{h}} \sqrt{\sum\nolimits_{t=1}^{T} \frac{(h_t - \overline{h})^2}{T-1}} \tag{3}$$

The formulas (1)–(3) represent measures of variation. A second possibility to approach volatility, especially seasonal fluctuations, is represented by measures of uneven distribution. In scientific research, the most common economic metrics are GINI coefficient or Herfindahl-Hirschman-Index (HHI), see e.g., [11, 12]. GINI measures the relative concentration, e.g., of traffic demand over the year, based on the number of observations n, the observation index (e.g., month) i and the corresponding demand x_i as shown in (4).

$$\text{GINI} = \frac{2 \sum_{i=1}^{n} i \bullet x_i}{n \sum_{i=1}^{n} x_i} - \frac{n+1}{n} \tag{4}$$

HHI is often used to calculate market shares of firms; however, it might be also transformed to shares of different time periods. The index represents the sum of the squared market shares of individual observations (5).

$$\text{HHI} = \sum_{i=1}^{n} \left(\frac{x_i}{\sum_{i=1}^{n} x_i} \right)^2 \tag{5}$$

The index is often normalized in a second step, fitting to an interval [0, 1]. The HHI is invariant regarding the number of observations. However, in our study, the number of observations is constant.

Considering that the paper primarily focuses on finding a valid metric for ATM purposes, we apply formula (1) on different spatial and periodical scopes first. Therefore, we use relative changes due to the heterogeneous size of the units, as well as absolute traffic figures in order to consider limitations in resource planning. In a second step, we will apply formulas (3)–(5) as well, compare the results, and discuss applicability and meaningfulness.

4 Application on Macro-level

4.1 Database

As stated in Sect. 2, volatility may be computed over various time periods and operational levels. Since environment and objectives differ between these levels, we follow a macroscopic and a microscopic approach. At ‘macro-level’ (ANSPs), we use

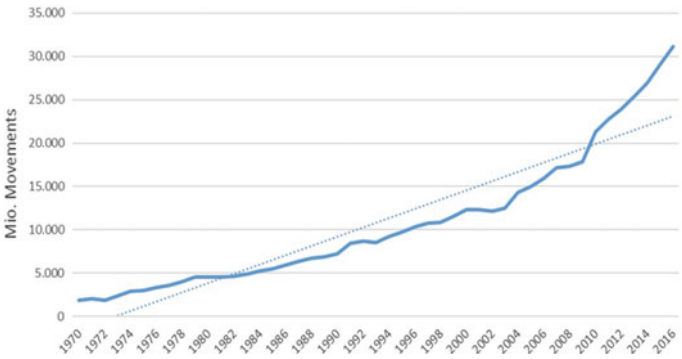

Fig. 1 Development of flight movements worldwide, 1971–2016 (Worldbank)

the Worldbank database for long-term investigations and data from the performance review unit (PRU) for medium- and short-term analysis [13–15]. We focus on ANSPs coordinated by EUROCONTROL.

Figure 1 shows the annual traffic movements between 1970 and 2016, based on Worldbank data. It emphasizes the need to consider multiple time periods: the overall (linear) trend is represented by the dotted line. Considering other time periods will result in another trend and, according to the definition in the previous section, in other volatility scores.

4.2 Long- and Medium-Term Analysis

As a first example, (1) was applied to the number of annual flights in European countries. The data was provided by Worldbank. R_i thus represents the change rate of flights in relation to the year before. A calculation example for Belgium is provided in Fig. 2. The red line shows the arithmetic mean μ, the green lines delimit the 66% confidence interval.

Since the calculation is based on growth rates, the relative differences R_i are available between 1971 and 2016. Applying formula (1) leads to a volatility score of $\sigma = 17.5\%$ for Belgium.

Figure 3 shows the long-term volatility scores for a selection of European countries. Bulgaria has the highest volatility score (33.9%) in traffic demand, while the United Kingdom has the lowest (4.1%). In general, (worldwide) volatility scores are characterized by a high level of scattering. However, high volatility scores are not common: The worldwide median is 16.8% in a long-term perspective. Since formula (1) is scale-dependent, countries with a relatively high traffic demand show low volatility scores. In contrast, countries such as Bulgaria and Hungary benefit from higher demands (and subsequently positive growth rates) due to the end of

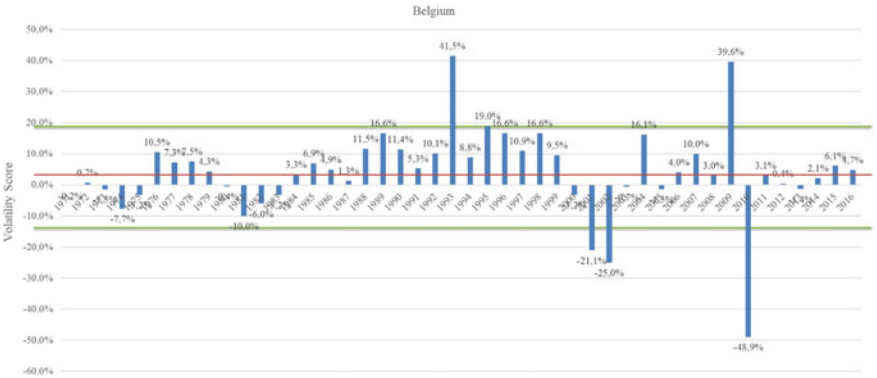

Fig. 2 Calculation example for long-term volatility for Belgium, 1971–2016, based on yearly traffic movements (Worldbank data)

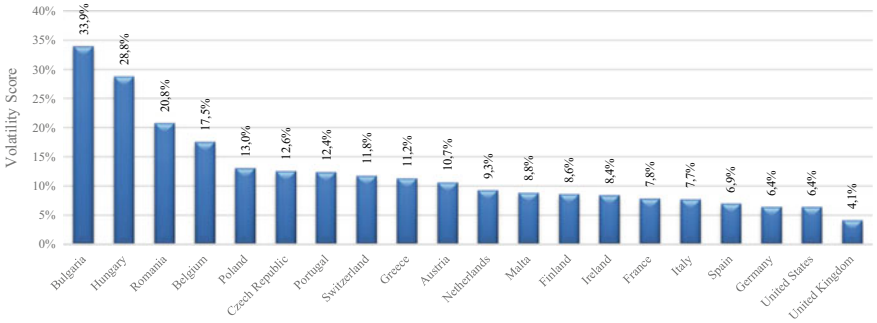

Fig. 3 Long-term volatility for a selection of European countries, 1971–2016, based on annual traffic movements (Worldbank data)

the political conflicts after 1990. Furthermore, growing traffic between the Arabic countries and Europe and/or America contributes to changes in growth rates.

High volatility scores may inhibit the resource planning of ANSPs. Fluctuations with high amplitudes, which is expressed by the volatility score, lead to high contingency costs. This is due to the necessity to provide staff and infrastructure for the case of maximum demand. However, the implementation of systems usually takes between 8 and 12 years.

It might be even more important to consider medium- and short-term fluctuation. A main cost driver of ANSPs is represented by human resources. The training of new controllers requires approximately five years and contingency costs might be higher than for infrastructure (hard and software) due to the annual costs per Air Traffic Control Officer (ATCO) or ATCO-hour. The medium-term analysis is based on PRU data, which is available for the years 2008–2017. It is beneficial to use time-based measures due to the possibility of subsumption.

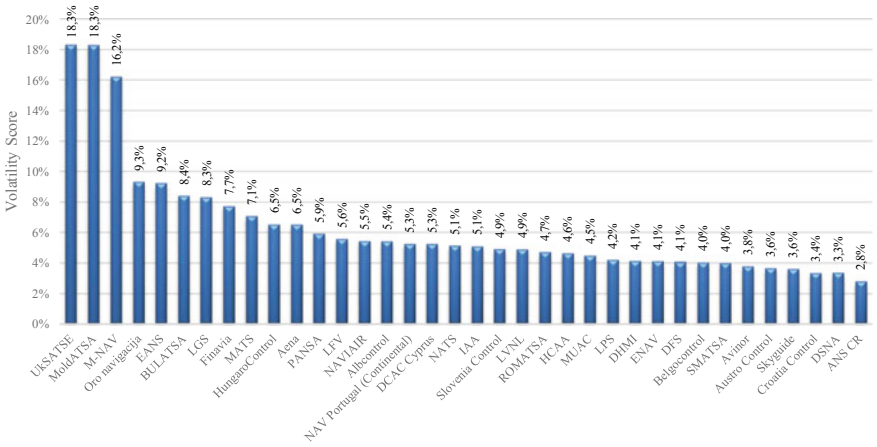

Fig. 4 Medium-term volatility, 2008–2014, flight hours (PRU data)

The medium-term perspective also enables the possibility to consider ANSPs instead of countries. Formula (1) was applied on EUROCONTROL ANSPs for a seven-year period (2008–2014). Figure 4 shows the medium-term volatility scores based on the change rates of 'IFR flight hours' (R_i). Scores are similar to those based on 'flights,' except for Malta Air Traffic Services (MATS) which is characterized by a deviation of about 6 percentage points. Volatility scores are lower than in the long-term perspective for majority of ANSPs.

4.3 Seasonality

As a further aspect, we consider seasonal demand shifts. The key underlying rationale is the same as for the long- and medium-term perspective: high fluctuations lead to high contingency costs. In order to calculate seasonal volatility, we used 2018 data provided by PRU dashboard (monthly flights). The data is available on daily basis. Formula (1) was applied on 'flights,' since 'flight hours' were not provided by the database [16].

Figure 5 shows the volatility according to the corresponding ANSPs, differentiated by summer and winter season. Since the scores differ between both seasons, classification is also different. The thresholds are shown in Table 1.

The applied volatility score is still based on growth rates. The figures show that volatility is higher in winter for the majority of ANSPs. There are some extreme values, represented by Norway for both periods, and the whole of Scandinavia for the winter season. The same effect is visible for FABEC-ANSPs: volatility decreases in summer and increases in winter. ANA LUX is confronted with the highest volatility in demand. This might be due to the overall smaller demand figures in winter (and

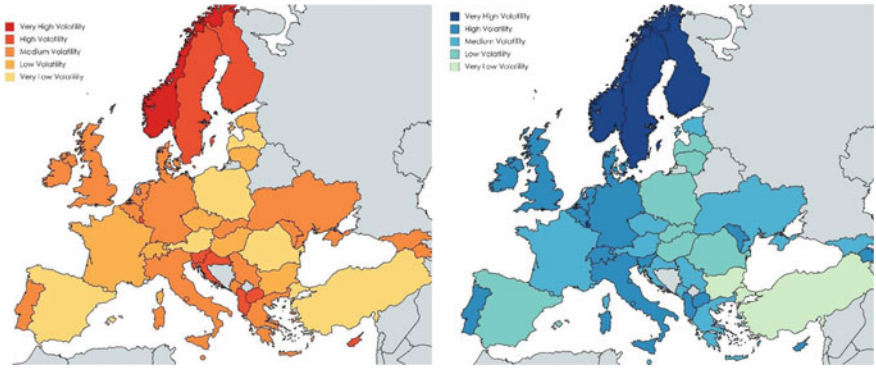

Fig. 5 Volatility score for summer (left) and winter (right), 2018

for ANA Lux). Subsequently, there is a higher (relative) change rate for a similar (total) shift in summer. For December, the high volatility can be explained by a demand fluctuation during Christmas time and New Year's Eve, given that demand figures are significantly lower on December 24th, 25th, and 31st. Due to illustrational reasons, the ANSPs are represented by the corresponding countries and MUAC is not included in the figures.

The results show some expected and some rather unexpected results. Especially the higher fluctuation of large-scale ANSPs might not be comprehensively covered by the relative measure of formula (1). Since ATCOs are licensed for a predefined number of sectors only, it is not possible to shift resources arbitrarily. Subsequently, it might be doubtful whether a metric based on formula (1) leads to meaningful results for seasonal volatility.

There are two possibilities to adjust the calculation of the score in order to improve the metrics. First, it is possible to use actual traffic figures instead of growth rates, but still apply formula (1). Second, as discussed in Chap. 3, there are potential alternatives, e.g., formulas (3)–(5).

These formulas were applied to PRU data [14]. The volatility scores are based on actual monthly flights in 2019. Furthermore, we calculated a peak load share (PLS). The metric divides the number of flights during the three most frequented months by the total number of flights in the whole year. Table 2 shows the results of all five indicators.

Table 1 Classification for seasonality

Class	Winter (%)	Summer (%)
Very high	>6	>15
High	10–16	10–15
Medium	7–10	5–10
Low	6–7	4–5
Very low	<6	<4

Table 2 Seasonal volatility metrics for a selection of ANSPs, 2019

ANSP	σ	CV (%)	HHI (%)	GINI (%)	PLS (%)
ANA LUX	596	9.0	8.4	4.7	27.1
Avinor	3.856	7.8	8.4	4.2	27.1
BULATSA	16.830	23.0	8.7	12.4	32.5
DFS	33.153	12.8	8.5	6.8	28.3
DSNA	48.413	17.6	8.6	9.5	30.0
ENAIRE	31.069	17.3	8.6	9.4	30.0
ENAV	36.114	23.7	8.8	12.9	32.6
IAA	7.869	14.6	8.5	7.9	29.0
LVNL	5.130	9.7	8.4	5.1	27.3
MUAC	16.045	10.3	8.4	5.6	27.8
NATS	28.649	13.6	8.5	7.3	28.8
Skeyes	6.670	12.5	8.5	6.7	28.3
Skyguide	18.067	16.5	8.5	8.9	29.6

The volatility score based on formula (1), σ. is scale-dependent and subsequently grows with the size of the corresponding unit. However, this might reflect the challenges of volatility more precisely. GINI and CV are highly correlated. These relative measures might be multiplied by the actual demand ore resource figures to calculate effects on the input- and output side. HHI seems to be unsuitable to compare volatility between single ANSPs. The peak load share might be of special interest for some ANSPs, e.g., if airspaces are primarily used in the summer or winter season. However, it gives no holistic description of the trend during a whole year. Subsequently, we suggest to use the CV or GINI coefficient.

Worldbank and PRU data allow only a very high aggregation level. Changing the perspective on lower operational levels will probably increase volatility since demand is expected to fluctuate more than in higher operational levels (law of large numbers). The application on a disaggregated level is discussed in section 0.

5 Application on Micro-level

Chapter 4 dealt with potential metrics to calculate volatility on the ANSP level. Most of the European ANSPs operate multiple area control centers (ACCs), dividing the corresponding national airspaces horizontally and/or vertically. The smallest structural unit is formed by the sectors, which can be combined or divided ('split') according to traffic demand. The possibility of combination, however, depends on the licensing of the air traffic controllers. Therefore, the sectors are allocated to sector families (SF). This operational level is defined as 'micro-level.' For volatility calculation, we use data provided by Deutsche Flugsicherung GmbH (DFS), containing

figures on sector family level for 'flights' and 'flight hours' (as demand), as well as 'ATCO-hours' (representing resources). The data is available for the ACCs Karlsruhe (ACC1), Bremen (ACC2), Langen (ACC3), and Munich (ACC4).

Figure 6 shows the number of IFR flight hours per year, differentiated by sector families. Due to the sensitivity of the data, the corresponding units are anonymized. Even though all sector families belong to the same ANSP, scattering is high: ACC1 SF1 flight hours are approximately seven times higher than the ones of ACC3 SF2. This divergence is caused by the different airspace characteristics: while some sector families are only responsible for upper airspaces, others supervise lower airspaces. The sector family ACC3 SF2 covers the southwestern area of Frankfurt airport, thereby controlling flights in the lower airspace, mostly with Frankfurt as their destination. As traffic composition in the lower airspace is more heterogeneous, capacity is lower due to the complexity and therefore comparatively less traffic is being controlled.

Traffic figures may vary significantly over time. As an example, most airspace units experience traffic peaks in summer. Table 3 shows the number of flights for each ACC for the years 2016 and 2017, as well as the mean, minimum, and maximum. The underlying annual shape of the demand curve is similar for all 4 ACCs.

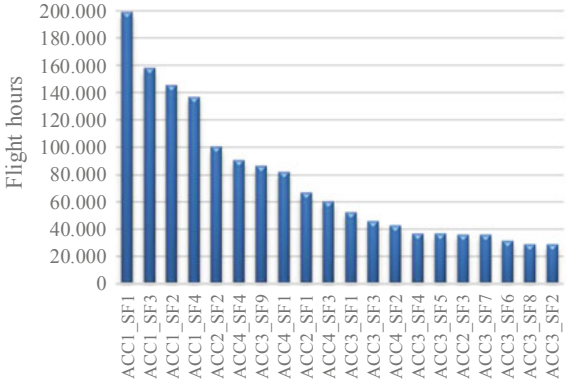

Fig. 6 Annual flight hours per sector family, 2017

Table 3 Descriptive statistics of traffic movements (based on monthly counts)

	Year	Sum	Min	Mean	Max
ACC1	2016	1,778,658	119,283	148,222	174,421
	2017	1,844,836	120,163	153,736	181,295
ACC2	2016	661,491	44,827	55,124	62,201
	2017	660,808	43,052	55,067	62,541
ACC3	2016	1,230,219	85,401	102,518	115,281
	2017	1,268,034	85,458	105,670	119,054
ACC4	2016	1,082,839	75,277	90,237	102,265
	2017	1,120,980	77,239	93,415	106,325

The largest number of flights occurs in summer, with the counter-peak in January or February. Karlsruhe controls about three times more flights than Bremen. However, the relative average is similar between all ACCs and all years (69–75%). Generally, higher volatility scores could be expected at the micro-level, as sectors control less flights compared to sector families, ACCs or ANSPs. The higher the amount of traffic the less volatility could be assumed, as one additional flight has a higher impact on lower operational levels.

The analysis on ANSP level demonstrated that fluctuations in traffic demand occur differently. In addition, pure demand figures on this operational level might not reflect changes in traffic flows appropriately. Therefore, it is useful to disaggregate the analysis by sectors, since capacity is basically provided within this smallest entity of the airspace.

Airspace structure is characterized by dynamic subdivisions. According to demand, sectors can be splitted or merged. Volatile traffic hampers efficient planning of these capacity enhancing measures significantly. However, sector data were not available for this research, so we applied the methodology on sector family data in order to calculate volatility. In this way we use 'flight hours' for demand.

Traffic demand fluctuates considerably over the year. The upper peak represents three times more flight hours than the lower peak, depending on the considered sector family. Furthermore, the data also reveal weekly and seasonal effects are also visible in the data.

According to Fig. 7, volatility metrics differ quite substantially between the sector families. On the one hand, the highest scores are shown for ACC2 sector families 1 and 3. On the other side, all three sector families with the lowest score are assigned to ACC1.

Comparing Fig. 6 with Fig. 7, there is no clear dependence between total overall demand and the volatility score. As a tendency, small units are characterized by a higher volatility (such as ACC 2). Further reasons might be the amount of military aircraft being controlled in different areas, which seems to lead to less volatility. In addition, the upper airspace (e.g., ACC 1 handling only traffic in the upper airspace)

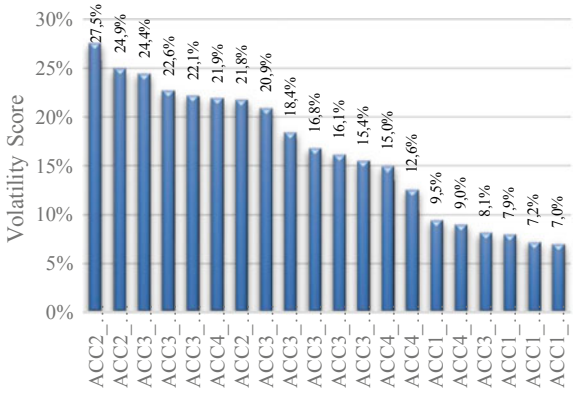

Fig. 7 Volatility of German sector families, monthly basis, 2017

and areas with a higher share of homogenous traffic (such as Approach Units of large Hubs like ACC3_SF9 and ACC4_SF1) seem to have a lower volatility, whereas the areas of responsibility that control flows to smaller airports, which tend to service low-cost carriers, are characterized by higher volatility.

In order to test the influence of volatility on performance, there are several analytical tools, such as regression analysis. This methodology enables the consideration of the interaction of several effects. Regression analysis is purely quantitative and thus does not require a priori assumptions. However, within this paper, we focus on the semi-quantitative approach of fuzzy cognitive mapping (FCM, Chap. 6). Furthermore, besides the analytical approaches, there is also the possibility of fast- or real-time traffic simulations (Chap. 7).

6 Fuzzy Cognitive Mapping

6.1 Approach and Methodology

Humans commonly tend to think that only direct causal relations exist between two concepts. Nevertheless, thanks to the understanding of complex systems we know that changes in one variable may influence variables which were not initially identified, or that one variable may generate an unexpected chain of events (commonly referred to as cascading effects). With this idea in mind, this paper is intended to better understand what and how volatility may affect or be affected by ATM. A fuzzy cognitive map is developed to this end.

Cognitive maps consist of a set of concepts and linkages which express cause-effect networks [17, 18]. However, causes are often uncertain, usually fuzzy. The notion of fuzziness was introduced into cognitive maps, giving rise to fuzzy cognitive maps [19].

FCM is a participatory, semi-quantitative method in which the experience, knowledge, and perceptions of the system of different experts on the topic (in our case, three air traffic controllers, two engineers specialized in performance management, one engineer with a focus on operational performance and two economists with specific knowledge of the European aviation sector) give rise to the construction of a graph structure that can be later used to simulate scenarios according to which policymakers may analyze how the system may behave under certain impacts [20]. In this way, these maps encourage systematic causal propagation (forward and backward chaining), helping to identify cascading effects and interdependencies across elements (including unexpected trade-offs and synergies) that otherwise would be difficult to analyze.

The approach is illustrated in Fig. 8. First, every concept (C) is defined at a discrete time, so its state may change over time. In a second step, all concepts are related to each other through directed arrows that indicate both the direction of the causality and the degree of influence one concept (C_2) can have on another (C_6) (positively or

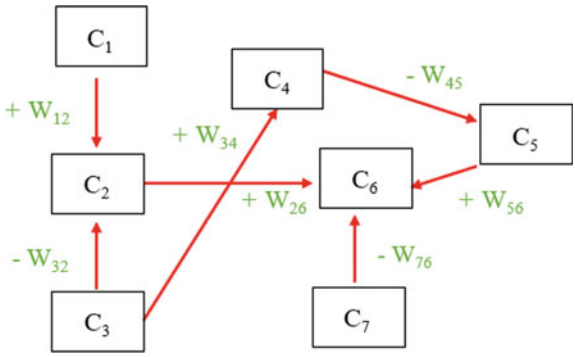

Fig. 8 Concept of a fuzzy cognitive map

negatively). Linkages are later labeled by weights (W_{26}), reflecting the strengths of the relationships between two concepts (C_2 and C_6). The weights are represented by a numerical scale from 0 to 1. Finally, once the map has been built-up, we can, on the one hand, perform scenario analysis to identify the cascading effects (in our case, the effects occurring in the whole system when there is a volatility problem in one part of it) and, on the other hand, estimate the following three indicators: Out-degree of a concept (a measure of the strength of the influence of one concept on other concepts in the network), In-degree of a concept (a measure of the dependency of a concept on other concepts in the network), and centrality (it denotes the individual importance of a concept).

6.2 Results

The eight experts found 39 concepts, such as ticket prices, wars/conflicts/crises, oil cost or airspace charges, among others. A complex map with these 39 concepts was built (Fig. 9), enabling us to show the relationships between them and to determine causes and effects of volatility that are usually not discernible at first sight.

According to our FCM, the concepts with the highest capacity to influence other variables or concepts (Out-degree) are 'predictability,' 'airspace complexity,' and 'economic activity.' By contrast, the concepts with the highest capacity for being influenced by the remainder (in-degree) are 'air traffic flow,' 'demand from airlines,' 'airspace complexity,' 'demand from passengers,' and 'predictability.' Centrality allows us to conclude that 'predictability' and 'airspace complexity' are the key variables to be considered when deciding certain policies or actions to reduce volatility by airlines and air navigation service providers.

When it comes to the scenario analysis, it involves examining what would happen in the whole system if there were a change in one of the concepts (e.g., a pandemic, like the COVID-19, or an increase of staff costs, among others). With this idea in mind, and after estimating a weight function and conducting the analysis with the software FCmapper [21], a common trend can be observed: the system reacts in a

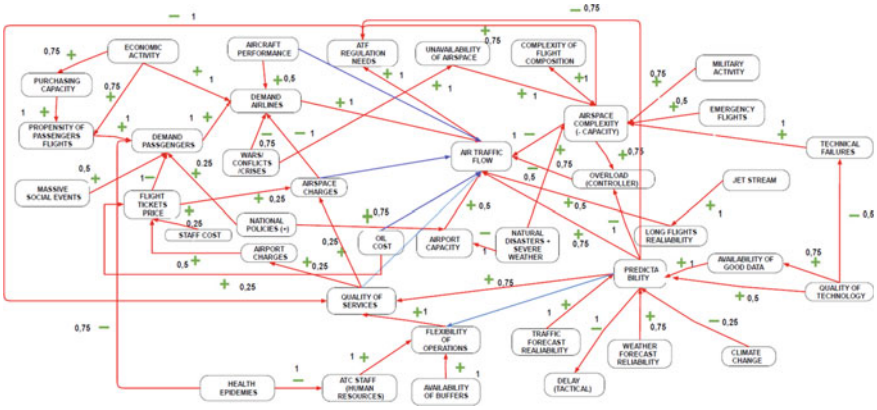

Fig. 9 Fuzzy cognitive map

similar way, irrespective of the fact in which concept a change (or shock) occurs. In other words, whether there is a change in one or another concept, the same variables are almost always the most affected by these changes. This means that these variables (in our case, 'airport charges,' 'airspace charges,' 'ATFM regulation needs,' 'demand from passengers,' 'demand from airlines,' 'flight ticket price,' 'air traffic flow,' 'quality of services,' 'overload (controller),' 'airspace complexity,' and 'complexity of flight composition') are the most sensitive in the case of external shocks, whatever they may be, so they should be taken into consideration by policymakers and air traffic managers when facing volatility in the performance and operation of the air system. This will help them to act accordingly, since they may decide whether or not to current buffers are appropriate or not or whether it is necessary to add some new buffers (see, for example, the case of overload for controllers).

In short, FCM is a very useful tool for understanding volatility, as it implies a high degree of complexity. It not only depends on certain obvious variables affecting it directly, but also on other variables that are indirectly relevant and that had not been identified if were not for the construction of this complex systems. Thus, the whole map should be seen in the context to prevent global consequences, as the impact of one variable may influence others in unexpected ways.

Moreover, despite being constructed by experts, the fact that it is easily to understand for the general public is what makes FCMs a very interesting alternative to be considered in policymaking.

7 Conclusion and Way Forward

The present paper develops a general definition to describe volatility of air traffic demand for a wide span of reference time periods, as well as for geographical scopes. Based on macro- and micro-level data, the method was applied on various examples

ranging from a 1 year to a >50-year period along the time axis and from sector family level to European airspace on the scope axis. The paper shows that volatility scores are sensitive to both factors. In addition, the highest volatility can be observed in December. By contrast, the low volatility scores for summer are rather unexpected. However, this picture changes when using a scale-dependent calculation basis, which might be more useful due to the nature of ANSP staff planning.

In addition, an FCM is applied to enable a holistic consideration of the whole system. In this way, it is possible to show which elements are sensitive to volatility, e.g., caused by external shocks. A quantification, e.g., by regression analysis, might be a subject for further research. Furthermore, the approach to simulate different traffic scenarios and their influence on sector configurations will lead to further insights with regards to resource planning.

The applied calculation methods represent one potential approach. Standard deviation and GINI coefficient are expected to match ATM requirements most. In further studies, it should be checked whether the formula must be adapted or substituted in order to calculate volatility based other time periods (e.g., day and night time differences).

Quantifying the impact on the performance of ANSPs (e.g., regarding cost effectiveness) might be another research focus. The simulation, which is currently work in progress, will represent a fundamental contribution. In addition, it might be beneficial to include sectors, sector families, and ACCs of other ANSPs. This would enable the consideration of particularly strong, unforeseen traffic fluctuations into regulatory measures, respectively, policy decision making.

Acknowledgments The authors would like to thank Marta Olazabal who supported the FCM progress, Ibon Galarraga and Prof. Alberto Ansuategi for methodological input regarding volatility metrics, and Prof. Hartmut Fricke for his profound ATM expertise.

References

1. FABEC, Volatility Task Force—Final Report (Langen, 2018)
2. FABEC, Volatility in ATM: Cases, Challenges, Solutions, World ATM Congress, Inter-FAB Panel, FABEC OPS Theatre Madrid (2018)
3. V. Deltuvaitė, Main determinants of volatility in air traffic and its impact on ANSPs' performance, in *FABEC Workshop on Volatility in air traffic and its impact on ATM Performance* (Warsaw, 2018)
4. D. Kügler, Volatility in ATM—challenges of sustainable air transportation, in *FABEC Workshop on Volatility in air traffic and its impact on ATM Performance* (Warsaw, 2018)
5. EUROCONTROL, *Performance Review Report (PRR) 2017* (Performance Review Commission, Brussels, 2019)
6. K.J. Daly, Financial volatility: Issues and measuring techniques. Physica A Stat. Mech. Appl. 2378–2393 (2008)
7. A. Hirsa, S. Neftci, *An Introduction to the Mathematics of Financial Derivatives* (Academic Press, 2013)
8. D.G. Luenberger, *Investment Science*, 2nd ed. (Oxford University Press, 2014)

9. R.A. Schwartz, J.A. Byrne, A. Colaninno, *Volatility: Risk and Uncertainty in Financial Markets* (Springer, 2010)
10. C. Hafner, *Nonlinear Time Series Analysis with Applications to Foreign Exchange Rate Volatility* (Springer Science & Business Media, 2013)
11. A. Bem, K. Daszyńska-Żygadło, T. Hajdíková, P. Juhás, *Finance and Sustainability, Proceedings from the Finance and Sustainability Conference* (Springer, 2014)
12. S.A. Rhoades, The Herfindahl-Hirschman index. Federal Reserve Bulletin (1993)
13. EUROCONTROL, OneSky Online, ACE Working Group, Brussels. Available at https://extra.euro-control.int/Pages/default.aspx. Accessed on 04 Mar 2020
14. EUROCONTROL, Data, Operations En-route, Available at: http://www.ansperformance.eu/data/. Accessed on 11 May 2019
15. Worldbank, World bank open data—free and open access to global development data. Available at https://data.worldbank.org/. Accessed on 20 Apr 2019
16. EUROCONTROL, Pan-European ANS Performance Data Portal, Performance Review Unit, Brussels (2016)
17. R. Axelrod, *Structure of Decision: The Cognitive Maps of Political Elites* (Princeton University Press, 1976)
18. J.H. Klein, D.F. Cooper, Cognitive maps of decision-makers in a complex game. J. Oper. Res. Soc. 63–71 (1982)
19. B. Kosko, Fuzzy cognitive maps. Int. J. Man Mach. Stud. 67–75 (1986)
20. M. Olazabal, M.B. Neumann, S. Foudi, A. Chiabai, Transparency and reproducibility in participatory systems modelling: the case of fuzzy cognitive mapping: transparency and reproducibility in fuzzy cognitive mapping. Syst. Res. Behav. Sci. (2018)
21. M. Bachhofer, M. Wildenberg, FC mapper software (2009). Available at: https://www.fcmappers.net/joomla/index.php. Accessed on 20 June 2019

Coordinated Sequencing of Traffic on Multiple En-Route Constraint Points

S. Abba Rapaya, P. Notry, and D. Delahaye

Abstract Air transportation traffic is progressively increasing over the years and dealing with it is an essential task to guarantee fluid flights in the future. Several works already indexed multiple aspects of aviation, among them, the E-MAN system. It introduced the sequencing of arriving traffic, starting from early stages of the En-route phase. This change facilitated the work for the approach controllers but also increased the workload of the En-route controllers. To handle that workload, controllers are now assisted by tools that consider the new constraints introduced by the arrival management system and propose advisories. From that same perspective, our project focuses on an algorithm for a helper tool that will combine both aspects of traffic sequencing in the En-route phase and conflict resolution. With this novel approach, we automatically generate near-to- optimal flight decisions, given that we can modify the speed and the flight level to respect the sequencing constraints and cut down potential conflicts. We categorize the problem as a mathematical optimization case. Thus, we describe a detailed mathematical model which covers all the aspects of the problem. This model gives a basis for the implementation of the flight optimizer. Later, we propose a solution based on a sliding window simulated annealing algorithm which reduces the complexity and takes into account uncertainties. Finally, we successfully test an implementation of the solution with real-life traffic data. It corresponds to flights within France going towards Paris CDG airport over a period of 24 h. The results demonstrate a total conflicts resolution with satisfying compliance with sequencing constraints.

Keywords Air traffic management · Traffic sequencing · Arrival management · Conflict resolution · Multi-objective optimization · Simulated annealing · Sliding window

S. Abba Rapaya (✉) · P. Notry · D. Delahaye
OPTIM, ENAC-LAB, ENAC, French Civil Aviation University,
7 Avenue Edouard Belin, 31055 Toulouse, France
e-mail: souleymanr@gmail.com

P. Notry
e-mail: philippe.notry@enac.fr

D. Delahaye
e-mail: delahaye@recherche.enac.fr

Air Traffic Management and Systems IV, Lecture Notes in Electrical Engineering 731,
https://doi.org/10.1007/978-981-33-4669-7_3

1 Introduction

The air traffic has been increasing lately. In its Global Market Forecast (GMF) [1], Airbus has predicted that the global air traffic will encounter an annual growth of 4.4% for the next coming 20 years. With that increase of traffic, some major airports will now rely on arrival management systems such as the Extended-Arrival MANager (E-AMAN [6]) system to help them manage their flow of traffic and generate efficient flights sequencing. However, most of the workload is now transferred to the En-route controllers since they will have to deal with occurring conflicts and also try to respect new constraints imposed by the E-AMAN to flights. In En-route, the airspace is characterized by several route flows crossing into potential conflict points. To avoid those conflicts, some separation constraints are defined for the flights and controllers need to make sure they are respected by using classic methods like vectoring, speed controlling or flight level changes. Each decision applied to an aircraft can have an impact on surrounding flights. This research aims to develop an algorithm that will assist the controllers. Based on the traffic flows analysis, this algorithm will provide near optimum flight decisions in order to remove conflicts at the crossing points. From the controller's side, the main objective is to reduce the workload and minimize the frequency occupation. This will be done by automatically eliminating conflicts due to lack of separation at crossing points and route links. It also implies reducing the number of flight level changes and simplifying the instructions given to pilots. Another objective is to integrate our tool with an E-AMAN system by generating decisions compatible with E-AMAN constraints. Finally, from the airlines point of view, we will need to take into consideration the preferred flight profile by generating decisions not far from that profile. The first part of the paper introduces some previous related works linked to arrival manager optimization in a wide sense. The second part presents the associated mathematical model. The meta-heuristic (simulated annealing) used for solving the underlying optimization problem is presented in the third part. Finally, the fourth part presents the results given by the algorithm on a real case at Paris Chales De Gaulle (CDG, airport code: LFPG).

2 State of the Art

This section presents the concepts and previous works related to our problem. It focuses on points around air traffic sequencing, conflict resolution and mathematical optimization methods. It is concluded by a synthesis which serves as baselines for our modeling and solution approach.

2.1 Extended AMAN

The Cross-border SESAR Trials for Enhanced Arrival Management (X-STREAM) project main objective is to extend the current horizon of the Arrival Management System beyond 200 NM towards the upstream Area Control Center (ACC). Extended-AMAN (E-AMAN) [6] allows for the sequencing of arrival traffic much earlier than is currently the case, by extending the AMAN horizon from the airspace close to the airport to further upstream and so allowing more smooth traffic management. Controllers in the upstream sectors, which may be in a different control center or even a different Functional Airspace Block (FAB), obtain system advisories to support an earlier pre-sequencing of aircraft. Controllers implement those advisories by, for example, instructing pilots to adjust the aircraft speed along the descent or even before top-of-descent, thus reducing the need for holding and decreasing fuel consumption.

2.1.1 Features

The traffic begins to be processed at the Eligibility Horizon (EH) and controllers are provided with AMAN advisories from the Active Advisory Horizon (AAH) onward [5]. EH is the spatial horizon where aircraft start to be considered by the AMAN and AAH is the spatial horizon where actions computed by the AMAN are executed by the aircraft. With the extension of the horizon of the AMAN to the En-route phase, as illustrated on Fig. 1, the EH goes further to around 180–200 NM which supports the controllers in applying more efficient arrival management techniques. The typical optimum top of descent is approximately 100–120 NM from touchdown which implies that up to 100 NM of flight within the extended AAH will be in En-route airspace.

2.1.2 Decisions on Flights

AMAN advice may be in the form of a Target Time at the Initial Metering Point (IMP) or Time To Lose (TTL)/Time To Gain (TTG) advisories to controllers calculated by AMAN working back from the runway time [5]. Upstream ACC controllers can then provide instructions to pilots to make adjustment of speed to meet TTL/TTG need, by executing advisories for speed coming from tools like Speed And Route Advisory (SARA)[1] or to delegate responsibility for adherence to a Controlled Time of Arrival (CTA) to flight crew.

[1] Speed and Route flight Advisory.

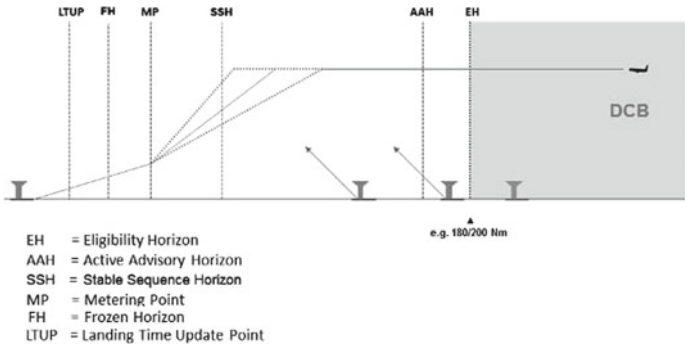

Fig. 1 Simple horizon extension

2.2 Previous Works

Optimization problems involve the minimization (or maximization) of a function by choosing input values from a given set of data and computing the value of the function. Nowadays, many studies have been conducted on the resolution of air traffic conflicts and the sequencing using various mathematical optimization techniques. This section will present a few of those works. Vela et al. in [10] presented a new approach based on concepts of speed control and flight-level assignment for conflict resolution over predefined routes. The resolution of this model was based on a Mixed Integer Linear Programming approach (MILP). The way it was formulated helped to reduce fuel burn over time horizons between 15 and 45 min. Qing et al. [7] proposed a flight scheduler for En-route air traffic. It was based on the application of delays or route changes to flights to produce an ordered merged sequence of flights at the exit nodes. They didn't tackle the conflict resolution aspect in that paper. During the 2017 SESAR Innovation Days, Couchelle et al. [3] presented a method to perform small changes on aircraft speed in order to resolve conflicts. In their model, they considered that the True Air Speed (TAS) was constant for each aircraft in the airspace and the uncertainties appeared due to wind components, with wind data collected from MétéoFrance PEARP (Prévision d'Ensemble ARPège). A protection area, as illustrated in Fig. 2, is defined around each aircraft to represent its potential positions. Thus, two overlapping protection areas imply a potential conflict between

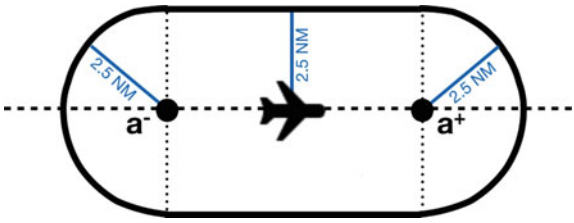

Fig. 2 Protected area around the aircraft. If two areas overlap, there is a potential conflict

the two aircraft that must be dealt with. The solution was implemented in Python using a simulated annealing algorithm. As a result, the algorithm was able to solve at least 70% of virtual conflicts with a computing time of 30 min to 2 h for a 4 h traffic data depending on the refinement of the parameters. On the other hand, Barragan et al. [2] presented their work at the 29th Congress of the International Council of the Aeronautical Sciences (ICAS). It was done on a study for a collaborative tool that aimed at helping controllers with the integration of the Extended Arrival Manager. They studied the aircraft sequencing problem as an optimization problem under different resolution methods (Linear programming, non-linear programming, heuristic methods). The objective function took into consideration the runway capacity, the delays and the fuel consumption. They also didn't consider the conflict resolution aspect.

2.3 Synthesis

As seen in this section, the Extended Arrival Management tool gives advisory directives to controllers to help create an efficient sequence of flights starting from a distant En-route point. However, it is still up to the controller to decide how he will implement those directives taking into account the potential occurring conflicts. A tool like SARA, in combination with E-AMAN, can help controllers by giving speed directives but no global conflict resolution is provided. Thus, it will be an added value for our solution to provide both sequencing and conflict resolution capabilities. Moreover, most of the previous works done on the optimization of the traffic focused on changes made on aircraft speed or route to delay or advance a flight. Therefore, not many alternatives were given for conflict resolution when there is a dense traffic. In that case, we can introduce changes on flight levels to broaden the solutions possibilities as suggested by Courchelle et al. [3]. As for the optimization method to apply, the nature of our problem makes it more appropriate for a meta-heuristic method, given the dimension of the problem. Also, the simulated annealing appears as a good choice regarding its stability, its memory consumption profile and its speed. Ji et al. [8] introduced an implementation of the simulated annealing algorithm coupled with the sliding window concept, the base of our implementation will be that algorithm. Another added value we can integrate in our solution is the collaboration with multiple E-AMAN tools at the same time. The state of the art review enabled us to define basis for our study case. In the next section, we will define a detailed mathematical model for the problem. This will highlight abstract concepts useful for the design of our solution.

3 Mathematical Model

This section focuses on an abstract mathematical modeling of our problem. Each aspect of the problem is represented using mathematical notations that can be interpreted into any optimization algorithm later. It presents the global network representation, how uncertainties are modeled, equations related to conflict detection, the optimization objective function definition and an evaluation of the complexity of the problem. To simplify our model, we made some assumptions. The TAS of each flight will be considered as constant all along its route in the airspace of interest. Each plane will be flying a constant flight level all along its route in the airspace. For that, we suppose that the application of any decision to change the flight level is performed before entering the airspace of interest. We assume that the time for the aircraft to perform a climb or descend operation is negligible. In other words, we will not consider the time for flight level changes. The wind direction will be considered as constant in all the airspace. Only its intensity will be randomly varying (a more realistic wind may be included in the future). We will not consider uncertainties on the time of entry of a flight in the airspace. Regardless of any action done on a flight prior to its entry in the airspace, we will always use the planned entry time as time of arrival at the entry point.

3.1 Constraints

We have identified some constraints for our model. They are elements that will influence the way the tool will handle the optimization process.

Sequencing constraints: those constraints are coming from the sequencing system. The E-AMAN generates a TTL or TTG for flights. It must be considered during the optimization process.

Aircraft performances: those correspond to the physical performances of the aircraft. It consists of the minimum (maximum) speed and the minimum (maximum) flight level the aircraft can fly. Basically, our tool should not advise a flight to perform outside of its physical limits.

Flight preferred profile: It is a constraint that can be proposed by the airline. In our case, we will consider the preferred cruising flight level. It is a flight level which if cleared to the flight, will help the airline to better achieve their business objective.

Separation constraints: we have three types of separation: the *distance separation* which is a minimum defined distance should be maintained between two aircraft when crossing a specific point, the *time separation* for which two consecutive aircraft should reach a given location with a minimum defined time interval and the *wake turbulence separation* which is the separation distance between two consecutive aircraft flying on the same link at the same flight level and which depends on their wake turbulence categorization as defined by ICAO.

3.2 Network Modeling

The network of routes is modeled as an oriented graph with nodes and oriented links.

Nodes A node represents any point of interest on a route. Most of the time, it will be where two routes are crossing. We can define a separation constraint on them (distance or time separation). A node n is characterized by its cartesian coordinates $(x, y),\ x, y \in \mathbb{R}$, a minimum separation distance d_{sep}, in case of distance separation constraint and a minimum separation time t_{sep}, in case of time separation constraint. The set of nodes will be noted N: $\mathrm{N} = \{n_i \ / \ i \in \mathbb{N},\ i \leq nb_{\text{nodes}}\}$ where nb_{nodes} is the total number of nodes in the network.

Links A link is a portion of route between two nodes. It is oriented from an origin node to a destination node. Each link is characterized by an entry node n_{ori}, an exit node n_{dest} and a length $d_l = \text{dist}(n_{\text{ori}}, n_{\text{dest}})$. The set of links will be noted L: $\mathrm{L} = \{l_i \ / \ i \in \mathbb{N},\ i \leq nb_{\text{links}}\}. \forall l_i \in \mathrm{L},\ l_i = (n_{ori}, n_{\text{dest}}) \ / \ n_{\text{ori}}, n_{\text{dest}} \in \mathrm{N},\ n_{\text{ori}} \neq n_{\text{dest}}$ where nb_{links} is the total number of links in the network.

Routes A route is an ordered list of adjacent links and is characterized by a parity p which can be odd or even: $p \in \{\text{ODD, EVEN}\}$ and a list of available flight levels $fls = \{fl \ / \ fl \in \mathbb{N}\}$. We will use the semi-circular rule to determine those flight levels depending on the parity of the route. The set of routes will be noted R: $\mathrm{R} = \{r_i \ / \ i \in \mathbb{N},\ i \leq nb_{\text{routes}}\}, \forall r \in \mathrm{R},\ r = \{l_i \ / \ l_i \in \mathrm{L}\}$ where nb_{routes} is the total number of routes in the network.

3.3 Flights Modeling

A flight f is characterized by a speed V_f, a flight level FL_f, the time of arrival at the first node (entry in the airspace) $t_{f_{\text{init}}}$, a wake turbulence category $wtCat_f$ and a defined route $r_f \in \mathrm{R}$. Apart from those characteristics, a flight is also subject to some constraints: a maximum speed $V_f^{\max}$, a maximum flight level $FL_f^{\max}$, a preferred flight level FL_f^{pref} given by the airline and a time constraint ttl_f given by the sequencing system (a positive value means a time to gain and a negative value refers to a time to lose both before reaching the final exit node). The set of flights will be noted F. $\mathrm{F} = \{f_i \ / \ i \in \mathbb{N},\ i \leq nb_{\text{flights}}\}$ where nb_{flights} is the total number of flights in the network.

3.4 Decision Variables

During the optimization process, two features of the flights are modified: the speed and the flight level. For that, we are using two decision variables which are the speed delta and the flight level delta.

Speed delta As in the model used by Courchelle et al. [3], we propose to use small speed changes to control flights speed. Each speed delta ΔV is an integer in the range of -6 to $+3$, expressed in percentage. $\forall f_i \in \mathrm{F},\ \Delta V_i \in \mathbb{Z} \cap [-6, +3]$. The new TAS V_i of flight f_i can be expressed as follow: $V_i = \frac{\Delta V_i}{100} \times V_{0_i}$ where V_{0_i} is the initial TAS.

Flight level delta The second decision variable we are using is the flight level delta. It represents the number of levels an aircraft should climb or descend. It is expressed as an integer varying from -2 to 2. A positive value represents a climb whereas a negative value represents a descend.

$$\forall f_i \in \mathrm{F},\ \Delta FL_i \in \mathbb{Z} \cap [-2, +2]$$

3.5 Uncertainties

In our assumptions, we supposed that the TAS of flights is constant all along its route. However, in the real world, each flight is subject to wind influence in the air which can affect the ground speed. This section presents how we model the wind and how it generates uncertainties in our model.

Wind modeling: we use a simplified model for the wind. The wind vector is characterized by a constant direction all over the airspace (it is represented as an angle α_w relative to the geographical north) and an intensity Ws randomly varying within a range of values, with $Ws \in [Ws_{\min}, Ws_{\max}]$.

Flight uncertainty: the ground speed Gs of the aircraft is the resultant from both the TAS component and the Wind Speed component ($\overrightarrow{Gs} = \overrightarrow{TAS} + \overrightarrow{Ws}$). Let's assume a flight arriving at the entry node n_{ori} of a link l at t_{ori}, its time interval of arrival at the exit node n_{dest} will be: $[t_{\text{dest}_{\min}}, t_{\text{dest}_{max}}]$,$= [t_{ori} + \frac{d_l}{V_{f_{\max}}}, t_{ori} + \frac{d_l}{V_{f_{\min}}}]$. This interval is built with the earliest time of arrival at the exit node $t_{\min}$ which depends on $V_{f_{max}}$ which is the maximum ground speed of the aircraft and the latest time of arrival at the exit node $t_{\text{dest}_{\max}}$ which depends on $V_{f_{min}}$ which is the minimum ground speed of the aircraft.

3.6 Conflicts Identification

We will consider two types of conflicts: node conflicts and link conflicts.

Node conflicts They are detected using the separation constraints. Depending on the type of separation constraint at the node (time or distance separation), the equations to detect node conflicts will differ. To detect a distance separation conflict, a circular protection area with a diameter of d_{sep} is defined around the node. Each flight arriving at the node will be monitored using four different times: an early time of entry in the

protection area $t^{\text{in}}_{\text{min}}$, a late time of entry in the protection area $t^{\text{in}}_{\text{max}}$, an early time of exit from the protection area $t^{\text{out}}_{\text{min}}$ and a late time of exit from the protection area $t^{\text{out}}_{\text{max}}$. Two consecutive flights are considered to be in conflict at the node when they are both present within the protection area at the same time. In other words, the trailing flight enters the protection area before the leading flight exits it. Let's consider two flights f and g with f leading. $\forall f, g \in \text{F},\ cflt(f, g) = 1$ if $t^{f,\text{out}}_{\text{max}} - t^{g,\text{in}}_{\text{min}} < 0$; (0 otherwise). To detect a time separation conflict, a separation time t_{sep} is defined on the node. Each flight arriving at the node will be monitored using two different times: an early time of arrival at the node t_{min} and a late time of arrival at the node t_{max}. Two consecutive flights are considered to be in conflict at the node when the time interval between the two of them crossing the node is less than the separation time. Let's consider two flights f and g with f leading. $\forall f, g \in \text{F},\ cflt(f, g) = 1$ if $|t^{f}_{\text{max}} - t^{g}_{\text{min}}| < t_{\text{sep}};\ (=$ 0 otherwise).

Link conflicts Link conflicts are essentially detected using wake turbulence category separation. Three situations are analyzed to detect those conflicts: at the entry node of the link, at the exit node of the link and catch-ups along the link itself. To detect entry conflicts, two different times are monitored at the entry of the link: an early time of arrival at the entry node $t^{\text{in}}_{\text{min}}$ and a late time of arrival at the entry node $t^{\text{in}}_{\text{max}}$. Two consecutive flights are considered to be in conflict at the entry of a link when the distance between them is less than the required wake turbulence separation distance. Let's consider two flights f and g with f leading. $\forall f, g \in \text{F},\ cflt(f, g) =$ 1; if $\text{dist}_{\text{ori}}(f, g) < wTCat_{\text{sep}}(f, g)$; (0 otherwise).

$$\text{dist}_{\text{ori}}(f, g) = V^{f}_{\text{min}} \times (t^{f,\text{in}}_{\text{max}} - t^{g,\text{in}}_{\text{min}})$$

With $wTCat_{\text{sep}}(f, g)$ the wake turbulence separation distance between f and g. To detect exit conflicts, two different times are monitored at the exit of the link: an early time of arrival at the exit node $t^{\text{out}}_{\text{min}}$ and a late time of arrival at the exit node $t^{\text{out}}_{\text{max}}$. Conflicts at the exit of the link are detected the same way as at the entry of the link. The distance between two consecutive flights is computed by using the exit times: $dist_{dest}(f, g) = V^{g}_{\text{max}} \times (t^{g,\text{out}}_{\text{min}} - t^{f,\text{out}}_{\text{max}})$. Conflict detection at entry and exit only checks if the aircraft are properly separated when entering or exiting the link. However, within the link, faster aircraft can catch-up slower ones and cross them, thus implicating a loss of separation during the crossing. To detect catch-up conflicts, a comparison is made between the entry and the exit sequence of flights. Let's assume $\text{S}^{l}_{\text{entry}}$ and $\text{S}^{l}_{\text{exit}}$ respectively the sequences of flights at the entry and at the exit of the link l, $pos : (\text{F}, \text{S}) \rightarrow \mathbb{N}$ the function that gives the position of a flight in a sequence. There is a catch-up conflict if: $\exists f \in \text{F}/\ pos(f, \text{S}^{l}_{entry}) \neq pos(f, \text{S}^{l}_{\text{exit}})$.

3.7 Objective Function

The mathematical modeling of the problem leads to a multi-objective optimization problem which aims at minimizing parameters linked to conflict occurrences, flight level modification, speed modification and also flights timing. The main objective is to reduce the global conflict count both on nodes and links. Let's consider c_{obj} the total conflict objective value.

$$c_{\text{obj}} = \sum_{n \in \text{N}} c_n + \sum_{l \in \text{L}} c_l$$

Two values related to flight level modifications are evaluated in the objective function:

$$fl_{\text{obj}} = fl_{\text{changes}} + fl_{\text{gap}}$$

where fl_{changes} represents the total number of aircraft which decision implies FL change and fl_{gap} is the summation of the difference between the final flight level and the preferred flight level of each flight. As for the flight level gap objective, we also want to minimize the gap between the initial speed and the final speed for each flight. For that, the speed objective s_{obj} is expressed as follows.

$$s_{\text{obj}} = \sum_{f \in \text{F}} |\Delta V_f|$$

Finally, we also want to make sure that the flights will arrive at their last node at the requested time with a reasonable (minimal) error margin. Thus, the time objective is expressed as follows.

$$t_{\text{obj}} = \sum_{f \in \text{F}} |t_{\text{max}}^{f,\text{last\_node}} - t^{f,\text{last\_node}_{\text{planned, max}}}|$$

The global objective function f is the sum of all the objectives listed above.

$$f = c_{\text{obj}} + fl_{\text{obj}} + s_{\text{obj}} + t_{\text{obj}}$$

The complexity of our model mainly depends on the dimension of the problem (number of flights involved) and the range of the decision variables. If we consider n_s options for the speed changes and n_{fl} options for the FL changes, then for N_f flight the size of the solution space is given by $(n_s \times n_{fl})^{N_f}$. In our model, $\Delta V \in [-6, +3]$ and $\Delta FL \in [-2, +2]$, the size of the solution space can be expressed by $(10 \times 5)^{N_f}$. To address such combinatorial complexity, we have developed a meta-heuristic based on a sliding-window simulated annealing.

4 Simulated Annealing

This method, as described by Soliman et al. [9], is based on the annealing process which is a physical process consisting of heating up a solid until it melts, then cooling it down in order to obtain a perfect crystallized form. During this process, the resulting structural properties depend on the residual energy in the material which is influenced by the rate of cooling. Thus, the cooling phase must be controlled in order not to get trapped in a locally optimal structure with high energy crystals, resulting in imperfections. In combinatorial optimization, the equivalent process is the simulated annealing which aims at finding a solution with minimal cost.

4.1 Principle

Let's consider the model presented by Henderson et al. [4]. Let Ω be the solution space (the set of all possible solutions). Let $f : \Omega \rightarrow \mathbb{R}$ be an objective function defined on the solution space. The goal is to find a global minimum, ω^* ($\omega^* \in \Omega$ such that $f(\omega) \geq f(\omega^*)$ for all $\omega \in \Omega$). The objective function must be bounded to ensure that ω^* exists. Define $N(\omega)$ to be the neighborhood function for $\omega \in \Omega$. Therefore, associated with every solution, $\omega \in \Omega$, are neighboring solutions, $N(\omega)$, that can be reached in a single iteration of a local search algorithm. Simulated annealing starts with an initial solution $\omega \in \Omega$. A neighboring solution $\omega^{'} \in N(\omega)$ is then generated. The candidate neighboring solution is accepted as the current solution based on the acceptance probability.

$$P\{\text{Accept}\,\omega^{'}\,\text{as next solution}\} =$$

$$\begin{cases} \exp[-(f(\omega^{'}) - f(\omega))/T_k)] & \text{if} f(\omega^{'}) > f(\omega) \\ 1 & \text{if} f(\omega^{'}) \leq -f(\omega). \end{cases}$$

where T_k is a parameter which control the probability of accepting a degraded solution. As illustrated in Fig. 3, each solution vector $\mathbf{X}$ which gather together the decision variables of aircraft is evaluated in a simulator process. This simulation is very powerful in the sense it can take into account many realistic aspects of the operational system. The result of the simulation generates the objective function which will be used by the optimizer (simulated annealing). The initial temperature is essential to define the behavior of the algorithm when it comes to the acceptance of solutions. We have set the initial temperature in order to get 80% of solutions to be initially accepted. We have used a geometric cooling law ($T_{k+1} = \alpha \cdot T_k$ with α in the range [0.8, 0.99]. Efficient stopping criterion can prevent the simulated annealing algorithm from performing unnecessary computations [4], thus reducing its global execution time. In our case, three criteria are used to stop the cooling procedure: when the final temperature T_{final} reaches a defined fraction of the initial temperature T_{init}, when the

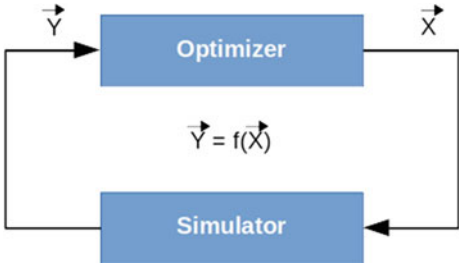

Fig. 3 Simulated annealing principle

evaluated criteria reach the value zero, or when the evaluated criteria remain constant over a defined number of iterations.

4.2 Neighborhood Function

Small changes on a local solution are performed using a neighborhood function. The efficiency of simulated annealing is highly influenced by the neighborhood function used. In our case, each solution is a set of flight decisions and determining a neighbor solution consists only on randomly modifying a flight decision in our set. The method used to choose the random flight is similar to the roulette wheel selection presented by Ji et al. [8]. On each flight decision, a performance criterion is evaluated, it corresponds to the sum of the total number of conflicts on the flight and the resulting delay. All the decision performances are added up together then a target value is randomly chosen between zero (0) and the total performance sum. Then, the cumulative sum of decision performances is calculated starting from the first decision until the cumulative sum reaches the previously chosen target value. The index at which it stops marks the flight decision on which a change will be done to generate a neighbor solution. Choosing the decision to change with this method guarantees that the selected flight is the one which is most likely to generate more conflicts and a large absolute delay. Given a flight decision, generating a neighbor solution consists in modifying the flight level delta ΔFL and the speed delta ΔV. Both modifications are done within their respective discrete range of values $[-2, +2]$ and $[-6, +3]$, with the same probability of occurrence $p = 0.5$.

4.3 Sliding Window

The sliding window approach as proposed by Ji et al. [8] is a technique based on the receding horizon control. It consists into dividing the entire time horizon into smaller equal intervals and thus evaluating the state of the network within the small time intervals. The evaluation interval starts from the earliest time and progressively

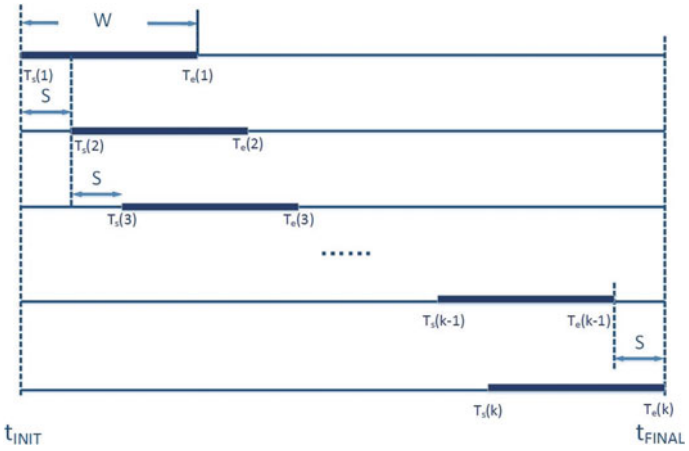

Fig. 4 Sliding window principle [8], W: the length of the sliding window, S: time shift of the sliding window

moves forward in time with a defined step until reaching the latest times. With this approach, it is not necessary to evaluate all the flights at once during the optimization since not all flights are involved in each sliding window interval. This method is more convenient in a dynamic environment with uncertainties and improves the computational time of the optimization process. Figure 4 illustrate how the sliding windows are generated all along the global optimization time interval.

5 Results

This section presents the results of our algorithm on real-life traffic data at Paris CDG. Paris CDG TMA is accessible through four entry points: OKIPA, MOPAR, LORNI and BANOX. Our experimentation airspace is focused on the En-route portion of traffic arriving at CDG airport which corresponds to four areas each having a TMA entry point as last node as we can see in Fig. 5.

All nodes (waypoints) except the four entry points are constrained with a 5NM separation minimum. As for the TMA entry points, the minimum separation between aircraft is 8NM. Concerning the wind data, we considered wind components with an angle of 30° relative to the geographical north. The wind intensity has been set within the range 25–35 kts all over the test airspace. A simple analysis of the network structure shows 742 different nodes with 817 links. This will contribute to increase the complexity and so the resolution time. In our scenario, we will consider a 24-h traffic data of 690 flights corresponding to the filed flight plans arriving at LFPG on July 28th, 2016. The arrivals are distributed among the four entry points of CDG Terminal Area (TMA) with the majority of flights arriving at LORNI and OKIPA

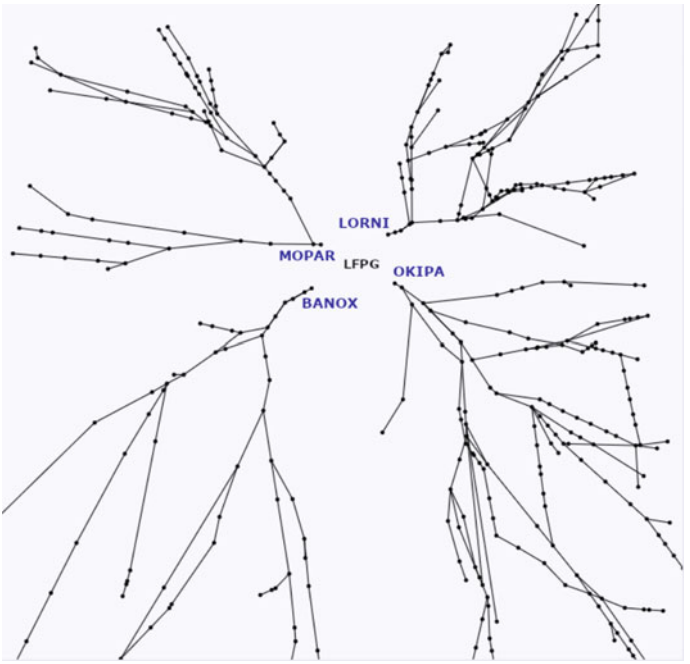

Fig. 5 Routes towards Paris CDG airport

Table 1 Flights distribution by TMA entry point

	BANOX	LORNI	MOPAR	OKIPA
Medium	85	163	75	167
Heavy	13	57	72	58
Total	98	220	147	225

nodes (Table 1). There is also a distribution of medium and heavy wake turbulence category aircraft with a majority of medium aircraft.

5.1 Statistics

Our algorithm written in Java 8 has been executed on an Ubuntu 18.04 operating system PC equipped with an Intel Core i5-3230M processor (4×2.60 GHz) and 8 GB of memory. The simulated annealing algorithm has been tested with the parameters in Table 2. Given the length of the sliding window (2 hours) and the distribution of flights, each resolution step on a sliding window will handle around 100 flights on average. A first analysis of the flight data detected 407 conflicts.

Table 2 Simulated annealing/sliding window test parameters

Parameter	Value
Temperature reduction coefficient (α)	0.95
Number of iterations at each temperature step	200
Cooling stopping temperature	$10^{-4}.T_{\text{init}}$
Maximum repetitions	35
Sliding window time shift (S)	30 min
Sliding window time length (W)	2 h
Probability of speed change	0.5
Probability of flight level change	0.5

Table 3 Optimization results on LFPG data

Criteria	Value
Initial conflict count	407
Solved conflicts	407
Solved conflicts ratio	100%
Climbed flights	61
Descended flights	66
Total FL changes	127
FL changes ratio	18.41%
Accelerated flights	4
Slowed down flights	4
Speed changes	8
Speed change ratio	1.16%
Total speed variation	35.029 kts
Average speed variation	4.38 kts
Total absolute delays	611 s
Average absolute delays	76 s
Execution time	11 min 23 s

The optimization algorithm analyzed the 690 flights and has solved the sequencing and the conflicts within a computation time of 11 min and 23 s. It solved all the 407 initially identified potential conflicts, which gives an efficiency rate of 100%. It changed flight levels on a total of 127 flights: 67 climbs and 66 descents. As for the speed, 4 flights have been accelerated and 4 slowed down which make a total of 8 speed changes. At the end, a total absolute delays value of approximately 611 s has been generated for the flights with speed changes which gives an average of approximately 1 min per modified flight (the 8 flights with speed modification). Very few flights have been affected by speed variations, also, the generated absolute

delays, an average of 76 s per modified flight is still acceptable. Table 3 summarizes all those changes.

6 Conclusion

This paper introduced the work done on the sequencing of the air traffic in En-route segments influenced by constraint points. We saw that En-route controllers are getting more involved in the pre-sequencing of arriving flows when they are still in the cruising phase which causes an increase of their workload. On the other hand, airlines wish to have efficient flights with few flight level changes around a certain preferred vertical profile and also less maneuverings due to conflict avoidance. To solve those issues, we have developed a decision support tool which can assist controllers in their tasks for sequencing traffic and solving conflicts in En-route airspace. After reviewing the concepts and previous works related to our subject, we based our study on a mathematical modeling of the problem followed by an optimization algorithm in order to extract traffic sequences. Using the simulated annealing algorithm for optimizing flights decisions appeared to be a good choice given its efficiency and adaptability properties. A first trial of our solution on real traffic data over Paris airspace displayed a resolution ratio of 100% for conflict solving and an acceptable level of speed and flight level changes. Also, the generated delays due to the compliance with sequencing constraints and conflict resolution appeared within an acceptable range. Moreover, a preliminary version of the algorithm was able to generate flights instructions that can be directly applicable by controllers. Apart from this first test scenario, the solution as it has been designed is able to simultaneously provide En-route sequencing for several airports arrival flows. Even if it has not been used in the Paris CDG case, the algorithm can also manage time constraints for some points in the airspace (points connecting countries with letter of agreement). On the other hand, it can also be helpful for airports not yet equipped with an arrival management system as long as the constraints at TMA entry points are well defined. As another advantage, our solution will facilitate novel arrival techniques and procedures such as Continuous Descent Operation (CDO) and Point Merge System (PMS).

References

1. Airbus, *Global Market Forecast: Growing Horizons 2017/2036* (2017)
2. R. Barragan, J.A. Pérez Castan, M. Sadornil, F.S. Nieto, J. Crespo, R. Arnaldo, C. Cuerno. Optimised algorithms for extended arrival managers, 9 (2014)
3. V. Courchelle, D. Delahaye, D. Gonzalez-Arribas, Simulated annealing for strategic traffic deconfliction by subliminal speed control under wind uncertainties (2017)
4. D. Henderson, S.H. Jacobson, A.W. Johnson, The theory and practice of simulated annealing, in *Handbook of Metaheuristics* (Springer, 2003), pp. 287–319

5. SESAR JU, Integrated sequence building/optimization of queues. Technical report (2015)
6. SESAR JU, Extended arrival management (aman) horizon (2018). Accessed on 03 July 2018
7. Q. Li, Y. Zhang, R. Su, A flow-based flight scheduler for en-route air traffic management **49**, 353–358 (2016)
8. M. Ji, Aircraft merging and sequencing problems in TMA. Master's thesis (2015)
9. S.A.-H. Soliman, A.-A.H. Mantawy, *Modern Optimization Techniques with Applications in Electric Power Systems*, vol. XVIII (Springer, 2012)
10. A. Vela, S. Solak, W. Singhose, J.-P. Clarke, A mixed integer program for flight-level assignment and speed control for conflict resolution, in *Decision and Control* (IEEE, 2009), pp. 5219–5226

Macroscopic Analysis to Identify Stage Boundaries in Multi-stage Arrival Management

E. Itoh, Y. Miyazawa, M. Finke, and J. Rataj

Abstract Accommodating the air traffic growth, reducing arrival delay is one of the most important functions of designing the ATM system. One of the newest concepts to further optimize arrival flows is multi-stage arrival management, proposed by DLR, in which different guidance principles to manage the arriving traffic are implemented in different stages. These stages are optimized to the core management task to be done in a certain area of the arrival stream and the conditions of the surrounding environment. This paper discusses this concept through a macroscopic analysis on the overall arrival traffic flows. Further, this paper analyzes parts of the multi-stage arrival management concept applied to Tokyo International Airport as a case study. A stochastic characteristic of arrival trajectories will be discussed as a counterpart of conventional deterministic trajectory-based operation based on data-driven analysis and arrival procedures at the airport. The best strategies of shifting arrival flow control to time-based management are analyzed based on the stochastic data analysis. Impacts of pop-up aircraft are discussed as one of the causes to increase uncertainties in aircraft trajectory management.

Keywords Arrival management · Multi-stage · Arrival delay · Air traffic management

E. Itoh (✉) · Y. Miyazawa
ATM Department, Electronic Navigation Research Institute (ENRI), National Institute of Maritime, Port and Aviation Technology (MPAT), Tokyo, Japan
e-mail: eri@mpat.go.jp

Y. Miyazawa
e-mail: miyazawa_y@mpat.go.jp

M. Finke · J. Rataj
Department of Controller Assistance, Institute of Flight Guidance, German Aerospace Center (DLR), Braunschweig, Germany
e-mail: michael.finke@dlr.de

J. Rataj
e-mail: juergen.rataj@dlr.de

Air Traffic Management and Systems IV, Lecture Notes in Electrical Engineering 731,
https://doi.org/10.1007/978-981-33-4669-7_4

1 Introduction

Highly frequented airports are the critical elements in air traffic. In the most cases, they are directly or implicitly the origin of delays in the air traffic system. Therefore, arrival management is an essential part in air traffic management. To clarify the meaning of arrival management, the following definition from EUROCONTROL [1] is used: "Arrival management is a general term given to the process of safely and effectively arranging arrivals into a smooth efficient flow for landing at a destination airport." To improve the arrival management process, controllers (ATCo) are supported by a family of decision support systems called arrival managers (AMANs). According to [1], an AMAN is defined as a software specifically designed to provide assistance in metering and sequencing arrival streams and that delivers information needed to implement an efficient arrival management. Following this definition, the first AMANs were built already more than 20 years ago. The tasks, where the controller is usually supported by an AMAN, are:

- Build an arrival sequence.
- Assign an arrival time at the runway threshold and other significant waypoints for each aircraft in the sequence.
- Predict a trajectory for each aircraft which implements the assigned landing time.
- Transform the trajectory into appropriate guidance instructions which are transmitted to the pilot.

2 Drawbacks of Modern Arrival Management Systems

One drawback of current AMAN designs is the effect of model uncertainties in the trajectory calculation and the probability of disturbances. As a consequence, the individual trajectory reliability decreases considerably with increasing distance of the aircraft to the airport. Hence, the drawback of the extension of the current planning horizon from 80 NM by a factor of 5 is the decreasing predictability and accuracy of the calculated trajectory. Furthermore, horizons of 500 nautical miles and more causes that some aircraft in the approach flow are still on the ground, as they are departing from airports that are less than 500 nautical miles away from the destination. Because the uncertainties as well as the probability of disturbances for a flight on ground are much higher as it is the case for airborne flights, the predictability and the quality of the trajectory are even worse. Hence, without additional effort concerning the concept of operation and the used methods as well as the existing planning mechanisms, the new approach results in decreased prediction quality of arrival time, and increased number of arrival sequence changes with negative effects on the aircraft, ATC, and airport operation. Moreover, corrective measures for an individual aircraft far away from the airport may become useless due to unexpected new disturbances that again reduce efficiency.

The trajectory-based operational concept recently described by SESAR provides a 4D trajectory for each aircraft, the so-called business trajectory [5]. This trajectory is designed so that the flight can be managed as closely as possible to the airspace user's ideal profile. Besides the three spatial dimensions, the trajectory also contains the dimension "time." 4D trajectories for the arrival phase can be planned by arrival management systems with long lead times which are conflict free, with an optimized landing sequence [1]. Nevertheless, in a pure trajectory-based ATM, this logically requires that all flights follow exactly these planned trajectories also in reality to guarantee that they stay free of conflicts and to avoid any corrective actions by ATC. The constraint to stay on a preplanned trajectory results in an increased number of control actions for the aircraft due to uncertainties and disturbances, like wind effects. Negative consequences of increased control actions are again an increased fuel consumption and, more important, an increased maintenance effort for the engines as well as a low acceptance by the pilots due to their increased workload. Additionally, some disturbances might have such an impact that increased control actions alone cannot maintain the optimized and conflict-free trajectory situation, like suddenly occurring emergency flights treated with absolute priority.

The described drawbacks require the development of new concepts of operation, methods, and planning algorithms for AMANs, taking the drawbacks into account, which stem from uncertainties and disturbances. Different solutions for airborne arrivals and arrivals that are still on ground at their departure aerodrome are needed as the different status has a significant influence on the uncertainties as well as the probability of disturbances impacting a flight. Hence, using todays planning and guidance functionalities for arrival management is disadvantageous.

The future arrival management will further be strongly influenced by the introduction of new wake turbulence categories. In the past, a 3 * 3 matrix was used to define the separation distances between the subsequent aircraft. These aircraft categories are heavy, medium, and light, and the number of different separations in the 3 * 3 matrix is 3 (4, 5, 6 NM) [5]. In this case, the controllers are able to remember this low amount of numbers of different separation minima for the aircraft pairs; hence, no further support was required to apply them to the aircraft on final approach. With the introduction of RECAT-EU, as an example, the number of aircraft categories increases to 6 and the number of different separation values to 8 in a 6 * 6 matrix [6]. The new wake turbulence categories increase the complexity for the controller considerably. To deal with that the controller needs additional support tools to create an efficient arrival sequence. Further considerations go in the direction to assign every individual aircraft pair an individual separation [7]. To guide such a separation scheme, it is indispensable to intensively support the controller with technical means.

3 Concept of Multi-stage Arrival Management

Following the description in the previous chapters, it becomes apparent that more and more tasks of the arrival management are collected under an AMAN, which makes

these systems more and more complex. By extending the planning horizon considerably, arrival management starts much earlier than in the past. The implementation of new separation values requires new support elements in the AMAN close to the runway.

It can be concluded that the driving requirements rules to be followed and constraints to be considered in future arrival management will at least depend on

- the distance of the airplane to the destination aerodrome,
- the characteristics and local constraints of main arrival flows,
- the diversity of involved aircraft type performance and equipment,
- the flight phase,
- predictability of traffic as well as accuracy and uncertainty of planning systems.

Although the list of dependencies can surely be further extended, state-of-the-art AMANs are still using the same algorithms for the whole traffic up to the planning horizon while not or not sufficiently considering the items contained in the list above. In addition, especially trajectory-based deterministic calculations seem to be unsuitable without a minimum level of predictability and only tolerate minor uncertainties. A better solution could be to adapt and optimize the working principles of AMAN systems according to these dependencies taking into account system architecture considerations.

This would result in a "clustering" of coherent tasks, methods or procedures, following the "separation of concerns" software architecture principle [8]. Supplementary to "separation of concerns" is the "single responsibility principle" in the software engineering domain. Taking these software architecture principles into account, it is necessary to divide future AMANs with their various "concerns" in different modules.

This approach can be realized with a multi-stage AMAN design defined by DLR, where several different sub-systems can use different working principles on different flight phases, arrival flows, or distances from the destination aerodrome. This design allows using the working principle which fits best to the single stages and offers also a lot of optimization potential for the whole AMAN architecture at the individual airports (see Fig. 1).

At its current stage of development, the multi-stage AMAN concept includes the following types of stages already:

- classical 4D trajectory-based, fully deterministic stages,
- time-based stages
- flow-based stages
- stages using stochastic methods.

Further types of AMAN stages may be available in future.

In addition, inspired by electric circuit or space launcher construction principles, two different types of stage arrangements can be identified:

- serial arrangement, where one stage directly feeds the traffic into another stage,

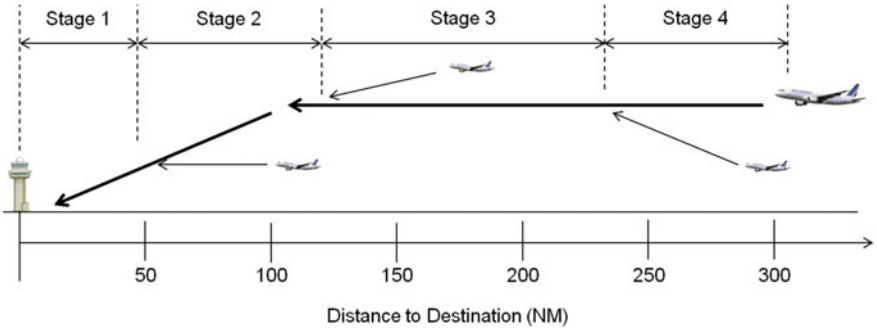

Fig. 1 Fictional example of a possible multi-stage AMAN design

- parallel arrangement, where separate airspaces, arrival flows, or otherwise, clustered arrivals are planned and handled by two stages in parallel.

Based on the description of the preceding chapters, a first stage/concern could be defined for the final approach area of an airport, where the main task is to create a tight sequence of aircraft on the center line by minimizing the used buffers on top of the minimum wake turbulence separation. At hub airports, this task is done by the so-called Director controller position which is very much specialized and focused just on this single task of creating the safe and effective sequence of aircraft on final track. Furthermore, the increasing task complexity by new wake turbulence categories and the focus on a time dependent separation between subsequent aircraft increases the distance of concerns to a trajectory-based approach.

A second stage/concern could be driven by trajectory-based operation with the goal to create an optimized aircraft sequence and feeding of the first stage defined above. Optimized aircraft sequence means that the order of the arriving aircraft corresponds to a previously defined optimization criterion. Furthermore, a high quality of the trajectory calculation is necessary to enable continuous descent approaches with engines in idle which are especially environment friendly. Here, it is important to start the calculation of the aircraft trajectory at least before the top of descent. In additional to sequencing, the trajectory-based approach enables a collision detection and avoidance in the TMA which is of utmost importance to ensure a safe and orderly traffic flow.

A third stage could be allocated to the arrival management of distant flights still in the en route phase of flight. Following the draw backs in chapter 2, another approach to guide the traffic should be taken into account here. This approach is based on statistical information which enables a continuous flow of aircraft to the airport without a high amount of corrective action. In contrast to this approach, precise trajectory-based operations would require a high amount of corrective actions of the aircraft as they have to follow their precisely planned but uncertain trajectories. More details concerning the statistical arrival management approach will be presented in a separate paper in the near future.

In order to build an AMAN system according to the multi-stage design, several decisions have to be made:

- type of the stage used for a defined part of the whole arrival management,
- serial or parallel arrangement of the individual stages,
- data exchange and transition conditions between the different stages,
- definite borders between the different stages/concerns.

A first scientific study has already been made by the Japanese research Electronic Navigation Research Institute (ENRI) on the definition of a possible border between flow-based and trajectory-based arrival management for Tokyo-Haneda International Airport, which is described in the following chapters.

4 Data-Driven Analysis

4.1 Case Study Data Description—Tokyo International Airport

Prior to discuss stage boundaries in the arrival management, this section introduces aircraft arrival operations at Tokyo International Airport, which this paper focuses on as a case study airport.

In total, maximum number of 447,000 departures and arrivals are accepted per year, with a maximum 80 operations in one hour. The airport makes use of four runways on daily basis, while the choice of the runway configuration depends on wind direction.

Over 60% of the domestic flights in Japan are concentrated at this airport. Figure 2 shows the distribution of departure airports with average number of departure aircraft arriving at Tokyo International Airport in Japan.

4.2 Stochastic Analysis on Air Traffic Arrival Flow

In order to characterize arrival traffic flow in each stage (see Fig. 1), a data-driven analysis is conducted using two years of radar tracks and flight plans in 2016 and 2017. Figure 3 shows definitions of aircraft flight time and inter-arrival time using concentric circles centered at Tokyo International Airport. In total, 29 datasets of aircraft flight time and inter-arrival time are defined when using a maximum radius of 300 NM with an increment of 10 NM. Aircraft inter-arrival time is defined as aircraft time-spacing between preceding and succeeding aircraft at each concentric circle. For example, the first dataset is difference of aircraft's crossing time after its proceeding aircraft crossed at the circle with 20 NM radius, the second dataset is the time difference at the circle with 30 NM radius, and so on.

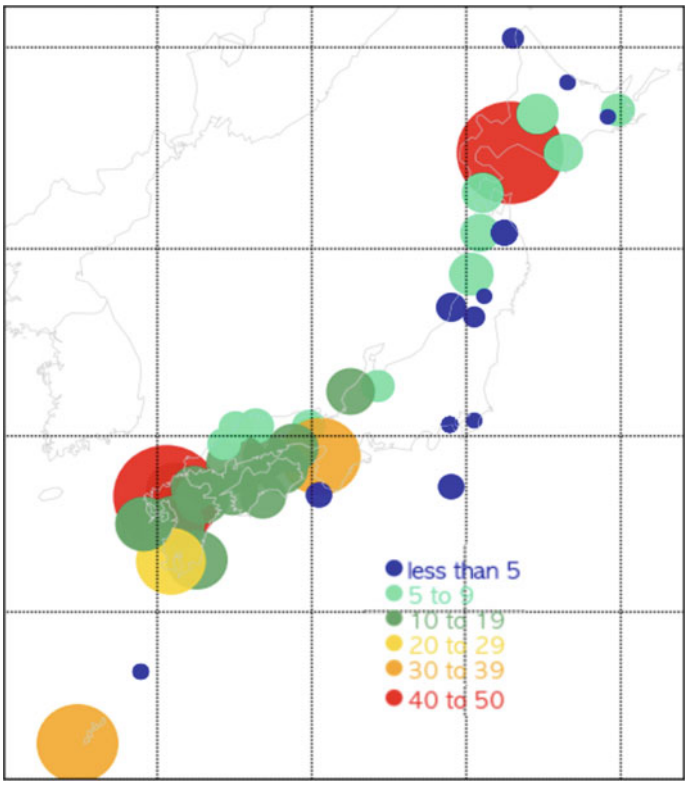

Fig. 2 Distributions of departure airports with average number of departures arriving at Tokyo International Airport in a day

Authors' past works indicated that the empirical distributions of the aircraft flight time could be numerically approximated using Gaussian distribution [9, 10]. The significant features of arrival traffic control appeared in the variances of the aircraft flight time distributions. Figure 4 compares flight time distributions corresponding to the arrival traffic flows from southwest direction. One of the most significant arrival strategies is illustrated in Fig. 4 for airspace between concentric circles 30 and 40 NM, 40 and 50 NM radii, where the variances grow dramatically in the arrival traffic flows from southwest direction. This explained by the fact that the arrival time-spacing was actively conducted by the air traffic controllers in the airspace between 30 and 50 NM away from the airport, just before the aircraft enter the terminal area. The increase in both the mean flight time and the flight time variance in the direction of the airport is due to the airspeed reduction that arriving aircraft undertakes prior to landing. For flight time, the mean and variance converge close to the circle of radius 200 NM. This circle captures current arrival strategies, since this is the airspace within which the traffic control capacity is met, and the spacing at merging points is filled. Between circles of radii 200 and 300 NM, air traffic controllers make an effort to maintain

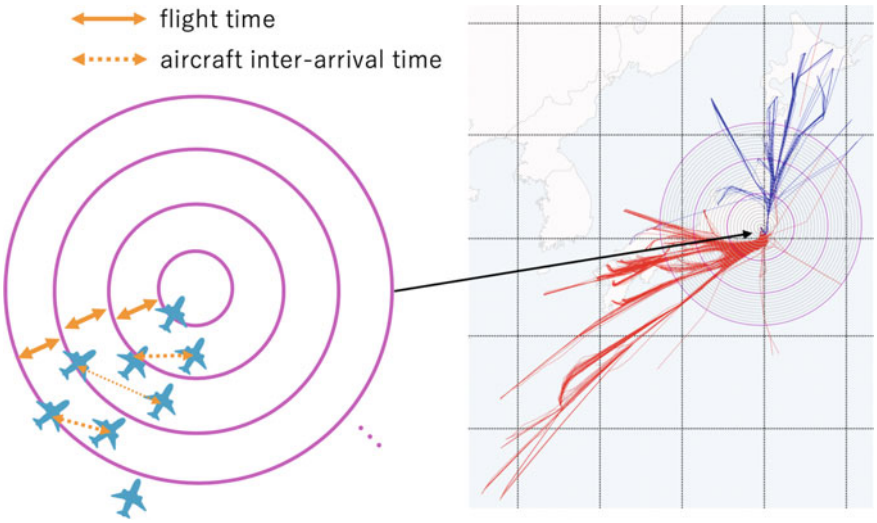

Fig. 3 Definitions of flight time and aircraft inter-arrival time in this paper. Map of Japan is drawn with flight tracks during an entire day in November 2016 [9]. The red tracks show the southwest traffic flow. The blue tracks show the north traffic flow.

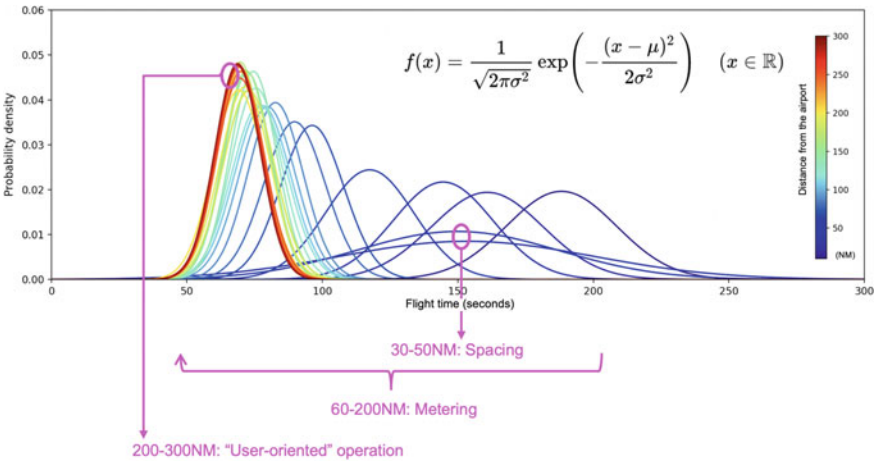

Fig. 4 Comparing flight time distributions every 10 NM radius, 10–300 NM

safe and efficient traffic flows by prioritizing airlines' own procedures. In summary, there are three main strategies illustrated in Fig. 4: (1) arrival time-spacing within the circle around 50 NM, especially between the 30 and 40 NM radii circles; (2) arrival metering for traffic capacity control and spacing at merging points between the 50 and 200 NM circles; and (3) maintaining efficient traffic flow by prioritizing

airlines' own procedures beyond the 200 NM circle. Minimizing arrival delays and operational costs requires great consideration in combining these different strategies.

Figure 5 compares exponential fittings and empirical probability densities of the aircraft inter-arrival time from the southwest direction at concentric circles with 50, 100, 150, and 300 NM radii [10]. The empirical distribution of the inter-arrival time is well approximated by an exponential distribution, where the arriving aircraft flies further than the circle around 150 NM radius. However, the inter-arrival times converge to a nearly Gaussian distribution toward the arrival airports.

The empirical coefficient is defined as $C_e = \sqrt{\sigma_A}/\mathbb{E}[A]$, where $\mathbb{E}[A]$ and σ_A are the mean inter-arrival time and variance of the inter-arrival time. When $C_e \to 1$, the empirical distribution of the inter-arrival time is well approximated by an exponential distribution. If C_e is much larger or smaller than 1, then the empirical distribution is deviating from the exponential distribution. According to the empirical data, $C_e = 0.4688, 0.6467, 0.8089, 0.8125$ corresponding to 50, 100, 150, and 300 NM radii of concentric circles.

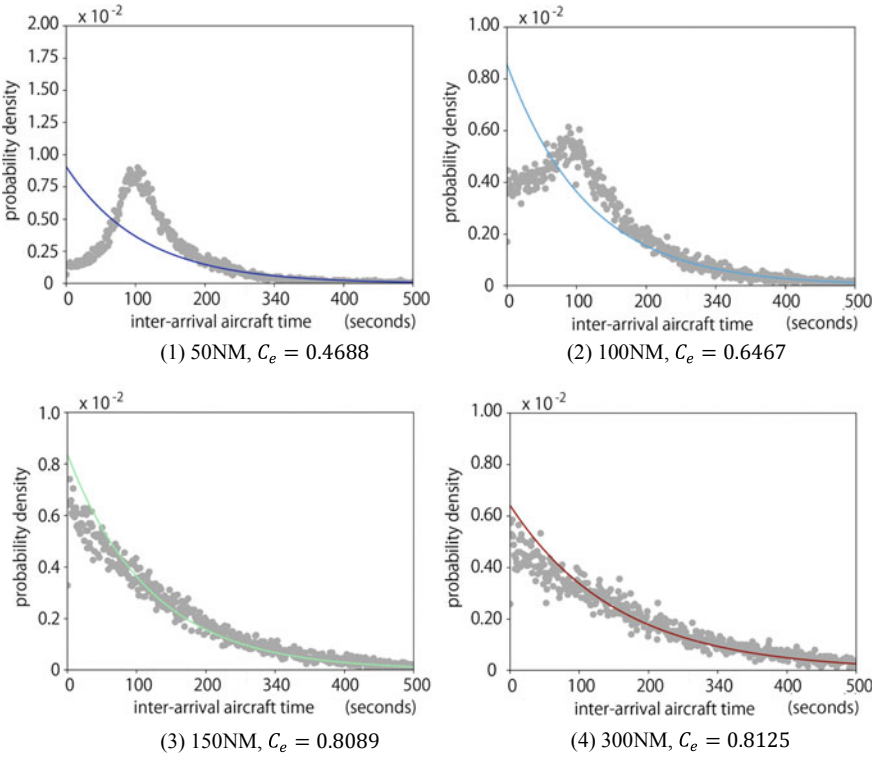

Fig. 5 Empirical distribution of the aircraft inter-arrival time and exponential fittings [10, 11]

5 Exploring Control Strategies in Future Arrival Management

5.1 Shifting Air Traffic Control Flow to Time-Based Traffic Management

One of the important arrival strategies to determine is where and how the aircraft arrival flow shifts to time management toward the arrival airport while minimizing arrival delay time. The first author's study clarified the best arrival strategy based on the analysis applying data-driven queuing models [10–12]. The proposed queue-based approach demonstrated that there are five parameters, which impact on arrival delay time as follows: (1) arrival traffic rate (2) airspace capacity (3) mean of aircraft flight time (4) variance of aircraft flight time (5) variance of aircraft inter-arrival time. All five parameters were estimated through data-driven analysis using the two years radar tracks and flight plans. Mean and variance of aircraft flight time, and variance of aircraft inter-arrival time were analyzed in Sect. 4.2 as shown in Figs. 4 and 5.

Figure 6 summarizes current arrival traffic rate in an hour at each concentric circle with 10–300 NM radii every 10 NM, focusing on arrival traffic from the north and southwest direction during the most congested time period 17:00 to 22:00 based on the data statistics. Arrival rate is well controlled at each airspace during the most congested time period; approximately, 10 aircraft from the north (see Fig. 6a) and 30 aircraft (see Fig. 6b) from the southwest arrives within 150 NM radius concentric circle in an hour [12].

Table 1 counted the number of aircraft from the southwest direction, which flew in the defined airspace, every 10 min during 17:00 to 22:00 time period in the two years. The values are relevant from operational point of views; 7 NM separation was given to arrival aircraft at 30–40 NM away from the airport before entering terminal area; thus, the number of aircraft between 30 and 40 NM radii concentric circles was 1 (see median value at 30–40 NM in Table 1.)

Approximately, 5 NM separation was given to initial approach fix, so the median took two aircraft in 10–20 NM and 20–30 NM airspace (see Table 1). In the queuing model, these values directory define the capacity at the assigned airspace. Based on the proposed queue-based approaches [10–12], the best arrival strategy to minimize arrival time delay is increasing airspace capacity within around 50 NM radius range. Extending aircraft flight time (with delay time) is more effective, where the variances of inter-arrival time are smaller, thus absorbing aircraft arrival delay closer to the airport is relevant operation for mitigating arrival delay time in the current arrival operation. According to the results of stochastic analysis using real data, the boundary to a fully deterministic time-based stage lay at around 30 NM away from the Tokyo International Airport. Transition area between the flow-based and time-based stage lay in-between 30 and 150 NM from the airport. Airspace further than 150 NM away from the airport could be assumed as the flow-based stage. However, the proposed queue-based approaches [10–13] showed that the best arrival strategy was shift these

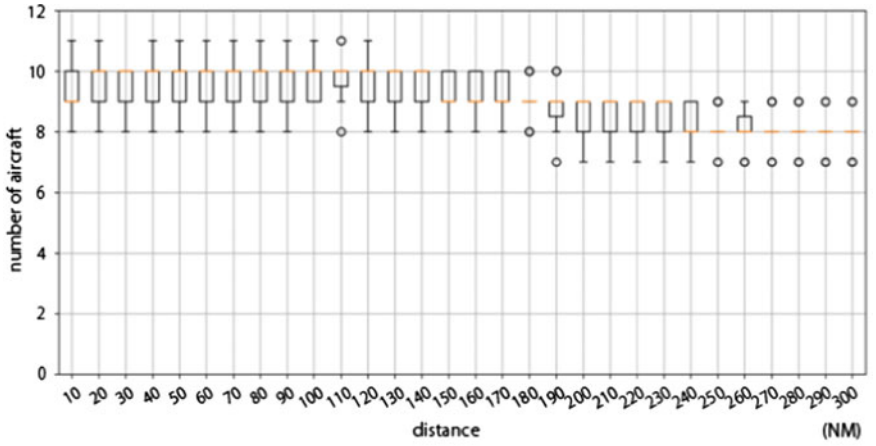

(1) Arrival traffic from the north direction, 17:00-22:00

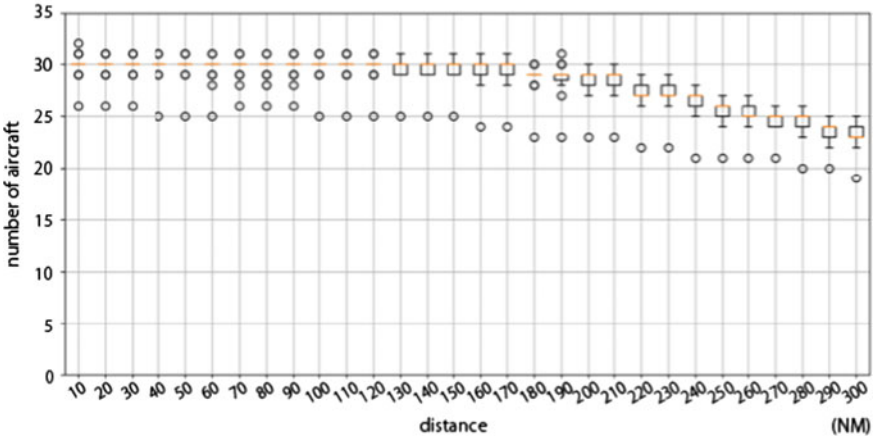

(2) Arrival traffic from the south-west direction, 17:00-22:00

Fig. 6 Arrival rate in an hour [12]. **a** Arrival traffic from the north direction, 17:00–22:00. **b** Arrival traffic from the southwest direction, 17:00–22:00

boundaries and transition area backwards: the boundary to a fully deterministic time-based stage at around 70 NM and the transition from the flow-based stage at further than 150 NM way from the airport.

Table 1 Arrival aircraft numbers served in the assigned airspace

Airspace (NM)	10–20	20–30	30–40	40–50	50–60	60–70	70–80	80–90	90–100	100–110
median	2	2	1	2	1	1	1	1	1	1
mean	1.79	1.85	1.38	1.66	1.52	1.10	0.908	0.875	0.812	0.819
STD	0.809	0.971	0.649	0.882	0.914	0.808	0.753	0.746	0.758	0.793
Airspace (NM)	110–120	120–130	130–140	140–150	150–160	160–170	170–180	180–190	190–200	200–210
median	1	1	1	1	1	0	1	0	0	0
mean	0.773	0.792	0.723	0.693	0.676	0.647	0.683	0.585	0.593	0.581
STD	0.801	0.861	0.790	0.802	0.794	0.779	0.806	0.745	0.734	0.771
Airspace (NM)	210–220	220–230	230–240	240–250	250–260	260–270	270–280	280–290	290–300	
median	1	0	0	0	0	0	0	0	0	
mean	0.807	0.555	0.654	0.627	0.542	0.603	0.518	0.626	0.536	
STD	0.837	0.715	0.804	0.783	0.744	0.755	0.699	0.739	0.709	

5.2 *Uncertainties in Time Management Due to Pop-Up Aircraft*

Although smaller variances of aircraft flight time and inter-arrival time mitigate arrival delay time under limited airspace capacities, uncertainties in aircraft time management increases in further airspace from arrival airport. One of the causes anticipated is the impact of pop-up aircraft departing within the considered horizon from the arrival airport, which merges into air traffic flow. As shown in Fig. 7, Osaka International Airport (RJOO) and Kansai International Airport (RJBB) locate between Fukuoka International Airport (RJFF) and Tokyo International Airport. Figure 3 also indicates that arrivals from these airports take a large amount in total amount of arrivals at Tokyo International Airport.

In order to analyze the impact of pop-up aircraft departing from RJOO and RJBB, Fig. 8 compares growth of standard deviation (STD) in flight time since the aircraft departing from RJFF, RJOO, RJBB, Naha International Airport (ROAH), and Asian countries crossed the 200NM radius circle centered at Tokyo International Airport. Figure 9 compares the horizontal and vertical track records in a day. Although variances of flight time impacted by the total amount of flight, Fig. 8 shows that the STD corresponding to arrivals from RJFF grows between 130 and 160 NM, where departing flights from RJOO and RJBB merge into traffic departing from RJFF. As

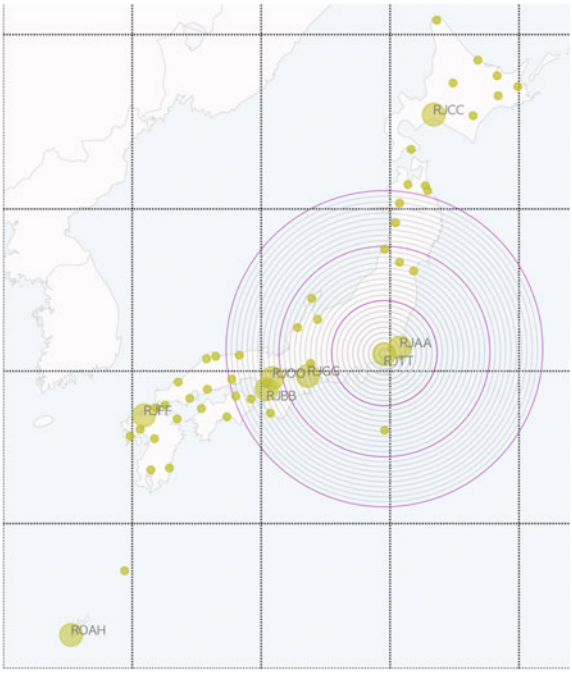

Fig. 7 Distributions of airports in Japan

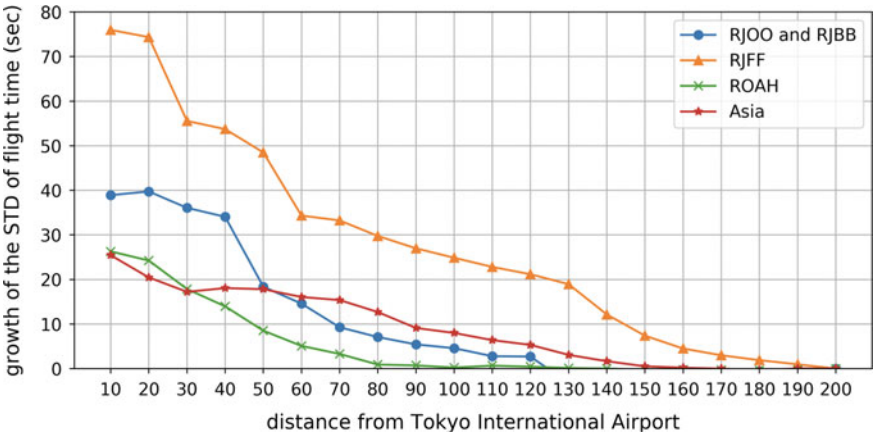

Fig. 8. Comparing growth of the flight time STD from these at 200NM

shown in Fig. 9, flight tracks of RJFF, RJOO, and RJBB merge not only horizontally, but also vertically below 30,000 ft airspace.

6 Discussion

This section discusses efficient arrival management strategies which can be applied in the stages of a multi-stage AMAN architecture (see Fig. 1) proposed in Sect. 3 based on the data-driven analysis in Sects. 4 and 5, and the first authors' work in [10–12].

Firstly, the best arrival strategy in the stage 1 is increasing airspace capacity, especially 30–50 NM distance from Tokyo International Airport for minimizing arrival delay time. This control would be done by achieving time management of aircraft inter-arrival time at around 70 NM from the arrival airport in the stage 2, suggested in [10]. Freeze horizon, where the AMAN calculates the optimal arrival schedules, is required to lie in the stage 3 prior to achieve arrival scheduling. Aircraft trajectories would be controlled between the freeze horizon and horizon, where time management is required to achieve.

Secondly, total aircraft arrival delay time is reduced if the flight time is extended in the airspace area, where the variance of aircraft inter-arrival time is smaller. As shown in Fig. 5, the variance of the inter-aircraft time grows in the farther airspace area from the arrival airport, and the distribution is near exponential at the airspaces farther than 150 NM. One of our future challenges is to propose the best way to draw horizons, which tailor arrival aircraft traffic prior to the conventional freeze horizon, in stage 3 and/or stage 4.

Thirdly, again it is repeated but controlling aircraft flight time, which increases the variance of aircraft flight time in arrival traffic flow, is allowed, where the variances

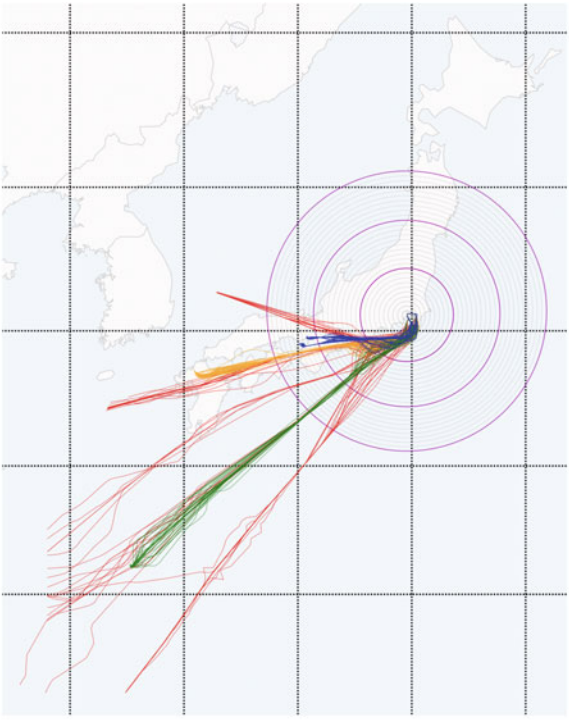

(1) Horizontal records

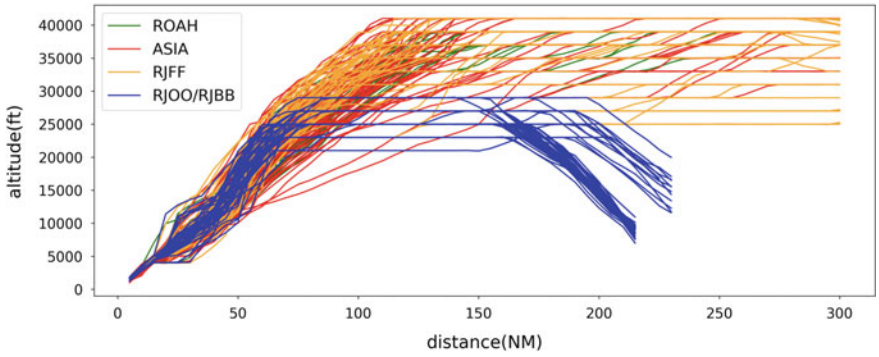

(2) Vertical records

Fig. 9. Flight tracks of arrival aircraft from RJFF, RJOO, RJBB, ROAH, and Asian countries in a day. **a** Horizontal records, **b** vertical records

of the inter-aircraft time is smaller. Otherwise, arrival delay time of the total arrival traffic increases. This also means that trajectory optimization targeting individual aircraft is not the solution to achieve minimum aircraft arrival delay because of the interference with surrounding traffic. Trajectory-based operation needs to be designed in order to reduce the variance of inter-arrival times in the arrival traffic.

Fourthly, pop-up aircraft also impacts on increasing the variances of aircraft flight time. Further, study will analyze the impacts on the arrival traffic delay and solutions to mitigate the impacts.

Lastly, applying new wake turbulence minima, so-called RECAT (Wake Turbulence Re-categorization), and point merge operation influences in the stage 1. Point merge operation is introduced in arrival traffic at Tokyo International Airport since July 2019. Figure 10 shows an example of point merge routes applying to arrivals from southwest direction, with flight tracks of arrivals in a day in 2017 and concentric circles drawn every 10 NM radius. There were two transition points named ADDUM and STONE previously; however, six transition points are newly prepared according to the expansion of terminal area. As shown in Fig. 10, the arcs of point merge routes locate within 50 NM radii concentric circle. Authors' future work will also analyze the impacts of the RECAT and point merge operations on the arrival aircraft traffic.

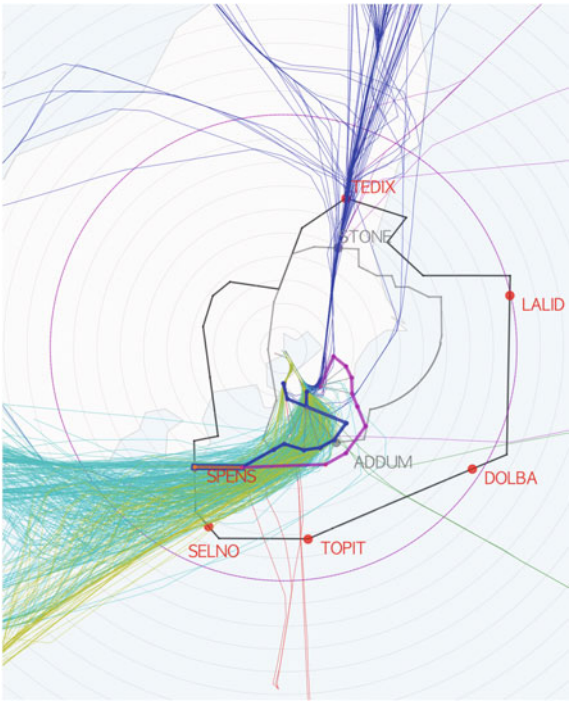

Fig. 10 One of the representative point merge operation at Tokyo International Airport

7 Conclusions

This paper introduced a multi-stage arrival management concept and discussed stage boundaries based on a data-driven analysis. Two years of data consisting of radar tracks and flight plans of air traffic arriving at Tokyo International Airport were analyzed as a case study. The analytical results characterized arrival traffic flow at each stage in the proposed concept. The best arrival strategy was discussed to shift air traffic flow control to time management. Authors' future works further discuss the efficient design of arrival management in each stage.

Design requirements of arrival management system depend on the characteristics of a given arrival air traffic flow and its surrounding environment, e.g., runway and airspace capacity, weather conditions, air routes, and other geographical constraints. This study further designs the multi-stage arrival management not only at Tokyo International Airport, but also different airports, e.g., German airports and conduct interoperability analysis in future.

Acknowledgments This research was conducted under CARATS initiatives supported by the Civil Aviation Bureau, Ministry of Land, Infrastructure, Transport and Tourism (MLIT) as the "Studies on the Extended Arrival Management." This research was also supported by the Ministry of Education, Culture, Sports, Science and Technology (MEXT) as the "Post-K Computer Exploratory Challenge" (Project ID: hp180188).

References

1. EUROCONTROL, Arrival ManagerxImplementation Guidelines and Lessons learned, Edition 0.1, December 2010, p. 14
2. SESAR Joint Undertaking, xStream Demonstration Plan, Edition 00.02.00, May 2018 (not published)
3. SESAR Joint Undertaking, iStream Demonstration Report, Edition 00.02.00, November 2016
4. Modern Airliners, https://www.modernairliners.com/airbus-a330/airbus-a330-specs/. Accessed on July 2019
5. SESAR Factsheet Business Trajectory, https://www.sesarju.eu/sites/default/files/documents/reports/SESAR_Factsheet_4DTrajectory__2_.pdf?issuusl=ignore
6. International Civil Aviation Organization (ICAO), Procedures for Air Navigation Services—Air Traffic Management, Doc 4444, 15th edn. (2007), pp. 4–11
7. EUROCONTROL, RECAT-EU—European Wake Turbulence Categorisation and Separation Minima on Approach and Departure, Edition 1.1, July 2015
8. https://ext.eurocontrol.int/lexicon/index.php/Pair-wise_separation. Accessed on July 2019
9. Effektive Softwarearchitekturen: Ein praktischer Leitfaden, Carl Hanser Verlag GmbH & Co. KG, ISBN-13: 978-3446452077
10. E. Itoh, Y. Miyazawa, A study on the stochastic modeling of traffic flows arriving to Tokyo International Airport, in *Proceedings of The 56thAircraft Symposium (written in Japanese)* (2018)
11. E. Itoh, M. Mitici, Queue-based modeling of the aircraft arrival process at a single airport", submitted to topical collection "air transportation-operations and management." Aerospace **6**(10), 103 (2019)

12. E. Itoh, M. Mitici, Analyzing tactical control strategies for aircraft arrivals at an airport using queue-based modeling. Submitted to J. Air Transp. Manage. (Under Review) (2019)
13. E. Itoh, M. Mitici, Evaluating the impact of new aircraft separation minima on available airspace capacity and arrival time delay. Aeronaut. J. **124**(1274), 447–471 (2019)

Analysis of Weather Impact on Flight Efficiency for Stockholm Arlanda Airport Arrivals

A. Lemetti, T. Polishchuk, R. Sáez, and X. Prats

Abstract Analysis of punctuality of airport arrivals, as well as identification of causes of the delays within transition airspace, is an important step in evaluating performance of the Terminal Maneuvering Area (TMA) Air Navigation Services. In this work we analyse how different weather events influence arrival punctuality and vertical flight efficiency on example of Stockholm Arlanda airport. We quantify the impact of the deviations from the flight plans influenced by different weather events, by demonstrating that they result in significant arrival delays, vertical inefficiencies and calculating how much extra fuel is wasted due to vertical flight inefficiency within Stockholm TMA.

Keywords Vertical flight efficiency · Punctuality · Weather impact

1 Introduction

Aviation, probably more than any other mode of transportation, is greatly affected by weather. Wind direction and speed can make a flight time quite different, for exactly the same journey. Flight routes can be altered to avoid convective weather, such as thunderstorms. Severe weather causes delays and cancellations. Airport capacity can be reduced considerably by low visibility, strong winds, thunderstorms in the terminal area and runway closures.

This research is a part of the IFWHEN project supported by the Swedish Transport Agency (Transportstyrelsen) and in-kind participation of LFV. It is also supported by the SESAR Joint Undertaking under the European Union's Horizon 2020 research and innovation programme under grant agreement No 783287.

A. Lemetti (✉) · T. Polishchuk
Communications and Transport Systems, ITN, Linköping University, Norrköping, Sweden
e-mail: anastasia.lemetti@liu.se

R. Sáez · X. Prats
Department of Physics, Technical University of Catalonia (UPC),
Castelldefels, Barcelona, Spain

Air Traffic Management and Systems IV, Lecture Notes in Electrical Engineering 731,
https://doi.org/10.1007/978-981-33-4669-7_5

There are several measures of convective weather. The most common is Convective Available Potential Energy (CAPE), which is an indicator of atmospheric instability that can predict severe weather. When the visibility at the airport drops below Runway Visual Range (RVR), the airport enforces Low Visibility Procedures (LVPs). LVPs mean procedures applied at an aerodrome for the purpose of ensuring safe operations such as spacing planes apart to reduce the risk of collisions, so it slows things down and decreases the airport capacity which in turn leads to delays and cancellations.

Reducing fuel waste has a significant environmental benefit as it reduces fuel emissions. One of the reasons for fuel waste is inefficient vertical profiles. During the descent phase Vertical Flight Efficiency (VFE) means aircraft leaves its cruising level at the optimum top of descent and avoids level-off segments after that.

In this paper, we study correlation between the punctuality of arrivals for the major Swedish airport Arlanda in 2018, and the following weather phenomena: wind, visibility and CAPE within the terminal manoeuvring area (TMA). We calculate delay statistics and additional fuel burn due to deviations from the flight plans. Furthermore, we compute VFE within Arlanda TMA, together with the associated fuel waste.

The rest of the paper is organized as follows. In Sect. 2 we review related work on the topic and provide background information on the methods we use for analysis of the performance of Stockholm Arlanda airport arrivals.

We present the results of data analysis in Sect. 3 and summarize our findings in Sect. 4.

2 Background

This section reviews previous work and provides background information related to analysis of the weather impact on the flight efficiency of airport arrivals.

2.1 Related Work

Classification and analysis of causes of airport delays was a topic of interest for many years. In early works [1, 2] weather uncertainties are mentioned as the main contributor to the deviations in airport schedules. According to [3] airport ATFM delays (19,704 min/daily) increased in May 2019 by 6.5% compared to May 2018 which had high delays due to weather and ATC industrial action.

Impact of deep convection and thunderstorms is also subject to ongoing research, e.g. Steiner et al. [4, 5] and Song et al. [6] investigated its implication both on the en-route flow management and for terminal area applications. Klein et al. [7] used a high-level airport model to quantify the impact of weather forecast uncertainty on delay costs.

Recent works [8, 9] confirmed the relevance and emphasized the importance of quantification and analysis of the weather impact on airport operation.

EUROCONTROL developed the methodology used by its Performance Review Unit (PRU) for the analysis of VFE during climb and descent [10]. Performance Review Commission of EUROCONTROL made an assessment of air traffic management in Europe for the year 2018, where among other indicators reviewed air traffic punctuality and vertical flight inefficiency at the top 30 European airports, including Stockholm airport Arlanda [11]. In addition, EUROCONTOL PRU continues working on the development and maintenance of the open access cloud based data repositories to enable stakeholders to reproduce the performance review results [12]. EUROCONTROL Experimental Center also develops new performance indicators targeting to capture different aspects of flight inefficiencies in TMA [13, 14], some of which we use in this work.

In [15] fuel consumption is evaluated for terminal areas with a Terminal Inefficiency metric based on the variation in terminal area fuel consumed across flights, reported by a major U.S. airline. Using this metric they quantify the additional fuel burn caused by Air Traffic Management (ATM) delay and terminal inefficiencies.

Estimation of the flight inefficiencies in terms of extra fuel burn calculated based on the algorithm proposed in [16] was considered in the scope of APACHE project (a SESAR 2020 exploratory research project) [17, 18], but mostly for en-route flight phase. Later Prats et al. [19] proposed a family of performance indicators to measure fuel inefficiencies. In this work, we apply similar techniques to fuel estimation during the descent phase within TMA.

Furthermore, in [20] and [21], an analysis of fuel savings of the Continuous Descent Operations (CDO) with respect to conventional procedures is analyzed. A reduction in fuel consumption of around 25–40% by flying CDO was reported.

2.2 Weather Phenomena and Metrics

We consider three weather metrics: wind gust, visibility and CAPE.

2.2.1 Wind Gust, Visibility

We use surface level measurements of wind gust and visibility, expressed in meters per second and meters respectively. Depending on cloud ceiling and runway visual range the spacing of aircraft on final approach must be increased. Low visibility reduces the runway capacity for landing aircraft. If this happens during a traffic peak hour, it causes major disruptions.

2.2.2 Convective Available Potential Energy (CAPE)

CAPE is the energy a parcel of air has for upward motion, measured in joules per kilogram of air (J/kg). The higher the CAPE, the faster and higher the air parcel can rise. Most thunderstorms form in moderately unstable conditions (CAPE up to 1000 J/kg) but any value greater than 0 J/kg indicates instability and an increasing possibility of thunderstorms and severe straight line winds.

2.3 KPIs

Here we list all the performance indicators we used in this work to evaluate TMA performance and explain how they are calculated.

2.3.1 Average Arrival Delay

First, we compute the average over the arrival delays for all flights delayed during the day of consideration. The delay is calculated as a difference between the scheduled arrival time and the actual time of arrival of the given flight.

2.3.2 ICAO KPIs

We use two KPIs proposed by the International Civil Aviation Organization (ICAO) [22]: Arrival punctuality and Level-off during descent.

According to ICAO, arrival punctuality (*KPI* 14.2*b*) is calculated as the percent of the flights arriving at the gate on-time (delayed less than 15 min according to the schedule). We use the inverse version of this KPI, i.e. percent for flights delayed more than 15 min.

Vertical inefficiencies during the descent phase result from the inability of flights to keep up CDO. This type of operations enables the execution of a flight profile optimized to the operating capability of the aircraft, giving as a result optimal continuous engine-idle descents (without using speed-breaks) that reduce fuel consumption, gaseous emissions and noise nuisance. If the aircraft levels at intermediate altitudes before landing, this descent is considered as vertical inefficient.

For evaluation of VFE we consider *KPI* 19.2, the average time flown in level flight inside TMA using the techniques proposed by EUROCONTROL in [10] with small changes. We identify the point of the trajectory in which the aircraft enters the TMA and use it as a starting point for the calculations (instead of the Top of Descent (ToD), which may lie outside of TMA). A level segment is detected when the aircraft is flying with the vertical speed below the certain threshold. We use the value of 300 ft per minute for this threshold, the minimum time duration of the level

flight is considered 30 s, and these 30 s are subtracted from each level duration as suggested in [10].

2.3.3 Additional Time in TMA

The additional time is calculated as the difference between the actual transit time and the time according to the flight plan. As stated in [14], it represents the extra time generated by the arrival management and "is a proxy for the level of inefficiency (holding, sequencing) of the inbound traffic flow during times when the airport is congested."

2.3.4 Fuel-Based PIs

Fuel-based PIs capture inefficiencies on tactical ATM layer in vertical domain as explained in [19]. The objective is to compare the fuel consumption of CDO trajectories with the actual flown trajectories. Fuel-based performance indicators are calculated using the 4.2 version of the Base of a Aircraft Data (BADA) [23].

The first expression used, known as the Total-Energy Model, equates the rate of work done by forces acting on the aircraft to the rate of increase in potential and kinetic energy, that is:

$$(T - D)V_{TAS} = mg\frac{\mathrm{d}h}{\mathrm{d}t} + mV_{TAS}\frac{\mathrm{d}V_{TAS}}{\mathrm{d}t} \tag{1}$$

Here T is the thrust acting parallel to the aircraft velocity vector, D is the aerodynamic drag, m is the aircraft mass, h is the geodetic altitude, g is the gravitational acceleration and V_{TAS} is the true airspeed.

The drag force is computed as follows:

$$D = \frac{1}{2} \cdot \delta \cdot p_0 \cdot \kappa \cdot S \cdot M^2 \cdot C_D \tag{2}$$

Here δ is the pressure ratio, p_0 is the standard atmospheric pressure at mean sea level (MSL), κ is the adiabatic index of air, S is the wing reference area, M is the Mach number and C_D is the drag coefficient. BADA proposes equations for computing C_D depending on the aircraft configuration, and modelled as a polynomial of lift coefficient C_L.

Three separate thrust models are proposed in BADA, depending on the engine type: turbofan, turboprop or piston. Each model includes the contribution from all engines and provides the thrust as a function of airspeed, throttle setting and atmospheric conditions. The general formula of the thrust force, T, is:

$$T = \delta \cdot W_{\mathrm{mref}} \cdot C_T \tag{3}$$

Here δ is the pressure ratio, m_{ref} is the reference mass (obtained from the Propulsive Forces Model (PFM)), W_{mref} is the weight force at m_{ref} and C_T is the thrust coefficient, which is a function of Mach number.

For the three engine types, BADA proposes different equations to compute the thrust coefficient C_T depending on the engine rating: maximum climb, maximum cruise, idle and no rating (direct throttle parameter input).

For estimation of the fuel consumption, BADA proposes once again a different model depending on the engine type, and also depending on the engine rating. Each model includes the contribution from all engines and provides the fuel consumption as a function of airspeed, throttle parameter and atmospheric conditions. The general formula for the fuel consumption, F, is:

$$F = \delta \cdot \theta^{\frac{1}{2}} \cdot W_{\text{mref}} \cdot a_0 \cdot L_{HV}^{-1} \cdot C_F \tag{4}$$

Here δ is the pressure ratio, θ is the temperature ratio, a_0 is the speed of sound at MSL in standard atmosphere, L_{HV} is the fuel lower heating value (obtained from the PFM) and C_F is the fuel coefficient, which depends on thrust for non-idle ratings. For each aircraft model, BADA provides an xml file with the corresponding aircraft performance data. For instance, the coefficients used to compute the thrust coefficient C_T of the thrust equation (3) are in this file. With the equations stated above, and the xml files for each aircraft, it is possible to compute the fuel consumption of a trajectory. The process followed is detailed below:

- **Thrust computation**: if the aircraft is climbing, max climb rating is chosen and the corresponding thrust formula (depending on the engine type) is applied. If the aircraft is descending, an idle rating is assumed. In level-offs, the total-energy model (Eq. (1)) is used in order to compute the corresponding aircraft thrust (drag is computed previously with Eq. (2)).
- **Fuel consumption computation**: for non-idle ratings, the thrust computed in the previous step is used to obtain the fuel coefficient C_F used in Eq. (4). For descents, idle rating is assumed.

Wind was considered when computing the fuel consumption, and it was obtained from historical weather data (detailed in Sect. 3.1). Furthermore, a 90% of the maximum landing mass has been assumed at the destination airport for all aircraft.

In order to generate the CDO trajectories an optimal control problem has to be solved as explained in details in [24]. First, a state vector with the initial conditions is needed. In this paper, it has been chosen as $x = [v, h, s]$, where v is the true airspeed, h—the altitude of the aircraft, and s—the distance to go. In order to obtain environmentally friendly trajectories, idle thrust is assumed and speed-brakes use is not allowed throughout the descent. In such conditions, the flight path angle is the only control variable in this problem, which is used to manage the energy of the aircraft and achieve different times of arrival at the metering fix with minimum fuel consumption and noise nuisance. Therefore, the control vector of the optimal control problem will be $u = [\gamma]$.

The dynamics of x are expressed by the following set of ordinary differential equations, considering a point-mass representation of the aircraft reduced to a "gamma-command" model, where vertical equilibrium is assumed (lift balances weight). In addition, the cross and vertical components of the wind are neglected, and the aerodynamic flight path angle is assumed to be small (i.e., $\sin\gamma \simeq \gamma$ and $\cos\gamma \simeq 1$):

$$\mathrm{f} = \begin{bmatrix} \dot{v} \\ \dot{h} \\ \dot{s} \end{bmatrix} = \begin{bmatrix} \frac{T_{\text{idle}} - D}{m} - g\gamma \\ v\gamma \\ v + w \end{bmatrix} \tag{5}$$

where $T_{\text{idle}} : \mathbb{R}^{n_x} \to \mathbb{R}$ is the idle thrust; $D : \mathbb{R}^{n_x \times n_u} \to \mathbb{R}$ is the aerodynamic drag; g is the gravity acceleration; w is the wind and m—the mass, which is assumed to be constant because the fuel consumption during an idle descent is a small fraction of the total m [25]. The longitudinal component of the wind $w : \mathbb{R} \to \mathbb{R}$ is modelled by a smoothing spline [26]:

$$w(h) = \sum_{i=1}^{n_c} c_i B_i(h) \tag{6}$$

$B_i, i = 1, \ldots, n_c$, are the B-spline basis functions and $c = \left[c_1, \ldots, c_{n_c}\right]$ are control points of the smoothing spline. It should be noted that the longitudinal wind has been modelled as a function of the altitude only, as done in similar works [27]. The control points of the spline approximating the longitudinal wind profile are obtained by fitting historical weather data (detailed in Sect. 3.1).

In this paper, the trajectory is divided in two phases: the latter part of the cruise phase prior the ToD, and the idle descent down to the metering fix. Assuming that the original cruise speed will not be modified after the optimization process, the two-phases optimal control problem can be converted into a single-phase optimal control problem as follows:

$$J = \frac{f}{v_{\text{cruise}}} + \int_{t_0}^{t_f} (f_{idle} + \text{CI})\, \mathrm{d}t \tag{7}$$

where $f : \mathbb{R}^{n_x \times n_u} \to \mathbb{R}$ and $f_{idle} : \mathbb{R}^{n_x} \to \mathbb{R}$ are the nominal and idle fuel flow, respectively; and CI is the cost index, which is a parameter chosen by the airspace user that reflects the relative importance of the cost of time with respect to fuel costs [28]. The CI is estimated by assuming that the aircraft was flying at the optimal speed in the cruise phase, as shown in [29].

To generate the optimum trajectories, five input parameters are used: aircraft model, cruise altitude, distance to go (i.e., the distance remaining to the metering fix by following a given route), speed (i.e., the true airspeed of the aircraft in cruise), and the cost index.

3 Results

This section describes the data used in this work and presents the results of data analysis for the Stockholm Arlanda airport in the year 2018.

3.1 Data

In this work we use multiple sources of historical data related to the performance of Stockholm Arlanda airport in 2018. Flight plans are obtained from the Demand Data Repository (DDR2, m1 file format) hosted by EUROCONTROL. For the historical flight trajectories we use DDR2 (m3 file format) and the Historical Database of the OpenSky Network [30, 31]. The historical weather data is provided by the National Oceanic and Atmospheric Administration (NOAA) through the National Operational Model Archive and Distribution System (NOMADS) [32].

Aircraft performance parameters for CDO trajectory generation are inputed from BADA 4.2 [23]. In the case the aircraft model does not correspond to any of the BADA models, a comparable aircraft in terms of performance and dimensions is used.

3.2 Analysis of the Weather Impact on TMA Performance

We compare the punctuality statistics and additional time in Stockholm Arlanda TMA based on DDR2 data with the weather statistics of wind speed, visibility and CAPE values for the same dates. To calculate VFE KPI (time flown level) we use OpenSky Network states data as it provides more accurate vertical profile.

First, we plot the data (metrics and KPIs) by days of the year. At some days we observe strong dependencies of the chosen KPIs from the considered weather metrics, while at other days the dependency is weak. This can be explained by the influence of some other operational factors or weather phenomena not considered in this study. For example, in February 2018 (Fig. 1) we can see that the changes in wind gust enforce the increase of average additional time and average time flown level inside TMA. Low visibility events can increase the TMA KPIs, which is clearly the case on February 25. In July 2018 (Fig. 2) high values of the punctuality-related KPIs (average delay and percent of delayed flights) coincide on some dates with increased gust, for example on July 27. From July 10 to the end of the month punctuality KPIs follow the changes of CAPE.

We continue with the deeper analysis of the dependencies between the KPI-metric pairs by introducing the thresholds in the weather metrics. Because of the nature of different weather events they can influence the flight performance differently. Strong wind gust makes aircraft landing problematic or simply impossible especially when

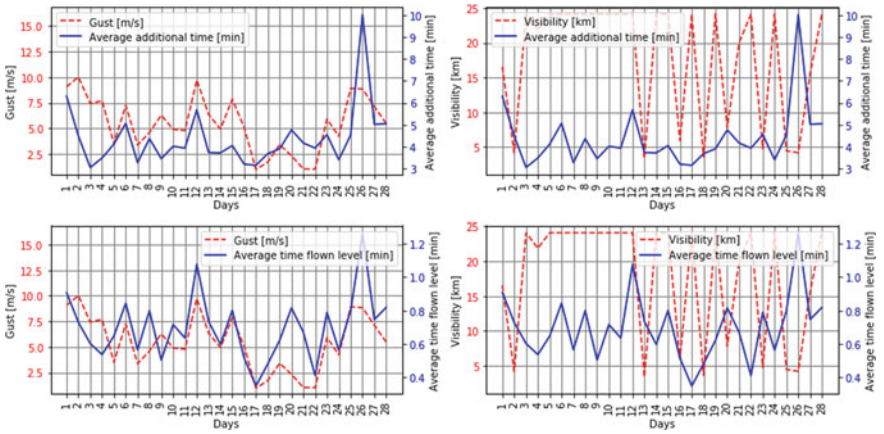

Fig. 1 Weather metrics (wind gust and visibility) and KPIs (average additional time in TMA and average time flown level) for the month of February 2018

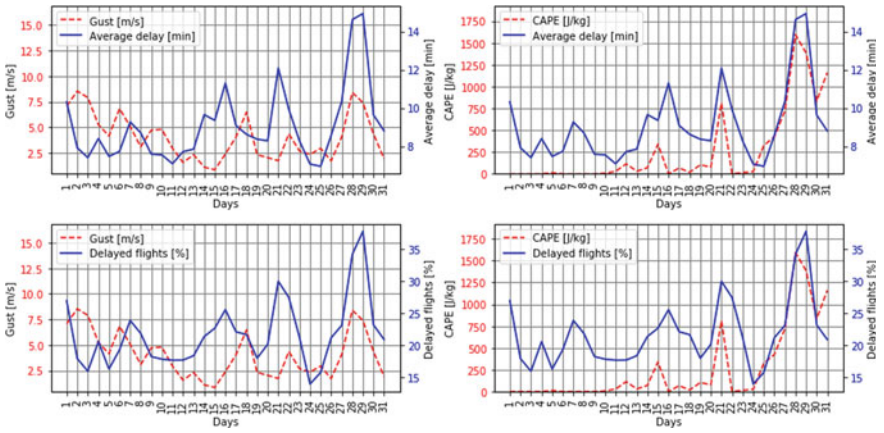

Fig. 2 Weather metrics (wind gust and CAPE) and KPIs (average delay and percent of delayed flights) for the month of July 2018

it is above 12 m/s. This obviously results in higher values of all KPIs chosen in this study, which is shown in Fig. 3.

We discovered, that with visibility lower 5 km significantly more flights are delayed, which indicates that there is an indirect dependency between the corresponding KPI and visibility. Similarly, we observe direct dependencies between all the KPIs and the other two weather metrics.

To examine the relationship between KPIs and weather metrics we apply regression analysis to the data for the whole year 2018. We clean the data by removing the KPI outliers. To remove skewness in weather metrics distribution we filter out

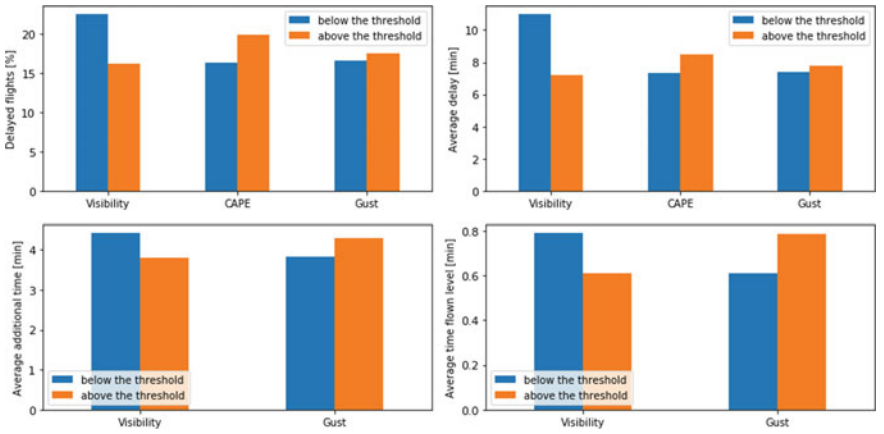

Fig. 3 Average KPIs over the year 2018 calculated with respect to the following thresholds in the weather metrics: visibility—5 km, CAPE—100 J/kg and gust—12 m/s

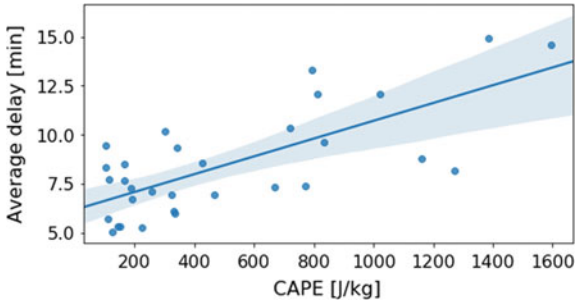

Fig. 4 Simple linear regression for average delay versus CAPE

data with the boundary values (more 24 km for visibility and less than 100 J/kg for CAPE).

Simple linear regression demonstrates moderate dependency between average delay and CAPE ($R^2_{\text{adj}} = 0.5052$), which is illustrated in Fig. 4. While the average delay and visibility show weak dependency in simple regression ($R^2_{\text{adj}} = -0.0131$), joining these two metrics in multiple linear regression results in better fitted model ($R^2_{\text{adj}} = 0.7524$). Figures 5 and 6 illustrate the corresponding results.

3.3 Additional Fuel Burn

In order to assess fuel efficiency within Arlanda TMA during the year 2018, we calculate the fuel waste associated with the vertical flight inefficiency for individual descent profiles within TMA. For actual trajectories we use both DDR2 and Opensky Network tracks and compare the results for additional fuel burn. The objective is to

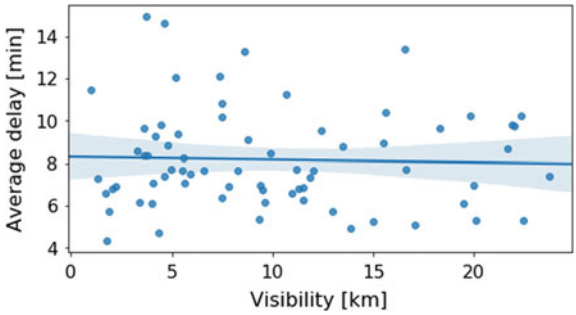

Fig. 5 Simple linear regression for average delay versus visibility

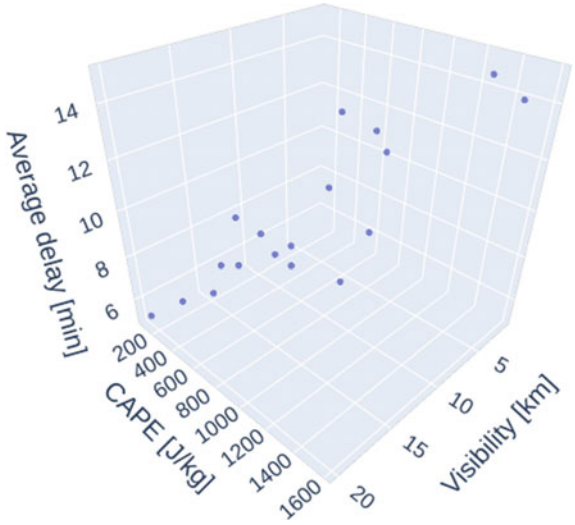

Fig. 6 Multiple linear regression for average delay versus visibility and CAPE

compare the fuel consumption of CDO trajectories with the actual flown trajectories. The CDO were only optimized for the vertical plane, so the distance to go was obtained from either DDR or Opensky.

First, we compare the fuel consumption of the actual trajectories obtained from DDR2 m3 data with the CDO profiles obtained with the trajectory optimization technique explained in Sect. 2.3.4. We calculate the additional fuel burn per day for all Arlanda airport arrivals during the months of February and July 2018, where we have discovered dependencies between the weather events and several KPIs. Figures 7 and 8 illustrate the results. We calculate that in both months CDO provide a reduction of fuel consumption around 60–65%, which constitutes significant inefficiency of the vertical profiles actually flown during these months.

It is important to recall that we calculate the fuel inside TMA only; if the whole descent was compared, the difference would have been lower, as level-offs at lower altitudes are more detrimental for efficiency than those at higher altitudes.

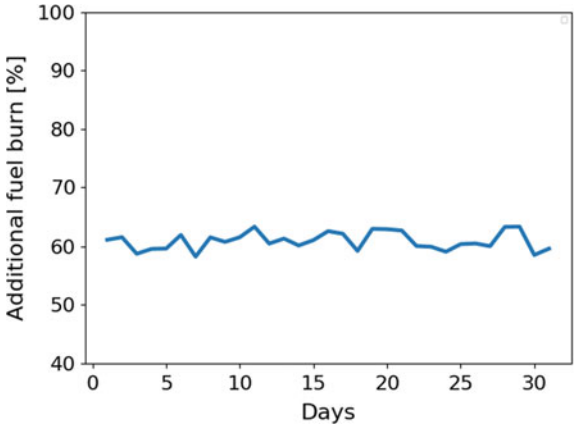

Fig. 7 Additional fuel burn (in percent per day) due to inefficient vertical profiles, calculated as the difference between the actual flown trajectories (DDR m3) and the optimal trajectories, in total fuel consumption per day inside TMA for the month of February 2018

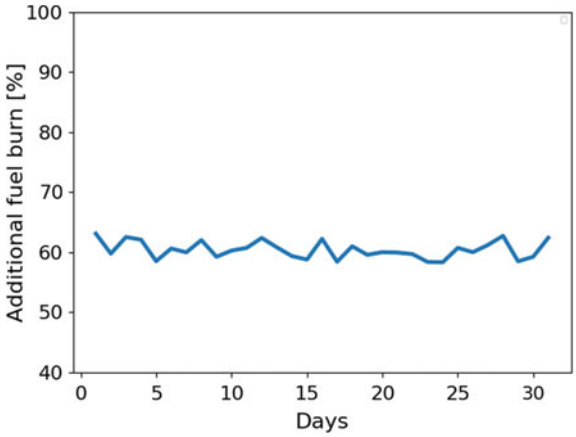

Fig. 8 Additional fuel burn (in percent per day) due to inefficient vertical profiles, calculated as the difference between the actual flown trajectories (DDR m3) and the optimal trajectories, in total fuel consumption per day inside TMA for the month of July 2018

Similar computations have been made by using Opensky data for the month of February and July 2018 (Figs. 9 and 10). While the fuel consumption is higher than with DDR (usually the difference is between 1 and 10%), the additional fuel burn with respect to CDO remains almost the same.

Absolute values for the fuel consumption are shown in Figs. 11 and 12, representing the average fuel consumption over the flights per day during the months of February and July 2018.

Fuel consumption suffers significant changes throughout the month. First of all, the calculation took into account wind components, which demonstrated the impact on the efficiency of vertical profiles. Hence, we observe the decrease of the fuel consumption during the corresponding days with the lowest gust values reported (e.g. on February 17, Fig. 1, gust-average time flown level plot), and increase of the fuel consumption during the days with the highest gust values (e.g. February 25–26). Moreover, the increase of the fuel burn during the days with low visibility

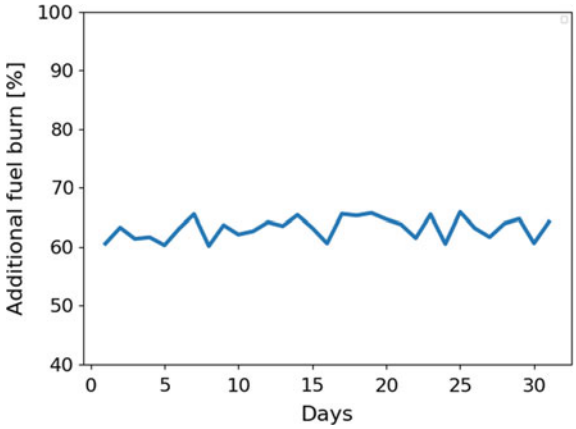

Fig. 9 Additional fuel burn (in percent per day) inside TMA due to inefficient vertical profiles, calculated as the difference between the actual flown trajectories (Opensky tracks) and the optimal trajectories, for the month of February 2018

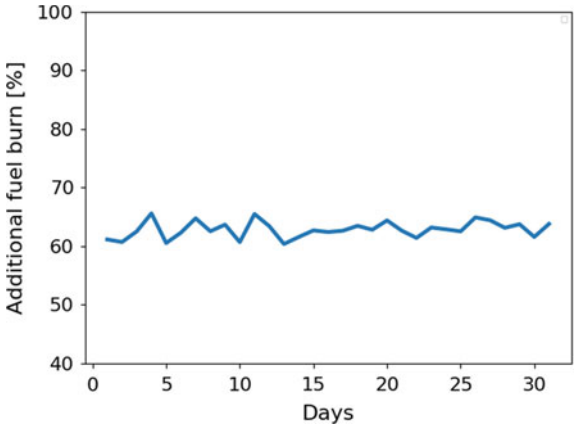

Fig. 10 Additional fuel burn (in percent per day) inside TMA due to inefficient vertical profiles, calculated as the difference between the actual flown trajectories (Opensky tracks) and the optimal trajectories, for the month of July 2018

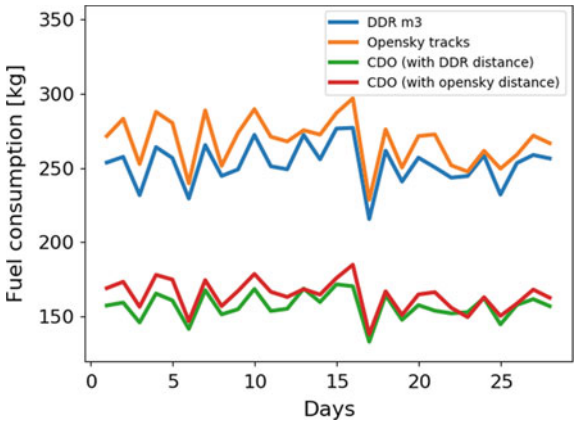

Fig. 11 Average fuel consumption over the flights per day (in kg) for actual flown trajectories (DDR m3 and Opensky tracks) and CDO within TMA for arrival flights in Stockholm Arlanda during the month of February 2018

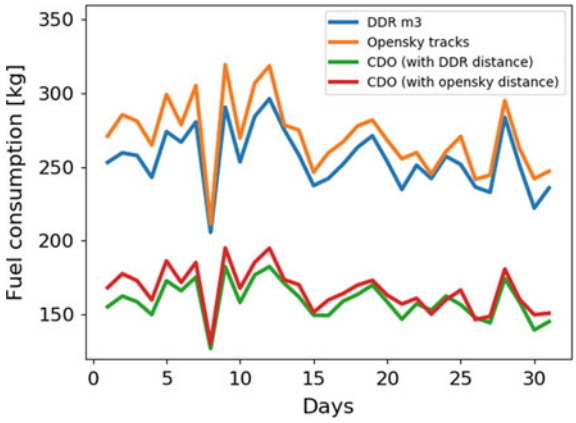

Fig. 12 Average fuel consumption over the flights per day (in kg)for actual flown trajectories (DDR m3 and Opensky tracks) and CDO within TMA for arrival flights in Stockholm Arlanda during the month of July 2018

(e.g. the same days February 25–26, visibility-time flown level plot on Fig. 1) can be a result of Low Visibility Procedures and the connected changes in the descent profiles because of the difficult weather condition.

The extreme CAPE values on 28–29 of July (CAPE curves on plot Fig. 2) result in the increased time flown level (the figure is not presented here), and correspondingly increases the fuel burn at the same days that can be explained by changed landing procedures during the days with high convective instabilities.

Finally, it is important to highlight the advantages (and some disadvantages) that Opensky data represents over DDR data. First, the better data granularity of Opensky data makes it a better option to estimate fuel consumption inside TMA. While DDR usually provides only 3 or 4 segments inside TMA, in Opensky there are about 60–80 waypoints (depending on the trajectory), which makes it more reliable. However, there are also some errors in Opensky data, which tend to cause very high values when computing the fuel consumption. Several data outliers were found in Opensky tracks. For instance, in some trajectories there are some repeated waypoints, even with the time advancing (which would mean the aircraft remains still, which is not possible). There are other situations where the latitude and longitude do not seem to correspond to the trajectory we are dealing with, and some of the speed values that could be extracted from Opensky tracks are wrong too. Since all these problems were found in less than 1% of flights, in this work we chose to remove these flights in order to have proper fuel consumption values. However, in future work it would be interesting to find an outlier removal method in order to efficiently solve this problem.

4 Conclusions and Future Work

In this paper we studied how different weather phenomena influence arrival punctuality and VFE on example of Stockholm Arlanda airport. We analyzed the dependencies between certain KPI-weather metric pairs. Performance degradation during the days when such weather events as low visibility, strong gusts or high thunderstorm probability were detected, result in significant amount of additional fuel burn. Our calculations show that CDO provide a reduction of fuel consumption around 60–65%, which constitutes significant inefficiency of the vertical profiles actually flown during the observed months. In addition, we shared our experience working with DDR and OpenSky data sources and discussed their applicability for calculations inside TMA, outlining the advantages and disadvantages of both.

The results of this work create a base for future studies of the impact of different factors such as ATM automation or different weather conditions on the arrival performance. In future work we plan to explore other sources of historical weather in order to add more weather metrics (snow, icing, cloud ceiling), as well as variations in the traffic intensity into our analysis.

References

1. S. Allan, J. Beesley, J. Evans, S. Gaddy, Analysis of delay causality at Newark International Airport, in *ATM Seminar* (2001)
2. R. Beatty, R. Hsu, L. Berry, J. Rome, Preliminary evaluation of flight delay propagation through an airline schedule. Air Traffic Control Quart. **7**(4), 259–270 (1999)
3. European Commission Network Manager. Monthly Network Operations Report (2019)
4. M. Steiner, R. Bateman, D. Megenhardt, Y. Liu, M. Xu, M. Pocernich, J. Krozel, Translation of ensemble weather forecasts into probabilistic air traffic capacity impact. Air Traffic Control Quart. **18**(3), 229–254 (2010)
5. M. Steiner, W. Deierling, K. Ikeda, E. Nelson, R. Bass, Airline and airport operations under lightning threats-safety risks, impacts, uncertainties, and how to deal with them all, in *6th AIAA Atmospheric and Space Environments Conference* (2014), p. 2900
6. L. Song, D. Greenbaum, C. Wanke, The impact of severe weather on sector capacity, in *ATM Seminar* (2009)
7. A. Klein, S. Kavoussi, R.S. Lee, Weather forecast accuracy: study of impact on airport capacity and estimation of avoidable costs, in *ATM Seminar* (2009)
8. S. Reitmann, S. Alam, M. Schultz, dvanced quantification of weather impact on air traffic management, in *ATM Seminar* (2019)
9. M. Steinheimer, C. Kern, M. Kerschbaum, Quantification of weather impact on air arrival management, in *ATM Seminar* (2019)
10. EUROCONTROL, *Analysis of Vertical Flight Efficiency During Climb and Descent* (2017)
11. EUROCONTROL, *Performance Review Report: An Assessment of Air Traffic Management in Europe during the Calendar Year 2018* (Draft Final Report for consultation with stakeholders)
12. E. Spinielli, R. Koelle, K. Barker, N. Korbey, Open flight trajectories for reproducible ANS performance review, in *SIDs* (2018)
13. R. Christien, E. Hoffman, K. Zeghal, Spacing and pressure to characterise arrival sequencing, in *ATM Seminar*
14. P. Pasutto, E. Hoffman, K. Zeghal, Vertical efficiency in descent compared to best local practices, in *ATM Seminar* (2019)

15. M.S. Ryerson, M. Hansen, J. Bonn, Time to burn: flight delay, terminal efficiency, and fuel consumption in the national airspace system. Transp. Res. Part A Policy Pract. **69**, 286–298 (2014)
16. G.B. Chatterji, Fuel burn estimation using real track data, in *11th ATIO Conference* (2011), p. 6881
17. X. Prats, C. Barrado, F. Netjasov, D. Crnogorac, G. Pavlovic, I. Agüi, A. Vidosavljevic, Enhanced indicators to monitor ATM performance in Europe, in *SIDs* (2018)
18. X. Prats, I. Agüi, F. Netjasov, G. Pavlovic, A. Vidosavljevic, APACHE-Final project results report (2018)
19. X. Prats, R. Dalmau, C. Barrado, Identifying the sources of flight inefficiency from historical aircraft trajectories, in *ATM Seminar* (2019)
20. H. Fricke, C. Seiss, R. Herrmann, Fuel and energy benchmark analysis of continuous descent operations, in *ATM Seminar* (2015)
21. F. Wubben, J. Busink, *Environmental Benefits of Continuous Descent Approaches at Schiphol Airport Compared With Conventional Approach Procedures* (Technical report, NLR, 2000)
22. KPI Overview. https://www4.icao.int/ganpportal/ASBU/KPI. Accessed on 29 Aug 2019
23. EUROCONTROL, User Manual for the Base of Aircraft Data (BADA) Family 4 (2014)
24. R. Sáez, X. Prats, T. Polishchuk, V. Polishchuk, C. Schmidt, Automation for separation with CDOs: dynamic aircraft arrival routes, in *ATM Seminar* (2019)
25. J.P. Clarke, N.T. Ho, L. Ren, J. Brown, K. Elmer, K.F. Zou, C. Hunting, D. McGregor, B. Shivashankara, K. Tong, A.W. Warren, J. Wat, Continuous descent approach: design and flight test for Louisville international airport. J. Aircraft **41**(5), 1054–1066 (2004)
26. C. de Boor, On calculating with B-splines. J. Approx. Theory **6**(1), 50–62 (1972)
27. P.M.A. de Jong, J.J. van der Laan, A.C. Veld, M.M. van Paassen, M. Mulder, Wind-profile estimation using airborne sensors. J. Aircraft **51**(6), 1852–1863 (2014)
28. Airbus, Getting to grips with the cost index—issue II. Technical Report 2 (1998)
29. R. Sáez, R. Dalmau, X. Prats, Optimal assignment of 4D close-loop instructions to enable CDOs in dense TMAs, in *DASC* (2018)
30. OpenSky Network. https://opensky-network.org. Accessed on 29 Aug 2019
31. M. Schäfer, M. Strohmeier, V. Lenders, I. Martinovic, M. Wilhelm, Bringing up opensky: a large-scale ADS-B sensor network for research, in *IPSN'14* (2014)
32. NOAA, https://www.ncdc.noaa.gov/data-access/model-data/model-datasets/global-forcast-system-gfs. Accessed on 29 Aug 2019

AcListant with Continuous Learning: Speech Recognition in Air Traffic Control

J. Rataj, H. Helmke, and O. Ohneiser

Abstract Increasing air traffic creates many challenges for air traffic management (ATM). A general answer to these challenges is to increase automation. However, communication between air traffic controllers (ATCos) and pilots is still widely analog and far away from digital ATM components. As communication content is important for the ATM system, commands are still entered manually by ATCos to enable the ATM system to take the content of the communication into account. However, the disadvantage of this procedure is significant additional workload for the ATCos. To avoid this additional effort, automatic speech recognition (ASR) can automatically analyze the communication and extract the content of spoken commands. DLR together with Saarland University invented the AcListant® system, the first assistant based speech recognition (ABSR) with both a high command recognition rate and a low command recognition error rate. Beside the high recognition performance, AcListant® project revealed shortcomings with respect to costly adaptations of the speech recognizer to different air traffic control (ATC) environments. Machine learning algorithms for the automatic adaptation of ABSR to different airports were developed to counteract this disadvantage within the MALORCA project, funded by Single European Sky ATM Research Programme 2020 Exploratory Research (SESAR-ER). To support the standardization of speech recognition in ATM, an ontology for ATC command recognition on semantic level was developed to enable the reuse of expensively manually transcribed ATC communication in the SESAR Industrial Research project PJ.16-04. Finally, results and experiences are used in two further SESAR Wave-2 projects. For the first time, this paper presents the evolution from the idea of ABSR born in an academic environment, starting with the project AcListant®, to industrialization ready research prototype of technology reediness level (TRL) 4. In this course, relevant industrial needs such as costs and necessary

J. Rataj (✉) · H. Helmke · O. Ohneiser
Institute of Flight Guidance, German Aerospace Center (DLR), Braunschweig, Germany
e-mail: juergen.rataj@dlr.de

H. Helmke
e-mail: hartmut.helmke@dlr.de

O. Ohneiser
e-mail: oliver.ohneiser@DLR.de

Air Traffic Management and Systems IV, Lecture Notes in Electrical Engineering 731,
https://doi.org/10.1007/978-981-33-4669-7_6

standardizations supported by tailored European funding scheme are considered. The addressed SESAR projects are MALORCA, PJ.16-04, PJ.10-96 HMI Interaction modes for ATC centre, and PJ.05-97 HMI Interaction modes for Airport Tower.

Keywords Assistant based speech recognition · Machine learning · AcListant® · MALORCA · PJ.16-04 · Ontology

1 Introduction

The increasing air traffic creates many challenges concerning safety, capacity, efficiency, and environmental performance for ATM. Additionally, economic pressure exists to increase productivity in ATC to keep flying affordable. The general answer of the main ATM development programs, such as SESAR (Single European Sky ATM Research) [1] in Europe, NextGen (Next Generation Air Transportation System) in US [2], CARATS (Collaborative Actions for Renovation of Air Traffic System) in Japan [3] or CAAMS (Civil Aviation ATM Modernization Strategy) in China [4] to fulfill these challenges is to increase digitization and automation considerably. In this case, digitization means to transform analog data into digital formats, which, in turn, is the basis for modern automation solutions. Already today, a high degree of digitization exists in ATM. Radar trackers, flight data processing systems (FDPS) as well as other systems represent the real world in digital environment. However, one central element of ATC, the communication between ATCos and pilots, is not digitized yet. The communication still relies on analog radio, which—independent of CPDLC (Controller Pilot Data Link Communications) [5–7]—will exist during the next decade or even longer.

The content of this communication is of utmost importance for the digital ATM systems world. Hence, the spoken commands of the ATCos must be digitized to be available in the digital world. Today, this is manually performed by ATCos via mouse or keyboard in parallel to their voice communication with the pilots. In this way, the digital world understands the impact of human communication on a certain traffic situation. As advantage of digitization, the controller can benefit from decision and negotiation support systems. However, a huge disadvantage is the significant effort for the ATCo concerning additional manual inputs into the digital system. Hence, the question arises whether the advantages by support systems, such as an arrival manager outweigh the disadvantages of additional controller workload.

An approach to avoid the above mentioned disadvantages is to use automatic speech recognition (ASR). ASR enables to automatically extract the content of uttered commands and digitize them for ATC systems without additional ATCo's workload. Therefore, such a technology seems to be very beneficial for further digitization of ATC and will increase automation. Additionally, speech recognition technology gathered a high interest based on popular consumer applications, such as "Siri" or "Alexa". Based on such applications and the large market behind, it can be

assumed that the technology will develop rapidly and can be adapted to ATC with moderate effort.

This article describes for the first time the entire development process of assistant based speech recognition (ABSR) in the academic environment and moving towards an industrializable prototype as well as first developments of standards in this context. Furthermore this work presents the references to our original work describing the algorithms, validation trials and the results. The special challenges presented in Sect. 2, which are posed especially to speech recognition in operational air traffic control environment, are the starting point for the novel approach to speech recognition are. In addition, Sect. 2 outlines the overall development process of the ABSR in air traffic control with the associated work in various projects. In Sect. 3, the paper discusses the novel approach utilizing predictions of ATCo behavior to improve speech recognition. An innovative problem solution in the academic environment is not always sufficient for the industrialization. For this reason, further research activities accompanying the industrialization to reduce implementation costs were necessary in order to utilize speech recognition in an operational environment. This is the subject of Sect. 4. The basic approach at this point was machine learning with the intervention that training of acoustic model, language model, and command prediction model iteratively enhance each other. Finally, Sect. 5 describes the standardization efforts required for industrialization, which took place in an industrial environment. This development was enabled by partially coordinated funding instruments mentioned in the article. The resulting projects were AcListant® based on the Helmholtz Validation Fund, MALORCA based on SESAR Exploratory Research and PJ.16-04 based on SESAR Industrial Research. Section 6 closes and gives an outlook.

2 Evolution of ASR in ATC

Based on the literature, speech recognition for ATC was used in some places with medium success [8, 9]. First attempts to use standard speech recognition for the controller working position in our labs led to disappointing results concerning the recognition rate. Tests in the DLR research simulator ATMOS (Air Traffic Management and Operation Simulator) with standard ASR systems—adapted to ATC environment—resulted in recognition rates from 65 to 85% per controller command. Such recognition rates will not be accepted by ATCos in an operational environment. It is known from other projects concerning Arrival or Departure Management that ATCos put very high demands on the capabilities of their support systems. If the system could not fulfill the expected abilities, the system will be rejected by the ATCos. Then, it is very difficult to get a second chance to introduce this new technology into ATC.

In order to avoid a rejection by the ATCos, it was assumed that high recognition rates are necessary not knowing exactly what *high* means. Based on this reasoning the first insight to solve the problem was to define a new assessment metric because

the metric, word error rate (WER), to evaluate the performance of an ASR system as used in the speech recognition domain [10], is not the deciding value for the ATCo's acceptance of the resulting system. More important is the correctness of the recognition on command level and not of single words. This insight creates a further considerable challenge for ASR, to deliver a high command recognition rate (CRR). The CRR hereby is defined as the percentage of correctly recognized commands divided by all given commands. An ATC command itself consists of several elements (e.g., callsign, command type, and command value) each consisting of several words, hence to achieve a low command recognition error rate (CER) is much more challenging than just a low WER. Details on CRR and CER calculation can be found in [11].

In discussions with ATCos from several European countries within the framework of the SESAR 2020 Industrial Research project PJ.16-04 CWP HMI (Controller Working Position Human Machine Interface), the requirements for ASR applications in ATM context were specified. The most important one is a low CER. Based on statements of ATCos, the CER is especially important, because it causes additional workload to detect an error. Hence, the ATCos prefer to manually input unrecognized commands instead of detecting wrongly recognized commands with additional manual correction effort. The decisive requirement follows from this that the CER of an ASR system should be exceptionally low. On the other hand, an acceptable high CRR is also indispensable.

To achieve both, high CRRs and low CERs, DLR together with Saarland University invented the AcListant® system [11], which will be detailed in the next section. This system bases on a specific context, which is gained using the knowledge of a controller assistant system. Hence, AcListant® (Active Listening Assistant) is denoted as Assistant Based Speech Recognition (ABSR) system, which creates a new class of speech recognition systems. AcListant® validation trials have demonstrated that both, high CRRs (>90%) and low CERs (<3%), are possible. Additionally, it was shown that controller assistant systems, e.g. Arrival Managers, benefit from the knowledge of the content of the communication between controller and pilot [12, 13].

The follow-up project AcListant®-Strips, led by DLR, successfully validates the hypothesis that ABSR reduces ATCo's workload for radar label maintenance. Beyond that, the reduced workload results in an increased controller performance. In Düsseldorf approach scenarios of the validation trials carried out with German and Austrian ATCos, the average flight time in the Terminal Maneuvering Area (TMA) was reduced by 77 s per aircraft and a reduced average flight length of 5 nautical miles was shown [14, 15].

The project also revealed an important shortcoming: The expensive adaptations of ABSR to different environments and user groups with respect to airspace, airports, dialects, local phraseology etc. After achieving the requirements of high CRR and low CER, reducing adaptation costs was the next challenge, which needed to be fulfilled for an industrialization of the research results. Hence, the next development step was driven by the question on how to reduce the costs for deployment and maintenance of an ABSR system. The considerations concerning cost reductions resulted in the idea

for the SESAR 2020 Exploratory Research project MALORCA (Machine Learning of Speech Recognition Models for Controller Assistance), which was led by DLR [16] The goal of this project was to substitute the expensive manual adaptation work of AcListant® by automatic procedures. In MALORCA a first set of mechanisms based on machine learning were developed by the project partners (Saarland University, Idiap, Austro Control, Air Navigation Service Provider of Czech Republic (ANS CR) and DLR) to enable an automatic adaption of AcListant® to a certain environment. These mechanisms were exemplarily applied to the approach areas of Vienna and Prague using recorded real controller communications. The resulting CER after learning for Vienna approach was 3.5%. For Prague a CER of 0.6% was achieved [17, 18].

In parallel to the work in SESAR Exploratory Research, activities to foster speech recognition in an industrial environment were performed in SESAR2020 Wave 1 with the ASR Activity in the Industrial Research solution PJ.16-04 CWP HMI led by DLR. The goal of this project was to increase the ATCos' productivity and to support the industrialization of speech recognition in ATC. The process of transforming an audio signal to a sequence of words is called transcription, i.e. the voice to text process. The transformation of the word sequence to the relevant ATC concepts is called annotation. MALORCA has shown that different experts agree on the transcription of a controller utterance, but their annotation results may be different. This creates a problem concerning automatic understanding of controllers' voice. Therefore, a set of rules for annotating a sequence of words to ATC concepts was developed, i.e. an ontology. This ontology was agreed in SESAR project 16-04 by 15 European ATC partners setting the basis for a standard in this field [19]. After having presented the evolution from AcListant® to an agreed ontology for command annotation the projects AcListant®, AcListant®-Strips, MALORCA and PJ.16–04 are presented in more detail.

3 AcListant® and AcListant®-Strips

Currently, ASR in ATC is only used in training, i.e. to replace pseudo-pilots. It is reasonable for training purposes to let an ATCo repeat utterances due to undesired deviations regarding the standard phraseology with resulting incorrect speech recognition. Furthermore, training situations are not as critical as real life situations, hence performance limits of ASR for training are acceptable, but not in an operational environment.

To enable the digital ATC world to understand the communication between ATCos and pilots is very beneficial, even more, if this requires no additional workload for the ATCo, which is possible by using speech recognition. As mentioned above to use ASR in operation, ATC specific requirements have to be taken into account, such as high CRRs and low CERs to be successful. In order to be successful, the gold standard in the ASR community, the WER, for assessment and evaluation has to be extended, because this standard is not descriptive enough as metric for ATC. The

specific ATC requirement is to know if the content of a controller command, the concept, is recognized. For example, in the utterance "good morning lufthansa one two three descend flight level one two zero" the meaningful concept from an ATC perspective is "DLH123 DESCEND 120 FL". Hence, to recognize "good morning" is not necessary, because it contains no relevant information and thus misrecognition is irrelevant. Taking this into account the new metrics CER and CRR [11] were defined for ATC applications.

The work concerning ASR started at DLR and Saarland University with a standard ASR with an acoustic model adapted to real ATCo-pilot communication. Many hours of speech samples were recorded, transcribed word-by-word, and annotated with the included semantic content afterwards. Although already considerable effort was spent it was decided to stop this approach of improving just a standard ASR engine. A radical new approach was necessary.

The new approach—patented and developed by DLR and Saarland University—bases on the intensive use of situational context to improve performance. ASR systems, which use current context are known, but not those that take a prediction of the situation into account. Possible sources for predictive context are controller assistant systems. These systems, such as an arrival manager (AMAN), predict the course of future situations to support the ATCo in planning his next actions. This prediction is considerably dynamic based on changing situation elements.

Using an assistant system, see Fig. 1, results in the new ABSR concept. For ABSR, the DLR AMAN 4D-CARMA (4 Dimensional Cooperative Arrival Manager) was used to provide the current and predicted situation of relevant air traffic. This comprises static and dynamic knowledge of the traffic and airspace situation handled by the 4D-CARMA—Core Components. Static knowledge considers e.g., airspace

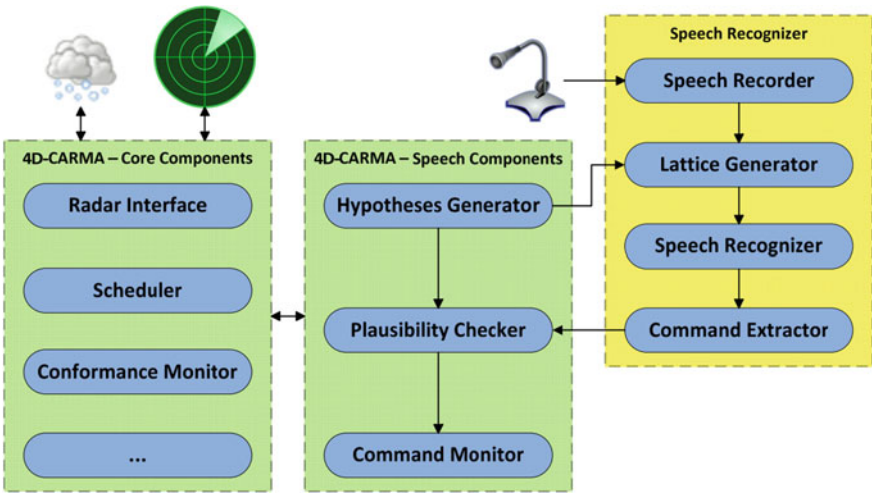

Fig. 1 Components of assistant based speech recognition [11]

structure with routes and waypoints, airspace sector frequencies, minimum separation, etc. Dynamic knowledge bases on the aircraft state vectors and flight phases as well as relevant planning from AMAN modules such as aircraft sequences or distances-to-go. Hence, commands should, e.g., only contain aircraft callsigns that are currently flying in the relevant airspace. Furthermore, knowing an aircraft is in its landing phase, descend and reduce commands are more probable than climb and increase commands. With the knowledge of the airspace structure, also reasonable heading values can be forecasted, because ATCo mostly follow certain routes or direct to certain waypoints.

This above described context knowledge of the assistant system is used by the 4D-CARMA Speech Components, starting with the "Hypotheses Generator" component. The "Hypotheses Generator" does not know exactly which commands the controller will give in the future, but it knows which commands have a higher probability than others in the current and future situation.

These hypotheses are used as input for the "Speech Recognition" block, which consists of the components: "Speech Recorder", "Lattice Generator", "Speech Recognizer", and "Command Extractor". A microphone is connected to "Speech Recorder" to record the signal as wave file. The "Lattice Generator" creates a search space for the "Speech Recognizer" using the output of the "Hypotheses Generator". Hypotheses are of good quality, if they are correct and if just a few commands are forecasted instead of everything that is possible in theory. Hence, the lower the number of hypotheses, the smaller the search space for the speech recognizer. The extracted commands are sent back to the "Plausibility Checker" component, which uses context knowledge and command hypotheses to reject recognized commands. The "Plausibility Checker" divides the recognized commands into three sets:

- Commands immediately accepted, i.e. recognized commands being predicted and also being plausible.
- Commands further monitored with respect to radar data, i.e. recognized commands which are either predicted or have high plausibility values.
- Commands immediately rejected, i.e. recognized commands which are not predicted and with low plausibility values.

The "Command Monitor" verifies commands monitored by continuous comparison to radar data. If, e.g. a descend command to flight level 90 was recognized and the aircraft did not descend after a predefined time, the command is transferred to the set of "commands rejected".

The validation of the ABSR system was performed in two related projects AcListant® and AcListant®-Strips. In AcListant® the recognized speech was used to support an AMAN as well as the ATCo by avoiding manual inputs to maintain the system. The flight information itself was documented on strips in electronic or paper form or on the radar screen in the aircraft label, depending on the simulation run. The information comprises of, e.g., callsign, destination, or route information, clearances regarding altitude, speed, direction, or procedures, as well as special flight situations like emergencies.

In AcListant® two dimensions of validation questions were addressed (see Fig. 2).

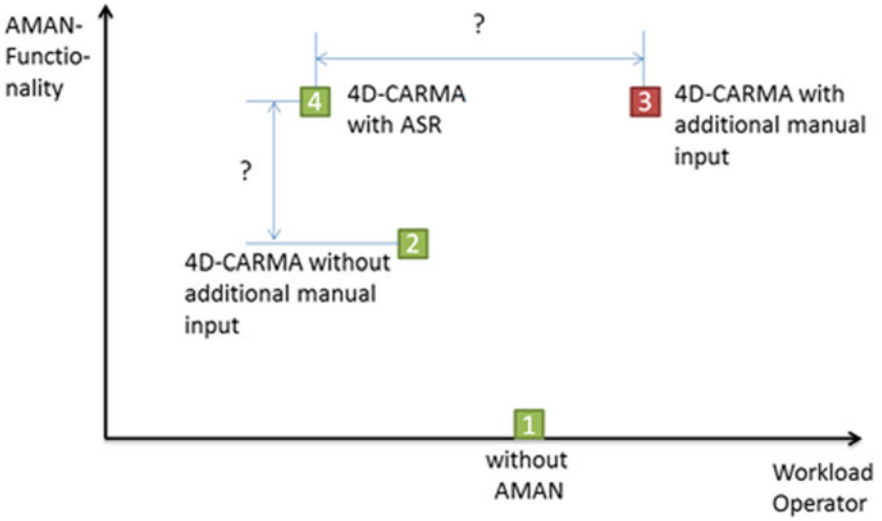

Fig. 2 AMAN functionality versus workload diagram

The first dimension concerns the functionality benefits for the AMAN depending on the input. The second addresses the workload of the ATCo depending on the kind of input. The difference between square 2 and 4 is the additional input for the AMAN based on ATCos' communication. The difference between square 3 and 4 is the kind of input. To validate the increasing functionality, simulation runs with standard AMAN (square 2) and runs with an AMAN supported by ASR creating additional inputs (square 4), were conducted. To quantity the workload reduction, additional runs with an AMAN, either with manual input device (square 3) or with ASR (square 4), were performed. Square 1 illustrates the situation without any controller support.

In the baseline scenario, i.e. square 2 in Fig. 2, for AcListant® trials the flight information were handled with paper flight strips as usual at Düsseldorf approach. In a second scenario, i.e. square 3, the ATCo had to manually input the clearances by mouse and keyboard, which emulates the situation with an electronic flight strip system.

The third scenario, i.e. square 4, based on ABSR usage. In this scenario, the ABSR system listened to the communication between ATCo and pilots. After the speech recognition, the ATCo had the possibility to confirm, correct, or reject the output of the recognizer. Two special test scenarios were chosen to be able to quantify the functionality benefits of a listening AMAN. The first one addressed an emergency situation caused by a sick person on board, the second one a runway closure. In these cases, an early re-planning of the AMAN was necessary to support the ATCo. The re-planning can be triggered by observing the radar data, by manual input of the commands or by speech recognition. Observing the radar data results in delayed system reaction and manual input results in additional ATCo workload. Using ABSR solves both issues by automatic and fast system input.

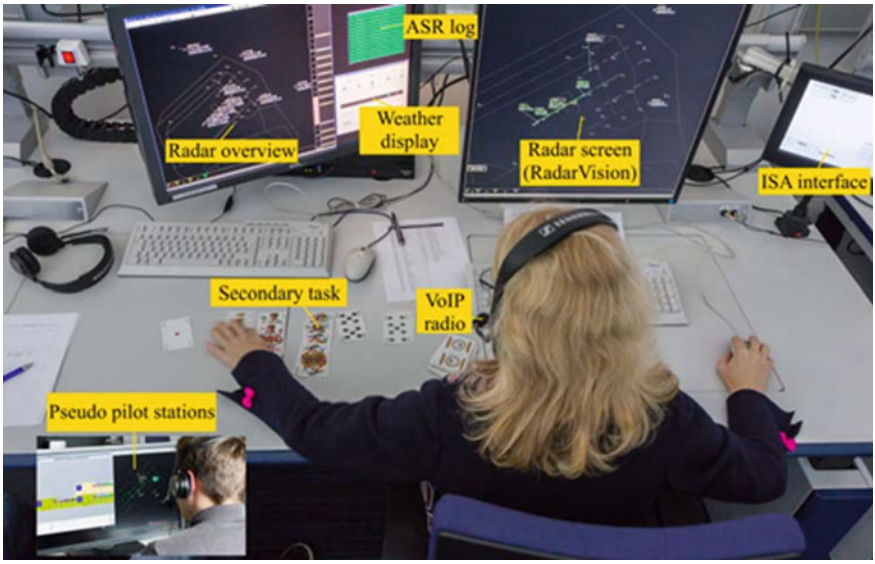

Fig. 3 Basic validation setup during final trials

The set-up for the validation trials consisted of a controller working position (CWP), a traffic simulation and two pseudo-pilot stations. The CWP comprised of radar screen, weather display, radar overview, speech log screen, mouse and keyboard (see Fig. 3). To measure the workload, an instantaneous self-assessment (ISA) test was used. For trials concerning speech recognition, it was necessary to involve different kind of voices. Hence, the participating controllers were selected in a way that there were male and female participants as well as speakers from different countries to take different accents into account.

In AcListant®, it was shown that CRRs of more than 95% are possible using an AMAN to reduce the search space of the speech recognizer. However, the CER was still above 7% and without "assistant based" nearly 20%, which is assumed to be not acceptable. Using also the knowledge from the assistant system to reject commands, i.e. the "Checker" component, the CER was reduced below 2.5%.

The prize for the checker is a decreased recognition rate from 95 to 91%, because correct recognitions were rejected also. The results in Table 1 are based on approx. 4,000 controller commands given in 23 simulation runs. The sum of CER and CRR can be above 100% due to the Levenshtein distance definition [10]. This distance is

Table 1 Command recognition and command recognition error rates

	Recognition rate (%)	Error rate (%)
ASR without AMAN	84.0	19.7
ABSR/AMAN	95.8	7.4
ABSR with checker	91.0	2.5

Table 2 Non-conformance of planned and flown trajectories when comparing different AMAN support levels

Support Condition	Baseline	AMAN	AMAN + ABSR
Average of 3 ATCos based on 69 aircraft (%)	18.7	19.9	8.5

defined here as the minimum number of deletions, substitutions, and insertions to transform one sequence of commands into another one. Hence, if only one command is really said, but three are accidently recognized, we have at least two insertions, which results for this example in a CER of at least 200%.

Furthermore, it was shown that speech recognition improves the adaptation speed of an AMAN on changes in the airspace situation. In the baseline, the AMAN output was not visible to the ATCo. Nevertheless, the AMAN runs in background generating trajectories which are compared with the ones resulting from the ATCo's commands. Table 2 shows the percentages of non-conformance of those trajectories.

Column "AMAN" shows the non-conformance if the AMAN supports the ATCo, but the AMAN gets no input from the speech recognizer. The column "AMAN + ABSR" shows the results, when the AMAN could rely on ABSR. In the case of the visible AMAN, the non-conformance increases from 18.7 to 19.9%. It seems that ATCos tend to slightly deviate if they see AMAN recommendations. When AMAN is supported by ABSR, non-conformance rate is decreased by more than 50%, from 19.9 to 8.5%.

Table 2 clearly shows that the internal plan of the AMAN is more conform to the mental picture of the controller if the AMAN is able to listen to the ATCo. The main results of AcListant® trials [11] are:

- AMAN adapts much faster if the ATCo deliberately deviates from the planning of the assistant system.
- ABSR reduces significantly the deviation between the ATCo's and the assistant system's plan.
- ABSR is able to achieve acceptable CRRs (>90%) and CERs (<3%).
- ABSR significantly reduces ATCo's workload.

In AcListant®-Strips only the difference between the manual input of flight information and ABSR was taken into account. The goal was to quantify benefits of using ABSR as input mechanism to maintain the digital ATC systems. Therefore, the focus was on the workload of the ATCo and the work efficiency. Additionally to known workload measurement tools, we used a secondary task to be performed by the ATCo. The goal of the secondary task was to sort a deck of 48 cards into six decks for each playing card type (9–10-Jack-Queen-King-Ace) and name at the end one to four randomly missing cards. The test subjects were instructed to stay at the ATC task as long as the task requires it. The time needed to sort cards and finally identify the missing ones served as an objective value for user workload. Beside the hypothesis to reduce the workload, it was further assumed that the working efficiency increases based on avoiding head down times and more remaining time to guide the air traffic.

Hence, in one of the two validation scenarios, a very high traffic density was chosen. Eight controllers from Germany and Austria performed different test runs with and without ABSR support [14].

The following results were found in these trials: The ATCos were able to sort twice as many decks of cards as without ABSR support and maintained flight information more precisely. The ATCos invest 30% of their working time to input issued commands by mouse, if no ABSR support is available. This effort is used exclusively to enter known information into an electronic system without any effect on efficiency and quality of the work of the ATCos. Using ABSR changes this situation considerably. The results of the trials have shown that ATCos use only 10% of their working time to maintain flight information when being supported by ABSR. These 10% of working time include the time to check, confirm, and reject outputs of the speech recognizer.

The ATCos were very confident with command recognition rates and command recognition error rates, i.e. they appreciated the automatic aircraft radar label input. They even encouraged having a reaction time of a few seconds to visually check the recognized commands in their HMI instead of actively acknowledging each recognized label input. If ATCos did not intervene during this time, the ATC system should automatically accept the displayed recognition output. It was further found that manual ATC system input by ATCos via mouse and keyboard showed no better quality with respect to accuracy of command values and completeness of inputs.

The trials have also shown that a significant reduction of ATCo workload has an effect on throughput and ATCo's efficiency. One to two inbounds per hour for Düsseldorf are possible. Increased throughput and ATCo's efficiency are possible, because released cognitive resources can be used to better guide air traffic. For the Düsseldorf TMA a benefit of 77 s reduced flight time was quantified. This additional flight time is mostly on downwind. If we assume flying in flight level 70 with 250 knots of calibrated air speed, an A320 consumes 2700 L per hour resulting in roughly 50–65 L of reduced fuel consumption per aircraft. One liter of kerosene is 0.8 kg resulting in 3.15 kg of CO_2. Therefore, application of speech recognition can relieve the environment by about 130 kg CO_2 per flight [15].

4 Implementation Costs

Even impressive results concerning ATC performance indicators by automatic maintenance of flight information are not sufficient to avoid critical questions concerning costs. Speech recognition induces costs by procurement, introduction, and maintenance. Procurement costs base on market driven company decisions. Introduction costs occur, because an ABSR system has to be adapted to users and environments. Maintenance costs are driven by adapting the ABSR system if environment changes. According to changes in the user group, an adaption is only necessary if these changes are significant. The main cost driver for the adaption is the manual work performed by experts. Experiences in AcListant® have shown that adaptation and maintenance

costs of about one million euros are reasonable adaptation cost for a midsize airport. To reduce such costs the manual work has to be automated.

Cost savings further allow a large number of midsize airports to use ABSR technology because it becomes affordable for them. If they use ABSR for flight information maintenance in the TMA, it is possible to save 130 kg CO_2 per flight to relieve environment, as outlined in Sect. 3. Collecting all additional airports, which are able to afford such a system in case of strongly reduced costs, will have a noticeable impact on the environment. Beside this benefit, additional benefits will occur, using ABSR in ATC, like the increased performance of controller assistant systems as shown above. Furthermore, the availability of transcribed and annotated controller commands can also be used for many off-line analyses.

To enable the work to achieve cost reductions, an extended team around the AcListant® partners gained funding from Horizon 2020 SESAR Exploratory Research for the, DLR coordinated project MALORCA. The goal of the project was to use machine learning algorithms to enable a generic, effective and especially cheap approach to adapt ABSR to a specific environment. A major step to achieve MALORCA goals was to separate environment and user dependent parts of the ABSR software from the independent ones. To achieve this, the ABSR system was disassembled into conceptual modules for the specific tasks INPUT, TEXT, COMMAND, and USER. The INPUT module supplies ABSR with voice signal input, surveillance data (e.g., radar data) and static airport dependent inputs (e.g., waypoints, frequencies). Based on data from INPUT, the TEXT module performs tasks related to the automatic speech recognition, i.e., transcription resulting in different sequences of words for one utterance. The COMMAND module translates sequences of words into controller commands using the output command prediction. Finally, the USER module provides the output of COMMAND to a user with an appropriate human machine interface or to another system. The conceptual modules consist of models, which are application (area) independent and models, which are application dependent. The models are automatically learned by machine learning algorithms.

The acoustic model is based on deep neural networks (DNN) and is automatically trained from transcribed and untranscribed data. If more than two hours of training data were available, speaker dependent acoustic models already outperform speaker independent models provided that the speaker is surely known. The lexicon, i.e. the word list and their pronunciation was manually updated by adding waypoints and some local words for greetings and good-bye. The language model consists of an N-gram statistical langue model and was trained by supervised learning.

For each command type (e.g., DESCEND, HEADING) a prediction area is created and subdivided into subareas of 1 nm by 1 nm. Additionally, a set of predefined rules to each command type is added, e.g. IF flight type is arrival AND controller working position is Feeder AND speed >220 knots. If the “Hypotheses Generator” detects that a lat/long position of an aircraft is inside an area of a specific command type and the rule condition for this area is true, the command values related to that flight and command type are predicted for that aircraft. For each command type the areas are learned by unsupervised learning, i.e. from automatically annotated commands.

The invention of the MALORCA project was that acoustic model, language model, and command prediction model iteratively enhance each other. The basic acoustic model results in automatic annotations of controller utterances. These annotations are used to train the command prediction model, which classifies the automatic annotations into good and bad training data elements. An automatic annotation, which is not predicted, is a bad training example. This classification is used in the next iteration to improve the acoustic model, which results in better annotations to improve the command prediction model etc. More details of model adaptation by machine learning are provided in [18] and [20].

After adapting all models the basic ABSR system could iteratively be improved with machine learning increasing the CRR from 80% to 92% for Prague, and from 60% to 83% for Vienna respectively. The 80% for Prague correspond to the case that no automatically transcribed data was available and the 92% include the usage of 18 h, i.e. 100%, of the automatically transcribed data set. The starting point of 60% CRR for Vienna data was on the one hand caused by worse audio quality and on the other hand by the higher variability of deviations from standard phraseology by Vienna ATCos. The CER could be reduced from 4.1 to 0.6% for Prague and from 10.9 to 3.2% for Vienna. For Vienna also 18 h of untranscribed and four hours of transcribed and annotated data were available.

5 ASR Towards Industrialization

In the SESAR2020 Industrial Research project PJ.16-04 the ASR activity is fostered on a broad basis by many project partners. Nineteen European affiliations from fifteen different countries contributed to maturing the technology readiness level (TRL) to TRL4. The overall aim of the project was to increase ATCo's productivity. Supporting companies consisted of European air navigation service providers, three ATM system providers, and research/consultancy organizations [21].

One achievement of the ASR activity was the definition of an ontology for annotation of ATCo commands [19]. The ontology is a set of rules on how to formally understand the content of an ATCo utterance which can consist of multiple concepts. Before extracting concepts, transcription of utterances is required. An example of a transcription and the agreed annotation of concepts from this example are shown in Fig. 4. Each utterance is annotated as a series of callsign-instruction pairs. The instruction can consist of a mandatory command part and optional conditions. The command itself is composed of a type (see example in Fig. 5) and in most cases of a value, a unit, a qualifier and a condition as shown in the given example above.

The developed ontology currently consists of 120 different command types for the en-route, approach and tower phase. It takes the ICAO phraseology and CPLDC protocol into account. However, the ontology sometimes goes beyond or is more general to satisfy the needs to harmonize integration of ASR into controller working positions.

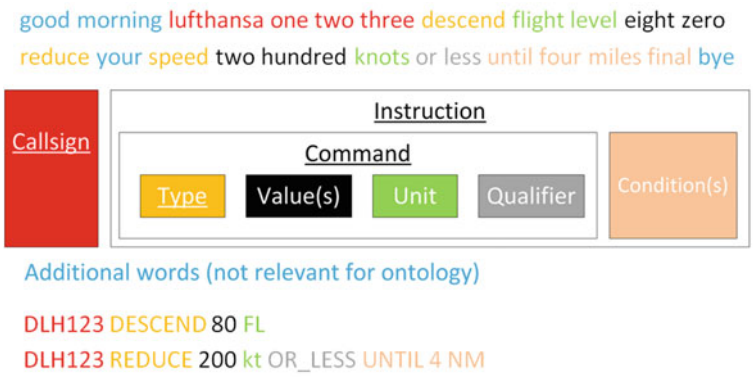

Fig. 4 Basic scheme of the ontology for controller command annotation with sub-parts of an instruction and example commands

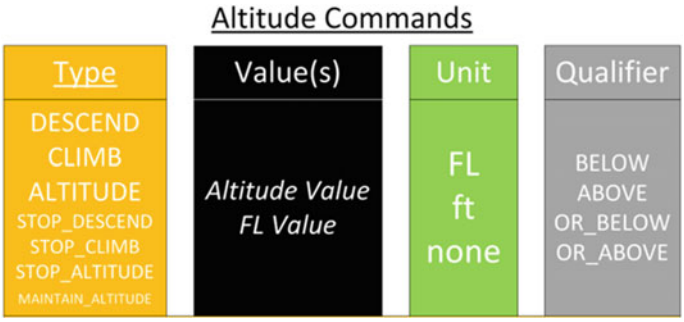

Fig. 5 Sub-parts of command annotation; example: altitude commands

The PJ.16-04 partners conducted several different validation exercises in 2018 and 2019 concerning ASR. One exercise from THALES, DLR, ANS-CR, Integra, and Austro Control (ACG) integrated different components to an ABSR system for Prague and Vienna approach [22]. DLR provided the hypotheses generator to predict controller commands and the checker component. They were used to improve the commercial ASR engine used by THALES. Validation trials with Czech and Austrian ATCos in the THALES SkyCentre proved that the hypotheses generator and the command checker significantly reduced the CER and thus in an environment similar to real ATC operations rooms.

Another exercise of PJ.16-04 compared issued clearances from Hungarian and Lithuanian ATCos in multiple remote tower environments with controller command predictions, developed by DLR [23]. To the best of our knowledge this was the first time that controller command prediction has been developed for a tower CWP.

Fig. 6 Multiple remote tower trials at DLR Braunschweig

Furthermore, it was the first to deal with a multiple remote tower environment forecasting controller commands for different airports in parallel. The command prediction was tested in a set-up for the PJ.05-02 multiple remote tower trials at DLR Braunschweig, see Fig. 6. The complete trials generated 107 recorded simulation runs. The command prediction error rate for annotated trials was 7.3%, i.e. 93% of the commands given by the ATCo were predicted [23].

6 Conclusions and Outlook

The paper presents the evolution of Assistant Based Speech Recognition (ABSR) introduced by DLR and Saarland University. AcListant® project has shown that both acceptable CRRs (>90%) and CERs (<3%) are possible.

AcListant®-Strips even improves ASR performance (above 95% and below 1.7%) and quantifies the benefits of ABSR: Controllers' "clicking time" is reduced by a factor of three resulting in two landings more per hour and 60 L of kerosene saving per inbound flight based on released cognitive ATCo resources. The command recognition and error rates were classified as totally sufficient by ATCos that participated in the ABSR trials.

MALORCA developed generic reusable modules and models. The latter ones can automatically be trained by machine learning algorithms. This result in reduced adaptation costs. SESAR2020s Wave 1 funded project 16-04 enables exchange of training data and reduced transcription and annotation effort, because the main European ATM players agreed on an ontology for command annotation.

SESAR2020s Wave 2 further promotes activities on ABSR with solutions PJ.10-96 and PJ.05-97 that were started end of 2019. Solution 97 foresees validation trials

with an ABSR system integrated into a tower environment. This comprises trials at DLR in Braunschweig and EUROCONTROL in Brétigny. ACG controllers will also perform ABSR trials in the Vienna approach operation's room in solution 96, the first time that an ABSR system will be directly integrated into the ops room of an air navigation service provider.

Acknowledgments The projects AcListant® and AcListant®-Strips were supported by DLR Technology Marketing and Helmholtz Validation Fund. The SESAR Exploratory Research project MALORCA and Industrial Research project PJ.16-04 CWP HMI also comprising the Automatic Speech Recognition activity (PJ.16-04-02) have received funding from the SESAR Joint Undertaking under the European Union's grant agreement No. 698824 respectively 734141.

References

1. Single European Sky ATM Research Joint Undertaking, https://www.sesarju.eu. SESAR Joint Undertaking, n.d.
2. Federal Aviation Administration, https://www.faa.gov/nextgen/, Modernization of U.S. Airspace, n.d.
3. Ministry of Land, Infrastructure, Transport and Tourism, https://www.mlit.go.jp/en/koku/koku_fr13_000000.html, Collaborative Actions for Renovation of Air Traffic Systems (CARATS), n.d.
4. International Civil Aviation Organization, https://www.icao.int/Meetings/a39/Documents/WP/wp_304_en.pdf, China's Strategy for Modernizing Air Traffic Management, n.d.
5. Eurocontrol, "LINK2000+: ATC data link operational guidance in support of DLS regulation," No 29/2009, vol. 6, 17 December 2012, online available at https://www.skybrary.aero/bookshelf/books/2383.pdf
6. O. Veronika Prinzo, Data-linked pilot reply time on controller workload and communication in a simulated terminal option, Civil Aeromedical Institute, Federal Aviation Administration, Oklahoma City, Oklahoma, USA, May 2001
7. ICAO, Global operational data link document (GOLD), 2nd edn. (2013)
8. D. Schäfer, Context-sensitive speech recognition in the air traffic control simulation, in *Eurocontrol EEC Note No. 02/2001 and PhD Thesis of the University of Armed Forces* (Munich, Germany, 2001)
9. J.M. Cordero, M. Dorado, J.M. de Pablo, Automated speech recognition in ATC environment, in *Proceedings of the 2nd International Conference on Application and Theory of Automation in Command and Control Systems (ATACCS '12)* (IRIT Press, Toulouse, France), pp. 46–53
10. V.I. Levenshtein, Binary codes capable of correcting deletions, insertions, and reversals. Soviet Phys. Doklady **10**(8) (1966)
11. H. Helmke, J. Rataj, T. Mühlhausen, O. Ohneiser, H. Ehr, M. Kleinert, Y. Oualil, M. Schulder, Assistant-based speech recognition for ATM applications, in *11th USA/Europe Air Traffic Management Research and Development Seminar (ATM2015)* (Lisbon, Portugal, 2015)
12. H. Gürlük, H. Helmke, M. Wies, H. Ehr, M. Kleinert, T. Mühlhausen, K. Muth, O. Ohneiser, Assistant based speech recognition—another pair of eyes for the Arrival Manager, in *IEEE/AIAA 34th Digital Avionics Systems Conference (DASC)* (Prague, Czech Republic, 2015)
13. AcListant homepage, www.AcListant.de, AcListant = Active Listening Assistant, n.d.
14. H. Helmke, O. Ohneiser, T. Mühlhausen, M. Wies, Reducing controller workload with automatic speech recognition, in *IEEE/AIAA 35th Digital Avionics Systems Conference (DASC)* (Sacramento, CA, USA, 2016)

15. H. Helmke, O. Ohneiser, J. Buxbaum, C. Kern, Increasing ATM efficiency with assistant based speech recognition, in *12th USA/Europe Air Traffic Management Research and Development Seminar (ATM2017)* (Seattle, WA, USA, 2017)
16. The project MALORCA, https://www.malorca-project.de, n.d.
17. M. Kleinert, H. Helmke, G. Siol, H. Ehr, M. Finke, Y. Oualil, A. Srinivasamurthy, Machine learning of controller command prediction models from recorded radar data and controller speech utterances, in *8th SESAR Innovation Days* (Belgrade, Serbia, 2017)
18. M. Kleinert, H. Helmke, G. Siol, H. Ehr, A. Cerna, C. Kern, D. Klakow, P. Motlicek et al., Semi-supervised adaptation of assistant based speech recognition models for different approach areas, in *37th AIAA/IEEE Digital Avionics Systems Conference (DASC)* (London, UK, 2018)
19. H. Helmke, M. Slotty, M. Poiger, D. Ferrer Herrer, O. Ohneiser, N. Vink, A. Cerna, P. Hartikainen, B. Josefsson, D. Langr, R. García Lasheras, G. Marin et al., Ontology for transcription of ATC speech commands of SESAR 2020 solution PJ.16-04, in *37th AIAA/IEEE Digital Avionics Systems Conference (DASC)* (London, UK, 2018)
20. M. Kleinert, H. Helmke, H. Ehr, C. Kern, D. Klakow, P. Motlicek, M. Singh, G. Siol, Building blocks of assistant based speech recognition for air traffic management applications, in *8th SESAR Innovation Days*, Salzburg, Austria, 2018.
21. The SESAR Project PJ.16-04, https://www.sesarju.eu/projects/cwphmi, n.d.
22. M. Kleinert, H. Helmke, S. Moos, P. Hlousek, C. Windisch, O. Ohneiser, H. Ehr, A. Labreuil, Reducing controller workload by automatic speech recognition assisted radar label maintenance, in *9th SESAR Innovation Days* (Athens, Greece, 2019)
23. O. Ohneiser, H. Helmke, M. Kleinert, G. Siol, H. Ehr, S. Hobein, A.-V. Predescu, J. Bauer, Tower controller command prediction for future speech recognition applications, in *9th SESAR Innovation Days* (Athens, Greece, 2019)

Airport Management

A Data-Driven Approach for Taxi-Time Prediction: A Case Study of Singapore Changi Airport

D. T. Pham, M. Ngo, N. Tran, S. Alam, and V. Duong

Abstract The ground movement is one of the most critical airside operations. It includes two sub-problems: routing and scheduling and serves the purpose of guiding aircraft on the surface of an airport to meet the departure schedule while minimizing overall travel time. To achieve that purpose, ground movement controllers manage the taxi-route assignments and taxi-time estimation for each aircraft in arrival or departure queue. A high-accuracy taxi-time calculation is required to increase the efficiency of airport operations. In this study, we propose a data-driven approach to construct features set and build predictive models for taxi-time prediction for departure flights. The proposed approach can suggest the taxi-route and predict the corresponding taxi-time by analyzing ground movement data. The controller's operational preferences are extracted and learned by machine learning algorithms for predicting taxi-route and taxi-time of given aircraft. In this approach, we take advantage of taxiing trajectories to learn the controller's decision, which reflects how the controller had decided the routing for a given situation. Two machine learning models, random forest regression, and linear regression are implemented and show similar performances in estimating the taxi-time. However, since the random forest is an ensemble method that has advantages in handling outliers, performing feature selection, and assessing feature importance, it can provide more stable results and interpretability, for real operations. The predictive model for taxi-time can predict the taxi-out time with high accuracy with given assigned taxi-route. The model can

D. T. Pham (✉) · M. Ngo · N. Tran · S. Alam · V. Duong
School of Mechanical and Aerospace Engineering (MAE), Air Traffic Management Research Institute (ATMRI), Nanyang Technological University (NTU), Singapore, Singapore
e-mail: dtpham@ntu.edu.sg

M. Ngo
e-mail: man.ngo@jvn.edu.vn

N. Tran
e-mail: thanhnam.tran@ntu.edu.sg

S. Alam
e-mail: sameeralam@ntu.edu.sg

V. Duong
e-mail: vu.duong@ntu.edu.sg

Air Traffic Management and Systems IV, Lecture Notes in Electrical Engineering 731,
https://doi.org/10.1007/978-981-33-4669-7_7

cover the controller's decision up to 70% in the top-1 and 89% in top-2 recommends. The mean absolute error is less than 2.07 min for all departure flights, and root mean square error is approximately 2.5 min. Moreover, the ± 3-minute error window can cover around 76% of departures, while more than 95% of departures are within the ± 5-minute error window.

Keywords Routing · Taxi-time prediction · Surface movement · Machine learning · Random forest · Linear regression

1 Introduction

In daily operations at an airport, the ground movement of aircraft is one of the most critical airside operations. The ground movement problem, including two problems: routing and scheduling, serves the purpose of guiding aircraft on the surface of an airport to meet the schedule while minimizing overall travel time. In which, the primary tasks of the ground movement controller are taxi-routes assignment and taxi-time estimation for each aircraft in arrival or departure queue [1]. A controller may select or modify taxi-routes based on his operational preferences or current runway–taxiway constraints that will lead to difficulty in taxi-time estimation.

Moreover, in Airport Collaborative Decision Making (A-CDM) [2], a high-accuracy taxi-time calculation is required to avoid generating and propagating delays in the air traffic management system because of the gap in time between estimated and actual taxi-time.

Several studies have focused on tackling taxi-time prediction [1, 3, 4] or taxi-route routing [5] problems. Previously, the limited availability of ground movement data such as aircraft surface movements, flight information, and airside operations information is the challenge for all studies. The research focuses on some aspects of the problem, such as taxi-out or taxi-in time prediction, considering traffic and data from a small set of stands, taxiways, airlines, and aircraft types. Recently, surface movement data from Advanced Surface Movement Guidance and Control System (A-SMGCS) [6] provides more opportunities for better analyzing surface movement at the system level and predicting aircraft route more accurately. However, extracting features from the surface movement data require an innovative data structure to capture the space and time dependency between airport airside traffic and airport airside infrastructure. Furthermore, the recommended taxi-routes are usually the output of a mathematical algorithm that does not consider controller preferences or operational strategy. Finally, even though those works have provided sets of useful explanatory variables for taxi-time prediction, data-driven features have not been well studied in the literature.

In this study, we focus on data-driven approaches to construct features set and build predictive models for taxi-route taxi-time prediction. By analyzing ground movement data, the controller's operational preferences can be extracted and learned by machine learning algorithms for predicting taxi-route and taxi-time of given aircraft. A set of

features is also obtained from the airport traffic network, weather information, and flight information.

The proposed algorithms can capture the existing pattern in movement data as controller preferences in handling taxiing and predict the taxi-route and taxi-time for each given departure aircraft. It is applied for Singapore Changi airport and evaluated with one-month Advanced Surface Movement Guidance and Control System (A-SMGCS) data.

This paper is organized as follows. Section 2 describes the overview of the proposed approach for taxi-route recommendation and taxi-time prediction. Section 3 discusses in detail our data processing steps, including data preparation, trajectory standardization, and movement pattern extraction using clustering. Section 4 introduces the list of features that are considered in this study. Section 5 describes our predictive models for predicting controller decision and taxi-time for departure flights. Section 6 then discusses the experiments and results. Finally, Sect. 7 presents our conclusions and future work.

2 Overview

Our proposed approach is presented in Fig. 1. The list of potential decisions is learned from data. The departure flights must be assigned route in sequence. This assumption

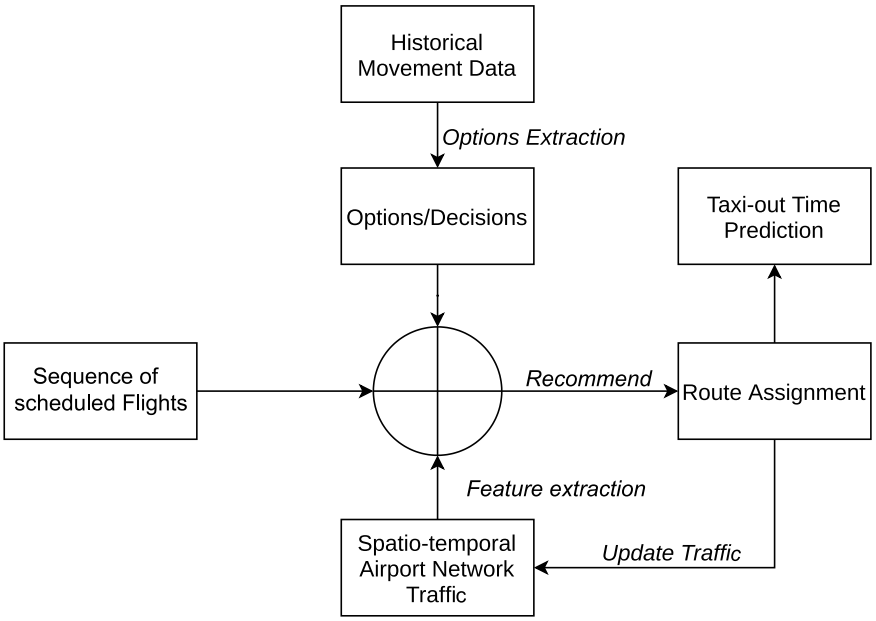

Fig. 1 A schematic illustration of the proposed approach

is made to ensure that at the decision time of a given flight, all previous departures are assigned taxi-route; thus, traffic scores can be computed. Based on the current information and predictions about future traffic, the list of options will be ranked and suggested. The taxi-time for each option or decision can also be computed from given features. When one option is chosen (the first ranked option in autonomous mode), the traffic will be updated for the next flights.

There are four main steps in this study: (1) standardizing trajectories data; (2) constructing a list of decision candidates (options); (3) extracting features from airport data including traffic conditions, weather, etc.; (4) developing predictive models for taxi-route and taxi-time for a given departure. Firstly, a map-matching technique is applied to standardizing actual trajectories using the airside graph. After this step, each trajectory is represented by a sequence of nodes with the corresponding timestamp. Secondly, we use Density-based Spatial Clustering of Applications with Noise (DBSCAN) [7] technique to cluster trajectories to form the list of common taxi-routes, called options. These options are what the controller will consider when making a taxi-route assignment for aircraft. Thirdly, features are extracted from the airport traffic network, weather data, and flight information data. The spatio-temporal airport network (airside) traffic is computed for each flight given its departure time. The traffic score will be computed for each option of that flight, which reflects how the decision relates to current traffic. Extracted features from different sources will be combined to form a set of input features for the machine learning model. These features are essential in explaining the controller's decision. Finally, the random forest method is selected as the predictive model because of its interpretability. Two predictive models are trained from preprocessed historical data to predict taxi-route and taxi-time.

3 Option Extraction

3.1 Data Preprocessing

3.1.1 Parsing Data

Advanced Surface Movement Guidance and Control System (A-SMGCS) is a system at airports having a surveillance infrastructure consisting of cooperative surveillance (e.g., multilateration systems) and a non-cooperative surveillance (e.g., SMR, microwave sensors, optical sensors, etc.). A-SMGCS data contains information about the movements of aircraft, including their trajectories.

The provided raw data is in Extended Data Recorder (EDR) extension, compressed messages, which are not suitable for performing analysis or developing a learning model. Thus, the first processing step is extracting and storing data into an analytical

Table 1 List of extracted features from raw data

9 features
Gate, Longitude, Latitude, Velocity in longitude, Velocity in latitude, Time of track, Measured flight level, Type of aircraft, Wake turbulence categorization

version. One month of data (October 2017) is extracted and stored in CSV (Comma-Separated Values) format. The final data contains more than 30,000 trajectories. The selected fields are listed in Table 1.

3.1.2 Preprocessing Data

The preprocessing process includes three steps:

- Detect different flights with the same ID: It is possible to have different flights with the same ID on one specific day; we should detect and separate them for further analysis.
- Detect whether the flight is arrival or departure.
- Determine the runway configuration.

Graph of Singapore Changi Airport Network: We construct and simplify Changi airport graph from taxiway and runway coordinates from NLR Air Traffic Control Research Simulator (NARSIM) [8].

3.2 Standardizing Trajectory

The original data based on the coordinates of airplanes through time is noisy and not well structured to be inputted to a machine learning model. The training model on noisy data can affect the accuracy of the model later. By matching the aircraft coordinates to the route on an airport graph (using map-matching algorithm), we can represent the trajectory of the airplane by the list of edge (taxiways); it helps to reduce the noise in training data before putting to the model. Besides, standardizing raw data can also reduce the complexity of our following clustering and learning problems since we only need to focus on a shared and well-defined graph with a finite number of edges and nodes. Finally, the output of the program will be delivered to air traffic controllers who are familiar with the list of taxiways that the airplane will follow, rather than the coordinates. So, the map-matching is the key to build the bridge from raw data to a more understandable data format for controllers.

3.2.1 Map-Matching Algorithm

There are several studies on map-matching. The most common approaches are point-to-point matching [9, 10] and point-to-curve matching [11] that map each point in the flight to the "closest" node or closest curve on the graph. Another approach is curve-to-curve matching [10, 11] that chooses the closest curve from the list of candidates (often was generated from a point-to-point matching) to the original curve. We observed that the flight data are dense, so we implemented the point-to-point matching with rule based to guarantee the result is a valid trajectory. The matching algorithm includes two steps:

- In the first step, we assigned each point of the flight to the node in the airport graph if the distance from this point to the nearest node is less than a predefined threshold. The result of the map-matching algorithm is a sequence of node id from the gate to first exit gate on the runway for departure flights and from the last exit gate to the gate for arrival flights.
- This approach may lead to some logical mistakes. For example, after step 1, the chosen trajectory can be: $O \rightarrow n1 \rightarrow n2 \rightarrow D$, but on the airport graph node, $n1$ and $n2$ do not have any connected edge. Thus, in the second step, we avoid these errors by connecting two unconnected nodes by the Dijkstra's shortest path between them. Let say that the shortest path from $n1$ to $n2$ is $n1 \rightarrow n3 \rightarrow n2$. The final trajectory is the sequence of connected nodes $O \rightarrow n1 \rightarrow n3 \rightarrow n2 \rightarrow D$. The matching result is illustrated in Fig. 2. Figure shows a sequence of track points (red dots) of a departure flight in Changi airport (gray segments), which is mapped to the airport graph and converted into a standardized trajectory (blue line).

3.2.2 Evaluate the Map-Matching Process

Noise trajectories can significantly affect the performance of the map-matching algorithm. The performance metric for this step is the distance percent error between the matched trajectory curves and original flight curves. The score is non-negative and the smaller it is the better the matching result is. By investigating the matching results, we can detect and remove the abnormal trajectories (Fig. 3). To maintain the quality of the dataset, we set a threshold $= 0.4$ (40%) to remove those trajectories which have high errors.

3.3 Clustering Using DBSCAN

We observe from historical data that the controllers have a pattern in assigning the taxiway for each departure in similar situations. However, those decisions can be affected by uncertainty such as weather, current airport traffic, etc. In general, they are limited and form a set of potential taxiways for each departure. Therefore, we

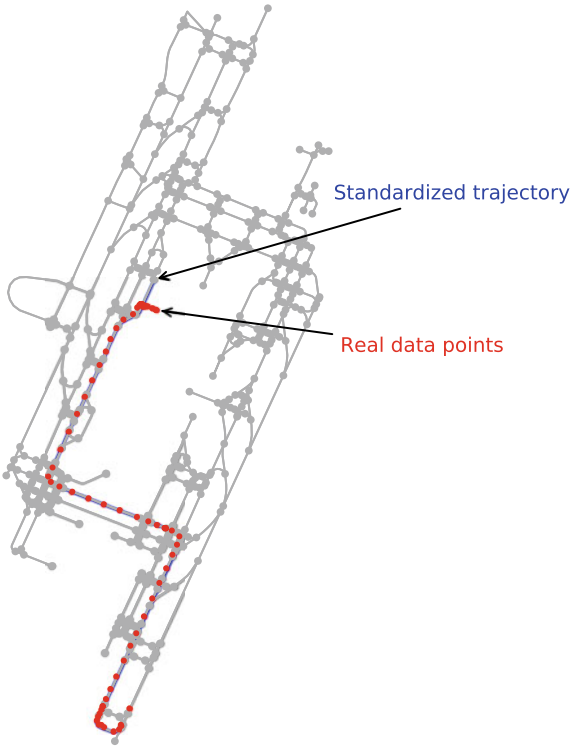

Fig. 2 An illustration of map-matching. Red dots represent real data points for one trajectory, and the blue line is the map-matching result of that trajectory over the graph of the taxi network of Changi airport

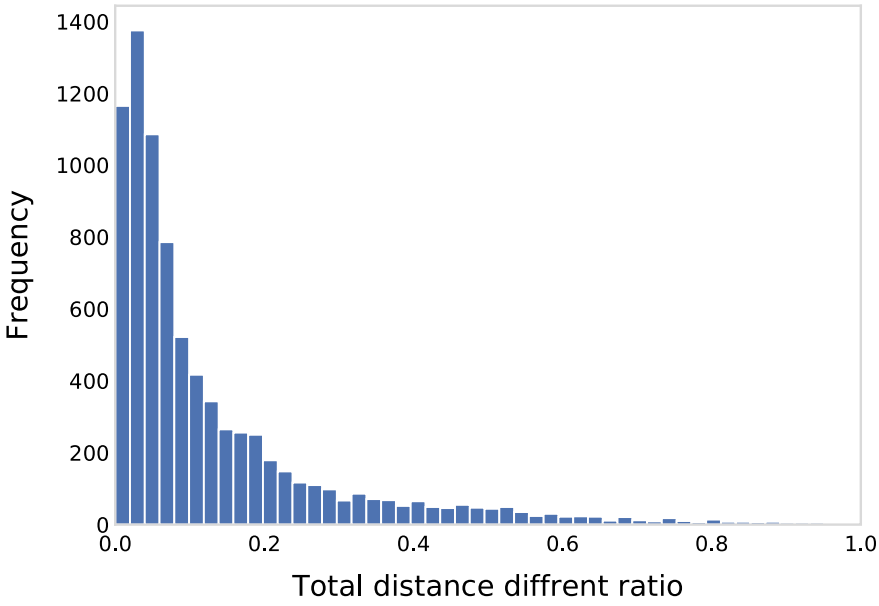

Fig. 3 Total distance different ratio distribution

can extract the pattern in the departure taxiway as controller's options from historical data by the clustering method.

We choose the DBSCAN algorithm as our clustering algorithm. One of the notable advantages of DBSCAN is that we are not required for a predefined number of clusters. It is an important feature because the number of options is different for each group of flight. Another advantage of DBSCAN is that it is able to identify outlier trajectories as noises so we can isolate those from processed data.

After the map-matching step, we can represent a trajectory as a list of nodes on the airport graph. Then, those trajectories are vectorized to input into the DBSCAN algorithm. We use Euclidean distance to define the difference between the two trajectories. The neighborhood threshold is 2 which means that we consider trajectories in one group are not different for more than two nodes. We only keep groups that contain more than three trajectories. An example of a clustering result can be observed in Fig. 4. Departure flights from gate B4 to runway 20C are grouped together for pattern extraction. Only two clusters are found, while the remaining trajectories are considered as noises.

Figure 5 shows the percentage of the clustered departures (after excluding the flights identified as noise) over total departures in each group (Gate runway). Thirteen groups keep less than 50% of the trajectories that reflect the high deviation of selected

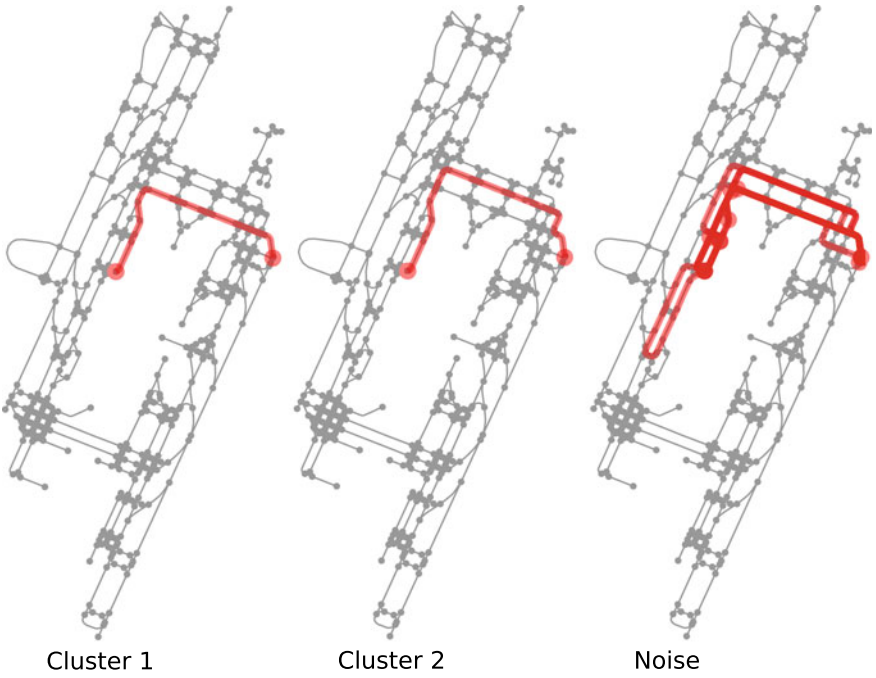

Fig. 4 Example of the clustering result for departure flights from gate B4 to runway 20C

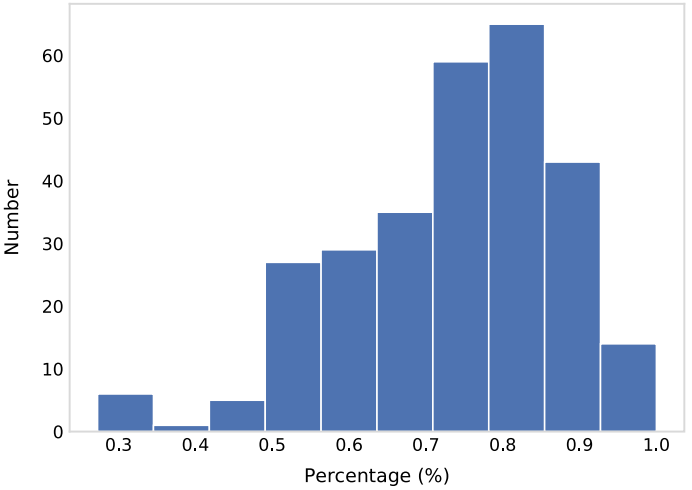

Fig. 5 Percentage of remaining clustered flights

taxi-routes. The average percentage of remaining flights is 75%, which means that the extracted options can cover 75% of the controller's decision.

4 Feature Engineering

The features which are considered in this study belong to four categories. The detailed description of those categories is mentioned in this session. The summary of all features is shown in Table 2.

Table 2 Summary of extracted features in four categories

Flight basic information	
5 features	Gate, runway, day-of-week, hour, aircraft_type
Selected option features	
2 features	estimated_travel_time (s), travel_distance (m)
Traffic features	
N features	traffic_score_0, …, $\text{traffic\_score}_{N-1}$
Weather features	
12 features	visibility (km), pressure (mbar), temperature (C), dewpoint (C), humidity (%), wind_speed (km/h), wind_dir_degrees(^{o}), fog ([0,1]), tornado ([0,1]), thunder ([0,1]), hail ([0,1]), rain ([0,1]),

4.1 Flight Basic Features

Each flight is specified by the gate, runway, and aircraft type features. Because those features are categorical, we encode them to the one-hot vector. Every value in an old column is split into a new column with two values one (exist) and zero (non-exist).

4.2 Selected Option Features

In our approach, to predict the taxi-time for departure flight, we first assign taxi-route for each flight and then estimate the travel time of each flight for given taxi-route. In this work, we only consider two features which are the estimated travel time and travel distance.

4.3 Traffic Features

Traffic features reflect the density of traffic of the airport at the time when the controller makes the decision of taxi-route assignment considering future aircraft movements. Given the flight plan of a departure aircraft which we want to assign taxi-route, we assume that all taxi-route of other aircraft in that period of time is fixed. Thus, we compute the traffic score for each option by computing the traffic score. Firstly, we introduce a trajectory prediction model for each flight on a taxiway based on combining the average travel time of road segments. Secondly, given a flight departure time, the traffic features for each option of that flight will be computed. In the given time window, we group the trajectory positions into multiple snapshots based on their timestamps with time step is 10 s. For each snapshot, we compute a traffic density map by mapping aircraft positions into a grid layer on the airport map with grid size is 100 m. The score of each cell is estimated by the number of aircraft in its area and the impact of neighboring traffic by spreading function.

4.4 Weather Features

The weather is also an important factor which affects controllers' decisions. Thus, we collect weather information at the airport updating every thirty minutes.

5 Predictive Models

5.1 Random Forest

Random Forest (RF) is an ensemble learning method for both classification and regression. It constructs multiple decision trees that are trained with different subsets of features and samples. The trees learn different knowledge from data and then vote for final prediction. It is highly robust with outliers/noises without skewing the prediction results and avoids overfitting due to the diversity of trees. One of the key advantages of RF, which suits our problem, is its capability to handle unbalanced datasets and to work with different types of features and range of feature values. Moreover, the interpretability of the model is also considered for understanding the impact of various features in prediction.

5.2 Predicting the Controller's Decision

A predictive model is built to predict controller decision in assigning a taxi-route for each departure flight. The features in flight basic information, traffic, and weather groups are used to predict the selected option of controllers in historical data. The possible decisions of controllers for each flight are the list of N extracted options in Sect. 4. The traffic scores are computed for N options to reflect the relationship between each option and the surrounding traffic. With this formulation, RF classifier is chosen as the predictive model. All the categorical features are encoded using a one-hot vector encoder that makes the total number of features for this model is 543 features.

5.3 Predicting Taxi-Time for Departure Flights

A predictive model is built to predict the travel time for each departure flight with assigned taxi-route. The features in all groups (flight basic information, selected option, traffic, and weather) are selected for the training of a predictive model. However, since the option is decided for a given flight, only the traffic score for that selected option is considered. With this formulation, the RF regressor is chosen as the predictive model. Similarly, a one-hot vector encoder is used for encoding the categorical features, and the total number of features is 153 features.

Table 3 Datasets and their size after each processing step

Version of dataset	Number of samples
Full one-month departure dataset	11,891
Preprocessing departure dataset	8128
Extracted option departure dataset	5875
Filtered departure dataset	4363

6 Experiments and Results

6.1 Dataset for Developing Predictive Models

From the original dataset, multiple processing steps have been performed on this data for cleaning and standardizing. Table 3 shows a summary of four versions of the datasets that we have produced. The total of departures in one-month data is 11891 movements. After the preprocessing step, only 8128 samples are kept. However, 2252 movements will be removed after the option extraction step since they are considered as noises by a clustering algorithm (DBSCAN). Finally, for each cluster, departures with abnormal taxi-time are removed. Thus, the final dataset only contains 4363 samples ($\approx$ 36.7% raw data). One of the future works is investigating new preprocessing and clustering algorithms to increase this percentage.

6.2 A Predictive Model for Controllers' Decision

To ensure the existence of departures from all pairs of gate and runway in both training and testing data, the data is grouped with each pair and then partitioned. We find the best RF model by applying grid search on the two main hyperparameters (the max depth and the number of estimators). We evaluated 25 sets of parameters which are combined from max depth in (50, 100, 150, 200, 250) and number of estimators in (50, 100, 150, 200, 250). The fivefold cross-validation method is used to assess the model performance for each set of parameters. Figure 6 shows the result of the tuning process. When the number of estimators is greater than 100 and the max depth is greater than 100, the model is converged. The best accuracy is 70.8% when max depth is 100 and the number of estimators is 150. This set of parameters is chosen for training our predictive model. Figure 7 shows the coverage of the controller decision for departures in top recommends. More than 70% of controller decisions can be found at the first suggestion while approximately 90% of the decision will be covered in the first two suggestions. This high coverage, like in other recommendation systems, will increase the acceptance of users since the relevant items are successfully retrieved within the top recommendations.

The list of the most important features is shown in Table 4. The features are ordered by Gini importance, which can be considered as the percentages of the contribution

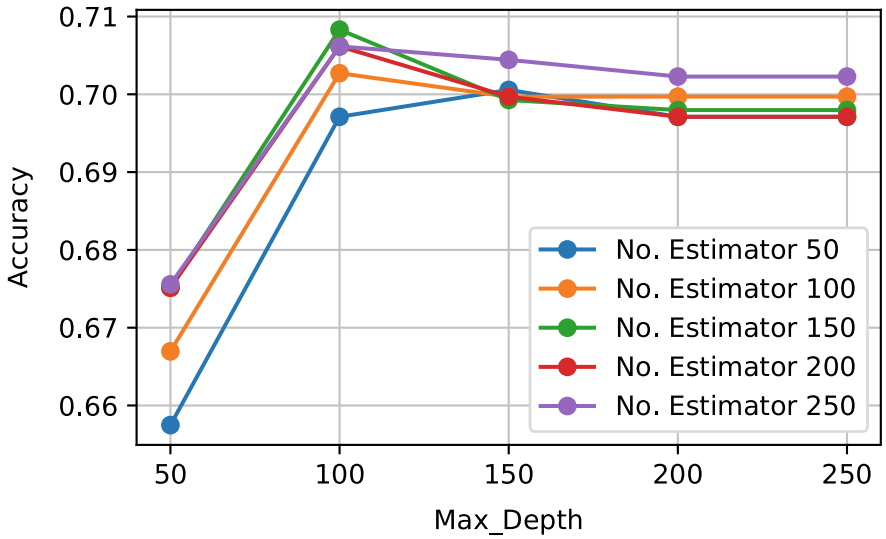

Fig. 6 Model performance for a different set of parameters

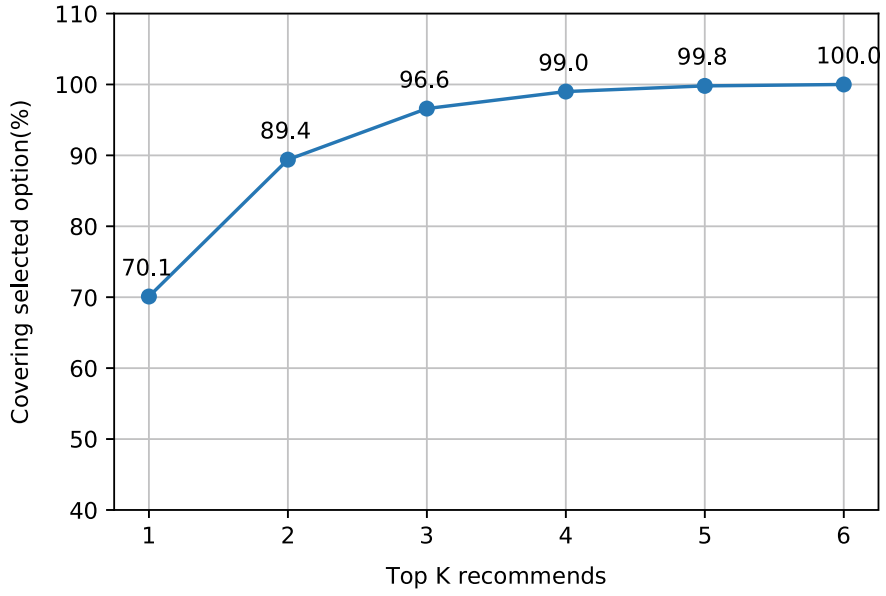

Fig. 7 Coverage of controller decision in top K recommends

Table 4 List of most important features for the taxi-route model

Index	Features	Gini importance (%)
1	Hour	3.30
2	Pressure (mbar)	2.96
3	Day-of-week	2.94
4	Wind_dir_degrees (°)	2.86
5	Temperature (°C)	2.81
6	Humidity (%)	2.75
7	Wind_speed (km/h)	2.72
8	Dewpoint (C)	1.97
9	Visibility (km)	1.76
10	Aircraft_type_H	0.74
11	Aircraft_type_M	0.73
12	Rain ([0,1])	0.46
13	Thunder ([0,1])	0.42

of each feature. Since we have several features and none of them dominates in the contribution, the Gini importance for all features is small (maximum 3.3%). However, the top 11 features have bigger contributions compared to the others. In which, the hour-of-day and day-of-week are two of the most important features which affect the controller's decision. The next ones are weather features such as pressure, wind direction, temperature, etc. Besides, aircraft type is also in the top features for predicting the controller's decision. Even though rain and thunder features are very important, their contributions are less than the others in our model. That happens due to the nature of our data, in which only less than 150 cases are recorded with rain or thunder conditions. With more dataset, which covers other seasons and weather conditions, we believe their importance can increase significantly.

6.3 A Predictive Model for Taxi-Time

We select the Dead Reckoning (DR) method as a baseline model. The DR method uses the tenth percentile value of taxi-time distributions for departures in the same group (in our case is the same option) as the predicted taxi-time [1]. To assess the performance of our predictive models for taxi-time, we apply the fivefold cross-validation method. Two algorithms, chosen for comparison, are: Random Forest (RF) and Linear Regression (LR). Table 5 shows the results of models with four metrics: Mean Taxi-Time Difference (MD), Mean Absolute Error (MAE), Root Mean Square Error (RMSE), Mean Absolute Percent Error (MAPE). Different metrics are used to provide better observation and assessment of model's performance.

The MAPE of RF and LR models is 22.06 and 23.46%, respectively, while the DR model error has higher error with 27.55%. The distributions of MAPE of RF and LR

Table 5 Comparison of performance metrics

Performance metrics	LR	RF	DR
Mean taxi-time difference (min)	0.15	0.22	−2.8
Mean absolute error (min)	2.01	2.07	2.96
Root mean square error (min)	2.52	2.56	3.91
Mean absolute percent error (%)	22.66	23.46	27.55

models (shown in Fig. 8) have power-law shape and are skewed to zero. LR model's performance is better than RF model on flights which have an absolute percent error of less than 10%. However, the difference between those two models is insignificant, around 1.4%. Besides, the distribution of MAPE in the DR model is flatter and has a high variance compared to those of the RF and LR models.

For more details, Table 6 compares the model performance by ± *k*-minute error metric. There are 76.71% of the flight's taxi-time predicted by the LR model, and 75.65% of the RF model has an error within 3 min, significantly better than DR with 58.9%. For the error range, ± 5-minute, that difference becomes more significant. That error range covers most of predictions by LR and RF (95.36 and 95.29%) while only 78.5% for DR. In conclusion, both models using RF and LR have similar performances and are much better than the baseline model (DR).

The list of the most important features is shown in Table 7. The features are ordered

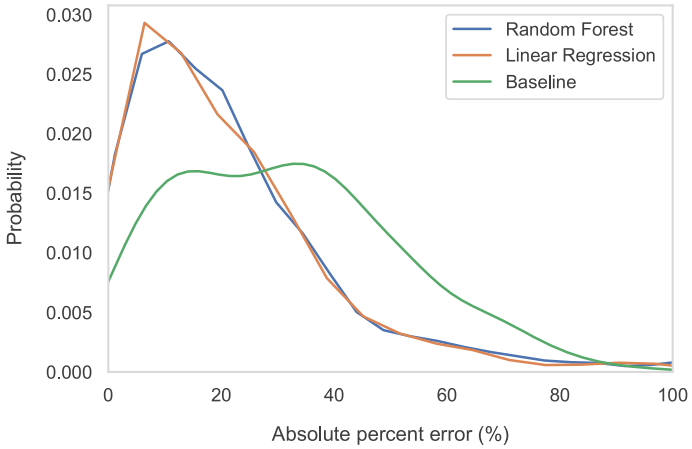

Fig. 8 Distributions of absolute percent error of taxi-time prediction

Table 6 Departures within ± *k*-minute error window

Error window	LR (%)	RF (%)	DR (%)
± 2-minute	56.30	56.02	45.11
± 3-minute	76.71	75.65	58.90
± 5-minute	95.36	95.29	78.75

Table 7 List of most important features for f taxi-time prediction models

Rank	Random forest	Linear regression
1	DR	Fog
2	Traffic score	Tornado
3	Hour	Aircraft type
4	Pressure	Gate–303
5	Wind direction	Hail
6	Estimated travel time	Gate–202L
7	Day-of-week	Runway
8	Wind speed	Gate–D40R
9	Visibility	Gate–462R
10	Temperature	Gate–462L

by Gini importance for the RF model and by weight for the LR model. We notice that although LR performs slightly better than RF, the list of feature importance of RF is more explainable and more general. This is reasonable since LR tends to stress the specific features related to rare events. Because RF combines the predictions from decision trees that it can produce more generalized results. Consequently, the most important features for taxi-time prediction include estimated travel time, traffic scores of options, hours, day-of-week, and weather features.

7 Conclusion and Future Work

7.1 Conclusion

In this work, we have proposed an approach which can both suggest taxi-route and predict the corresponding taxi-time. The taxi-route model is developed considering controller preferences, which are learned from historical data. Moreover, we also take advantage of taxiing trajectories to form the controller's decision that not only limits the potential options but also is more practical. As a result, the model can cover the controller's decision up to 70% in the top-1 and 89% in top-2 recommends. The second predictive model for taxi-time can predict the taxi-out time with high accuracy with given assigned taxi-route. The MAE is less than 2.07 min for all departure flights, and RMSE is approximately 2.5 min. Moreover, the $\pm$ 3-minute error window cover around 76% of departures while more than 95% of departures are within the $\pm$ 5-minute error window. Two machine learning models, RF and LR, show similar performances in estimating the taxi-time; however, from our observations, RF can provide a more stable result and interpretability due to its characteristics.

7.2 Future Work

To increase the performance of both models, the preprocessing step will be investigated with a better map-matching algorithm for standardizing data. More surface movement data will be collected and analyzed to propose new features for predictive models. Finally, the integration of ground movement and other surface operations will be investigated.

Acknowledgements This research is supported by the National Research Foundation, Singapore and the Civil Aviation Authority of Singapore, under the Aviation Transformation Program. Any opinions, findings and conclusions or recommendations expressed in this material are those of the author(s) and do not reflect the views of National Research Foundation, Singapore and the Civil Aviation Authority of Singapore.

References

1. H. Lee, W. Malik, Y.C. Jung, Taxi-out time prediction for departures at charlotte airport using machine learning techniques. in *16th AIAA Aviation Technology, Integration, and Operations Conference* (2016), p. 3910
2. S. Corrigan, L. Martensson, A. Kay, S. Okwir, P. Ulfvengren, N. McDonald, Preparing for airport collaborative decision making (a-cdm) implementation: an evaluation and recommendations. Cogn. Technol. Work **17**(2), 207–218 (2015)
3. S. Ravizza, J. Chen, J.A. Atkin, P. Stewart, E.K. Burke, Aircraft taxi time prediction: comparisons and insights. Appl. Soft Comput. **14**, 397–406 (2014)
4. S. Ravizza, J.A. Atkin, M.H. Maathuis, E.K. Burke, A combined statistical approach and ground movement model for improving taxi time estimations at airports. J. Oper. Res. Soc. **64**(9), 1347–1360 (2013)
5. I. Gerdes, A. Temme, Taxi routing for aircraft: creation and controlling. in *The Second SESAR Innovation Days* (2012)
6. Organisation de l'aviation civile internationale. in *Advanced Surface Movement Guidance and Control Systems (A-SMGCS) Manual. ICAO* (2004)
7. M. Ester, H.-P. Kriegel, J. Sander, X. Xu et al., A density-based algorithm for discovering clusters in large spatial databases with noise. Kdd **96**(34), 226–231 (1996)
8. J.M. Ten Have, The development of the NLR ATC research simulator (Narsim): design philosophy and potential for ATM research. Simulation Practice Theory **1**(1), 31–39 (1993)
9. W.Y.O Chieng, M.A. Quddus, R.B. Noland, Map-matching in complex urban road networks. Brazilian J Cartograp (Revista Brasileira de Cartografia) 55.2, 1–18 (2003)
10. D. Bernstein, A. Kornhauser, An introduction to map matching for personal navigation assistants (1996)
11. C.E. White, D. Bernstein, A.L. Kornhauser, Some map matching algorithms for personal navigation assistants. Transp Res Part C: Emerg Technol **8**(1–6), 91–108 (2000)

Dealing with Adverse Weather Conditions by Enhanced Collaborative Decision Making in a TAM APOC

F. Piekert, N. Carstengerdes, R. Suikat, and S. Schier

Abstract This paper will provide an insight into enhanced collaborative decision making being conducted in adverse weather conditions in a simulated Oslo airport environment. This simulation is part of the Total Airport Management (TAM) research in the Single European Sky ATM Research program (SESAR 2020) as project PJ.04. SESAR2020 is operated in two defined program waves, wave 1 covering the years 2016–2019 and wave 2 following until 2022. This paper will focus on a set of two out of seven V2 level validation exercises that are conducted in wave 1 of PJ.04′s Solution 2 (PJ.04–02), addressing concepts for Collaborative Airport Performance Management. The key objective of PJ.04–02 is to develop multi-stakeholder decision support for airport management stakeholders especially in adverse conditions (e.g. bad weather, union strikes or unforeseen events such as runway blockages). In the Oslo airport environment winter conditions are a major reason for performance degradation of airport operations. An enhanced integration of stakeholder actions and collaborative operations planning is expected to provide performance benefits. The philosophy of collaborative decision making advocated by SESAR 2020 is that of 'consensus' building amongst the different airport stakeholders through a common impact assessment and a structured solution finding process resulting in mutually agreed actions. The objective is to raise situation awareness and introduce a collaborative problem solving approach leading to better, earlier and therefore more stable solutions. Orchestrated by a moderator, the so-called airport operations center supervisor, the global impact assessment is supported by each stakeholder evaluating the consequences for their own operations, documented in an electronic impact and corresponding solution message. The validation and

F. Piekert (✉) · N. Carstengerdes · R. Suikat · S. Schier
Institute of Flight Guidance, DLR German Aerospace Center, Braunschweig, Germany
e-mail: Florian.Piekert@DLR.DE

N. Carstengerdes
e-mail: Nils.Carstengerdes@DLR.DE

R. Suikat
e-mail: Reiner.Suikat@DLR.DE

S. Schier
e-mail: Sebastian.Schier@DLR.DE

Air Traffic Management and Systems IV, Lecture Notes in Electrical Engineering 731,
https://doi.org/10.1007/978-981-33-4669-7_8

assessment of the underlying conceptual approach to collaborative airport performance management in adverse conditions requests for an artificial airport environment. In contrast to a real airport the simulated environment allows for any necessary changes in weather situation, traffic patterns or support system composition while keeping the operators in the loop. The target level for the validation experiments is V2 (referring to the European operational concept validation methodology), requiring the simulator to allow for an operational concept feasibility assessment while providing emulation of all airport processes and working positions of the airport management. The objective assessment of benefits credited to specific operational improvements under consideration of the validation exercises PJ.04–02.V2.04 and PJ.04–02.V2.09 requires a stepwise approach in which the functionality and system complexity is consecutively enhanced. The baseline was represented by the results achieved by SESAR 1, providing an airport operations center (APOC), basic processes and support system functionality. The functionality of the V2.04 setup reflected the SESAR2020 solution regarding advanced decision support, providing dynamic demand and capacity balancing alongside a guided enhanced collaborative decision making process and enhanced meteorological forecasts by weather alerts. The V2.09 solution setup provides additional information support by a performance dashboard, taking into account probabilities for additional diverted traffic. Two exercise simulation runs were executed for each setup, subjecting the Oslo operators with different meteorological phenomena and resulting operational challenges. The PJ.04–02 validation objectives were broken down into exercise specific objectives, allowing for an impartial feasibility assessment based on objective metrics and qualitative human performance criteria. Preliminary exercise analysis results indicate a well-received conceptual approach, the stepwise functionality enhancement complying with benefit increase expectations.

Keywords SESAR · Total airport management · Collaborative airport performance management · Collaborative airport decision making · Validation · PJ.04

1 Introduction

1.1 Total Airport Management Research

Total Airport Management (TAM) has a research history of more than twenty years. Foreseen in the beginning as a multi-modal airport management approach [1], the research of the German Aerospace Center (DLR) focused on airside, landside and the combined approach in varying projects [2–7].

When the European research program SESAR started to address TAM nearly a decade later, a focus on airside processes [8–10] had to be taken to not overlap with ground based transport research being conducted by the European Commission's other research programs.

Complementing the research on TAM, various DLR projects focused on evaluation and validation techniques of how to measure the benefits credited to TAM and how to build and operate adequate research environments [11–16]. DLR's work resulted in a simulated airport environment where all relevant parameters (e.g. traffic samples, weather impact, and resource availability) can be fully controlled [17–20]. This is used to study conceptual questions and is becoming more important due to the collaborative approach between various stakeholders interacting in airport operations centers (APOC).

1.2 The PJ.04 Total Airport Management Industrial Research Project

The research described in this work was conducted under the framework of the SESAR 2020 industrial research project PJ.04 Total Airport Management which is structured into the two solutions "Enhanced Collaborative Airport Performance Planning and Monitoring" (solution PJ.04–01) and "Enhanced Collaborative Airport Performance Management" (solution PJ.04–02). The work program of PJ04–01 is previously presented in [21] in more detail, the work laid out in this article contributes to PJ.04–02.

The work carried out by PJ.04–02 has to follow established processes and guidelines prescribed by the SESAR Joint Undertaking (SJU) [22–24]. Projects are expected to provide evidence of their claimed development success (concept and/or prototypes) by conducting validation activities. These follow the European Operational Concept Validation Methodology [E-OCVM; 25,26]. Having achieved a progressed project phase, PJ.04–02 is expected to provide evidence for its V2 maturity (proof of operational feasibility) at the end of its project's lifecycle. This guides the approach of the experimental designs required to gather all necessary evidences.

1.3 Solution PJ.04–02 Enhanced Airport Performance Management

The solution PJ.04–02 addresses four operational improvements regarding airport operations:

- Enhancement of airside / landside performance management
- Proactive management of meteorological impacts
- Proactive management of capacity shortfalls by taking airline priorities into account.
- Proactive management of environmental restrictions

These four improvements aim at a better collaborative management of airport processes and thus support the optimization of the airport's performance, especially in adverse weather conditions. The work that will be presented in this publication addresses the enhanced airside/landside performance management and the proactive management of meteorological impacts.

2 Deficiencies and Research Challenges

Regarding airside/landside performance management and proactive management of meteorological impacts, there is optimization potential regarding the collaborative decision making process [27]. Interviewing operational experts, this potential is specially revealed in adverse weather conditions. Meteorological forecasts are currently individually interpreted by each stakeholder of the airport management. As such stakeholders might come to different conclusions and different action plans. Hence situations might occur where airport and air traffic control plan to close down operations while airlines try to keep up their full operation as they do not read the forecasts to significantly impact the operations. In consequence, an imbalance between capacity and demand occurs.

Optimizing these operational situations requires a collaborative process where the individual impact assessment is aligned and all stakeholders agree on a common solution strategy. Ideally, this results in airport and air traffic control providing the resources necessary to conduct the essential flight operations (intercontinental flights, flights with multiple connections at other airports, etc.) while airlines try to delay or reduce traffic of less importance (dead-end flights, less occupied flights, etc.). Last but not least ground handling should align their resources to support a quick recovery of the operations once the cause for capacity shortfall has passed.

This objective can only be reached upon sufficient support of the stakeholders. As such three general improvements are focused within this paper [28, 33]:

- **Meteorological impact assessment:** Improved meteorological data must be provided to all stakeholders including a standardized impact analysis which considers agreed limits. Reaching those limits triggers the need for all stakeholders to take collaborative actions.
- **Collaborative procedure:** A common procedure must be designed which all stakeholders follow to assess the impact of a capacity shortfall and agree on necessary actions.
- **Demand capacity balancing:** Demand and capacity of all relevant airport resources must be constantly monitored, displayed to the airport management stakeholders and discussed upon a noticed imbalance.

These three general improvements are addressed in PJ.04–02 by a set of technical systems (cf. Fig. 1). The demand for a meteorological impact assessment is fulfilled by the Weather Information System for Airport and Decision Making (WISDAS) of LEONARDO. WISDAS provides detailed weather data and alerts to all stakeholders.

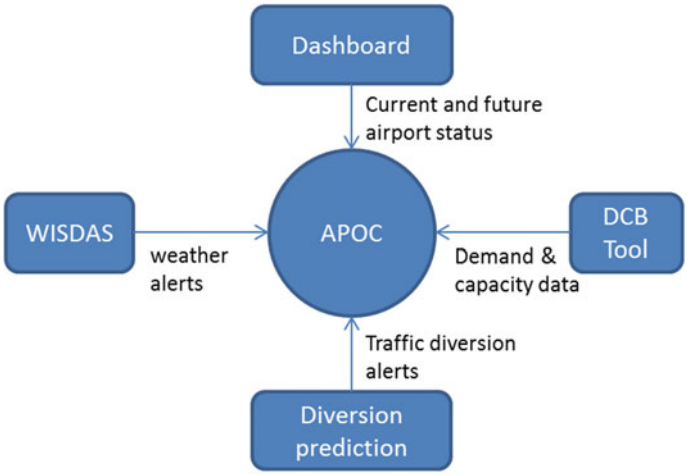

Fig. 1 Technical tools addressing the aimed improvements

The collaborative procedure was developed by operational experts and researchers within SESAR2020 contributed by EUROCONTROL's total airport management dashboard. This dashboard assures that all stakeholders are aware of the current and future airport status. The demand capacity balancing (DCB) is assured by the so-called DCB Tool of SINTEF. The DCB Tool constantly monitors runways, stands and ground handling capacities. It triggers the collaborative process once an imbalance is detected. The process is supported by a central messaging system and task assignment within the DCB Tool. Moreover a diversion prediction of the University of Warsaw on behalf of Polish Air Navigation Service Provider PANSA contributes to the demand assessment. This tool alerts the stakeholders once a high likelihood for reduced airport operations at one of the neighboring airports is detected. The diversion predication analyses the flightplan and trajectories to provide the stakeholders with an estimate number of diverting traffic.

The WISDAS, the dashboard, the DCB-tool and the diversion prediction encounter the existing operational challenge of collaborative adverse weather management in airport operations. This solution is designed as an enhancement of existing airport processes (e.g. Airport Collaborative Decision Making, A-CDM) and planning tools (e.g. Pre-departure sequencer and airport information sharing platform). It was validated by DLR utilizing a Human-In-The-Loop simulation to assess aspects like usability, trust and acceptance.

3 Validation Design

As a basis for the validation, DLR's ACCES facility (Airport Control CEnter Simulator) was utilized [29, 30]. The ACCES provides a simulation of the airport processes, close-to-reality user interfaces and the possibility to design multiple working positions in several airport and airline operations centers. For this validation the user interfaces and the simulation were adapted to Oslo airport.

3.1 Research Scenarios for Oslo

The exercise conducted a series of real-time simulation runs, covering Oslo Gaerdemoen airport (OSL). The full cycle of aircraft operations from outstation departure via approach, turnaround and the flight to the next station were simulated. The simulation provides all A-CDM milestones and procedures as well as Air Traffic Flow and Capacity Management (ATFCM). As such the stakeholders were able to apply regulations to Oslo airport as well as to conduct pre-departure sequencing.

The essence was to study the effects of the solution systems and procedures applied on strong wind and winter weather situations. Oslo was chosen since the operations are heavily affected by adverse weather such as snow fall. The tools developed in SESAR have a high potential to improve operations under the Oslo conditions.

The scenarios are real flight plans of a full operating day in Oslo (depicted in Fig. 2). The impacting snow and wind events were designed in a way that they hit the airport around 16:00 UTC and reduce capacity (dashed line in Fig. 2) by approx 85%. The airport stakeholders were able to influence the traffic according to the ATFCM and A-CDM procedures by changing flightplan times (e.g. Estimated or Target Off Block Times—EOBT / TOBT) or resource capacities (e.g. runway throughput, ground handling staff, stand assignment).

3.2 APOC Stakeholders

As shown in Fig. 3, the exercise placed five different operators from three stakeholder groups in the APOC, consisting of two ground handler station managers acting as airline representatives, one representative from the local air traffic control and two representatives from the local airport, whereas one acted as the APOC supervisor and the other one as the stand and gate allocation manager.

Additionally, three airline stakeholder operators where placed in a nearby room, each representing the flight dispatcher in the airline operation center (AOC). Figure 3 depicts this setup. Communication between APOC and AOCs was possible through electronic means (chat—messages, phone system); while within the APOC in addition the direct verbal channel was encouraged.

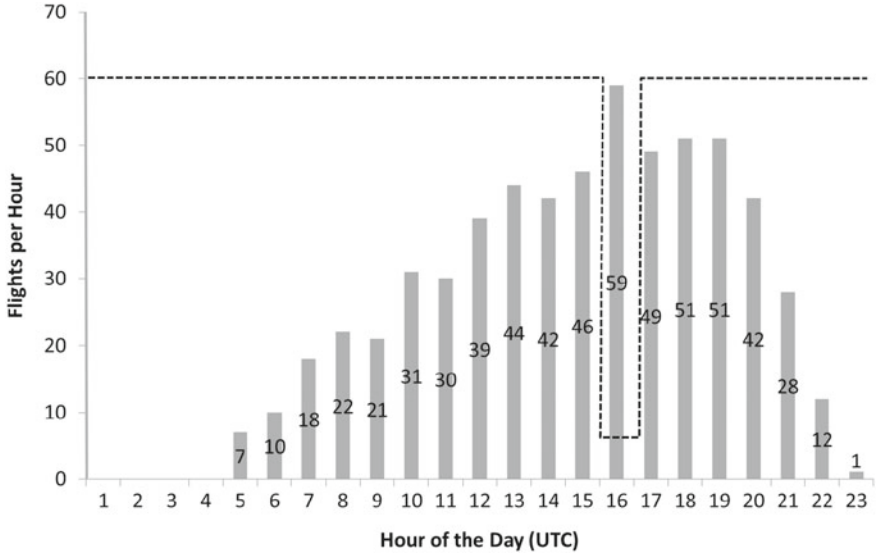

Fig. 2 Demand and capacity of the selected scenarios

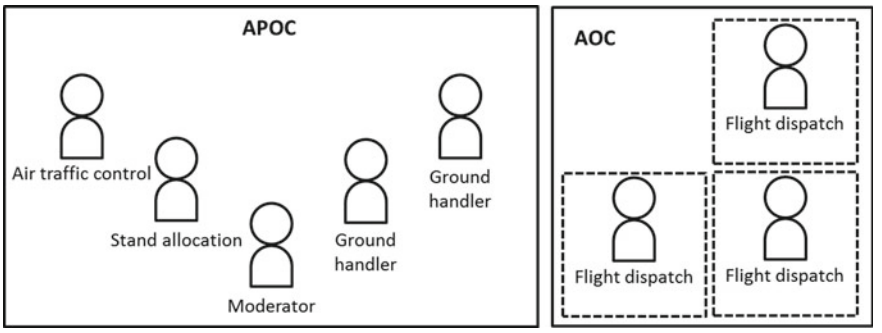

Fig. 3 APOC stakeholder group

The different stakeholders have appropriate roles (cf. [28]).

- The APOC supervisor oversaw and coordinated the planning process and actions among the other stakeholders.
- The air traffic control stakeholder was responsible for the runway management, pre-departure sequencing and defined the actual runway capacity during the degraded conditions in the scenario.
- The airport representative in this exercise conducted stand/gate allocation planning and management.

- The two ground handlers were responsible to manage the turnaround processes, control handling capacities and they acted as local representatives on behalf of the airlines, communicating with the airline stakeholders.
- The airline stakeholders worked as flight dispatchers being responsible for managing flight rotations plans.

In most APOCs, a representative of the local meteorological service provider ensures the timely delivery of metrological information and partially the expected impacts on operations. For the purpose of the exercise, this role was replaced by a simulation staff member. Also the multiple roles within the flow management chain have been replaced by simulation staff. The flow managers are responsible for collecting the constraints of airport and airspace control units. They forward them as traffic regulations to the central European network management in Brussels. The Network Management Operations Center (NMOC) applies the regulations by issuing slots to flights which are designated to a constrained area or airport. Except for the flow manager and the meteorologist, all roles were staffed by operational experts from European airports or airlines.

The different stakeholder participants in the exercise were provided with different systems, according to their role and responsibility in the APOC and exercise. Each working position was equipped with a common data display and an individual resource planning tool. The common data display was adapted to the look and feel of the operational information display at Oslo airport. The resource planning tools were provided by the simulation allowing the stakeholders to plan their resource (e.g. runway, stand, ground handling staff, aircraft).

3.3 Simulation Environment

The simulation environment consists of the hardware (e.g. monitors, keyboards, computers, phones, tables, and chairs), user interfaces and various simulation software components. The entire exercise was driven by a sophisticated array of simulation components [17, 19, 20, 31, 32] developed by DLR (Fig. 4). These provided the data for the user interface applications and the support systems.

The main driver of this simulation array is the milestone simulation which is a process simulation generating A-CDM milestones based on flightplan data and resource availabilities. The flightplan and milestone data is stored in an airport database (central element in Fig. 4). All user interfaces access this database for updating the information in the corresponding tools, reflecting changes of the airport processes' durations or sequences. For instance flight schedules can be adopted using the DLR airline rotation planner. The ground unit planner allows handling staff allocation. The pre-departure sequencer calculates target takeoff and startup times and the airport gate planner enables the stand and gate allocation. Moreover, systems to

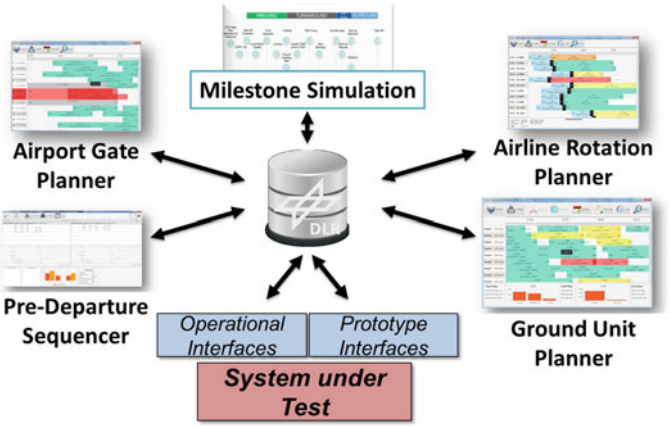

Fig. 4 DLR simulation environment

be tested on basis of the DLR airport management simulation can be connected to the platform either via operational or individual interfaces emulating real airport data exchanges.

3.4 DCB & CDM Process

The collaborative decision making (CDM) process used for the demand capacity balancing (DCB) was developed within SESAR 2020 and conducted according to the PJ.04–02 OSED [33] (Operational Services and Environment Description—the central concept document of Solution PJ.04–02). It was designed around the application of a series of use cases. The use cases defined sequences of activities to be executed by the appropriate APOC stakeholders under various conditions and prerequisites. It was used to capture the interactions between the operators in the APOC when they collaborate to resolve situations in a more formal manner.

A-CDM and SESAR 1 [34–38] do not prescribe a distinct collaborative decision making process. As such, a high level procedure as shown in Fig. 5 was assumed and provided to the stakeholders as the common process for the baseline.

For the solution runs PJ.04–02 used a more detailed and structured approach, targeted towards sustainable quality decision making routines. As shown in Fig. 6, this approach relies on the definition of three official messages which are distributed among all stakeholders. After the alert, an initial impact message is defined including the moderator's assessment of the situation. This initial message is enriched with the impact evaluation of the other stakeholders to receive the agreed impact message. Within the next step, the stakeholders develop a solution and publish a solution message to agree in a strategy solving the operational challenge. Finally this solution is implemented into the airport system.

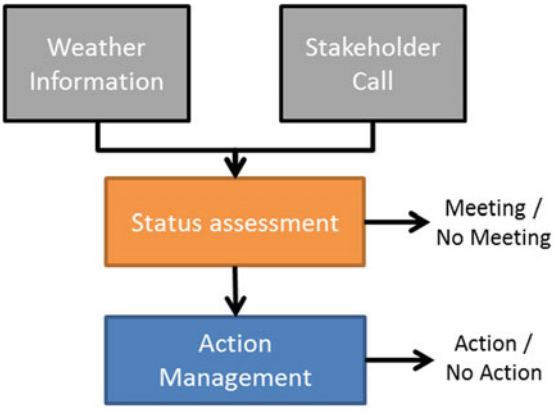

Fig. 5 The collaborative process in the baseline

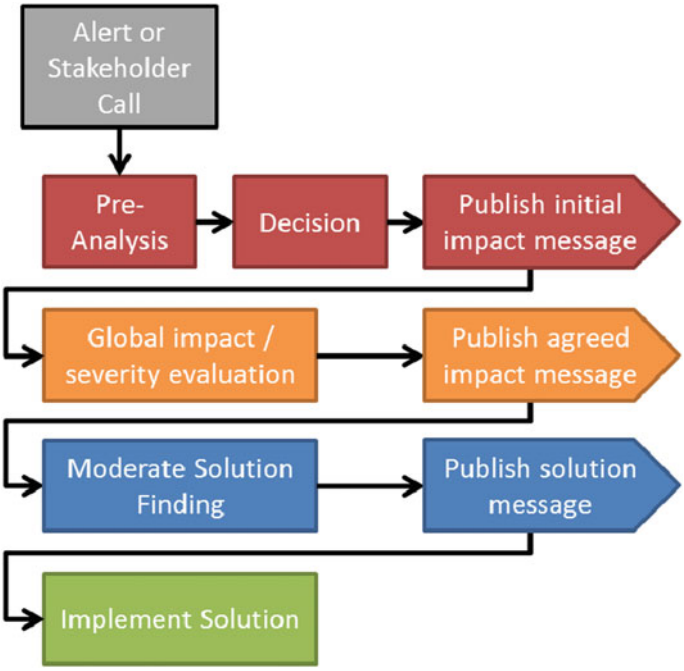

Fig. 6 The collaborative process in the solution

In SESAR 2020, it was prescribed to use a specific modelling tool for operational and technical level process modelling. The tool orients itself around the use of the Unified Modelling Language (UML) and expresses interactions between different entities in a graphical way. The model charts generated can vary from simplistic

towards very complex, depending on the task and the group of stakeholders/entities to involve.

The tool suite provided in the APOC simulation has been designed to implement those decision making flows, to support the APOC supervisor in initiating the most appropriate measures at the required moment and to start the discussion and decision making process between the relevant stakeholders. Tasks and information were exchanged electronically between the operators, the results were collected by the APOC supervisor and an overall impact assessment communicated. Later in the process the mitigation decision was communicated similarly, providing the agreed solution approach to all involved parties, followed by the plan implementation by the stakeholders.

4 Execution and Evidence

The validation exercise was executed over several consecutive days including multiple sessions for a single run. A combination of real-time interactive phases combined with fast-time based fast forwarding allowed the operators to take decisions over given situations and events and then, after the fast forward, see the simulated outcomes based on taken decisions.

This approach was considered necessary to assess the fulfillment of the high level validation objectives, e.g. OBJ-AO0813-VALST2.001 "To validate that collaborative recovery procedures and associated predictive and decision support when carried out with appropriate tools assisting airport, network, Air Space Users and Air Navigation Service Provider stakeholders to anticipate, understand and collaboratively manage large scale disruptive adverse events will reduce impact and knock-on effects, optimizing solutions whilst ensuring that users' end-to-end processes are managed."

After each session questionnaires were provided to the participants to obtain feedback used for post-exercise analysis and evidence gathering whether or not the exercise success criteria have been met, e.g. CRT-04.02-V2-VALP-EXE4–0011 "Decision support tools taking into account MET impact assessments in adverse weather conditions trigger appropriate pro-active CDM actions by the airport stakeholders."

The entire exercise was designed as a staged approach that involved the proper setting of a baseline result, going through a first enhancement evolution (named V2.04) and then complementing with the second evolutionary step (named V2.09). This approach was considered necessary to identify the different influences brought by the support system evolution and increased sophistication.

In total seven operational experts took part in the exercise.

4.1 Baseline and Solution Runs

To identify the effects that the introduction of the support systems and the concept brought, a baseline composition of systems and procedures was defined. This was based on previous SESAR 1 project results and the anticipated state-of-the-art brought in the future by the sister solution PJ.04–01, on which the solution PJ.04–02 bases [27]. Two exercise runs were executed for each of the three settings, varying between the two underlying central weather events that introduced the operational problems.

4.1.1 Baseline Reference

The reference scenario assumes an APOC where A-CDM processes with current procedures are employed as well as an advanced airport operation plan as defined in SESAR 1 [37, 38] is operational at the airport. Hence general information sharing between stakeholders is established and planning information (e.g. the target off-block time—TOBT) is exchanged. Basic demand and capacity predictions are available in an aggregated form. The operational procedures regarding bad weather operations are the ones currently in use at OSL airport. Weather information is available from standard forecast messages (TAF, METAR).

4.1.2 Solution Step 1: V2.04

The intermediate scenario comprised an established and controlled demand capacity process to jointly plan the airport resources and advanced meteorological prediction and alerting services to allow more precise forecasts and alert triggering based on predefined thresholds. As such WISDAS and the DCB tool were activated for the participants. WISDAS supported the APOC operators in assessing the operational impact of the predicted weather situation and the DCB tool guided the stakeholders through the structured DCB process and provided additional information on affected Key Performance Indicators (KPIs).

4.1.3 Solution Scenario 2: V2.09

The target solution scenario featured additionally to the previous step the EUROCONTROL dashboard to show the airport status. Further, anticipated additional demand due to diverted flights from neighboring airports due to weather is provided by the diversion prediction tool. The established CDM process remained unchanged.

4.2 Evaluation Method

The evaluation of the new concept and systems is based on subjective and objective data. The subjective data is gathered by questionnaires collecting operators' feedback. The objective data is provided by the simulation engine which records the generated flight data (A-CDM milestones, resource requests and clearances, etc.).

4.2.1 Questionnaires

Literature and state-of-the-art research offers a large variety of questionnaires that can be used for a multitude of different assessment purposes. Several are considered as standard works and some are custom-shaped (bespoke questionnaires) for singular purposes. In the exercise aspects of human performance, such as system acceptability, performance and operational concept feasibility were targeted and the operator responses captured in LimeSurvey.

To assess the human performance aspects of the exercise a subset of the EUROCONTROL SHAPE[1] questionnaires [39] SATI (SHAPE Automation Trust Index), AIM (Assessing the Impact of Automation on Mental Workload), STQ (SHAPE Teamwork Questionnaire) and SASHA (Situational Awareness for SHAPE) were used. Moreover the SUS (System Usability Scale [40]) and bespoke questionnaires were answered by the participants.

4.2.2 Objective Data Analysis

Objective data analysis was based on the recorded simulation and tool system data. The recorded data encompassed for example the full set of A-CDM event data for each flight operation, the updates to various data fields (e.g. the TOBT or stand allocation changes), allocated resources (e.g. stand allocation plans or ground handling crew assignments) or set capacities (for e.g. the runway or maximum handling capacities).

This data is analyzed according to the SESAR 2020 performance framework methods. In this framework distinct calculations and criteria are defined to determine and assess the KPIs like punctuality and predictability.

[1] https://www.skybrary.aero/index.php/SHAPE

5 Results

This paper focusses on the results of the bespoke questionnaire to provide some initial findings towards the major three improvements (meteorological assessment, collaborative process and demand capacity balancing). The results of the standardized questionnaires and the objective data are still under evaluation and will be presented in future publications.

For each of the improvements one bespoke questionnaire with multiple items was filled out by the participants. The feedback was given on a seven point Likert-scale, as shown in Table 1.

5.1 Meteorological Impact Assessment

The meteorological impact assessment was evaluated by seven questions ("*A*"-"*G*") shown in Fig. 7. The answers indicate an increase in assessment ability based on increased system support from reference via V2.04 towards V2.09 configuration.

Table 1 Likert scale rating options

x-axis	Description
0	strongly disagree
1	disagree
2	somewhat disagree
3	neutral
4	somewhat agree
5	agree
6	strongly agree

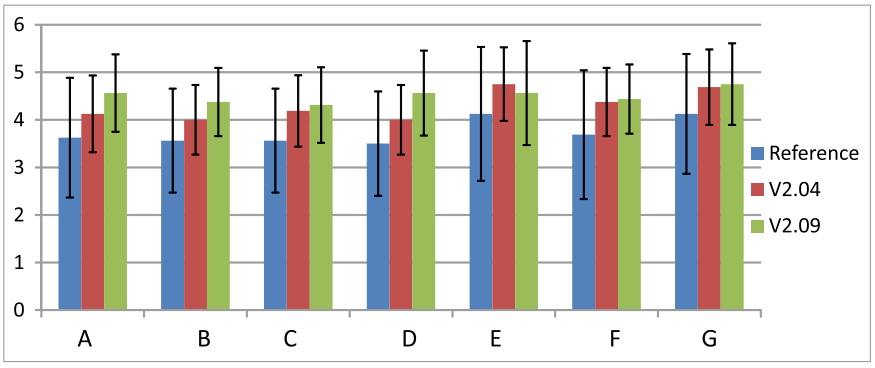

Fig. 7 Questionnaire results on usefulness of MET impact assessment

Table 2 *x*-axis descriptions of Fig. 7

x-axis	Description
A	I was able to assess the likelihood of key meteorological conditions
B	I was able to assess the intensity of key meteorological conditions
C	I was able to assess the duration of key meteorological conditions
D	I was able to assess the impact of occurrence of key meteorological conditions
E	I have confidence in the data provided
F	I have sufficient information on the impact of MET events
G	I trust the MET data provided

Starting around between "neutral" and "somewhat agree", the participants evaluated their ability increased towards "somewhat agree" / "agree". These results show that the participants felt to be better able to understand and evaluate the weather information regarding the anticipated impact on operations—as a team and on their own (Table 2).

The element "*E*" additionally increases from reference to solution and supports the feedback from the operators that the solution systems empower them to better understand the impact and have a higher confidence in the results. The negligible and not significant decrease from V2.04 to V2.09 configuration is a single feedback answer.

The final two items "*F*" and "*G*" follow the expected and observed increase-pattern and show that the new systems provide more and more trustworthy information.

5.2 Collaborative Process

Twelve questions regarding the collaborative process were posed. Selected four of the questions and ratings are given in Fig. 8 (Table 3).

The answers in Fig. 8 for the items "*H*", "*I*" and "*K*" showed an increase in agreement, starting with approximately "somewhat agree" for the reference, climbing

Table 3 *x*-axis descriptions of Fig. 8

x-axis	Description
H	The presented concept, procedures and tools facilitated a quicker solution finding
I	The presented concept, procedures and tools facilitated better resource planning
J	The presented concept, procedures and tools made savings in terms of human and infrastructure resources possible
K	The presented concept, procedures and tools improve situation awareness across team members

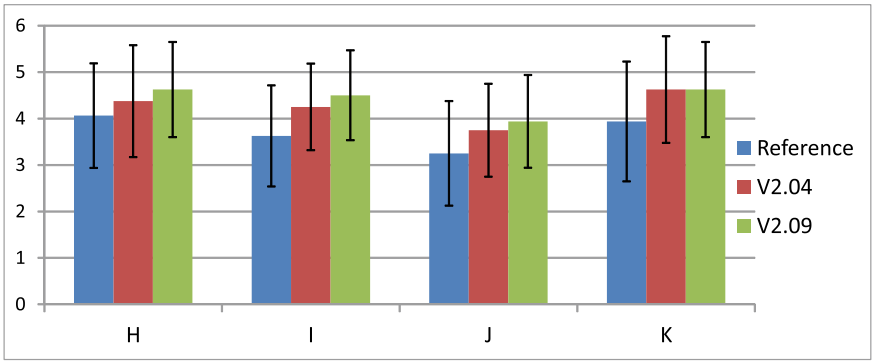

Fig. 8 Questionnaire results regarding the collaborative process

slightly towards "agree" with setup V2.09 always rated higher than or as high as V2.04 results.

The feedback for "*J*" started with an average of "neutral" and slightly increased to "somewhat agree" over V2.04 towards V2.09.

5.3 Demand Capacity Balancing

The operators were asked five questions and responded with any appropriate number of the above scale.

The questionnaire's answers in Fig. 9 clearly show a subjective improvement regarding the awareness of capacity decreasing events. The ratings of the five

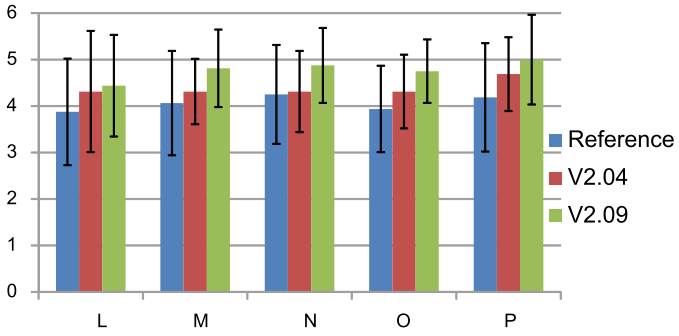

Fig. 9 Questionnaire results regarding usefulness of provided demand capacity balancing tools

Table 4 *x*-axis descriptions of Fig. 9

x-axis	Description
L	I understand the predicted data
M	I could detect any issue regarding the airport performance in advance
N	I could identify the causes of airport performance issues
O	The events were sufficiently accurately predicted
P	The uncertainty of the operations was acceptable

elements "*L*" to "*P*" increased subsequently when the additional systems were provided in first the V2.04 setup and second in the V2.09 solution setup (Table 4).

While the reference setup in the simulation environment already was assessed as "somewhat agree" to the positively formulated statements, the introduction of the novel support systems boosted it gradually to approximately "agree".

5.4 Discussion

The evaluation of all three improvements by the bespoke questionnaires indicates an improvement on the addressed challenges. Nevertheless it has to be considered that the bespoke questionnaires are only one part of the results. Debriefing, simulation and standard questionnaire data are still under evaluation. Moreover the results represent the opinion of seven operational experts working together in one team. To gain statistical validity additional simulation runs with other stakeholders are needed. Concluding this evaluation, an indication for a positive effect of the designed systems can be found, but needs to be confirmed by the other data sources and by additional simulation runs with additional participants.

Further, first steps in simulation data analysis have been conducted. Those results have been reported in the project's validation report [41]. In conclusion, there is some indication that the improved MET forecasting and alerting as well as the DCB process lead to a reduced capacity loss in bad weather situations. It therefor is assumed that in real operations with better MET forecasting and an adequately designed collaborative decision making process it is possible to reduce the loss of capacity and to improve the duration needed to recover from adverse weather conditions.

6 Outlook

The PJ.04–02 exercises addressed a great challenge in airport management: The efficient management of adverse weather situations in a collaborative manner is one of the important key capabilities to guarantee the stability of the European air traffic

network. The initial analysis of the conducted simulations indicates that the designed improvements are beneficial for the operations.

Beside the already discussed complete data analysis of the conducted exercise, the feedback of the operational experts suggests two additional focus points for future work. First, some of the stakeholders were challenged by assessing the future impact of the applied actions. The participants of the exercise agreed on measures like regulating the arrival traffic flow or cancelling a certain number of flights. As the impact of these actions is multiple hours in the future and might affect certain resources indirectly (e.g. ground handling staff), the impact is challenging to assess. As such, the operational experts requested for a tool where different actions can be played through and assessed before they are applied. This approach is called what-if and will be focused by DLR, Oslo airport and SINTEF in SESAR 2020 wave 2.

Moreover the experts highlighted that the simulation session gave them the possibility to align on each other and find detailed procedures to improve the airport operations. As such, a training and learning environment like the airport management simulation is highly needed. This gets even more important with Total Airport Management and other concepts that introduce new tools and procedures which need to be adapted to the local airport and then trained by the airport management stakeholders.

Acknowledgments The authors would like to thank Yves Günther, Anne Papenfuss, Lisa Oehmingen and Felix Timmermann of the DLR simulation team to support the conduction of the simulation exercises. Moreover, special thanks go to the participating partners: Avinor, Swedavia, EUROCONTROL, CCL, PANSA, SINTEF and LEONARDO.

SESAR 2020 Project "PJ.04 Total Airport Management" is co-funded by the European Commission and the SESAR Joint Undertaking under Grant ID 733121, subject to Horizon 2020 legislation. Project Coordinator is Groupe ADP, Solution 1 Management is conducted by ENAIRE and Solution 2 Management is conducted by DLR (AT-One). Deputy Coordinator and primary point of Communications is provided by EUROCONTROL.

The PJ.04 partners are ACG (COOPANS), ADP (SEAC2020), ATOS (FSP), Avinor (SEAC2020), CCL (COOPANS), DLR (AT-ONE), ENAIRE (INECO), EUROCONTROL, HAL (SEAC2020), INDRA, LEONARDO, LPS SR (B4), MUC (SEAC2020), NLR (AT-ONE), Naviair (COOPANS), PANSA (B4), SINTEF (NATMIG), SNBV (SEAC2020), Swed (SEAC2020), THALES AIR SYS.

For more information please visit the SESAR Joint Undertaking's website at https://www.sesarju.eu or refer to SESAR Joint Undertaking [42].

References

1. H. Hartmann, Final report of preliminary study total airport management, CARE Action "Innovation", DLR (Braunschweig, Germany, 2001), p. 33
2. Y. Günther, A. Inard, B. Werther, M. Bonnier, G. Spies, A. Marsden, M. Temme, D. Böhme, R. Lane, H. Niederstraßer, Total airport management-operational concept and logical architecture, DLR, (Braunschweig, Germany, 2006), pp. 44
3. G. Spies, F. Piekert, A. Marsden, R. Suikat, C. Meier, P. Eriksen, Operational concept for an airport operations center to enable total airport management. in: ed. by I. Grant, *26th Congress of International Council of the Aeronautical Sciences (ICAS)* (Alaska, USA, 2008)
4. F. Piekert, A. van Dongen, Total airport management negotiation of airport performance parameters. in 7th EUROCONTROL Experimental Center INO Workshop, EUROCONTROL, Brétigny sur Orge (France, 2008), pp. 7
5. T.A.M.S. Partners, *Gesamtvorhabensbeschreibung Leuchtturmprojekt TAMS-Total Airport Management Suite* (Nürnberg, Germany, TAMS Partners, 2011), p. 56
6. F. Depenbrock, B. Urban, A. Temme, Y. Günther, M. Schaper, S. Helm, *TAMS Operational Concept Document* (Braunschweig, Germany, DLR, 2012), p. 73
7. S. Helm, A.B. Claßen, F. Rudolph, C. Werner, B. Urban, Integration of landside processes into the concept of total airport management. in *Air Transport Research Society 2012 World Conference* (Tainan, Taiwan, 2012)
8. SESAR Consortium, SESAR Concept of Operations, (SESAR Consortium, Brussels, Belgium, 2007), p. 214
9. SESAR Consortium, D6—Work Programme for 2008–2013, SESAR Definition Phase-Air Transport Framework, (SESAR Consortium, Brussels, Belgium, 2008), p. 124.
10. SESAR Joint Undertaking, Total Airport Management in: SESAR Joint Undertaking (Ed.) CALL: SESAR2020 IR-VLD WAVE1, (European Commission, Brussels, Belgium, 2015)
11. R. Suikat, A. Deutschmann, Total airport simulation supporting research for future airport management concepts. in AIAA *Modeling and Simulation Technologies Conference and Exhibi*t, (American Institute of Aeronautics and Astronautics, Honolulu, Hawaii, USA, 2008)
12. M. Jipp, F. Depenbrock, R. Suikat, M. Schaper, A. Papenfuß, S. Kaltenhäuser, Validation of multi-objective optimization for total airport management in *8th Asian Control Conference*, ASCC Kaohsiung (Taiwan, 2011)
13. P. Förster, A discrete event modelling and simulation environment for applications in the TAM context, 60. Deutscher Luft-und Raumfahrtkongress 2011, (Bremen, Germany, 2011)
14. N. Carstengerdes, M. Jipp, F. Piekert, A. Reinholz, R. Suikat, Validation of the total airport management suite-research report, Deutsches Zentrum für Luft- und Raumfahrt e.V. (DLR), Institut für Flugführung, (Braunschweig, Germany, 2012), p. 153
15. R. Suikat, *TAMS Simulation Concept Document* (Braunschweig, Germany, DLR, 2012), p. 29
16. A. Deutschmann, understanding the dynamic system airport. in *World Conference on Transport Research, WCTR*, (Rio de Janeiro, Brasil, 2013), p. 6
17. S. Schier, F. Timmermann, T. Pett, Airport management in the box–a human-in-the-loop simulation for Acdm and airport management Deutscher Luft-und Raumfahrt Kongress 2016, (Braunschweig, Germany, 2016)
18. S. Schier, T. Pett, O.K. Mohr, S.J. Yeo, Design and evaluation of user interfaces for an airport management simulation. in *AIAA Aviation Modelling and Simulation Conference* (Washington, D.C., USA, 2016)
19. S. Schier, A. Duensing, Sparring partners for human-in-the-loop simulations-the potential of virtual agents in air traffic simulations, Deutscher Luft- und Raumfahrt Kongres 2017, (München, Deutschland, 2017), p. 10.
20. S. Schier, L. Rosenau, M. Freese, Trainieren mit CLAUDI–Das Potential kognitiver Agenten für Simulationen und Planspiele, 6. Interdisziplinärer Workshop Kognitive SystemeMünchen, (Deutschland, 2017)
21. F. Piekert, A. Marsden, O. Delain, *Europe's next Step in Airport Performance Management Research, EIWAC 2017* (ENRI, Tokyo, Japan, 2017).

22. E. Commission, COMMISSION IMPLEMENTING REGULATION (EU) No 409/2013 of 3 May 2013 on the definition of common projects, the establishment of governance and the identification of incentives supporting the implementation of the European air traffic management master plan (Text with EEA relevance), in *L 123/1*. ed. by E. Commission (European Commission, Brussels, Belgium, 2013), p. 7
23. E. Council, COUNCIL REGULATION (EC) No 219/2007 of 27 February 2007 on the establishment of a joint undertaking to develop the new generation European air traffic management system (SESAR), in *European Council*. ed. by E. Council (Belgium, Brussels, 2007), p. 18
24. E. Council, COUNCIL REGULATION (EC) No 1361/2008 of 16 December 2008 amending Regulation (EC) No 219/2007 on the establishment of a joint undertaking to develop the new generation European air traffic management system (SESAR), in *European Council*. ed. by E. Council (Belgium, Brussels, 2008), p. 6
25. EUROCONTROL, E-OCVM Version 3.0, in EUROCONTROL (Ed.) *European Operational Concept Validation Methodology*, (EUROCONTROL, Brussels, Belgium, 2010), p. 76.
26. EUROCONTROL, E-OCVM Version 3.0 Annexes, in EUROCONTROL (Ed.) *European Operational Concept Validation Methodology*, (EUROCONTROL, Brussels, Belgium, 2010), p. 144.
27. F. Piekert, O. Delain, E. Martin Dominguez, A. Marsden, *Europe's next step in total airport management research,* ATRS 2017 (ATRS, Antwerp, Belgium, 2017), p. 32
28. C. Rahatoka, S. Busoni, B. Desart, R. Suikat, A. Marsden, D. Defourny, E. Miklos, P. Nechaj, F. Piekert, *SESAR Solution PJ04-02: V2 Validation Plan (VALP)-Part I* (Braunschweig, Germany, DLR, 2019), p. 178
29. R. Suikat, S. Kaltenhäuser, J. Hampe, F. Timmermann, B. Weber, ACCES-A gaming and simulation platform for advanced airport operations concepts. in *AIAA Modeling and Simulation Technologies Conference*, American Institute of Aeronautics and Astronautics 2010
30. F. Piekert, N. Carstengerdes, S. Schier, R. Suikat, A. Marsden, A high-fidelity artificial airport environment for sesar APOC validation experiments, in *The 19th ATRS World Conference Singapore* (2015), p. 16
31. S. Schier, Y. Günther, S. Lorenz, R. Suikat, F. Piekert, Ein Flug durch Raum und Zeit–Entwurf und Evaluation einer Simulationsdynamik für das Flughafenmanagement, Simulation technischer Systeme inklusive der Grundlagen und Methoden in Modellbildung und SimulationUlm, Germany, 2017, p. 6
32. F. Piekert, N. Carstengerdes, S. Schier, R. Suikat, A. Marsden, A high-fidelity artificial airport environment for sesar apoc validation experiments. J. Air Transp. Stud. **8**, 20 (2017)
33. J. Busink, E. Derogee, B. Desart, A. Grimm, R. Grosmann, Y. Günther, F. Hølvold, A. Inard, L. Lapteva, I. Larsson, G. Marrazzo, A. Marsden, E. Miklos, P. Nechaj, T. Robinson, M. Sinen, D. Skoglund, T. Verhoogt, Sesar Solution PJ.04–02 SPR-INTEROP/OSED for V2-Part I, DLR, (Braunschweig, Germany, 2019), p. 353
34. EUROCONTROL, Airport CDM Operational Concept Document, EUROCONTROL, (Brussels, Belgium, 2006), p. 54
35. EUROCONTROL, Airport Collaborative Decision Making (A-CDM), EUROCONTROL, (Brussels, Belgium, 2015)
36. M. Linde, A. Marsden, E. Goni Modrego, F. Vormer, O. Delain, E. Callejo Tamayo, J.L.M. Sánchez, T. Verhoogt, D02-AOP Update Concept Document, SESAR WP 6.5, (SJU SESAR Joint Undertaking, Brussels, Belgium, 2011), p. 37.
37. H. Bogers, M. Linde, J.R. Matas Sebatia, I. Álvarez Escotto, J.I. Martin Espinosa, B. Ciprián Tejero, C. Druce, A. Knight, A. Von Eckartsberg, D. Bourguignat, O. Delain, R. Ten Hove, R. Grosmann, R. Wyss, A. Marsden, A. Wennerberg, N. Halwachs, D. Fuchs, A. Arvidsson, R. Dekker, R. Breuer, S. Foetsch, E. Goni Modrego, J.A. Ubeda Torres, D16-OFA 05.01.01 Consolidated OSED, Part 1, SESAR Consortium, (Brussels, Belgium, 2015), p. 608
38. H. Bogers, M. Linde, J.R. Matas Sebatia, I. Álvarez Escotto, J.I. Martin Espinosa, B. Ciprián Tejero, C. Druce, A. Knight, A. Von Eckartsberg, D. Bourguignat, O. Delain, R. Ten Hove, R. Grosmann, R. Wyss, A. Marsden, A. Wennerberg, N. Halwachs, D. Fuchs, A. Arvidsson, R. Dekker, R. Breuer, S. Foetsch, E. Goni Modrego, J.A. Ubeda Torres, D16 - OFA 05.01.01 Consolidated OSED, Part 2, SESAR Consortium, (Brussels, Belgium, 2015), p. 244.

39. D.M. Dehn, Assessing the impact of automation on the air traffic controller: the SHAPE questionnaires. Air Traffic Control Quarter **16**, 127–146 (2008)
40. J. Brooke, SUS: a retrospective. J. Usabil. Stud. **8**, 29–40 (2013)
41. F. Rousseau, B. Desart, A. Marsden, E. Miklos, C. Lopez, C. Rahatoka, R. Salomon, R. Suikat, *SESAR Solution PJ04-02: Validation Report (VALR)* (Braunschweig, Germany, DLR, 2019), p. 284
42. SESAR Joint Undertaking, *SESAR 2020 Membership Reflects Growing Europe-Wide Commitment to ATM Modernisation* (SESAR Joint Undertaking, Brussels, Belgium, 2016).

Precision Approach Procedures with General Aviation Aircraft and Helicopter at Braunschweig Research Airport

T. Feuerle, T. Rausch, T. Lueken, and S. Schmerwitz

Abstract The European funded project "GNSS Solutions for Increased GA and Rotorcraft Airport Accessibility Demonstration—GRADE" is a very large demonstration (VLD) project within the SESAR2020 program. In the context of this VLD, several SESAR solutions are demonstrated in simulation and real flight test campaigns. This paper presents the demonstration and evaluation of capabilities of a common used general aviation (GA) aircraft, namely Cessna 172N, performing different precision approach procedures. In parallel, an EC135 helicopter is demonstrating the possibilities of point in space (PINs) approaches. The project team consists of European partners representing different stakeholders involved in air traffic. Initially, fast time simulations took place where air traffic controllers were confronted with aircraft approaching on curved approaches paths using performance-based navigation (PBN) procedures. A flight test campaign has been conducted in July and September 2019 in Braunschweig. The two project partners TU Braunschweig (TUBS) and German Aerospace Centre (DLR) conducted several approaches in parallel using a GA aircraft (TUBS) and a research helicopter (DLR) in order to demonstrate a simultaneous non-interfering (SNI) approach to the Braunschweig airport.

Keywords Precision approach procedures · General aviation · Demonstration of novel SESAR approach procedures

T. Feuerle (✉) · T. Rausch
Institute of Flight Guidance, Technische Universitaet Braunschweig (TUBS), Braunschweig, Germany
e-mail: t.feuerle@tu-braunschweig.de

T. Rausch
e-mail: thomas.rausch@tu-braunschweig.de

T. Lueken · S. Schmerwitz
Institute of Flight Guidance, Deutsches Zentrum Für Luft- Und Raumfahrt (DLR) E.V, Brauschweig, Germany
e-mail: thomas.lueken@dlr.de

S. Schmerwitz
e-mail: sven.schmerwitz@dlr.de

Air Traffic Management and Systems IV, Lecture Notes in Electrical Engineering 731,
https://doi.org/10.1007/978-981-33-4669-7_9

1 Introduction

In the coming decades, general aviation (GA) aircraft and rotorcraft, especially the small ones for personal transportation, will have an increasingly important role in air traffic. These vehicles usually have basic on-board equipment, only some of them are equipped for instrument procedures like the instrument landing system (ILS). Therefore, in the terminal phases of the flight, they often fly according to visual flight rules and perform non-precision approaches, significantly affecting the operations of the other airspace users. As already done for better equipped commercial aircraft, the exploitation of Global Navigation Satellite System (GNSS) for navigation during instrument approach and landing could allow GA aircraft and rotorcraft to improve their navigation (guaranteeing the required performance) and to increase tasks automation (thus reducing pilot workload), while ensuring higher levels of safety. For the application, the availability of affordable flight deck displays and decision support tools is necessary. Consequently, it will facilitate the integration of such aircraft in future air traffic scenarios and systems [1, 2].

Moreover, the exploitation of GNSS navigation procedures will allow the definition of more flexible approach procedures, providing benefits in terms of minimizing the interference with commercial aircraft for landing on congested airports and the avoidance of sensitive zones (e.g. due to obstacles, security and noise constraints) for landing on small airports placed, e.g. in urbanized area.

One of the aims of the "*GNSS Solutions for Increased GA and Rotorcraft Airport Accessibility Demonstration* (GRADE)" project is to demonstrate the capability of GA aircraft, equipped with SBAS (space-based augmentation system) as well as GBAS (ground-based augmentation system) receivers, to perform precision curved approaches with required navigation performance (RNP) below 0.3 NM [3–5]. A general overall overview of the project can be found in [6].

The project demonstration itself includes two steps, the first one consists of real-time simulations (RTS) with human and hardware in the loop and the second one of flight trials (FT) [7]. The paper [7] analyses the results of the first demonstration step for fixed-wing GA aircraft, aimed at the fine adjustment up of the prototype systems to be integrated in the flying test beds.

This paper summarizes the trials conducted in Braunschweig. Due to the nature of the very large demonstration (VLD) project, the focus was laid on the demonstration of the technological achievements of previous SESAR projects. A detailed explanation of the setup and the results will be given herein.

2 Experimental Setup

This paper focusses on the flight trials at Braunschweig research airport (EDVE). The two project partners TU Braunschweig (TUBS) and German Aerospace Centre (DLR) have conducted several approaches with a GA aircraft (Cessna 172N) and a helicopter (EC135). The procedures which have been flown will be explained in more detail in Chap. 5.

The C172N is equipped with several high performance GNSS navigation equipment, namely a prototype of a ground-based augmentation system (GBAS) receiver for GA, a commercial off-the-shelf (COTS) space-based augmentation system (SBAS) receiver, a GNSS reference unit and a prototype system of a human–machine interface (HMI). The objective of the flight trials is the demonstration of different SESAR solutions for GA from a technical perspective as well as the collection of pilot feedback, i.e. collection of operational feedback. Procedures to be covered will be SESAR 1 solution #51 "Enhanced terminal operations with LPV procedures", #55 "Precision approaches using GBAS CAT II/III based on GPS L1" and solution #103 "Approach procedure with vertical guidance".

The operational scope of the flight test campaign in Braunschweig was the demonstration of the feasibility and benefits of the execution of the SESAR 1 solution Sol#113 "Optimized Low-Level IFR routes for rotorcraft", which covers the demonstration of standard point in space (PinS) helicopter procedures as well as low-level IFR routes for helicopters. In addition, it has been demonstrated, that the PinS procedure can be conducted independently from approaching fixed-wing traffic resulting in a simultaneous non-interfering (SNI) operation. The same guidance tools as used in the real-time simulation have been integrated into DLR's research helicopter active control technology / flying helicopter simulator (ACT/FHS). This included head-down display prototypes of an enhanced primary flight display with course deviation indicator (CDI), as well as a navigation display for presenting guidance information to the pilot.

3 Research Aircaft Cessna C172N

The research aircraft is a standard Cessna C172N (see Fig. 1). It has been modified with several additional sensors and antennas as well as pilot interfaces. It is certified with a permit to fly which limits the flights to daytime and visual flight conditions. Nevertheless, it can be used for experimental flight trials easily (see also [8]).

For the GRADE project and the trials described in this paper, a prototype of a GBAS receiver has been installed. It is located in the middle part of the flight deck below the GARMIN 430WAAS (see Fig. 2). Deviation indications from both devices

Fig. 1 Research aircraft cessna 172N "D-EMWF"

Fig. 2 Cockpit of cessna 172N

can be displayed on the cross deviation indicator, which is also located in the middle part of the cockpit panel. With this installation GBAS as well as SBAS approaches can be performed using standard instruments. It has been used within the project to assess the flyability and acceptability of novel approach procedures in conventional cockpit layouts. Besides these conventional instruments, a portable moving map device was installed into the aircraft as well. (Fig. 3).

Fig. 3 DLR's research helicopter active control technology / flying helicopter simulator (ACT/FHS)

4 Research Helicopter EC135

The ACT/FHS "flying helicopter simulator" of the DLR is based on a standard Eurocopter EC 135 type helicopter, which has been extensively modified for use as a research and test aircraft. The mechanical controls, for example, have been replaced by a fly-by-wire/fly-by-light (FBW/FBL) flight control system. As a result, the control commands are transferred by electric cables and fibre optic cables instead of control rods.

The application portfolio of the FHS covers pilot training, trials of new open and closed-loop control systems, up to simulation of the flight characteristics of other helicopters under real-environmental conditions. The FHS is equipped with two engines, a bearingless main rotor and a Fenestron tail rotor as standard; its key features are notably quiet operation and high manoeuvrability and safety. The fly-by-light control system is a ground breaking new system, where, in contrast to fly-by-wire, the control signals between the controls, the flight management computer and the actuators for rotor blade control are transferred optically via fibre optic cables instead of electrically.

The advantages compared with electrical data transfer are the high transmission bandwidth, high reliability and low weight. The fly-by-light flight control system consists of a quadruple redundant computer and is designed such that the stringent safety criteria of the European aviation authorities are met in full.

FHS is the first helicopter in the world with this flight control system. The cockpit layout provides seats for a safety pilot, the test pilot and the flight trial engineer. A comprehensive equipment line-up with sensors and systems for on-board data recording and processing is used to record the data from the flight trials. This data is available to users and engineers for analysis on board and—via telemetry—on the

ground. Furthermore, additional vision systems and an experimental flight management system (FMS) can be integrated in order to generate adequate head-down symbology for PinS guidance.

At the end of 2016, DLR has designed an experimental graphics computer called JCONV2 for high performance graphics calculations and presentations on a helmet mounted display system. As part of the GRADE project, the ability of this computer has been extended to allow the display of additional information to be displayed on the evaluation pilot's head-down display at the same time. To realize this capability, a cable was laid between the JCONV2 and the side panel near the flight test engineer. From there, the video signal was routed to the evaluation pilot's head-down display.

5 Procedures Flown

Two independent flight test procedures were designed: One for the fixed-wing demonstration and one for the rotorcraft demonstration. The procedures described in this chapter have been demonstrated in flights either by the Cessna 172 solely, the FHS solely, or by both aircraft simultaneously.

Flight trials for the fixed-wing demonstration exercises consist of reference scenarios (standard instrument RNAV arrival and approach procedures as published in AIP) and solution scenarios designed for the flight exercises in the GRADE project. These solution scenarios included shorter routes and additional turning points compared to the reference scenarios. The additional turning points were set to already available visual reporting points to ease the flight operations including air traffic control and other traffic. The intention was to generate curved and segmented pre-defined approaches as given in the different SESAR solutions (see Chapter 2).

Figure 4 shows, from left to right, the reference scenario for the runway 08, the solutions scenario route for runway 08, solution scenario route for runway 26 and the reference scenario for runway 26.

The pilot was supported by a GNSS-based navigation prototype on a portable display (showing a map display and a course deviation indicator) during the whole approach, and for the final approach of the solution scenarios additionally either by GBAS or SBAS information. Off-nominal scenarios like simulated GBAS outage or display outage were included in the exercises.

Flight trials for the rotorcraft demonstration exercises consist of an en-route segment of a low-level route (LLR), a PinS approach and a PinS missed approach. A LLR network in conjunction with SNI PinS procedures allows to circumvent the problem of merging rotorcraft and fixed-wing traffic, or, in general, slow traffic from fast traffic.

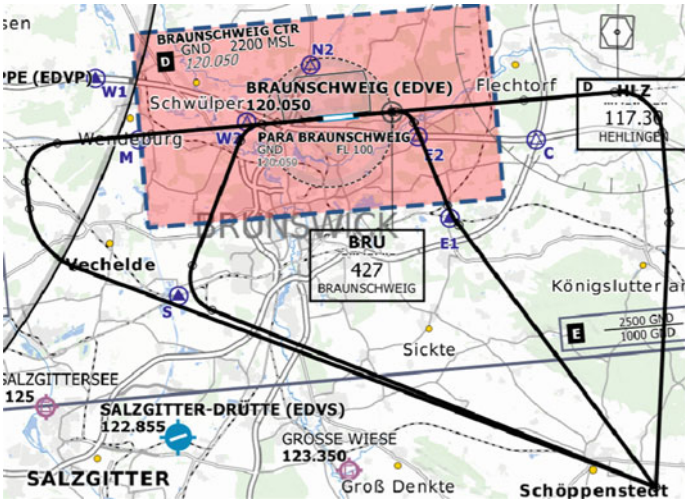

Fig. 4 Reference and solution scenario routes for the fixed-wing demonstration exercises

At the airport, the rotorcraft flies a PinS procedure, which was designed to be an SNI approach with fixed-wing aircraft approaching at the same time on conventional RNP or ILS approaches. Final approach separation for the rotorcraft on the PinS is assured by a visual procedure from the missed approach point to a dedicated helipad on the apron. If visual reference is not established at the PinS, the rotorcraft will execute a SNI missed approach procedure. The design of the PinS ensures that all separation limits are respected according to SESAR 4.10 Deliverable 23. The low-level route is designed at an altitude below minimum radar vectoring altitude. At the same time, ATC surveillance is assured and the flight path is monitored by a controller.

Figure 5 shows the LLR network for the GRADE project integrated into a departure chart for runway 26 at EDVE. The design altitude for all segments is 2200 ft, roughly 2000 ft above ground level. The approach procedure (see also Fig. 6) commences at point LELUH near Wolfenbuettel. The procedure as depicted can be coded and flown as standard or advanced PinS, but is optimized using radius to fix (RF) before the final approach point (FAP) and in the missed approach. The final approach begins at the FAP and is a localizer performance with vertical guidance segment (LPV) with a fictitious threshold point located such that the glide path intercept point is exactly at the desired helipad. Vertical guidance is an ILS look-alike guidance provided by the SBAS system using a 4.4° glide path angle. Minimum descent altitude is 628 ft MSL (350 ft GND), thereafter proceed visually if the helipad is in sight.

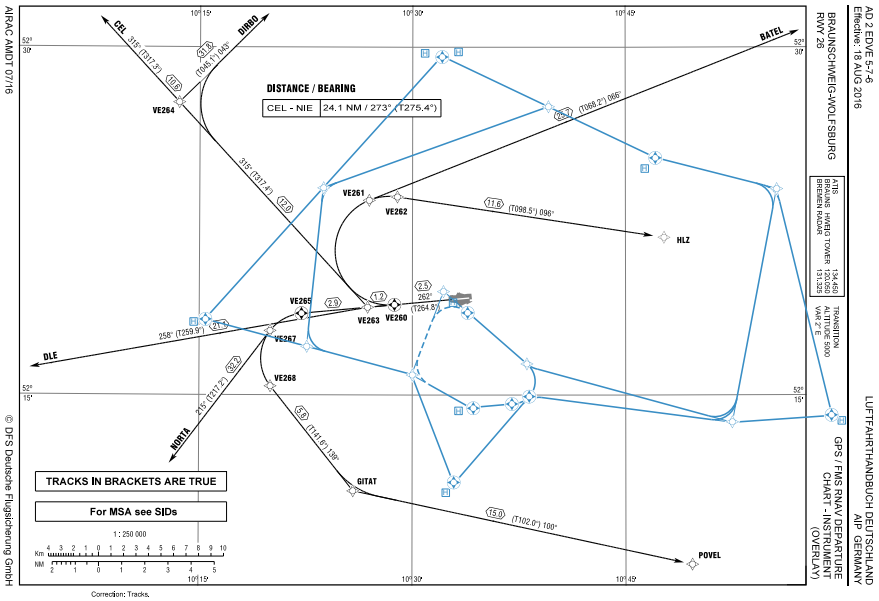

Fig. 5 Possible low-level route network

The missed approach commences upon abortion of the approach procedure, i.e. if no visual references are established by the time the aircraft reaches the missed approach point (MAPt). The pilot must initiate a climb to 2200ft MSL and follow the track as depicted. Upon crossing the MAPt, an immediate left turn to WP4 is required. For advanced PinS, this leg is coded as a RF to WP4 with a radius of 1 NM. In lieu of the RF, a fly-by waypoint FB5 can be used, but for track keeping accuracy and separation assurance, we strongly recommend using RF. Upon reaching WP4, a 1.5 NM straight leg follows to WP6. After WP6, if an advanced PinS is desired, the leg from WP6 to WP7 can be coded as RF with a radius of 2.75 NM. If an advanced PinS is not desired, FP8 can be used in lieu of the RF. After WP7, the aircraft returns to LELUH with a track to fix of length 5.1 NM. We designed the missed approach track along the track of the city tangent motorway to reduce noise exposure of downtown Braunschweig.

As an example, with this network, it would be possible to transport patients from whatever hospital required to the airport under IMC. In detail, there are six hospitals, a federal police force heliport and the airport EDVE connected to this network. The rotorcraft can follow a LLR network from one hospital to another or to a local airport under IFR. This use case of urgent medical transport is just one of many, but for the demonstration of LLR and SNI, it serves as the driving use case.

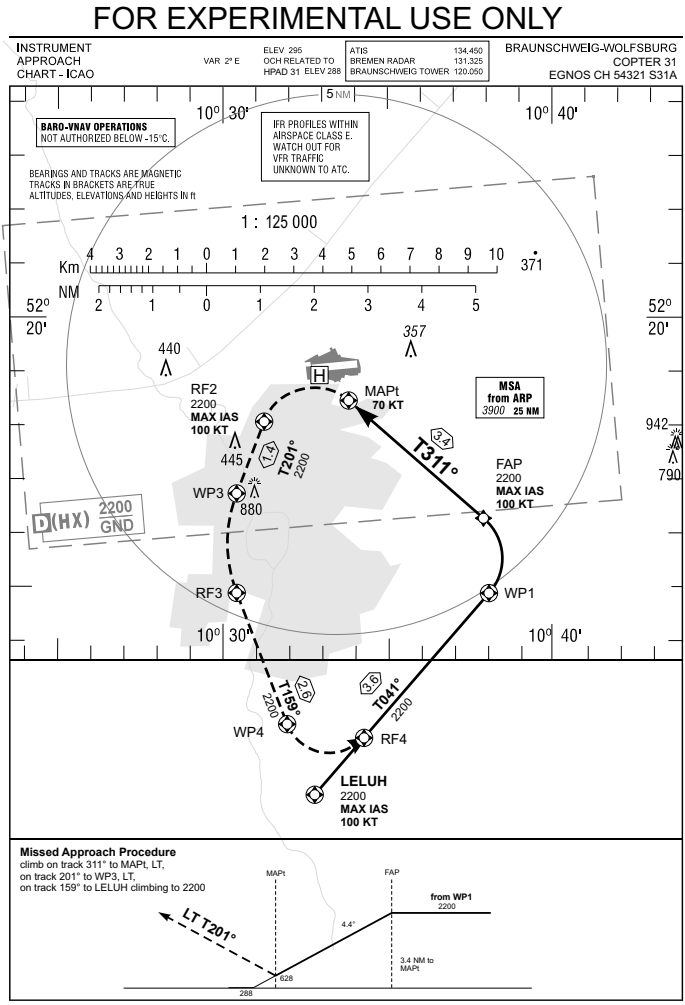

Fig. 6 Possible simultaneous non-interfering approach

6 Results and Evaluation of the Trials

The fixed-wing flights have been carried out between 18th July and 12th September 2019; three different pilots were involved. 20 approaches and a total flight time of about 7:30 h on 6 different days were executed.

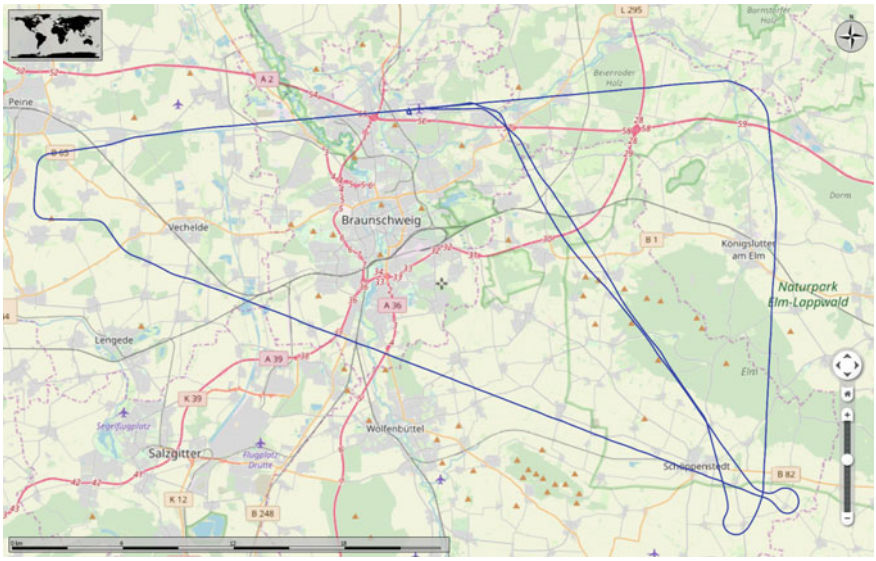

Fig. 7 Reference scenario flight path of the fixed-wing demonstration exercise (with ATC intervention during RWY08 approach)

Figure 7 shows one flight with reference scenario approaches inbound runway 26 and runway 08. The complete flight trajectory is displayed with the outbound trajectories in the middle and the approach trajectories to the right (for runway 26) and left (for runway 08). The approaches all started at the initial waypoint south east of Braunschweig airport. The approaches inbound runway 26 were flown without ATC delays. The approach to runway 08 shows a small deviation due to ATC vectoring.

Figure 8 depicts the flight trajectories of solution scenario approaches. All three approaches were flown on runway direction 26 with different length of initial approach segment. The intermediate approach segments have been flown using augmented GNSS while the final approach segment has been flown using either SBAS or GBAS (as GBAS is not available for terminal approach path procedures so far).

An inspection of the recorded flight path data showed that pilots were able to follow the defined approach path closely. In all the executed approaches, values lower than 0.3 NM for the deviation from the defined approach path were achieved.

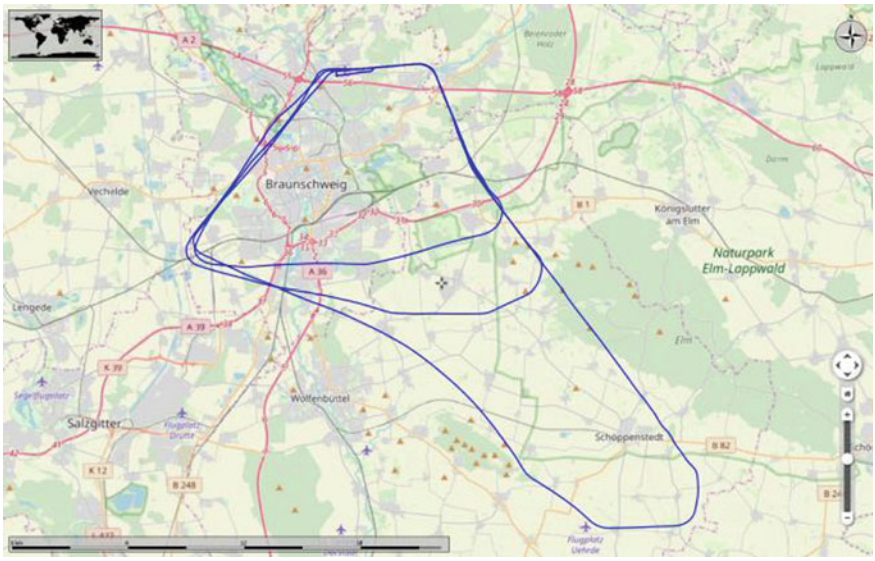

Fig. 8 Solution scenario flight path of the fixed-wing demonstration exercise, RWY26

For human performance analyses, questionnaires have been filled out, addressing the objectives of acceptability of the tested operations by pilots, feasibility and flyability of the designed procedures (accurate and efficient completion of operations), cognitive workload (using the NASA Task Load Index (TLX) assessment), situational awareness (using the NASA Situation Awareness Rating Technique (SART) assessment), and the capability of the HMI to provide the pilot with clear and complete information to execute the landing procedures with a sufficient level of confidence and precision.

The resulting subjective total workload of the fixed-wing pilots ranges from 38% to 44%, the resulting subjective total situational awareness score ranges from 5.6 to 9.2 (on a scale ranging from −5 to 13). This shows a generally moderate workload combined with a good situational awareness.

Figures 9, 10, 11 and 12 show some further pilots' answers to the questionnaire items.

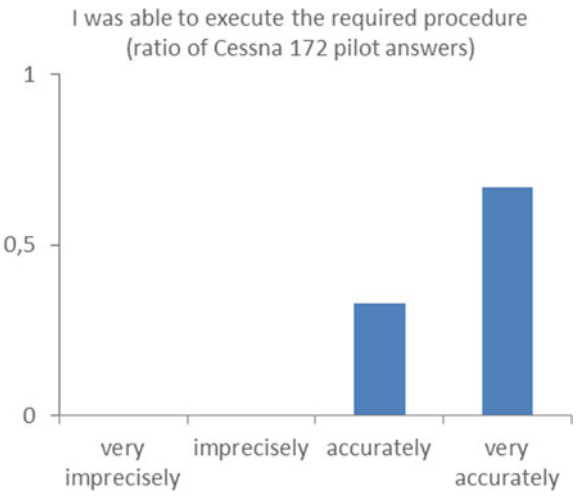

Fig. 9 Exemplary questionnaire answers for the fixed-wing flights (procedure)

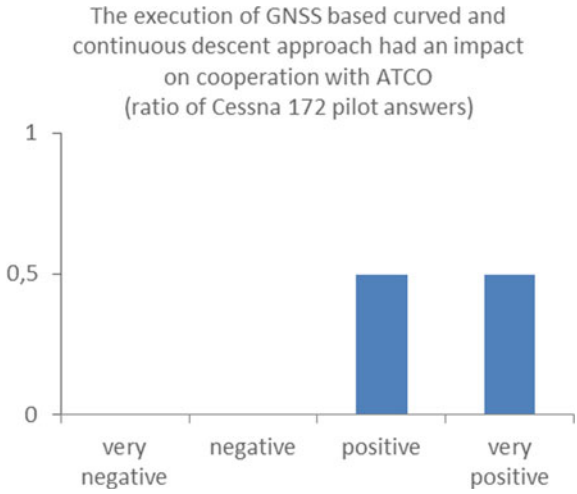

Fig. 10 Exemplary questionnaire answers for the fixed-wing flights (impact on ATCO)

Comments to the procedure layout were also collected. Beside the fact, that the final was quite short but manageable, no major findings were drawn. A rationale for this statement is the fact that the procedure has been adapted especially for relatively slow flying GA aircraft.

Regarding the helicopter flight trials, these exercises were supported by two different types of flight guidance displays (Fig. 13). The standard PFD display has been complemented by a course deviation indicator (CDI) and so-called bugs for desired speed, barometric altitude, and heading. The final approach point "FAP" defines the position where the display of the PFD is switched from RNP/VNAV (green) to angular deviation of the LPV (magenta). A tunnel-in-the-sky synthetic

Fig. 11 Exemplary questionnaire answers for the fixed-wing flights (situational awareness)

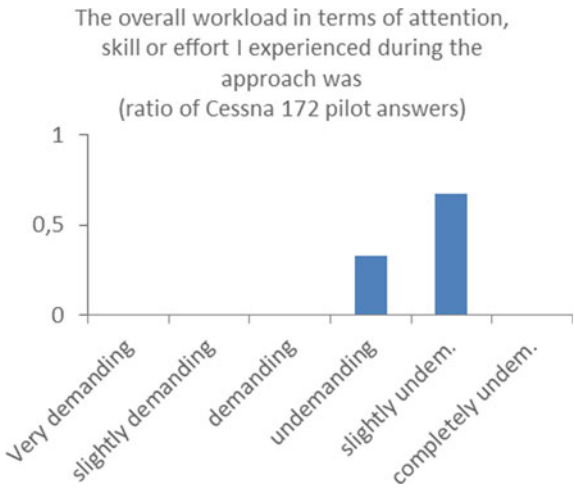

Fig. 12 Exemplary questionnaire answers for the fixed-wing flights (workload)

vision system (SVS) was implemented as an alternative primary flight display. To minimize the cross-track error especially, in curved segments, a flight path marker and a flight director as parts of the tunnel display supported the pilot during turns.

The flight trials have been carried out from 20th of August until 18th of September. With respect to the preparation of these flight trials, many different experts on different focal areas have been involved in these experiments:

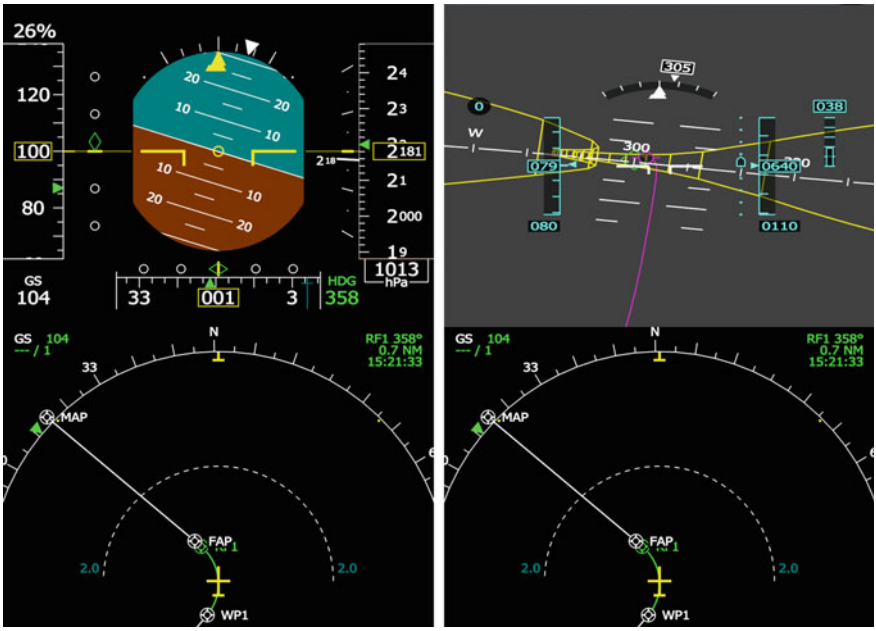

Fig. 13 Solution scenario (Sol #113) of first helicopter demonstration exercise including tunnel- (SVS), navigation- and PFD flight guidance displays.

- 4 technical experts / engineers (prototype implementation, flight trials preparation, and demonstration day technical preparation and presentation);
- 3 DLR test pilots (same pilots who carried out preceded real-time simulations in fall 2018) [9];
- 1 human factors expert.

In total, 2 shakedown runs and 24 repeated approaches during 10 h of flight time on 6 different days were conducted during the flight trials.

Flight data records were made to subsequently provide quantitative statements regarding e.g. tracking accuracy, cross-track errors, etc. For human performance analyses, questionnaires have been filled out: 8 NASA TLX, 8 3D SART, and a debriefing questionnaire by each pilot.

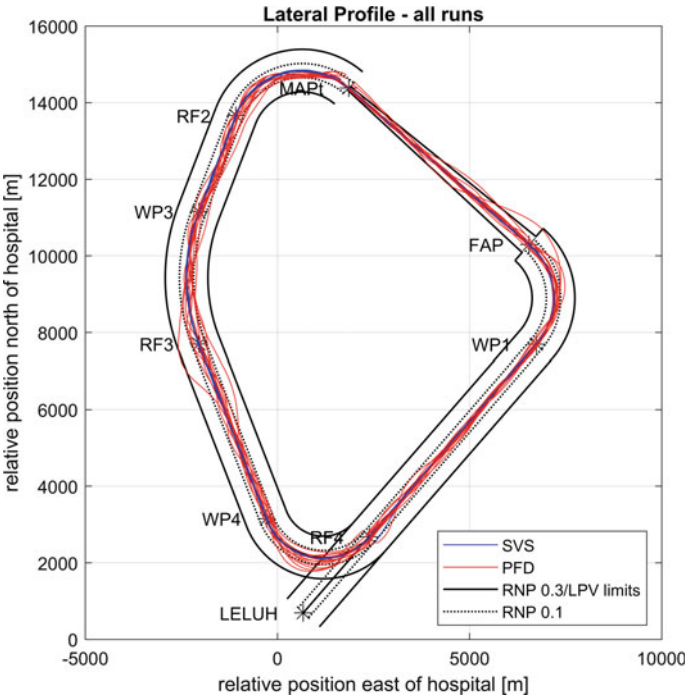

Fig. 14 Lateral profile of all runs per display type with RNP limits

Figure 14 depicts the recorded lateral profile for all runs with the RNP 0.3 limits and a second limit of RNP 0.1. It can be seen that all pilots managed to stay within the RNP 0.3 limits during the approach phase regardless of the guidance display type. During the LPV approach between FAP and the MAPt, two runs under PFD with CDI configuration show deviations larger than the LPV allows. In both cases, the pilots managed to capture the calculated localizer again. It can be observed that in general, all flights under PFD with CDI configuration pilots tend to react later on deviations from the route. With SVS guidance, the lateral accuracy was always significantly better than RNP 0.1 except for two flights close to the start of the procedure.

Table 1 Flight time within RNP limits during the approach phase in percent

	PFD (%)	SVS (%)
$X \leq$ RNP 0.1	95.50	99.81
RNP 0.1 $< X \leq$ RNP 0.3	4.50	0.19
$X >$ RNP 0.3	0.00	0.00

Tables 1 and 2 show the percentage of flight time within or outside the lateral RNP 0.1 or RNP 0.3 limits. It can be seen that during the approach phase more than 95% of the flight time the performance was at least RNP 0.1 for both guidance options. During the missed approach segment, the performance is 6% worse for the PFD guidance and constantly good for the SVS guidance.

Figures 15 and 16 show the box-whisker plots from NASA TLX and 3D SART questionnaire per display type. The PFD provoked much more workload for the pilots than the SVS. Nevertheless the variation of the ratings for the PFD is very high. The ratings for the situation awareness barely shows enough SA for the PFD and fair ratings for the SVS. It can be argued that in comparision with the SVS display pilots feel much less aware of their situation and what pilots state as being "behind" the helicopter. As a result, pilots with CDI guidance always have to reduce an already build up deviation. It is much easier with a tunnel-in-the-sky guidance to prevent a deviation to build up at all.

Table 2 Flight time within RNP limits during the missed approach phase in percent

	PFD (%)	SVS (%)
$X \leq$ RNP 0.1	89.20	100.00
RNP 0.1 $< X \leq$ RNP 0.3	10.60	0.00
$X >$ RNP 0.3	0.20	0.00

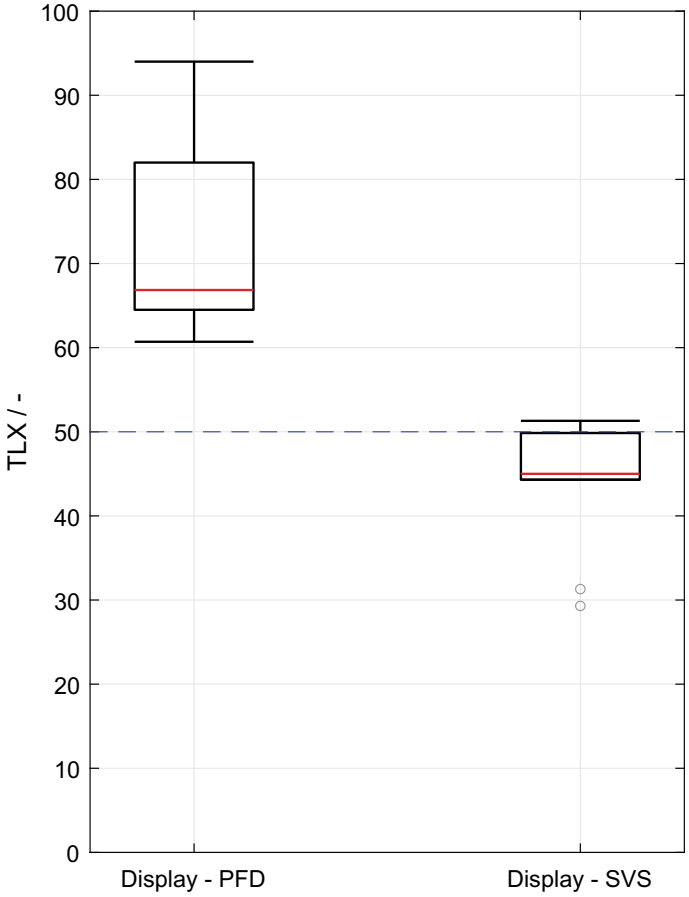

Fig. 15 NASA Task load index, absolute index per display type

More details to the results of GRADE's helicopter flight trial demonstration will be presented on 46th European Rotorcraft Forum ERF 2020 in Moscow [10].

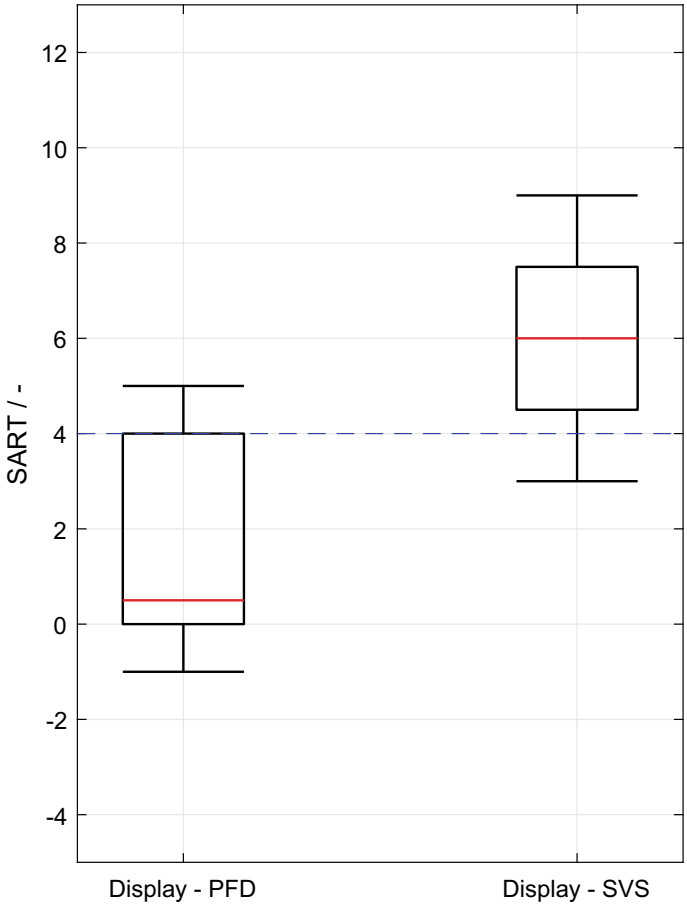

Fig. 16 3D situation awareness rating technique, absolute score per display type

7 Conclusions

The GRADE project demonstrated that GNSS-based approach procedures are well suited not only for business and transport aircraft but also for rotorcraft and general aviation aircraft. With the performed study including demonstration flights into Braunschweig research airport, the feasibility has been demonstrated. With the highly flexible GNSS procedures and the corresponding avionic equipment approaches can be flown with less impact on environment (e.g. circumnavigation of noise sensitive areas) as well as separation between different kinds of traffic.

Acknowledgments The project "GRADE – GNSS Solutions for Increased GA and Rotorcraft Airport Accessibility Demonstration" is funded by the SESAR Joint Undertaking under the Grant Agreement No. 783170. The authors want to acknowledge especially the active support of the air

traffic controllers at Braunschweig research airport. Furthermore, the authors would like to thank all persons involved in the preparation and conduction of the flight trials for their help and support.

References

1. P. Neri, Use of GNSS signals and their augmentations for civil aviation navigation during approaches with vertical guidance and precision approaches, PhD Thesis, University of Toulouse, November (2012)
2. M. Steen, T. Feuerle, M. Stanisak, T. Yoshihara, P. Hecker, GBAS curved approach procedures: advantages, challenges and applicability. in: *28th International Congress of the Aeronautical Sciences (ICAS 2012)* (Brisbane, Australia, September 2012).
3. R. Geister, T. Dautermann, V. Mollwitz, C. Hanses, and H. Becker, "3D-precision curved approaches: a cockpit view on ATM. In: *Tenth USA/Europe Air Traffic Management Research and Development Seminar (ATM2013)*, June (2013)
4. ICAO, in *Doc. 9613—Performance-based navigation manual*, 3rd edn. (Montréal, Quebec, Canada, 2012)
5. R. Geister, C. Hanses, H. Becker, Curved approach procedures enabled by a ground based augmentation system. in: *31st DASC* (Williamsburg, VA (USA), October 2012)
6. A. Vitale et al., *Solutions for Increased General Aviation and Rotorcraft Airport Accessibility–the GRADE Project", SESAR Innovation Days (SID)* (Salzburg, Austria, December 2018)
7. U. Ciniglo et al., Real-time testing of GNSS based curved and continuous descending approach for general aviation aircraft. in: *38 th Digital Avionic Systems Conference (DASC) Digital Avionic Systems Conference (DASC)* (San Diego, USA, September 2019)
8. T. Feuerle et al., GBAS Flight trials with general aviation aircraft. in: *International Symposium on Precision Approach and Performance Based Navigation (ISPA)*, November, (Munich, 2017)
9. Schmerwitz, Sven und Dautermann, Thomas und Lenz, Helge und Lüken, Thomas, GNSS solutions for increased GA and rotorcraft airport accessibility demonstration. in: *45th European Rotorcraft Forum (ERF) 2019*, September, (Warsaw, Poland, 2019)
10. T. Lueken, T. Dautermann, J. Ernst, S. Schmerwitz, Flight trial demonstration of increased general aviation and rotorcraft operations supported by GNSS solutions. in: *46th European Rotorcraft Forum (ERF) 2020, September*, (Moscow, Russia, 2020)

An Optimistic Planning Approach for the Aircraft Landing Problem

S. Ikli, C. Mancel, M. Mongeau, X. Olive, and E. Rachelson

Abstract The Aircraft Landing Problem consists in sequencing aircraft on the available runways and scheduling their landing times taking into consideration several operational constraints, in order to increase the runway capacity and/or to reduce delays. In this work we propose a new Mixed Integer Programming (MIP) model for sequencing and scheduling aircraft landings on a single or multiple independent runways incorporating safety constraints by means of separation between aircraft at runways threshold. Due to the NP-hardness of the problem, solving directly the MIP model for large realistic instances yields redhibitory computation times. Therefore, we introduce a novel heuristic search methodology based on Optimistic Planning that significantly improve the FCFS (First-Come First-Served) solution, and provides good-quality solutions in reasonable computational time. The solution approach is then tested on medium and large realistic instances generated from real-world traffic on Paris-Orly airport to show the benefit of our approach.

Keywords Aircraft landing problem · Mixed integer programming · Optimistic planning

S. Ikli (✉) · C. Mancel · M. Mongeau
ENAC, Université de Toulouse, Toulouse, France
e-mail: sana.ikli@recherche.enac.fr

C. Mancel
e-mail: catherine.mancel@recherche.enac.fr

M. Mongeau
e-mail: mongeau@recherche.enac.fr

X. Olive
ONERA DTIS, Université de Toulouse, Toulouse, France
e-mail: xavier.olive@onera.fr

E. Rachelson
ISAE-SUPAERO, Université de Toulouse, Toulouse, France
e-mail: emmanuel.rachelson@isae-supaero.fr

Air Traffic Management and Systems IV, Lecture Notes in Electrical Engineering 731,
https://doi.org/10.1007/978-981-33-4669-7_10

1 Introduction

The International Air Transport Association (IATA) expects 7.8 billion passengers to travel in 2036, which represents nearly double the passengers recorded in 2016 [1]; this increasing demand on air transportation exposes the available infrastructure to a risk of saturation. Constructing new infrastructures (runways, airports) is a solution to increase the capacity, however, it may not always be feasible due to the huge cost incurred. The alternative is to optimize the use of current infrastructure, especially the runway which is recognized to be the bottleneck of the whole Air Traffic Management (ATM) system.

Since the runway sequence is one of the key factors that determines runway capacity [2], several researchers were interested in the optimization of runway sequences, which corresponds in the literature to the following problems:

- The Aircraft Landing Problem (ALP) aims at sequencing arriving aircraft on the available runways and scheduling their landing times taking into consideration several operational constraints.
- The Aircraft Take-off Problem (ATP) consists in scheduling take-off slots to departing aircraft
- The Aircraft Scheduling Problem (ASP) consists in sequencing and scheduling simultaneously departing and arriving aircraft.

According to the survey [3] by Bennell *et al.*, the ALP received much more attention in the literature than the ATP or the ASP. Several approaches are proposed in the literature for the three above-mentioned problems, and can be classified in two main categories:

- Exact approaches, mainly MIP-based approaches [4–9] and Dynamic Programming [6, 10, 11]
- Heuristic approaches [4, 9, 12] and Meta-heuristics, such as Simulated Annealing [13–16], Tabu Search [8, 17], Genetic Algorithms [18, 19], Ant Colony Optimization [20, 21], and Variable Neighborhood Search [13, 22].

Interested readers may refer to [3] for a comprehensive review of existing approaches to the ALP.

In this work, we are interested in sequencing and scheduling aircraft landings at the runway threshold. Each aircraft has a target landing time and an authorized landing time window, expressed as an earliest and a latest acceptable landing time based on fuel considerations. Deviations from the target times will cause a cost that depends on each aircraft, and the aim is to minimize the total deviations from target times, which is more general than minimizing only total schedule tardiness. To model the problem, we propose a novel MIP formulation that takes into consideration safety constraints by imposing separation between aircraft at the runway threshold (Table 1). The proposed formulation is adapted to airports that involve multiple independent runways. Due to the NP-hardness of the problem [4], solving directly the MIP model for large realistic instances leads to redhibitory computation times, which

Table 1 Final-approach separation matrix (in seconds) according to ICAO's basic wake-turbulence categories (*source* [10])

		Following aircraft		
		H	M	L
Leading aircraft	H	96	157	196
	M	60	69	131
	L	60	69	82

is unsuited for the dynamic nature of the problem that requires air-traffic controllers to make quick but good decisions. Therefore, we introduce a novel heuristic search methodology based on Optimistic Planning [23], that provides good-quality solutions in a negligible time. We then evaluate empirically our approach on realistic instances generated from real-traffic data from Paris-Orly airport.

The remainder of this paper is organized as follows. In Sect. refsec:problem we describe the ALP and highlight the operational constraints. Next, Sect. 3 presents our proposed MIP formulation and the constraints taken into account. Then, in Sect. 4, we explain our proposed solution approach. Section 5 presents computational results that show the benefits of our approach, and finally in Sect. 6 we summarize the contributions of this work and suggest some perspectives for future research work.

2 Problem Description

Given a set of aircraft near the terminal area of an airport, the ALP consists in mapping each aircraft to a landing time such that a given criterion is optimized while operational constraints are satisfied. When the airport has more than one runway, a decision with respect to the landing runway has to be made by controllers; the runway assignment depends on several factors such as the airport configuration and the direction of arriving aircraft.

The most common approach used by controllers to sequence aircraft is the First-Come First-Served (FCFS) rule, where aircraft land according to the order of the scheduled times of arrival at the runway, and air-traffic controllers ensure only the minimum separation requirements. This FCFS heuristic is easy to implement and guarantees equity between aircraft. However, it is rarely optimal in terms of runway throughput, especially in congested airports [10], simply consider the large separation requirement in some scenarios where a heavy aircraft is followed by a light aircraft (Figure 1). This motivates the development of efficient methods that compute optimal sequences while satisfying several operational constraints such as minimum separation, authorized time windows and constrained-position shifting.

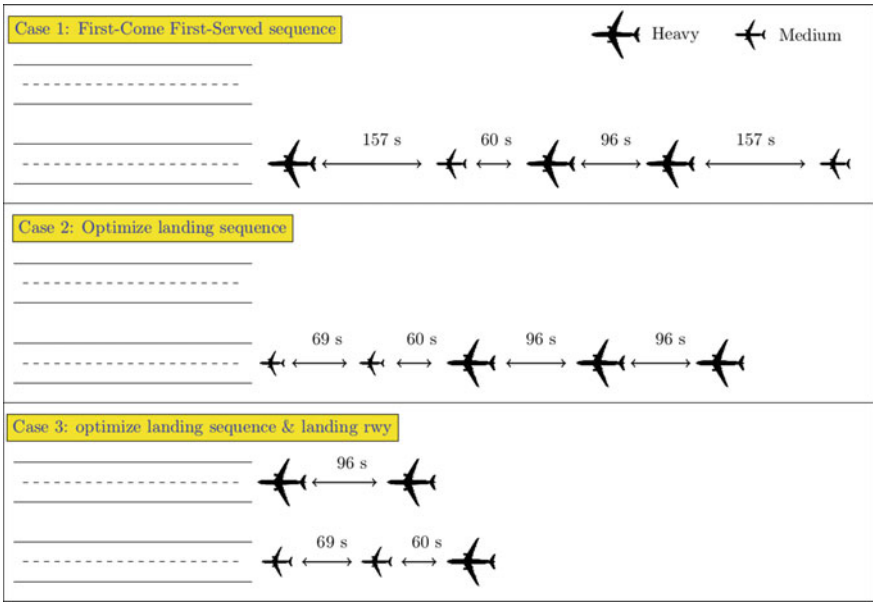

Fig. 1 Comparison of three landing sequences. Case 1 illustrates the FCFS sequence. In case 2, the landing sequence is optimized with respect to wake turbulence separation, and in case 3 the landing sequence is further optimized by runway assignment

- The **minimum separation** constraint guarantees that no aircraft is affected by the wake-vortex turbulence generated by a leading aircraft, especially during take-offs and landings. The International Civil Aviation Organization (ICAO) classifies aircraft in three main categories, namely Heavy (H), Medium (M) and Light (L), and the separation requirements are defined depending on the category of both the leading and the following aircraft. Separation requirements are given in Nautical Miles (NM), but can be converted to seconds as explained in [2] and summarized in Table 1.
- **Time-windows** constraints are defined by an earliest and a latest possible landing times, based on fuel availability or on possible speed-ups. Indeed, once an aircraft arrives at the boundary of airport control centers, decision-support tools compute an Estimated-Time of Arrival (ETA) at the runway threshold. If the aircraft speeds up, the Actual Landing Time (ALT) may be earlier than the ETA. On the other hand, aircraft may be delayed after entering the radar range and, in this case, the ALT will be later that the ETA and the latest possible landing time is limited by the available fuel [24].
- The **Constrained-Position Shifting** (CPS) constraint limits the deviation from the FCFS sequence for equity reasons. This constraint ensures that an aircraft is not deviated from its initial position in the FCFS sequence by more than a given number of positions called maximum position shifting and denoted m, which is

usually small; $m = 3$ or 4 [10]. This constraint does not only ensure equity between aircraft, but it also reduces the complexity of the problem.

In the following section, we introduce a MIP formulation for the ALP involving one or multiple runways, and we show how we can incorporate different operational constraints in the model.

3 Mathematical Modeling

Runway assignment and scheduling aircraft at each runway is formulated as a MIP model which decides the landing dates at each runway threshold, while respecting safety requirements so as to optimize a given objective. We leave the control problem, i.e. how aircraft can be controlled so as to implement the solution of our decision problem, for future research work.

3.1 Input Data

Consider a set of arriving aircraft $\mathcal{A} = \{1, 2, ..., N\}$, and a set of available runways $\mathcal{K} = \{1, 2, ..., R\}$. Without loss of generality, let us assume that each aircraft index $i \in \mathcal{A}$ represents its position in the FCFS sequence. Then, for each flight $i \in \mathcal{A}$, the given input data are presented in Table 2.

For each aircraft $i \in \mathcal{A}$, the earliest acceptable landing times E_i is chosen to be 60 seconds before the target time T_i, because it is the most economic for arriving aircraft according to [25]. The latest landing time L_i is set to 1800 s after the target time due to the limited fuel on board [25].

3.2 Decision Variables

Our proposed model involves binary optimization variables for sequencing and runway assignment, and continuous optimization variables for assigning times at the runway threshold. The binary variables are defined as follows:

Table 2 List of input data

Notation	Parameter
T_i	Target landing time
$[E_i, L_i]$	Landing time window ($L_i > E_i$)
S_{ij}	Minimum separation time (≥ 0) between aircraft i and j, where i lands before j
c_i^-	Penalty cost (≥ 0) per time-unit for landing *before* the target time T_i
c_i^+	Penalty cost (≥ 0) per time-unit for landing *after* the target time T_i

- $a_{ik} = \begin{cases} 1 & \text{if aircraft } i \text{ is assigned to runway } k, \\ 0 & \text{otherwise,} \end{cases}$
- $\delta_{ijk} = \begin{cases} 1 & \text{if aircraft } i \text{ and } j \text{ are assigned to runway } k, \text{ and } i \text{ lands before } j, \\ 0 & \text{otherwise,} \end{cases}$
- $y_{ij} = \begin{cases} 1 & \text{if aircraft } i \text{ lands before} j, \\ 0 & \text{otherwise,} \end{cases}$

For each aircraft $i \in \mathcal{A}$, the continuous variables are:

- t_i : landing time
- t_i^-, t_i^+: deviations from the target landing time T_i (before and after T_i, respectively).

3.3 MIP Model

Our objective minimizes the total deviation cost from target times (T_i) which is more general than minimizing only the total schedule delay. The complete model is given by (1)–(12)

$$\min_{\delta,y,a,t} \sum_{i\in\mathcal{A}} c_i^- \overbrace{\max(0, T_i - t_i)}^{t_i^-} + c_i^+ \overbrace{\max(0, t_i - T_i)}^{t_i^+} \tag{1}$$

$$t_i = T_i - t_i^- + t_i^+ \qquad i \in \mathcal{A} \tag{2}$$

$$E_i \le t_i \le L_i \qquad i \in \mathcal{A} \tag{3}$$

$$y_{ij} + y_{ji} = 1 \qquad i, j \in \mathcal{A} : \ i < j \tag{4}$$

$$\sum_{k\in\mathcal{K}} a_{ik} = 1 \qquad i \in \mathcal{A} \tag{5}$$

$$\sum_{k\in\mathcal{K}} \delta_{ijk} + \delta_{jik} \le 1 \qquad i, j \in \mathcal{A} : \ i < j \tag{6}$$

$$\delta_{ijk} + \delta_{jik} \ge a_{ik} + a_{jk} - 1 \ \ i, j \in \mathcal{A} : i < j, k \in \mathcal{K} \tag{7}$$

$$2(\delta_{ijk} + \delta_{jik}) \le a_{ik} + a_{jk} \ \ i, j \in \mathcal{A} : i < j, k \in \mathcal{K} \tag{8}$$

$$t_j \ge t_i - M_1(1 - y_{ij}) \qquad i, j \in \mathcal{A} : i \ne j \tag{9}$$

$$t_j \ge t_i + S_{ij} - M(1 - \delta_{ijk}) \ \ i, j \in \mathcal{A} : i \ne j \tag{10}$$

$$i - m \le N - \sum_{j\in\mathcal{A}, j\ne i} y_{ij} \le i + m \quad i \in \mathcal{A} \tag{11}$$

$$\delta_{ijk}, y_{ij}, a_{ik} \in \{0, 1\} \qquad i, j \in \mathcal{A} : i \ne j, \ k \in \mathcal{K} \tag{12}$$

In the above formulation, constraints (2) are introduced to linearize the objective function; constraints (3) represent the time window restrictions; constraints (4) enforce the order precedence relationship between flights i and j at landing; con-

straints (5) ensure that an aircraft is assigned to exactly one runway; constraints (6) enforce the order precedence relationship between flights landing on the same runway; constraints (7) and (8) enforce the logical relationship between δ_{ijk} and a_{ik}; constraints (9) relates precedence relationships between landings to landing times; constraints (10) ensure the separation requirements between aircraft landing at the same runway; constraints (11) impose the CPS constraint, and constraints (12) enforce the binary restrictions of our discrete variables.

Before reporting numerical results obtained with this formulation, we shall first present a novel alternate methodology to solve the ALP, since solving directly the MIP leads to redhibitory computation times, as we shall show in Section 5.

4 Optimistic Planning

The dynamic nature of the ALP requires air-traffic controllers to make quick but good decisions; the computation time of any solution is thereby a critical issue. Given the complexity of the problem, the computation time to find an optimal solution either with our MIP model or with other exact approaches is unsuited for real-time applications. Therefore, we introduce a novel heuristic search approach based on the *Optimistic Planning* (OP) paradigm [23, 26], capable of computing solutions that do not deviate too much from the FCFS solution sequence and that are relatively close to optimal solutions, within an acceptable computational time.

Our approach models the ALP as an environment defined by *states*, *transitions*, *actions*, and *costs* where:

- each ***state*** denoted x, is a partition $(I, \bar{I})$ of the set of aircraft, where $\bar{I}$ is the (ordered) set of aircraft that have already landed, and I is the set of aircraft that have not landed yet.
- each ***action*** denoted u is an aircraft index $i \in I$ that we decide to land, while satisfying the CPS constraints.
- each ***transition*** is defined as follows. If we execute action $u = i \in I$ from a given state $x = (I, \bar{I})$, then the system generates the unique next state $x' = (I', \bar{I}')$, where $I' = I \setminus \{i\}$, and $\bar{I}' = \bar{I} \cup \{i\}$ (aircraft i landed).
- when the environment transits from the state x to the new state x' defined above, the estimated value c (***cost***) of the the new state is defined by

$$c = f(\bar{I}') + g(I'), \tag{13}$$

where $f(\bar{I}')$ is the delay cost of the (landed) sequence $\bar{I}'$. Indeed, aircraft in the set $\bar{I}$ are already sequenced. Thus, computing the landing times for aircraft in this

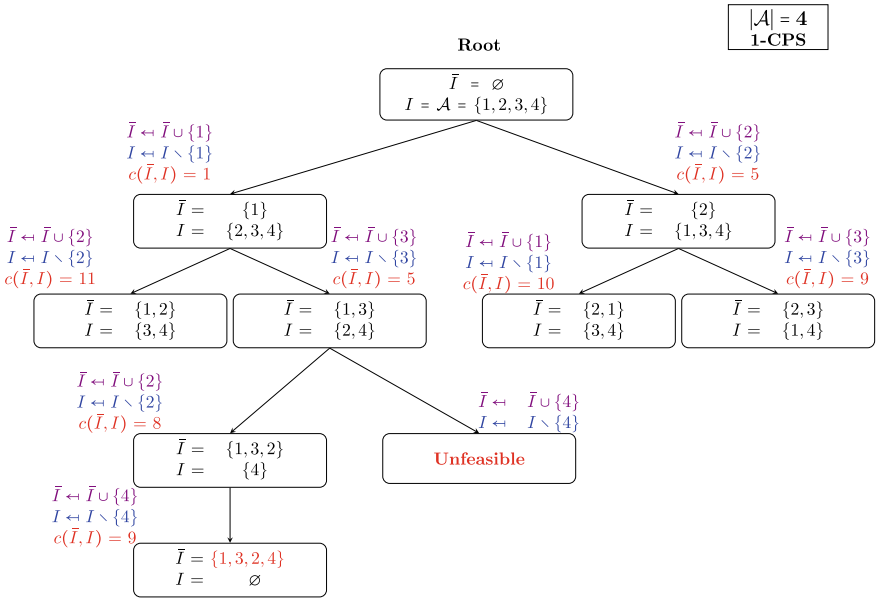

Fig. 2 An OP tree illustration for $|\mathcal{A}| = 4$ and $m = 1$

sequence is straightforward, and $f(\bar{I})$ is simply the weighted [1] sum of aircraft delays. $g(I')$ is a function that estimates the lowest cost among all sequences obtained from I' that satisfy the CPS constraints. In our numerical experiments, the FCFS rule is chosen as the estimation heuristic g, i.e. $m = 0$.

Optimistic Planning is the method that incrementally explores this search tree so as to identify an optimal branch as quickly as possible. Figure 2 illustrates an example of this tree for 4 aircraft ($\mathcal{A} = \{1, 2, 3, 4\}$), and a maximum position shifting of 1 ($m = 1$). Nodes are labeled by states, arcs are labeled by actions and costs. Near the nodes, the update process of the two sets $\bar{I}$ and I and the estimated costs are highlighted. Remark that the values of the costs in this figure are randomly chosen for the sake of this illustration.

The algorithm starts from the initial state where the set $\bar{I}$ is empty, and $I = \mathcal{A}$ (all aircraft available to land). At each iteration, its main loop seeks to determine which aircraft to land based on the optimistic evaluation c, and it updates $\bar{I}$ by adding this aircraft, until a stopping criteria is met, i.e., all aircraft are landed or a time limit is reached. Only actions that satisfy the operational constraints are available in a given state.

[1] These individual weights are provided with the data (*e.g.*, delay cost in Table 3).

5 Results and Discussion

In this section we report the computational results of the MIP formulation (1)–(12) and of our Optimistic Planning approach. Experiments are run on a personal computer under GNU/Linux operating system, processor Intel(R) Core(TM) i7-4700M with 8 GB of RAM. The MIP model was implemented in DoCplex, and solved using IBM CPLEX (version 12.8). Before reporting the computational results, we first present the test instances used in this paper.

5.1 Test Instances

Our test instances are generated from data sets from a benchmark test-problem set under construction at ENAC, obtained from real traffic in Paris-Orly Airport, that features two runways (06/24 and 08/26 as shown in Fig. 3), which are considered independent (runway 02/20 is rarely used for commercial traffic).

The test-problem sets are constructed from two traffic days obtained from the OpenSky Network [27]: one in July 2018 containing mostly data about landed aircraft on runway 06/24, and one in April 2019 containing data about landed aircraft on runway 08/26. We merge these two traffic days and artificially add light aircraft to obtain larger and also more congested data sets.

We construct four data sets of 40 flights, named `alp_40_1.txt`, `alp_40_2.txt`, `alp_40_3.txt`, and `alp_40_4.txt`. They contain data about aircraft whose scheduled time of arrival (sta) lies between 07:00–08:10, 11:00–12:30, 15:00–16:10, and 19:00–20:00. These data sets are available at [28]. A test instance of size $|\mathcal{A}|$ is obtained by considering the first $|\mathcal{A}|$ lines of data from one of these data sets.

Table 3 shows an example from [28], which is the most congested data set among the four, named `alp_40_4.txt`. In Table 3, the fourth and fifth columns, denoted "sta" and "sta_s", indicate the scheduled time of arrival in HH:MM:SS format and in seconds respectively. The sixth column displays the delay cost per time unit of each aircraft, that we computed following a similar approach to that used in [8].

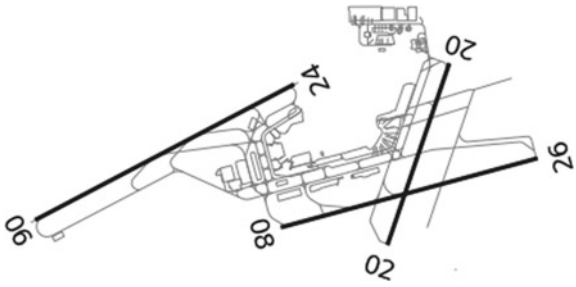

Fig. 3 A representation of Orly runways

Table 3 Example of a data-set features with $|\mathcal{A}| = 40$ aircraft

Index	mdl	category	sta	sta_s	Delay cost
1	B738	Medium	19:00:00	68,400	7
2	A320	Medium	19:00:00	68,400	5
3	B738	Medium	19:00:00	68,400	7
4	–	Light	19:00:00	68,400	1
5	B744	Heavy	9:00:00	68,400	22
6	B737	Medium	19:05:00	68,700	6
7	A320	Medium	19:05:00	68,700	5
8	B738	Medium	19:05:00	68,700	7
9	B738	Medium	19:05:00	68,700	7
10	-	Light	19:10:00	69,000	1
11	A319	Medium	19:10:00	69,000	4
12	AT43	Medium	19:10:00	69,000	1
13	A320	Medium	19:10:00	69,000	5
14	A320	Medium	19:10:00	69,000	5
15	B744	Heavy	19:10:00	69,000	22
16	A320	Medium	19:15:00	69,300	5
17	A321	Medium	19:15:00	69,300	7
18	B738	Medium	19:20:00	69,600	7
19	A320	Medium	19:20:00	69,600	5
20	A318	Medium	19:25:00	69,900	3
21	AT45	Medium	19:25:00	69,900	1
22	A320	Medium	19:25:00	69,900	5
23	CRJX	Medium	19:25:00	69,900	2
24	E145	Medium	19:30:00	70,200	1
25	A319	Medium	19:35:00	70,500	4
26	AT45	Medium	19:35:00	70,500	1
27	A320	Medium	19:35:00	70,500	5
28	–	Light	19:35:00	70,500	1
29	B744	Heavy	19:35:00	70,500	22
30	CRJ7	Medium	19:40:00	70,800	3
31	A320	Medium	19:40:00	70,800	5
32	CRJX	Medium	19:40:00	70,800	2
33	B738	Medium	19:45:00	71,100	7
34	E145	Medium	19:45:00	71,100	1
35	B744	Heavy	19:50:00	71,400	22
36	–	Light	19:50:00	71,400	1
37	A321	Medium	19:50:00	71,400	7
38	CRJX	Medium	19:50:00	71,400	2
39	A319	Medium	19:50:00	71,400	4
40	A320	Medium	19:55:00	71,700	5

In particular, the delay cost for each aircraft is obtained by multiplying the aircraft average pax number (in hundreds of seats) by its fuel consumption (in ton/hour), then round the results to the nearest integer. These individual delay costs are used as weights to compute the total cost of a given fixed sequence of aircraft. In particular, they are used in the computation of c from Eq. (13), as well as in the computation of %improv in Eq. (14).

5.2 Computational Results

We first report results obtained from implementing our MIP model involving a single runway ($|\mathcal{K}| = 1$), for different values of the maximum position shifting $m = 2, \ldots, 6$. Figure 4 illustrates the evolution of the computation time in seconds for each value of m and for a set of 8 test instances of various sizes $|\mathcal{A}| = 16, 18, \ldots, 30$, obtained by simply considering the first $|\mathcal{A}|$ lines of the data set `alp_40_4.txt`, presented in Table 3. We impose a time limit of 1800 s (30 min) in CPLEX.

Figure 4 exhibits the expected exponential growth of the computing time with the size of the instance, $|\mathcal{A}|$, and with increasing values of m, (recall that the ALP is an NP-hard problem). The saturation effect than can be observed is simply due to our time limit.

Table 4 reports the performance of the MIP model on various test instances, obtained this time from the four data sets of [28], by considering the first $|\mathcal{A}|$ lines of each of the four data sets. Results for each instance size are averaged over the four tests. Throughout Table 4, column "$|\mathcal{A}|$" represents the size of the instance, column "m" shows the value of the maximum position shift parameter, column "% improv (MIP)" displays the percentage improvement of the MIP approach, and the

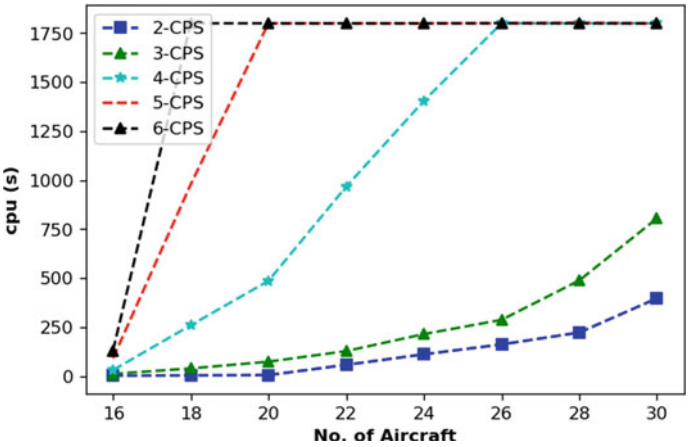

Fig. 4 Computational time of the MIP approach for different maximum position shifting values

Table 4 MIP-approach performance on different instances from the four data sets [28]

$\|\mathcal{A}\|$	m	%improv (MIP)	cpu (s)
18	2	22	1.3
	3	34	12
20	2	21	3
	3	32	17
22	2	28	3
	3	37	26
24	2	26	4
	3	37	40
26	2	25	5
	3	36	45
28	2	26	8
	3	35	68
30	2	27	30
	3	37	164
32	2	26	46
	3	37	410
34	2	25	70
	3	36	550
36	2	24	208
	3	34	974
38	2	24	482
	3	35	1110
40	2	24	1090
	3	33	1400

last column reports the computing time in seconds. The percentage of improvement obtained by a method M (here M = MIP) is computed with respect to the FCFS solution as:

$$\%\text{improv (M)} = \frac{C_{\text{FCFS}} - C_{\text{M}}}{C_{\text{FCFS}}} \times 100, \tag{14}$$

where C_{FCFS} and C_{M} are the cost of the FCFS sequence and that of the solution provided by the method M, respectively.

It can be concluded from Table 4 that significant improvements can be obtained with the MIP approach, starting from $m = 3$, but this requires large computation times, which make it non-adapted to the dynamic nature of our problem, especially since the complexity scales exponentially with the number of aircraft, and since future ATM systems will have to deal with very large ALP instances.

Table 5 Algorithm performance details (average improvement) for one runway

$\|\mathcal{A}\|$	%improv (OP) m = 2			%improv (OP) m = 3		
	2*s*	5*s*	15*s*	2*s*	5*s*	15*s*
18	12	12	12	2	15	15
20	18	18	19	10	23	24
22	23	22	21	19	32	33
24	19	25	26	22	26	31
26	14	19	20	11	24	31
28	15	16	24	9	23	29
30	14	18	24	8	21	36
32	14	18	26	2	22	37
34	14	12	25	6	23	28
36	13	13	25	7	24	24
38	12	13	26	8	23	26
40	12	13	25	7	22	26
min	12	12	12	2	15	15
max	23	25	26	22	32	37
avg	15	16	20	28	23	29

We report the results of the OP approach on different instance sizes $|\mathcal{A}| = 18, 20, \ldots, 40$ involving a single runway (Table 5), and imposing each time a limited computational time-budget of $\{2, 5, 15\}$ s. For each instance size, we evaluate the approach on different instances of the same size—generated from the four data sets [28]—and report the average, minimum and maximum improvement over the FCFS solution.

Table 5 shows the average percentage improvement of the total cost given by Eq. (14) for two values of the maximum position shifting parameter, $m = 2$ and 3. It can be observed that large instances of sizes greater than 30 can benefit from a significant improvement (on average more than 21%) for a maximum position shifting of $m = 3$, within only 5 seconds.

Finally, Table 6 reports an example of the solution provided by our OP approach on the instance given in Table 3 with $|\mathcal{A}| = 22$ aircraft, and imposing a computational budget of 2 s. The first column displays the aircraft position in the solution sequence. The "index" columns corresponds to the aircraft index from Table 3 occupying each position. The "landing" columns report the landing times. For this example, the percentage improvement of the FCFS sequence is 35%. Moreover, remark that for this scenario, the utilization of the runway in terms of the makespan i.e. length of the sequence is also optimized. Indeed, the last landing in the sequence for the FCFS is 7:41:20 while the last landing with our approach is at 7:40:45.

Table 6 Example of solutions provided by FCFS and by our optimistic approach

Position	FCFS		OP	
	Index	Landing	Index	Landing
1	1	7:00:00	3	7:00:00
2	2	7:03:16	5	7:01:36
3	3	7:04:16	4	7:03:12
4	4	7:05:52	1	7:04:48
5	5	7:07:28	2	7:08:04
6	6	7:10:05	6	7:10:00
7	7	7:15:00	8	7:15:00
8	8	7:16:00	9	7:16:36
9	9	7:17:36	7	7:19:13
10	10	7:20:13	10	7:20:22
11	11	7:21:22	12	7:25:00
12	12	7:25:00	13	7:26:09
13	13	7:26:09	11	7:27:18
14	14	7:30:00	15	7:30:00
15	15	7:33:16	14	7:31:00
16	16	7:34:25	17	7:33:37
17	17	7:35:34	20	7:35:00
18	18	7:36:43	21	7:36:09
19	19	7:37:52	16	7:37:18
20	20	7:39:01	18	7:38:27
21	21	7:40:10	19	7:39:36
22	22	7:41:20	22	7:40:45

Our computational experiments on the MIP formulation and the heuristic search approach show that the latter is more suited and more promising to solve the ALP with large congested instances, since it can provide good solutions in short computation time.

6 Conclusion

Runway sequence optimization is an ongoing challenge for researchers and controllers due to the dynamic nature of the problem and to the various operational constraints that must be taken into consideration. In this work, we proposed an exact approach (MIP) to solve the deterministic case of the ALP as well as a novel method based on Optimistic Planning to solve medium and large challenging instances.

Our computational experiments show that computation times for our MIP model (and other exact approaches) are very high for large congested instances, which make them unsuited to the dynamic nature of ALP. With the constrained-position shifting restrictions, the complexity of the problem can be reduced, but the problem remains untractable for increasing values of the maximum position-shifting parameter and the number of aircraft. On the other hand, our proposed heuristic search approach based on optimistic planning is able to find good quality solutions that significantly improve the FCFS sequence within a limited time budget, making it a promising method for solving the ALP in real time.

In future studies, we plan to extend our heuristic search approach to the multiple-runway case. Furthermore, instead of using the First-Come First-Served rule as the estimation heuristic, we are planning to construct more accurate functions to help the search to explore the most promising nodes first, so as to identify an optimal branch faster. Taking into consideration uncertainty on the arrival times is also a future track of research, since the solutions of our two deterministic approaches (MIP and the heuristic search) cannot be straightforwardly applied in the presence of uncertainty.

Acknowledgements The authors would like to thank Serge Roux, from ENAC, for his assistance with technical support. The authors also thank the anonymous referees, whose suggestions greatly improved the quality and the presentation of this paper.

References

1. The International Air Transport Association (IATA). [Online]. Available: https://www.iata.org/pressroom/pr/Pages/2017-10-24-01.aspx
2. A. Odoni, R. De Neufville, *Airport Systems: Planning, Design, and Management* (McGraw-Hill, New York, 2003)
3. J.A. Bennell, M. Mesgarpour, C.N. Potts, Airport runway scheduling. 4OR **9**(2) (2011)
4. J.E. Beasley, M. Krishnamoorthy, Y.M. Sharaiha, D. Abramson, Scheduling aircraft landings—the static case. Transport. Sci. **34**(2), 180–197 (2000)
5. F. Furini, C.A. Persiani, P. Toth, Aircraft sequencing problems via a rolling horizon algorithm," in *International Symposium on Combinatorial Optimization* (Springer, Berlin, 2012), pp. 273–284
6. D. Briskorn, R. Stolletz, Aircraft landing problems with aircraft classes. J. Scheduling **17**(1), 31–45 (2014)
7. A. Ghoniem, H.D. Sherali, H. Baik, Enhanced models for a mixed arrival-departure aircraft sequencing problem. INFORMS J. Comput. **26**(3), 514–530 (2014)
8. F. Furini, M.P. Kidd, C.A. Persiani, P. Toth, Improved rolling horizon approaches to the aircraft sequencing problem. J. Scheduling **18**(5), 435–447 (2015)
9. A. Faye, Solving the aircraft landing problem with time discretization approach. Eur. J. Oper. Res. **242**(3), 1028–1038 (2015)
10. H. Balakrishnan, B. Chandran, Scheduling aircraft landings under constrained position shifting, in *AIAA Guidance, Navigation, and Control Conference and Exhibit* (2006), p. 6320
11. A. Lieder, D. Briskorn, R. Stolletz, A dynamic programming approach for the aircraft landing problem with aircraft classes. Eur. J. Oper. Res. **243**(1), 61–69 (2015)
12. L. Bianco, P. Dell'Olmo, S. Giordani, Scheduling models for air traffic control in terminal areas. J. Scheduling **9**(3), 223–253 (2006)

13. A. Salehipour, M. Modarres, L.M. Naeni, An efficient hybrid meta-heuristic for aircraft landing problem. Comput. Oper. Res. **40**(1), 207–213 (2013)
14. G. Hancerliogullari, G. Rabadi, A.H. Al-Salem, M. Kharbeche, Greedy algorithms and metaheuristics for a multiple runway combined arrival-departure aircraft sequencing problem. J. Air Transp. Manage. **32**, 39–48 (2013)
15. A. Rodriguez-Diaz, B. Adenso-Diaz, P.L. Gonzalez-Torre, Minimizing deviation from scheduled times in a single mixed-operation runway. Comput. Oper. Res. **78**, 193–202 (2017)
16. J. Ma, D. Delahaye, M. Sbihi, P. Scala, M.A.M. Mota, Integrated optimization of terminal maneuvering area and airport at the macroscopic level. Transport. Res. Part C Emerging Technol. **98**, 338–357 (2019)
17. B. Soykan, G. Rabadi, A tabu search algorithm for the multiple runway aircraft scheduling problem, in *Heuristics. Metaheuristics and Approximate Methods in Planning and Scheduling* (2016), pp. 165–186
18. G. Bencheikh, J. Boukachour, A.E.H. Alaoui, F.E. Khoukhi, Hybrid method for aircraft landing scheduling based on a job shop formulation. Int. J. Compu. Sci. Network Secur. **9**(8), 78–88 (2009)
19. X.B. Hu, E.A.D. Paolo, A ripple-spreading genetic algorithm for the aircraft sequencing problem. Evol. Comput. **19**(1), 77–106 (2011)
20. G. Bencheikh, J. Boukachour, A.E.H. Alaoui, Improved ant colony algorithm to solve the aircraft landing problem. Int. J. Comput. Theory Eng. **3**(2), 224 (2009)
21. Y. Jiang, Z. Xu, X. Xu, Z. Liao, Y. Luo, A schedule optimization model on multirunway based on ant colony algorithm. Math. Probl. Eng. **2014**, Article ID 368208 (2014)
22. A. Salehipour, L. Moslemi Naeni, H. Kazemipoor, Scheduling aircraft landings by applying a variable neighborhood descent algorithm: runway-dependent landing time case. J. Appl. Oper. Res. **1**(1), 39–49 (2013)
23. R. Munos, From bandits to Monte-Carlo tree search: The optimistic principle applied to optimization and planning. Found. Trends Mach. Learn. **7**(1), 1–129 (2014)
24. H. Lee, H. Balakrishnan, A study of tradeoffs in scheduling terminal-area operations, in *Proceedings of the IEEE* (2008), pp. 2081–2095
25. R. Prakash, R. Piplani, J. Desai, An optimal data-splitting algorithm for aircraft scheduling on a single runway to maximize throughput. Transport. Res. Part C Emerg. Technol. **95**, 570–581 (2018)
26. J.F. Hren, R. Munos, Optimistic planning of deterministic systems, in *European Workshop on Reinforcement Learning* (Springer, Berlin, 2008), pp. 151–164
27. The OpenSky Network. [Online]. Available: https://opensky-network.org
28. S. Ikli, *The Aircraft Landing Problem instances*. [Online]. Available: https://personnel.isae-supaero.fr/emmanuel-rachelson/alp-instances.html

Passengers on Social Media: A Real-Time Estimator of the State of the US Air Transportation System

P. Monmousseau, A. Marzuoli, E. Feron, and D. Delahaye

Abstract This paper aims at investigating further the use of the social media Twitter as a real-time estimator of the US Air Transportation system. Two different machine learning regressors have been trained on this 2017 passenger-centric dataset and tested on the first two months of 2018 for the estimation of air traffic delays at departure and arrival at 34 different US airports. Using three different levels of content-related features created from the flow of social media posts led to the extraction of useful information about the current state of the air traffic system. The resulting methods yield higher estimation performances than traditional state-of-the-art and off-the-shelf time-series forecasting techniques performed on flight-centric data for more than 28 airports. Moreover the features extracted can also be used to start a passenger-centric analysis of the Air Transportation system. This paper is the continuation of previous works focusing on estimating air traffic delays leveraging a real-time publicly available passenger-centered data source. The results of this study suggest a method to use passenger-centric data-sources as an estimator of the current state of the different actors of the air transportation system in real-time.

Keywords Delay estimation · ATM performance measurement · Big data · Machine learning

P. Monmousseau (✉) · D. Delahaye
Ecole Nationale de l'Aviation Civile (ENAC), Universite de Toulouse, Toulouse, France
e-mail: philippe.monmousseau@recherche.enac.fr

D. Delahaye
e-mail: delahaye@recherche.enac.fr

A. Marzuoli · E. Feron
School of Aerospace Engineering, Georgia Institute of Technology, Atlanta, GA, USA
e-mail: amarzuoli3@gatech.edu

E. Feron
e-mail: feron@gatech.edu

Air Traffic Management and Systems IV, Lecture Notes in Electrical Engineering 731,
https://doi.org/10.1007/978-981-33-4669-7_11

1 Introduction

The Air Transportation System is a complex interconnected system that carried more than 631 million passengers on domestic flights in the United States in 2010 according to the Bureau of Transportation Statistics (BTS) [1]. Flight delays are still a major issue both in the United States with 27.0% of departing flights and 27.8% of arriving flights experiencing delays in 2017 [1].

Most previous studies aimed at predicting or classifying flight delays were centered on flight-centric information coming from a variety of sources with different levels of public availability, and using only very little passenger-centric data. Mueller and Chatterji [2] created a probabilistic model of delays by fitting Poisson and Normal distributions to the historic delay data from 10 airports. Rebollo and Balakrishnan [3] implemented a network model to classify and predict future delays on specific links or specific airports using two years of flight-centric and weather-related data. Klein et al. [4] and [5] focused on predicting short-term weather-related delays using only past and current weather information. Aljubairy et al. [6] used Internet of Things in order to analyze flight-related sensors in real-time and classify the delay of an upcoming flight.

Over the past few years, NextGen [7] in the United States has been advocating a shift from flight-centric metrics to passenger-centric metrics to evaluate the performance of the Air Transportation System. The failures and inefficiencies of the air transportation system not only have a significant economic impact but they also stress the importance of putting the passenger at the core of the system [8, 9]. Several studies have highlighted the disproportionate impact of airside disruptions on passenger door-to-door journeys. Flight delays do not accurately reflect the delays imposed upon passengers' full multi-modal itinerary. Cook et al. [10] designed propagation-centric and passenger-centric performance metrics, and compare them with existing flight-centric metrics. Wang [11] showed that high passenger trip delays are disproportionately generated by canceled flights and missed connections. Nine of the busiest thirty-five airports cause 50% of total passenger trip delays. Congestion, flight delay, load factor, flight cancellation time and airline cooperation policy are the most significant factors affecting total passenger trip delay. NextGen intends to not only improve the predictability and resilience of the US Air Transportation System, but also to reduce door-to-door travel time for passengers.

Passengers are at the core of this system and, yet, limited quantitative information about passenger movements is publicly shared. Each aviation stakeholder only has access to a partial view of the passenger-side of air transportation operations making a system-wide data-driven picture of passenger behavior difficult to implement. The BTS provides aggregated passenger data per market but no granular information. Passenger surveys conducted by airports or airlines, while very detailed, remain limited to small samples of passengers and short time periods, and may not be representative.

Precursor work was made by Marzuoli et al. in [12] and [13] using mobile phone data in order to analyze the performances of airports from the passengers' perspective.

These studies validated the use of passenger-centric data to better assess the overall health of the Air Transportation System. However mobile phone data is proprietary data and is not often publicly available. In order to operate in real-time, it is thus necessary to also look into other sources of passenger data available on a national scale.

Another popular source of data previously used for studying large-scale behaviors with real time availability is social media, in particular Twitter. With more than 68 millions active users in the United States [14], Twitter is an important pool of user-created data that is still not fully leveraged. Twitter has already been the main focus of many studies focused on its real-time availability, especially during natural disasters with multiple works by Palen et al. [15–17]. Terpstra et al. also studied how a real time Twitter analysis could have provided valuable information for the operational response of a natural disaster crisis management with the case of the storm hitting a festival in Belgium [18]. Regarding the air transportation field, most works mining Twitter data focus on how airlines are perceived by passengers by means of sentiment analysis [19] or sentiment classification [20]. Though these works give a good insight on how passengers perceive the state of some specific actors within the air transportation system, it does not give a global idea of its health. Monmousseau et al. in [21] used publicly available social media data created by passengers to accurately estimate and predict the hourly aggregated status of the US air transportation system.

This paper proposes to build on this previous work in order to estimate the state of the air transportation system to a finer level. Rather than predicting the number of delays across all the United States, the proposed passenger-centric models are improved and tuned to accurately estimate the state of delays for each of the 35 major airports within the United States. The created models are based on three different levels of content-related features created from the flow of social media posts. First results indicate that these new models can estimate the number of hourly delays with a mean absolute error of less than 3 flights for 26 of the considered airports, and of less than 6 flights for the 9 remaining airports.

The rest of the paper is structured as follows: Sect. 2 describes the datasets and the feature extraction process. The methodology and results of the training process are shown in Sect. 3, before being analyzed and exploited in Sect. 4. Section 5 concludes this study and discusses possible future steps.

2 Dataset description and feature selection

2.1 Dataset description

Following the initial work performed in [21], the goal here is to use passengers behavior on social media - in particular on Twitter - in order to analyze and estimate the flight-centric health of the US air-transportation system at an airport level. In this

Table 1 Twitter handles used for gathering tweets

Category	Twitter handles
Airlines	@united, @Delta, @AmericanAir, @SouthwestAir, @SpiritAirlines, @VirginAmerica, @JetBlue
Airports	@JFKairport, @ATLairport, @flyLAXairport, @fly2ohare, @DFWAirport, @DENAirport, @CLTAirport, @LASairport, @PHXSkyHarbor, @MiamiAirportMIA, @iah, @EWRairport, @MCOAirport, @Official_MCO, @SeaTacAirport, @mspairport, @DTWeetin, @BostonLogan, @PHLAirport, @LGAairport, @FLLFlyer, @BWI_Airport, @Dulles_Airport, @MidwayAirport, @Reagan_Airport, @slcairport, @SanDiegoAirport, @flyTPA, @flypdx, @flystl, @flySFO,@HobbyAirport, @flynashville, @AUStinAirport, @KCIAirport

study, the flight-centric health of an airport is described by delay related information contained within BTS data. This data is publicly available usually with a two to three month delay and this study limits itself with the BTS data from January 2017 to February 2018.

The Twitter dataset available for this study is the same as in [21] and consists of all the tweets found using a basic search for each handle of 7 major US airlines as well as 34 major US airports (one of them having two Twitter handles). The full list of handles can be found in Table 1. Each entry consists of a timestamp, a user id, the content of the tweet and the handle used to retrieve the tweet. This dataset spans the entire period from January 1st 2017 to February 28th 2018. The extraction of features from this dataset has been improved since the previous study and is described in Sect. 2.2.

Figure 1 plots the total number of tweets related to each handle over the year 2017 against the total number of flights flown by each airline or to and from each airport. Airlines tend to gather more tweets than airports, and the number of tweets is not necessarily correlated to the number of flights flown per airline. The handle "@Delta" gathered the most tweets over 2017 even though Southwest Airlines carried out the most flights in 2017. Most airports are regrouped around a cluster of 10k tweets and 200k flights over 2017, with Los Angeles International airport (LAX) and Hartsfield-Jackson Atlanta International airport (ATL) being exceptions due to their higher number of tweets.

In order to estimate the flight-centric health of each considered airport, this information first needs to be extracted from the BTS dataset for each airport. Only two types of delayed flights are considered here from a passenger's perspective: Flights departing with any amount of delay, and flights arriving with a delay greater than 15 minutes. Once all the flights departing an airport and all the flights arriving at the same airport are selected, the following values can be aggregated per hour:

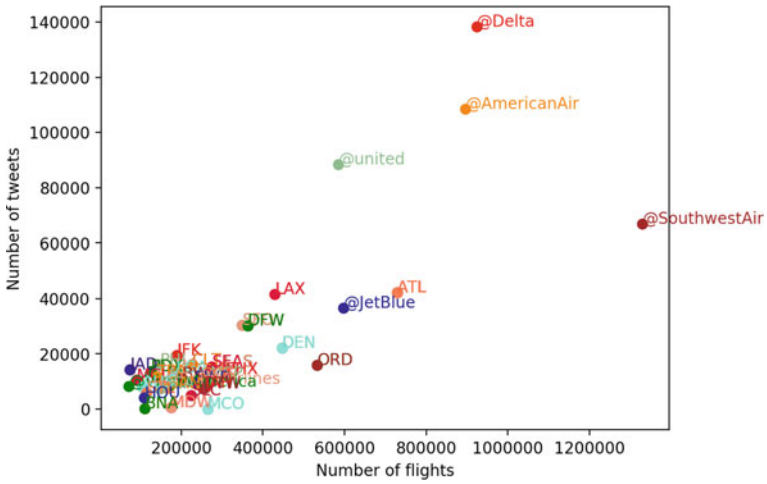

Fig. 1 Number of tweets over the number of flights during the year 2017 for the considered airlines and airports

- NumDepDelay: Number of flights departing with a delay
- NumArrDelay15: Number of flights arriving with a delay greater than 15 min

The aim of this study is to accurately estimate these two values for each airport at every hour using a single passenger-centric dataset.

2.2 Feature Selection on Twitter Data

2.2.1 Volume Features

Features were extracted identically for all search handles presented in Table 1, for the exception of @MiamiAirportMIA, which does not gather enough tweets. In addition to the raw number of tweets per hour per search handle, keyword related information is also extracted from the Twitter dataset. In order to keep all the relevant tweets without having to decline all the possible forms of the chosen keywords (e.g. "delay", "delayed", "delays", etc.), simple regular expression filters were created for each keyword: Any tweet containing a word starting with the related keyword is kept and the resulting tweets are then aggregated per hour. Five keywords were chosen for this study: 'delay', 'wait', 'cancel', 'hours', 'refund'.

2.2.2 Topic Features

Another way of exploiting information from the content of these tweets is to perform a topic analysis of the tweet database using Latent Dirichlet Allocation [22] (LDA). In LDA, each document - here each tweet - is modeled as a finite mixture of topics. A topic is defined as a distribution over the words composing the full set of considered documents. The topic distribution of each document and the word distribution of each topic can be determined using variational Bayes approximations and was implemented in Python by Rehurek and Sojka [23] within the Gensim library.

A first step in topic analysis is to clean the documents analyzed, here the tweets. This cleaning process was already performed in [13] and [21] and consists of the following steps: Any reference to websites or pictures was replaced by a corresponding keyword. Every mention to another Twitter user within a tweet (@someone) as well as most emojis were similarly replaced. Since this database contains many replies from airlines to their customers, individual signatures of each agent were also replaced by a keyword. Dates and times were also generically replaced by keywords (e.g. "3rd Jan 2017" becomes "DATE" and "4pm" becomes "TIME"). Common bigrams and trigrams, i.e. combination of two or three words, are also considered as single words. The resulting text was then filtered from common stop-words and from words occurring only once in the whole year of 2017.

For this study, the choice of 100 topic is made and the topic distribution determination algorithm is run five times and the best topic representation is chosen using the coherence measures introduced in [24]. The aim of these coherence measures is to select topics with word distributions the more human understandable possible for a better explainability. As an example, the top five words of a created topic are: "toknowmeistoflywithme", "nut_allergy", "restrictions_apply", "comfortable_journey" and "mins_secs". The first word represents a *hashtag* for the phrase "To know me is to fly with me" and the other words are actually bigrams. The combination of these five words indicate a topic around passenger well-being aboard a plane.

The topic mixture of each tweet is then calculated based on this choice of 100 topics. Topic related features are then created by averaging the distribution of each topic per hour and per search handle. The hourly standard deviation of each topic distribution is also extracted.

This cleaning process introduces two additional keywords that enables a quick filtering of tweets, and therefore two additional features to add per search handle: tweets containing a picture and those containing a website link. Thus seven keywords are actually considered for feature extraction: 'delay', 'wait', 'cancel', 'hours', 'refund', 'PICTURE', 'WEBSITE'.

2.2.3 Sentiment Features

Sentiment analysis is also used here to enhance the feature set considered. Two different datasets and cleaning method were used to train three different regressors

Table 2 Emoji sentiment association

Category	Emojis
Positive	":)", "=)", ":-)", ";)", ";-)", ":-D", ":D", "=D"
Negative	":(", ":-(", "=(", ":-@", ":'(", ":-|"

each. The first dataset used was the labelled dataset used in a Kaggle competition [25] and was cleaned using the same process as for the previous LDA learning. The generic keywords from the cleaning process (e.g. 'WEBSITE', 'DATE') were removed before creating the associated dictionary, as well as words appearing in less than 20 tweets or in more than 75% of the full dataset. A second dataset and cleaning process was generated based on the work of Read [26]. Emoji filters were used to extract tweets from the initial dataset and automatically label them with a positive or negative sentiment according to Table 2. The text cleaning process is improved by merging negation words ("no", "not" and "never") with the word that follows it. The tokens used for the creation of the dictionary are the resulting bigrams, i.e. combinations of two words that follow each other in a tweet, with the same frequency filter as the first method described.

For both methods, three classifiers are trained (a random forest classifier, a naive Bayesian classifier and a logistic regressor) using the scikit-learn library [27]. A sentiment score is then calculated for each tweet by averaging the output of these classifiers, 0 meaning a unanimous negative sentiment and 1 a unanimous positive sentiment. The hourly average of these scores are added to the Twitter feature set.

2.2.4 Summary

Given the temporal nature of the data analyzed, the following features were chosen to keep track of the date: month of the year, day of the month, day of the week and hour in the day. In summary the following 8484 features are considered:

- Hourly volume of tweets for each search handle (7 airlines and 33 airports giving 40 features): Num_tweets_*handle*
- Hourly volume of keyword-related tweets for each search handle (40 × 7 features): Num_tweets_*keyword_handle*
- Hourly average of tweets' sentiment (40 × 2 features): Mean_sent_*method_handle*
- Hourly average of topic distribution for each search handle (40 × 100 features): Mean_*topic_handle*
- Hourly standard deviation of topic distribution for each search handle (40 × 100 features): Std_*topic_handle*
- Month of the year, Day of the month, Day of the week and Hour in the day (4 features)

3 Estimating Delays

The aim of this section is to see how well it is possible to estimate per airport the number of flights departing with a delay and the number of flights arriving with a delay greater than 15 minutes using the features extracted from the Twitter dataset. The dataset was split into a training set consisting of the data from the year 2017, and a testing set with the data from January and February 2018.

3.1 Methodology

For each BTS value at each airport, two different machine learning regressors were trained on the training data set: a Random Forest regressor and a Gradient Boosting regressor. These regressors were implemented from scikit-learn [27] with identical hyper-parameters. The maximum depth of each regressor was limited to ten, the minimum number of samples for a split was fixed to two and the maximum number of trees was fixed at ten. These parameters were chosen following the results from the initial work performed in [21].

As a comparison benchmark, we used Facebook's time-series forecasting tool Prophet [28] on the 2017 BTS data to forecast the full two first months of 2018. The Prophet tool is based on an additive model where non-linear trends are fit with yearly, weekly, and daily seasonality [29]. It is described as robust to outliers and missing data with no parameter tuning necessary, therefore the default parameters of the Prophet tool was used for this forecasting benchmark.

Lastly, the standard deviation of the BTS values in the training set were calculated to illustrate the added value of the trained regressors. The performance measures used to compare the different regressors are presented in Sect. 3.2.

3.2 Estimation Performance Measures

In order to measure the performance of the different models, two different indicators were used: the R^2 score and the mean-absolute error (MAE).

The R^2 score, also known as the coefficient of determination, is defined as the unity minus the ratio of the residual sum of squares over the total sum of squares:

$$R^2 = 1 - \frac{\sum_i (y_i - f_i)^2}{\sum_i (y_i - \bar{y})^2} \tag{1}$$

where y is the value to be predicted, $\bar{y}$ its mean and f is the predicted value. It ranges from $-\infty$ to 1, 1 being a perfect prediction and 0 meaning that the prediction does as well as constantly predicting the mean value for each occurence. In the case of

a negative R^2, then the model has a worse prediction than if it were predicting the mean value for each occurence and therefore yields no useful predictions.

Regarding the mean-absolute error, the smaller its value is, the more accurate the prediction is. It is calculated using the following formula:

$$\text{MAE} = \frac{1}{n} \sum_i |f_i - y_i| \tag{2}$$

where n is the number of values being predicted.

3.3 Estimation Results

Figure 2 shows a comparison per airport of the mean-absolute error of the two trained regressors along with the chosen benchmark for the estimation of the number of flights departing with a delay. The standard deviation of the number of delayed departing flights at each airport during the year 2017 is also included for comparison. The Random Forest models have the best results in this case: they outperform the Gradient Boosting models at all-but-one airports (LAX) and the Facebook Prophet tool on 31 airports out of 34. For 26 airports, the Random Forest models are able to estimate the hourly number of delayed departing flights with a mean-absolute error of three flights or less, and with an error of less than six flights for the remaining airports.

Figure 3 shows a comparison per airport of the mean-absolute error of the two trained regressors along with the chosen benchmark for the estimation of the number of flights arriving with a delay greater than 15 minutes. The standard deviation of the number of delayed arriving flights at each airport during the year 2017 is also included for comparison. The Random Forest models also have the best results in this case though their relative performance are not as important as for delayed departing flights : they outperform the Gradient Boosting models at 27 airports out of 34 and the Facebook Prophet tool on 28 airports out of 34. The absolute performance is however better than for estimating the number of delayed departing flights. For 28 airports, the Random Forest models are able to estimate the hourly number of delayed departing flights with a mean-absolute error of less than three flights, and with an error of less than five flights for the remaining airports.

Figure 4 shows a comparison per airport of the R^2 score of the two trained regressors along with the chosen benchmark for the estimation of the number of flights departing with a delay. The Random Forest models still have the best results in this case, but the model associated with LAX airport also shows the only negative score. They outperform the Gradient Boosting models at 27 airports out of 34 and the Facebook Prophet tool on 28 airports out of 34.

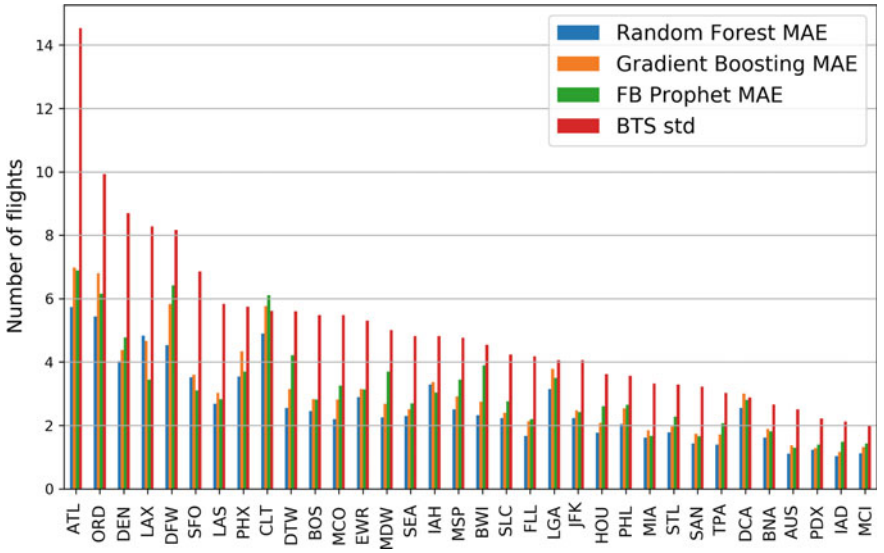

Fig. 2 Comparison of the mean absolute errors per airport for the trained regressors for the estimation of the number of delayed departing flights. The standard deviation of the BTS value on the training set is included for comparison

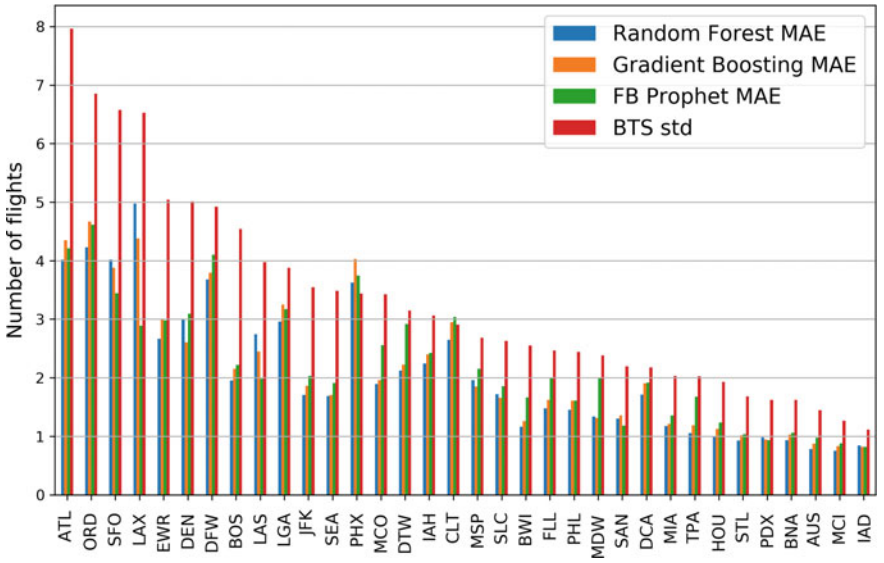

Fig. 3 Comparison of the mean absolute errors per airport for the trained regressors for the estimation of the number of flights arriving with a delay greater than 15 min. The standard deviation of the BTS value on the training set is included for comparison

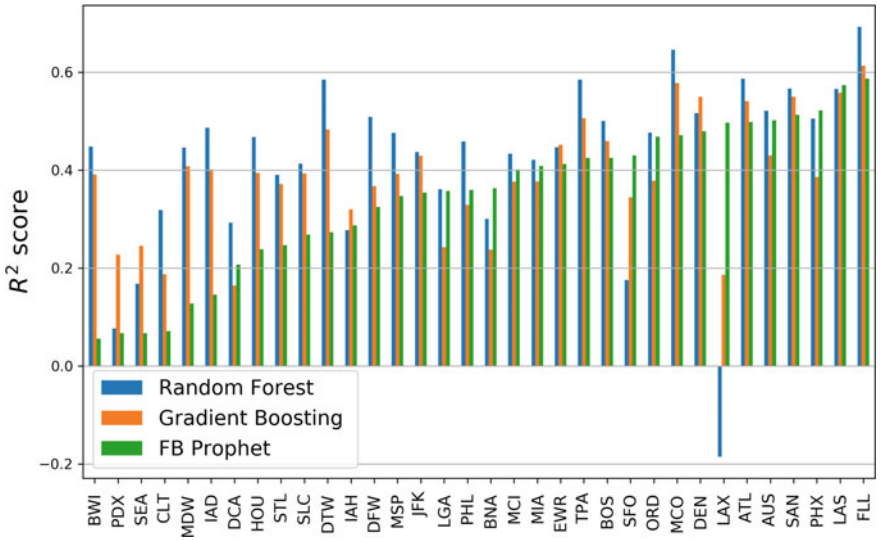

Fig. 4 Comparison of the R^2 scores per airport for the trained regressors for the estimation of the number of delayed departing flights

4 Analysis and Applications

The aim of this section is to analyze the differences between the chosen models as well as explore possible applications resulting from the extracted features.

4.1 Model Analysis

Figure 5 shows the hourly prediction of the number of delayed departing flights at Atlanta airport (ATL) over the period January 12th–16th for the two trained regressors along with the benchmark and the actual values. This airport was chosen since it has the highest BTS standard deviation for the number of delayed departing and arriving flights, and the period was chosen to illustrate the high variability of the number of delays from a day to another. In this example, January 12 has more than twice as many delayed flights than any other day, as well as important hourly variations.

Figure 5 illustrates the main differences between the different models: The Prophet tool predicts for each day a similar daily variation with three peaks during the day yet with amplitudes varying depending on the month and the day of the week. It also predicts negative values, which underlines some limitations of the model in this case. The added value from passenger-centric data-sources is better seen on January 12 and 13, where only the Random Forest regressor is able to estimate the higher number of delays on January 12 before correctly estimating the more usual levels of January

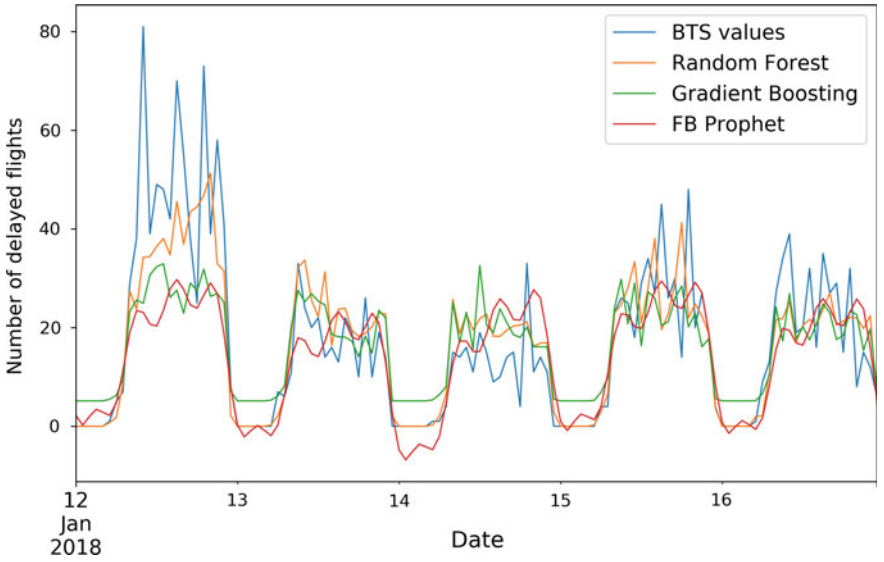

Fig. 5 Predicted number of delayed departing flights at ATL by the trained regressor over the period January 12th, 2018 to January 16th, 2018. The actual number of delayed departing flights is indicated for comparison

13. The Gradient Boosting regressor doesn't estimate outliers as well as the Random Forest regressor due to the difference in their loss functions. That difference is also illustrated by the non-zero minimum of the Gradient Boosting estimation during night time.

4.2 Other Applications

4.2.1 Real-Time Sentiment Analysis

The extracted features can be fed to the trained models for accurately estimating the number of delayed flights, but they can also be used directly in order to sense the overall passenger mood. Once the sentiment analyses are conducted on the tweets, it is possible to merge them into one score per airline and monitor their evolution.

Figure 6 shows the hourly average mood for three major airlines during the North-eastern bomb cyclone studied in [13]. These three airlines have a similar passenger mood evolution at the beginning and the end of the period, yet United Airlines shows a drop in passenger mood on January 4th, the day when the bomb cyclone actually hit the East coast. Though all three airlines have hubs in New York, United Airlines is the only airline with a hub at Newark International Airport (EWR) and not John F. Kennedy International Airport (JFK) nor LaGuardia Airport (LGA), which were both

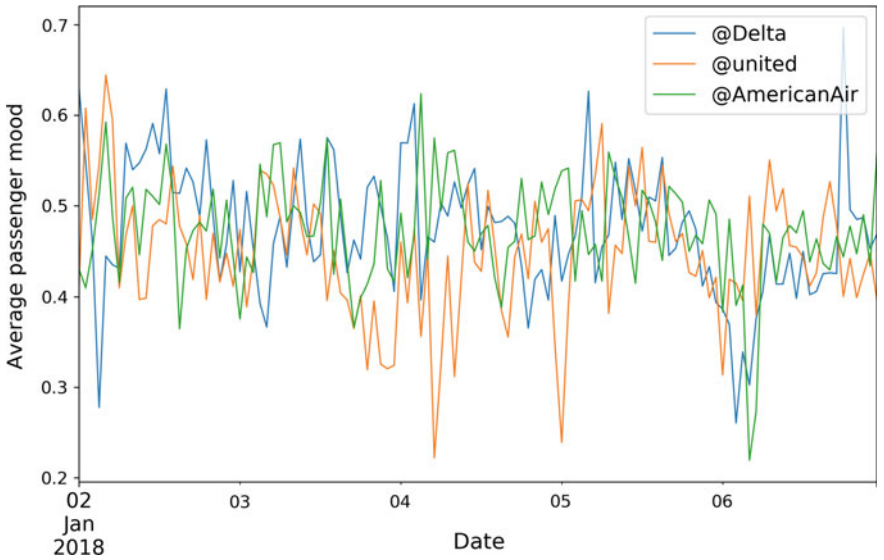

Fig. 6 Average passenger sentiment with respect to three major airlines over the period January 2nd, 2018 to January 6th, 2018, corresponding to a bomb cyclone hitting in the North-East of the US

closed during the bomb cyclone, meaning that United Airlines probably had more dissatisfied passengers to handle on site during these extreme weather conditions.

4.2.2 Airports Passenger Map

After training the Random Forest models, it is possible to search for the most important features within the 8484 initial features for each airport. This is achieved by using the Mean Decrease Impurity measure defined by Breiman in [30] and normalizing the obtained feature importances so that the sum of all feature importances is equal to one. Table 3 shows the ten features with the highest feature importances for predicting the number of delayed departing flights in ATL. Besides date related features, four of the top ten features are related to the volume of tweets containing delay keywords.

Once the features gathering 99% of the total importance for estimating the number of delayed flights are extracted, it is possible to group these features per origin in order to gain some insight on how airports are related from a passenger perspective. For example, once the most important features for estimating the number of delays at ATL are extracted, it is possible to count how many of these features are issued from tweets gathered using the handle of John F. Kennedy International Airport (JFK).

Figure 7 shows how ATL is connected to the other airports from this perspective. The larger the link between ATL and another airport, the more features were kept

Table 3 Top ten features for predicting the number of delayed departing flights at ATL

Rank	Feature	Rank	Feature
1	Hour	6	DayOfMonth
2	Month	7	delay_@SouthwestAir
3	DayOfWeek	8	num_ATL
4	delay_@Delta	9	delay_JFK
5	delay_ATL	10	mean_63_BWI

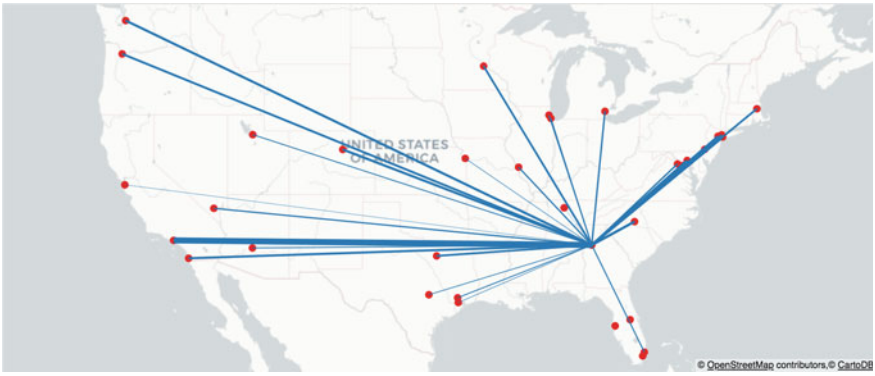

Fig. 7 Map of feature links between Atlanta airport (ATL) and the other airports for estimating the number of delayed departing flights. The larger the link, the more features were kept among the features gathering 99% of the total importance for estimating the number of departing delayed flights at ATL

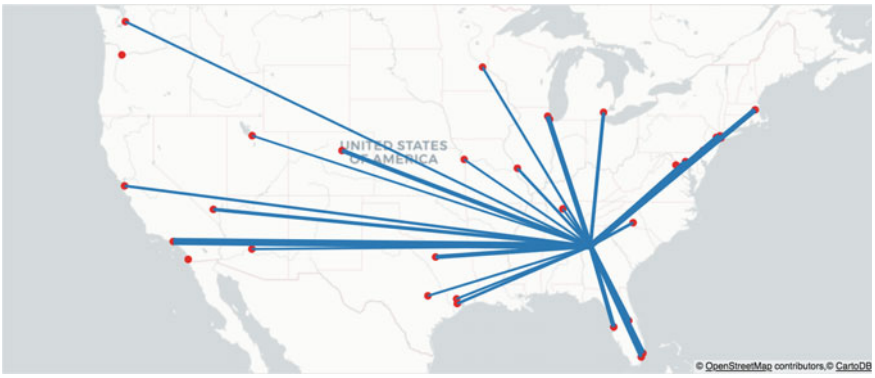

Fig. 8 Map of delay links between Atlanta airport (ATL) and the other airports. The larger the link, the more flights departed with a delay during 2017 from ATL towards the connecting airport. Only links with more than 1000 delayed flights in 2017 were considered

among the features gathering 99% of the total importance for estimating the number of departing delayed flights at ATL. Interestingly, this airport graph is different from the graph built from the actual BTS values. Figure 8 shows how ATL is connected to the other airports using the number of delayed departing flights from ATL. For example, although there are many delayed flights departing to Florida, few features from Floridan airports are kept. The opposite observation can be made regarding Portland (PDX): there were less than a thousand delayed flights from ATL to PDX, yet features from PDX were kept.

This example illustrates the possibility of creating a yearly review of airport relationship from a passenger point of view. Future studies should investigate more thoroughly the possible correlation and relation between the passenger connection map and the delay connection map.

5 Conclusion

This paper aimed at investigating further the use of the social media Twitter as an estimator of the US Air Transportation system. Exploiting both raw volume information as well as different levels of content information within the Twitter stream enables to accurately estimate for each airport the number of flights departing with a delay and the number of flights arriving with a delay greater than fifteen minutes. This passenger-based estimation yields a better estimation performance for a majority of airports compared to using a state-of-the-art and off-the-shelf forecasting tool on the flight-centric data alone. Moreover, the methods used to extract relevant features from this passenger-centric data-source can be used to gain additional real-time insight on how passengers relate to the Air Transportation system.

This study confirmed that information contained in passenger-centric datasets are useful for a better understanding of the different stakeholders within the air transportation system, and have the added benefit of being more readily and publicly available than flight centric datasets. Future studies should focus on analyzing cases when the estimation is less accurate, implying differences between the handling of passengers and that of planes. Another direction of study considered is to validate this method to other countries or regions (e.g. the European Union) where sufficient flight-centric data is available.

Acknowledgements The authors would like to thank Nikunj Oza from NASA-Ames, the BDAI team from Verizon Media in Sunnyvale as well as the French government for their financial support.

References

1. Bureau of Transportation Statistics, in *Bureau of Transportation Statistics, About BTS* (2018). [Online]. Available http://www.rita.dot.gov/bts/about
2. E. Mueller, G. Chatterji, Analysis of Aircraft Arrival and Departure Delay Characteristics, in *AIAA's Aircraft Technology, Integration, and Operations (ATIO) 2002 Technical Forum* (American Institute of Aeronautics and Astronautics, Los Angeles, California, 2002)

3. J.J. Rebollo, H. Balakrishnan, Characterization and prediction of air traffic delays. Transport. Res. Part C Emerg. Technol. **44**, 231–241 (2014)
4. A. Klein, C. Craun, R.S. Lee, Airport delay prediction using weather-impacted traffic index (WITI) model, in *29th Digital Avionics Systems Conference*, Salt Lake City, UT, USA. IEEE (2010), pp. 2.B.1-1–2.B.1–13
5. B. Sridhar, N.Y. Chen, Short-term national airspace system delay prediction using weather impacted traffic index. J. Guidance Control Dyn. **32**(2), 657–662 (2009)
6. A. Aljubairy, A. Shemshadi, Q.Z. Sheng, Real-time investigation of flight delays based on the Internet of Things data, in *Advanced Data Mining and Applications*, ed. by J. Li, X. Li, S. Wang, J. Li, Q.Z. Sheng, vol 10086 (Springer International Publishing, Cham, 2016), pp. 788–800
7. V. Cox, M. Romanowski, NextGen implementation plan, in *Federal Aviation Administration* (2009)
8. World Economic Forum, *Connected World: Transforming Travel, Transportation and Supply Chains*. http://www3.weforum.org/docs (2013)
9. World Economic Forum, *Smart Travel: Unlocking Economic Growth and Development Through Travel Facilitation*. http://www3.weforum.org/docs/GAC/2014 (2014)
10. A. Cook, G. Tanner, S. Cristóbal, M. Zanin, *Passenger-Oriented Enhanced Metrics* (2012)
11. D. Wang, D.L. Sherry, D.G. Donohue, Passenger trip time metric for air transportation, in *The 2nd International Conference on Research in Air Transportation* (2006)
12. A. Marzuoli, E. Boidot, E. Feron, A. Srivastava, Implementing and Validating Air Passenger–Centric Metrics Using Mobile Phone Data. J. Aerospace Inform. Syst. **16**(4), 132–147 (2019)
13. A. Marzuoli, P. Monmousseau, E. Feron, Passenger-centric metrics for air transportation leveraging mobile phone and Twitter data, in *Data-Driven Intelligent Transportation Workshop—IEEE International Conference on Data Mining 2018*, Singapore (2018)
14. Statista, Monthly active Twitter users in the United States (2018). [Online]. Available: https://www.statista.com/statistics/274564/monthly-active-twitter-users-in-the-united-states/
15. L. Palen, K. Starbird, S. Vieweg, A. Hughes, Twitter-based information distribution during the 2009 Red River Valley flood threat. Bulletin Am. Soc. Inform. Sci. Technol. **36**(5), 13–17 (2010)
16. S. Vieweg, A.L. Hughes, K. Starbird, L. Palen, Microblogging during two natural hazards events: what twitter may contribute to situational awareness (2010), p. 10
17. K. Kireyev, L. Palen, K.M. Anderson, *Applications of Topics Models to Analysis of Disaster-Related Twitter Data* (2009), p. 4
18. T. Terpstra, R. Stronkman, in *Towards a realtime Twitter analysis during crises for operational crisis management* (2012), p. 10
19. J. O. Breen, Mining twitter for airline consumer sentiment, in *Practical Text Mining and Statistical Analysis for Non-structured Text Data Applications*, vol. 133 (2012)
20. Y. Wan, Q. Gao, "enAn ensemble sentiment classification system of Twitter data for airline services analysis, in *2015 IEEE International Conference on Data Mining Workshop (ICDMW)* (IEEE, Atlantic City, NJ, USA, 2015), pp. 1318–1325
21. P. Monmousseau, A. Marzuoli, E. Feron, D. Delahaye, enPredicting and Analyzing US Air Traffic Delays using Passenger-centric Data-sources, in *Thirteenth USA/Europe Air Traffic Management Research and Development Seminar (ATM2019)*, Austria, Vienna (2019)
22. D.M. Blei, A.Y. Ng, M.I. Jordan, enLatent Dirichlet allocation. J. Mach. Learn. Res. 993–1022 (2003)
23. R. Rehurek, P. Sojka, Software Framework for Topic Modelling with Large Corpora, in *enLREC 2010 Workshop on New Challenges for NLP Frameworks* (2010)
24. M.Röder, A. Both, A. Hinneburg, Exploring the space of topic coherence measures, in *Proceedings of the Eighth ACM International Conference on Web Search and Data Mining—WSDM '15* (ACM Press, Shanghai, China, 2015), pp. 399–408
25. Kaggle, in*Twitter US Airline Sentiment*. https://www.kaggle.com/crowdflower/twitter-airline-sentiment (2018)

26. J. Read, enUsing emoticons to reduce dependency in machine learning techniques for sentiment classification, in *Proceedings of the ACL Student Research Workshop on—ACL '05* (Association for Computational Linguistics, Ann Arbor, Michigan, 2005), p. 43
27. F. Pedregosa, G. Varoquaux, A. Gramfort, V. Michel, B. Thirion, O. Grisel, M. Blondel, P. Prettenhofer, R. Weiss, V. Dubourg, J. Vanderplas, A. Passos, D. Cournapeau, enScikit-learn: machine Learning in Python. *enMachine Learning in Python* (2011)
28. S.J. Taylor, B. Letham, Forecasting at scale. Am. Statistician **72**(1), 37–45 (2018)
29. Facebook, *Prophet—Forecasting at Scale* (2018). [Online]. Available: https://facebook.github.io/prophet/
30. L. Breiman, *Classification and Regression Trees* (Routledge, London, 2017)

Trajectory Management

A Human-In-The-Loop Simulation Study on the Requirements of Air Traffic Control Operations for Expanding Continuous Descent Operations

H. Hirabayashi, N. K. Wickramasinghe, and D. Toratani

Abstract Continuous descent operations (CDO) is an efficient aircraft descent procedure that results in minimal fuel consumption because aircraft descend from their optimal top of descent (TOD) at idle engine thrust. To expand the implementation of CDO, we focus on enhancing the decision-making abilities of air traffic controllers (ATCOs). We conducted a series of human-in-the-loop (HITL) simulations to understand the issues involved in CDO approval decision making by ATCOs and to provide effective inputs to support the decision making. From our initial simulation results, we identified several issues that can affect ATCO CDO-specific decisions. As a proposal to solve these issues, we then created support information displays and evaluated them in follow-on simulations. Our support displays were found to be increasingly effective if their information was sufficiently accurate to avoid premature judgment. It was also found necessary to provide support information to ATCOs to enable more proactive air traffic control (ATC) measures for CDO execution.

Keywords Air traffic control · Continuous descent operations · Human-in-the-loop simulation

1 Introduction

Continuous descent operations (CDO), in which aircraft descend at idle engine thrust from their top of descent (TOD), is an efficient aircraft descent procedure [1]. Performing CDO affords minimum fuel consumption and also prevents early

H. Hirabayashi (✉) · N. K. Wickramasinghe · D. Toratani
Air Traffic Management Department, Electronic Navigation Research Institute (ENRI), National Institute of Maritime, Port and Aviation Technology (MPAT), Tokyo, Japan
e-mail: h-hirabayashi@mpat.go.jp

N. K. Wickramasinghe
e-mail: navinda@mpat.go.jp

D. Toratani
e-mail: toratani-d@mpat.go.jp

Air Traffic Management and Systems IV, Lecture Notes in Electrical Engineering 731,
https://doi.org/10.1007/978-981-33-4669-7_12

descent, leading to noise reduction at localities situated around airports, so it is desirable for all descending aircraft to follow CDO from the viewpoints of efficient aircraft operations and reduced environmental impact. Thus, CDO has been specified by the International Civil Aviation Organization (ICAO) as one of the modules to be implemented in its Global Air Navigation Plan (GANP) modernization program [2].

Efforts to enable more flights to conduct CDO are being made around the world. In the USA, the introduction of Optimized Profile Descents (OPD) is being actively promoted. OPD procedure design and post-implementation evaluation methods have been studied [3], and OPDs are being introduced at many major airports [4]. An OPD is specified as an RNAV (Area Navigation) standard terminal arrival (STAR) procedure. OPD STARs contain upper / lower altitude limits and speed constraints at several waypoints, so the descent is not completely free, but it is possible to descend from cruise with fewer level flight segments than a conventional procedure. In Europe, the Continuous Climb and Descent Operations (CCO/CDO) task force was launched in 2015, and conducted a detailed analysis of actual traffic data. The results showed that continuous descent from TOD had only been achieved by 24% of flights in nominal CDO procedures, and task force activities to expand the use of CDO are still ongoing [5].

In Japan CDO routes, which approve the entire flight trajectory from the TOD to the end of the STAR, are currently designed and published for three airports [6–8], but their operation time window is restricted to late-night when the air traffic volume is low because of difficulties in maintaining the required separations between aircraft in higher traffic situations. However, simple comparisons between radar track trajectories and simulated CDO trajectories have demonstrated that there are sometimes traffic gaps (intervals) in the airspace during which CDO can be implemented even during day light hours when the traffic volume is heavy [9]. Enabling such potentially CDO-capable flights to execute CDO can extend current CDO operations from light traffic to regular air traffic scenarios.

The aim of our study is to expand CDO in Japan and more widely beyond its current usage and limitations. Since CDO is initiated with air traffic control (ATC) approval, we focus on assisting and enhancing the air traffic controller's (ATCO's) CDO approval decision-making abilities. Therefore, to expand CDO beyond its current usage and limitations, in this study, we conducted a series of human-in-the-loop (HITL) simulations with the assistance of experienced former ATCOs to determine the relevant issues and identify the requirements for ATC operation involving CDO approval specific decision making. HITL simulation is very important for evaluating the feasibility of a proposed operational procedure. HITL simulation has been used to evaluate the support information required by pilots during CDO operations [10], but prior to our study, there have been no published HITL studies focusing on ATC procedures and ATCO performance during CDO operations.

2 Cdo Procedures

2.1 CDO at Kansai International Airport

In our HITL simulations, we utilized certain target scenarios relevant to Kansai International Airport (ICAO code "RJBB"), one of the three airports where CDO routes are established. RJBB is a 24-h international airport located offshore on an artificial island close to the highly populated Kansai region. There are two parallel runways (RWY06R/L and RWY24R/L), which are mainly used as dedicated runways for departure and arrival, respectively. The airport operator Kansai Airports reported 189,658 aircraft movements in fiscal year 2018 [11], an increase of 1.8 since fiscal year 1995, the year after the airport was opened, mainly due to traffic connecting the Asia region.

RJBB offers several CDO routes in the late-night to early-morning time window [6]. During the most recent two years (1 Jan. 2017 to 31 Dec. 2018), the daily average number of CDO requests was 2.6, and the approval rate of CDO requests was 78% [12].

Each CDO route is set via a "transfer point" to the end point of the STAR. Here, transfer point refers to a waypoints at which ATC responsibility for arriving flights is transferred from en-route radar control to terminal radar control, indicated by the star in Fig. 1 which shows the location of the transfer point in an airspace vertical view.

The RJBB CDO routes are indicated by blue lines in Fig. 2. There are five transfer pints (indicated by stars), and CDO routes are available from three of these. For each of these transfer points, three CDO routes are defined depending on the landing runway. In the RJBB procedure designs, the end point of the STAR is collocated with either the Initial Approach Fix (IAF) or an Intermediate Approach Fix (IF) at 4000 ft.

The CDO procedure, triggered by pilot request, is as follows:

(1) A flight requests CDO from ATC at least 10 min before reaching TOD, giving the TOD position and estimated time at the transfer point.

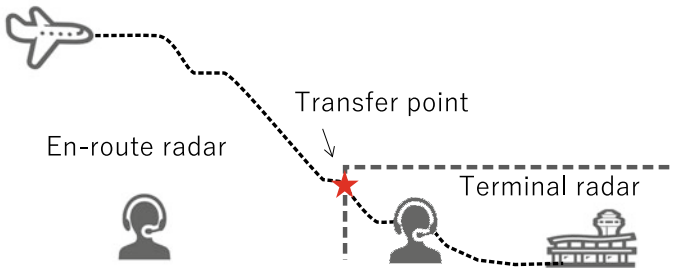

Fig. 1 ATC transfer from en-route radar to terminal radar

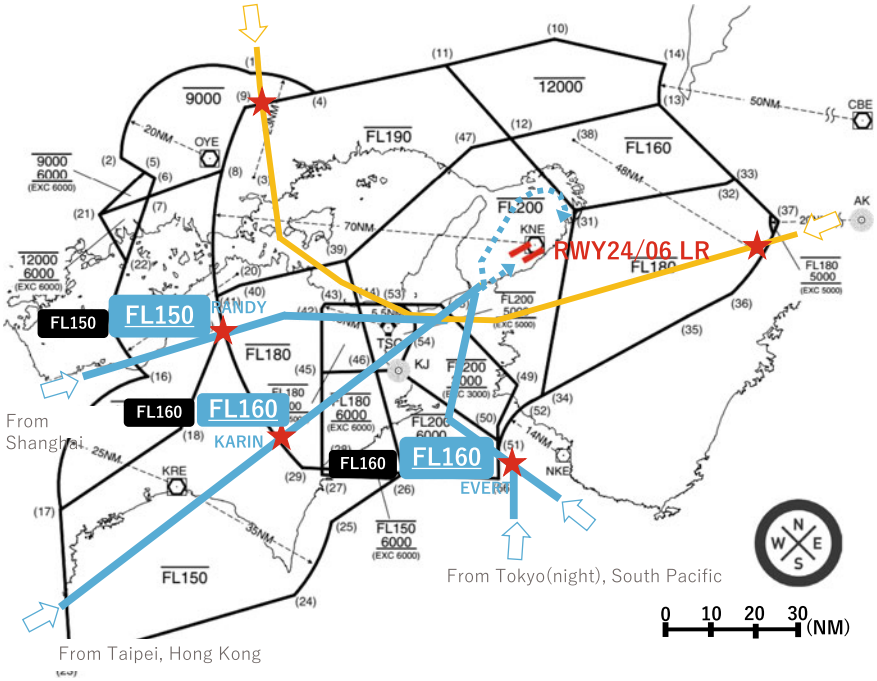

Fig. 2. Outline of CDO routes at RJBB

(2) ATC issues CDO approval clearance if it is determined that the requesting aircraft can fly the CDO route and that there will be no conflicting aircraft during the CDO descent. This procedure is almost the same at the other two airports.

Maintaining safe separation between aircraft is an essential part of an ATCO's role. When approving a CDO, ATCOs must ensure adequate separation from other traffic during the CDO descent, which we call "competing" traffic in this paper. Aircraft flying along airways or departure routes that cross the CDO route and aircraft landing at the same airport from different directions, may be candidates for competing aircraft (Fig. 3). ATCOs must issue instructions to aircraft, including the CDO aircraft, in a timely manner to ensure safe separation from the other traffic. However, as the traffic volume increases, the number of competing aircraft and ATCO workload increases correspondingly. To ensure a reasonable workload to maintain airspace capacity as traffic volume increases, it becomes necessary to impose descent constraints that deviate from the ideal, such as descending aircraft prior to their ideal TOD (early descent).

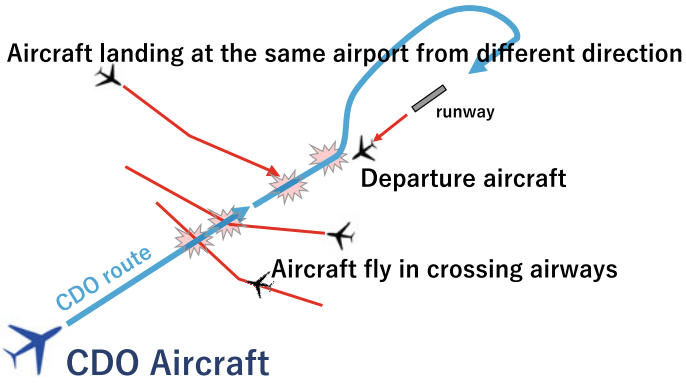

Fig. 3 Competing aircraft

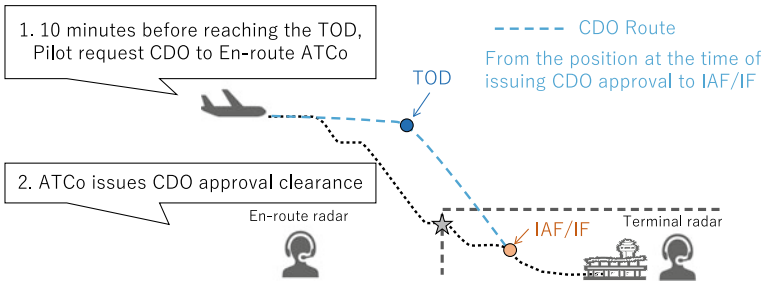

Fig. 4 Vertical view of CDO procedure

Fig. 5 Horizontal view of CDO procedure

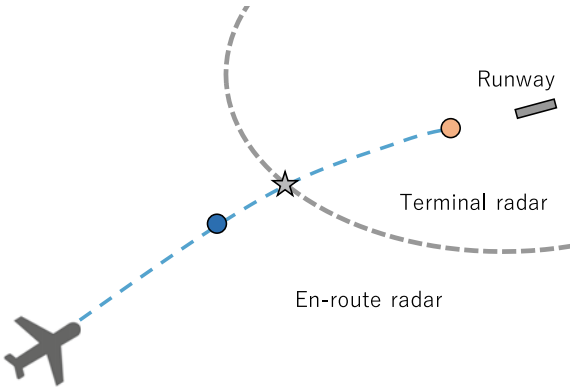

2.2 ATC Operation for CDO

Figures 4 and 5, respectively, show the schematics of a CDO route in vertical and horizontal views. Since the TOD is located before the transfer point, CDO must be requested within en-route radar control airspace. The gray dotted line in Fig. 4 indicates a conventional descent for comparison, which has a different vertical profile.

Figures 6 and 7 clarify the differences in the ATC processes between conventional and CDO descents. For a conventional arrival, the en-route ATCO first provides a descent instruction to the aircraft to cross the transfer point at the prescribed altitude, and ATC responsibility is transferred to the terminal radar ATCO at the transfer point. The terminal radar ATCO then assumes responsibility for the flight until giving a runway approach clearance. Both ATCOs proactively issue ATC instructions to the aircraft to ensure adequate separation from other traffic by repeatedly searching for potential "conflicts" with competing aircraft from a few minutes to tens of minutes ahead. For en-route ATCOs, the major competing aircraft is aircraft on crossing airways and other arrivals with the same transfer point. For terminal ATCOs, the primary competing aircraft arrivals to the same airport and departure / arrival traffic at nearby airports. For a CDO arrival, a pilot CDO request triggers a CDO-specific conflict search by both the en-route radar ATCO and terminal radar ATCO (as indicated by the red rectangles in Fig. 7) before the CDO can be approved. Since the CDO clearance includes approval up to the STAR end point, a conflict search up to about 30 min ahead is required. At first, conflict searches are conducted separately by the en-route and terminal radar ATCOs to ensure that there are no conflicts along the CDO route within their areas of responsibility, then coordination between the ATCOs is required, as indicated by the area highlighted in yellow color in Fig. 7. The crossing altitude at the transfer point varies for each CDO operations, which forms another element of the coordination.

Although the ATC process for a CDO arrival is more complex than for a conventional arrival with regards to conflict search and coordination, the CDO process requires fewer communications between the CDO flight and ATCOs. With a conventional arrival, ATCOs have to issue multiple instructions at the proper instances, but a CDO arrival requires only a single CDO approval clearance to descend from the TOD to the STAR end point.

Upon comparing the two ATC processes, it could be argued that the CDO-specific ATC operation is a reactive task while conventional ATC operation is proactive. For a conventional arrival, ATC instructions are issued actively according to minute-by-minute predictions of the traffic situation. On the other hand, for a CDO arrival, it is necessary to continually monitor whether the aircraft can fly as per long-term predictions, and if a competing aircraft appears, the CDO is canceled and the procedure reverts to the conventional descent.

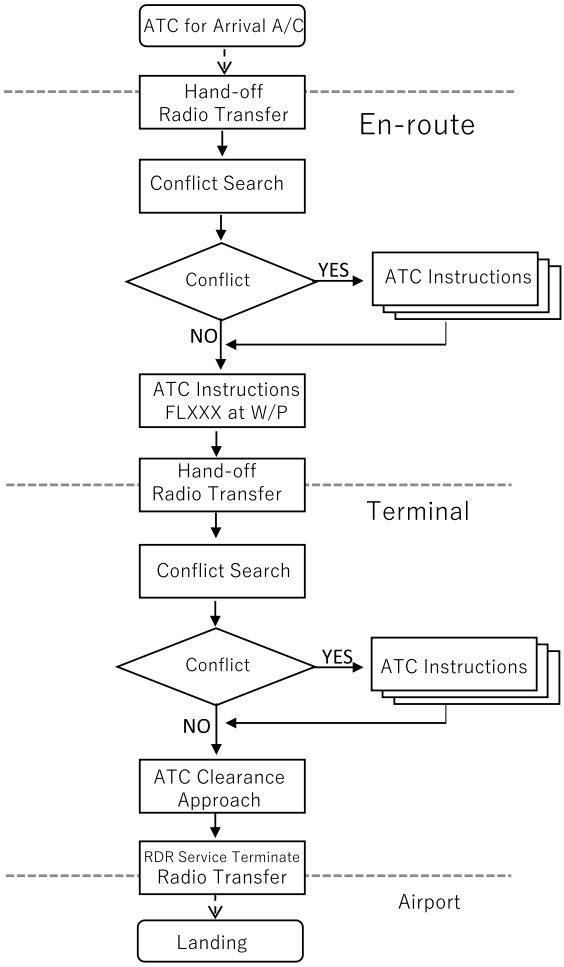

Fig. 6 ATC task flow (conventional descent)

Abbreviation	Explanation
A/C	aircraft
FLXXX	Flight Level altitude
Hand-off	radar transfer
RDR	radar
FLXXX at W/P	an example of instruction to cross the waypoint (W/P) at altitude FLXXX

3 Human-in-The-Loop Simulation

In the CDO procedure, the en-route and terminal radar ATCOs have to judge whether or not a requesting aircraft can execute the CDO; that is, whether or not CDO is applicable to the aircraft. If the determination is made as “CDO-applicable”,

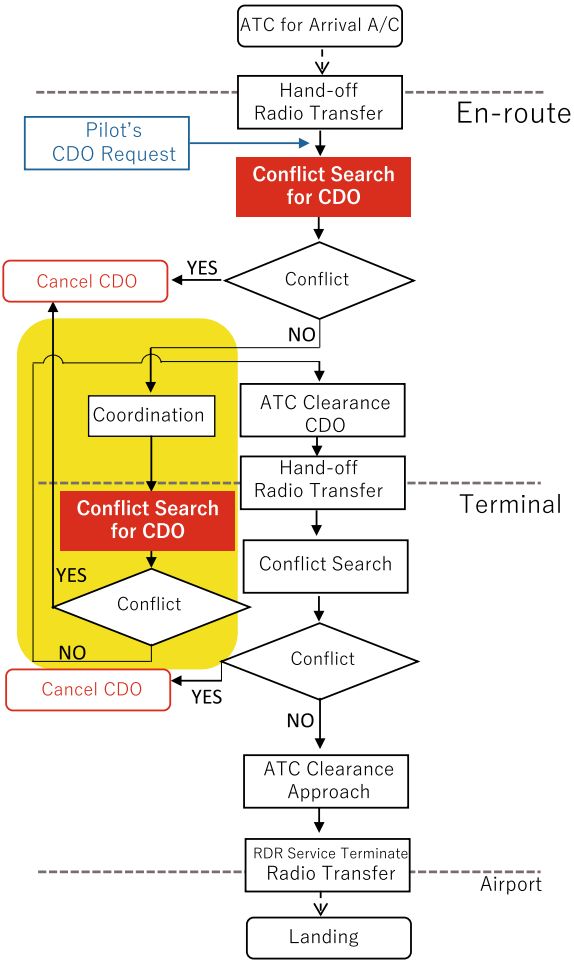

Fig. 7 ATC task flow (CDO descent)

CDO approval clearance is issued after coordination between the en-route radar and terminal radar ATCOs. Since the CDO approval clearance is made through the end point of the STAR, the ATCOs have to consider the entire aircraft trajectory from the point at which the request was made to the IAF/IF point (corresponding to approximately 30 min of flight time in the case of an RJBB arrival), and conduct corresponding conflict searches within their airspaces of responsibility.

HITL simulations were conducted with experienced former ATCOs to determine the relevant factors and necessary information pertaining to the "CDO-applicable" decision making. That is, the main questions addressed through the simulations were as follows: What are the relevant issues to consider, and what is the information required for deciding on whether CDO can be applied when CDO is requested?

Fig. 8 HITL simulation examination

3.1 Decision Support Tool for Simulation Experiments

In the HITL simulations, we utilized a decision support tool customized for CDO. The tool was developed at ENRI, and has two functions: a fast-time simulation function for CDO flight trajectory calculation, and a real-time air traffic simulation function that reflects input ATC instructions. The tool presents the traffic situation on simulated radar screens and has several support information displays. The real-time simulation function was used for our experiments.

Figure 8 shows the setup for the simulation experiments. There were three simulated controller-working positions (CWP) corresponding to en-route radar control, terminal radar control, and traffic flow coordination. ATC instructions to aircraft were input directly at the CWP user interface rather than by voice. The traffic flow coordinator was also responsible for inputting system commands. Figure 9 shows the radar simulation screen used in the experiments.

3.2 Participants and Scenarios

Three former ATCOs who were familiar with ATC operation in the target area participated in our experiments. Two participants were utilized as the ATCOs directly involved in the CDO procedure outlined in Sect. 2, that is in the roles of en-route radar ATCO and terminal radar ATCO, while a third participant acted as the traffic flow coordinator.

The simulation airspace range was approximately 200 NM from the target airport (RJBB). The ATCOs input instruction commands to the tool to ensure adequate separations between aircraft according to the following prerequisites:

- All aircraft arriving at RJBB request CDO.
- ATCOs can apply speed adjustment to the CDO aircraft. If an change to vertical profile or flight course is required, CDO is cancelled.

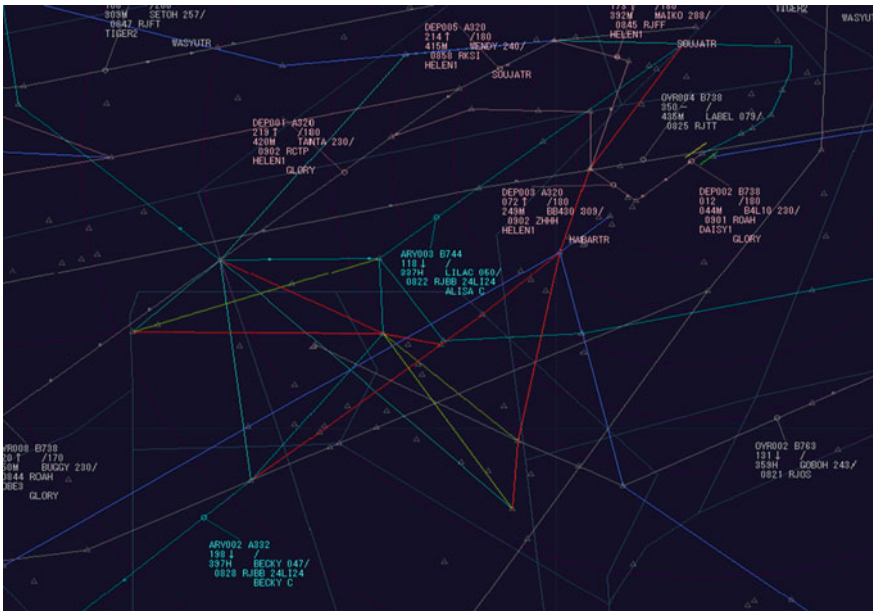

Fig. 9 Radar simulation screen

- The longitudinal separation between aircraft crossing the same transfer point must be 10 NM or more.
- All actual operational restrictions (no-fly zone, STAR restrictions, etc.) are applicable.

Ten simulation experiments were performed over a period of 7 days, including familiarization with the tool.

Scenarios were created based on historical flight plan data. Two days in 2016 and 2017 were selected for the scenarios: One day was focused on RWY06 arrivals while the other day was dedicated to RWY24 arrivals. On each day, traffic scenarios for three time periods were created from corresponding flight plan data: (a) 0000–0800 JST (Japan Standard Time), (b) 1000–1300, and (c) 2100–2400. Scenarios (a) and (c) include several hours after and before the current CDO operation time period at RJBB, respectively. The arrival rate during the CDO operation period was 0–1 flights every 10 min, but increased to 1–3 flights/10 min. During the one-hour time periods immediately before and after CDO operation period. These scenarios were prepared to examine the CDO operability during time periods spanning several hours earlier and/or later than current CDO operations. Scenario (b) includes the peak traffic time period during each day, and was prepared to extract issues and to study the feasibility of HITL simulation of CDO in heavy traffic environments. A total of six scenarios was, therefore, prepared for two runway operation configurations and three time periods. The simulations were conducted reflecting the wind conditions during the selected days.

To create realistic traffic flows, the time and altitude of entry of flights into the simulation were set based on historical radar track data, and the subsequent flight trajectories were calculated using an aircraft type-dependent performance model and the wind conditions. In addition to RJBB arrival traffic flows from multiple transfer points (refer Fig. 2), the RJBB departure traffic flows, crossing airway traffic flows, and traffic flows at nearby airports were also simulated.

The scenarios were not arranged to be conflict-free; that is, loss of separation could occur if all RJBB arrivals executed CDO, so participants had to give ATC instructions to ensure separation. For example, eight arrivals in 30 min were set in a time period during which traffic volume gradually increased. If all aircraft executed CDO without speed restrictions or route stretching, two pairs of aircraft executing CDO would lose longitudinal separation prior to reaching the IAF/IF, and there were other competing aircraft such as RJBB departures and crossing airway traffic.

4 Results and Discussions

4.1 Issues Concerning CDO-Specific ATC Operations

From the HITL simulation experiment, we identified several influences that affected ATC CDO operations and considered the underlying issues. These influences and issues are summarized in Table 1.

4.1.1 Wide Variation in CDO Trajectories

The first issue is the wide variation in CDO trajectories. Figure 10 shows the differences between conventional and CDO descent trajectories in vertical view. In a conventional descent, an aircraft crosses the transfer point at a predetermined altitude, whereas for a CDO descent, the speed and angle of descent are determined by each aircraft, so the TOD position and the position of entry into the terminal

Table 1 Issues and their influences in CDO-specific ATC operation

Issues	Influence
CDO trajectories vary widely	Transfer operation occurs outside airspace interest
Difficulty in predicting flight trajectory (Particularly altitude)	Inapplicable vertical separation Reduction in airspace capacity
Early CDO approval estimation times	Difficulty of predicting competing aircraft
Prioritization of CDO	Increase in burden of both CDO and competing aircraft

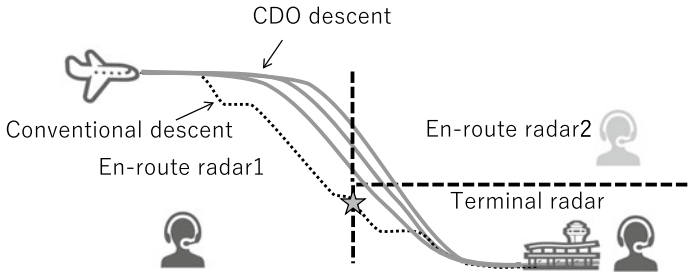

Fig. 10 Differences conventional descent and CDO descent trajectories

radar airspace vary from flight to flight. Figure 11 shows the actual TOD positions of CDO flights (the TOD positions of 56 CDO flights over 84 days in 2018 extracted from radar data provided by the Japan Civil Aviation Bureau). The TOD positions are widely spread, and the vertical profiles also vary significantly. Table 2 lists the altitude-related statistics of CDO flights at their transfer points calculated from radar data. In a conventional descent, an aircraft is instructed to descend to cross the transfer point at 16,000 feet, but on the other hand, a CDO descent profile is optimized for an idle thrust descent, and so the altitude at the transfer point varies widely. Another

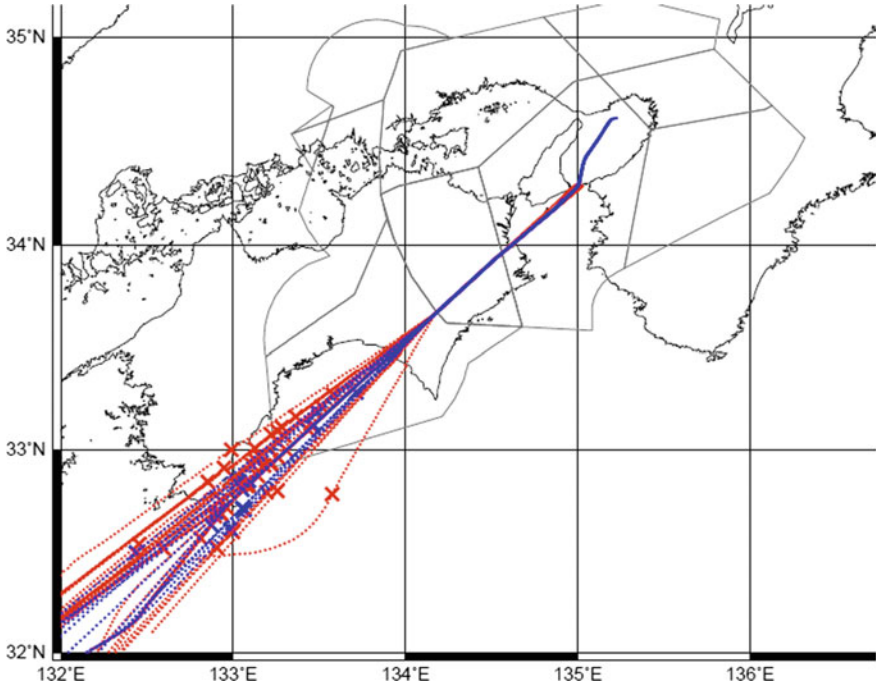

Fig. 11 TOD positions of CDO flights

Table 2 Statistics of transfer point crossing altitude of CDO flights

	Transfer point for RWY06	Transfer point for RWY24
Number	41	12
Max	24328	24072
75%	17749	21358
Median	16744	18718
25%	15741	17368
Min	15607	15809
Average	17059	19289
SD	1706	2865

Altitude is expressed in units of feet

factor in the wide scatter of CDO transfer point crossing altitudes relative to conventional descent operations is that ATC transfer occurs outside the airspace of interest. This also requires additional coordination between the ATCOs.

4.1.2 Difficulty of CDO Trajectory Prediction

The wide variation of CDO trajectories also causes difficulty for ATCOs in accurately predicting the flight trajectory. This difficulty is captured in Table 1 along with its issues in the second row. In a conventional descent, ATCOs issue altitude instructions as they desire. However, in the CDO case, these instructions are not provided because CDO clearances involve aircraft descending as they wish. It is difficult for ATCOs to accurately predict the descent trajectory based only on human experience and judgement, and as a result, ATCOs could not apply vertical separation, which one of the separation standards. Moreover, because of uncertainty of the trajectory, ATCOs may need to set an extra buffer to maintain separation. This difficulty also leads to reduction in the airspace capacity. Assistance from automation such as a trajectory prediction function is required to enable ATCOs to estimate the crossing altitude accurately.

4.1.3 Early Judgement for CDO Approval

The third issue involves the necessity of early judgement when issuing a CDO approval. A CDO approval clearance is issued only when competing aircraft are not predicted on the estimated CDO trajectory. However, it is difficult to carry out this prediction precisely. In particular, when a departure is a competing aircraft, an estimate of its relationship with the CDO profile must be made before it has even become airborne, which is difficult even if the predicted take-off time is accurate.

4.1.4 Prioritization of CDO

The fourth issue was whether or not to prioritize CDO flights. In the HITL simulation experiments, the ATCOs ensured ATC separations to prioritize CDO flights to the maximum extent possible. The HITL simulations were mainly of time periods slightly outside the current CDO window, wherein the traffic volume increased / decreased gradually. It was necessary to issue speed adjustment (mostly speed reduction) instructions to proceed with CDO in many of the cases considered.

4.2 Supporting ATC Operations for Expanding CDO

To enhance the ATCO judgement for CDO approvals, we integrated two decision support displays based on a ground-based trajectory prediction function into the HITL simulation tool at CWPs. One is a matrix display for the en-route radar ATCO which displays the existence of potentially competing aircraft against CDO trajectories as a time series, with altitude and time on the vertical and horizontal axes, respectively. The other display is a timeline display for the use of the terminal radar ATCO, which shows time intervals between landing aircraft on the vertical axis with the timeline at specified waypoints or runways. Figure 12 shows images of these support displays. As a result of comparing the experiment with and without supporting screens, we found that these displays could facilitate proactive ATC operations and support the CDO approval process.

In our interviews with the ATCOs participating in the HITL simulations, they commented that our proposed displays would be feasible if the provided information were accurate. It is widely expected that improvement of highly accurate trajectory prediction will increase the effectiveness of ATCO support functions. Furthermore, the en-route ATCO commented that it would be easier for decision making if competing aircraft were clearly indicated, rather than be shown as only a probability on the matrix screen. The terminal radar ATCOs stated that the timeline display was effective for future predictions because it visualized the time intervals between aircraft, but because it did not show distance intervals it could not be used to judge whether the distance-based radar-separation criteria would be satisfied. It was remarked that both these displays would be more useful for the flow coordinator, who manages the traffic flow comprehensively, than for tactical radar ATCOs.

In this study, we attempted the following to prioritize CDO: (1) speed adjustment (of both CDO and competing aircraft), (2) delaying the take-off of departing aircraft, and (3) per-flight adjustment of the STAR before the TOD to avoid competing traffic. Regarding (1), we note that speed adjustment has been implemented in actual CDO operations, and is considered acceptable from the perspective of ATCOs because it is effective in maintaining adequate aircraft separation. However, there were several cases in the experiments when excessive speed adjustments had to be imposed to avoid radar vectors and improve the CDO success rate (i.e., the rate at which an approved CDO is successfully completed without being aborted). It is necessary to

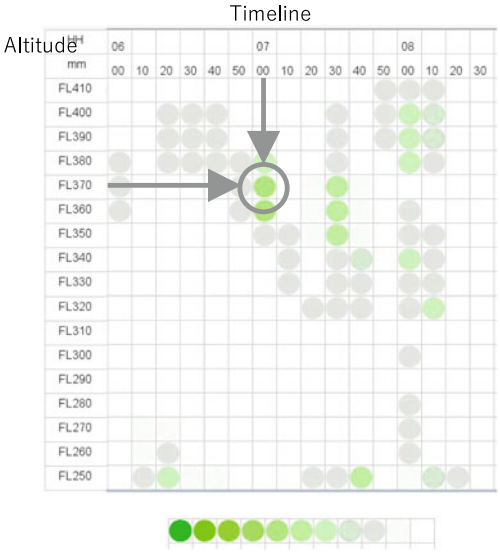

In the example in this figure, possibility of competing aircraft existence is shown when crossing the determined point from 07:00 to 07:10 at altitude FL370. The darker the color, the longer the competitor will exist in 10 minutes.

Matrix Screen

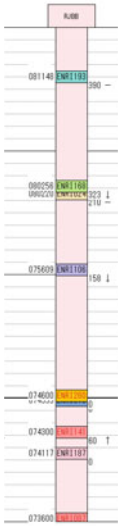

The timeline shows the aircraft time interval at a determined location. The example shows the aircraft time interval on the runway. Arrival aircraft shown by black character and departure aircraft shown by red character. The auxiliary lines are shown at one minute intervals.

Current Time

Timeline Screen

Fig. 12. ATCOs' decision supporting screens

consider aircraft operating efficiency to carry out speed adjustment to achieve overall effectiveness. Regarding (2), take-off delay was considered for the CDO routes that are mostly affected by departing aircraft. To ensure CDO success, competing departure aircraft required up to 7 min of delay. Regarding (3), the probability of competing aircraft existing on the CDO trajectory decreased and the CDO success rate increased. However, the STAR revisions involved path stretching to avoid competing traffic near the runway. This caused an approximately 12.6 NM stretch to original CDO route. For the issue of prioritization of CDO, both the advantages and disadvantages of CDO become very important in considering its overall effectiveness and feasibility.

In cases (2) and (3), priority given to CDO resulted in inefficiency for other and own aircraft. Further consideration is needed on acceptable departure delays, route stretch, etc.

5 Conclusions

To determine the issues involved in CDO-specific ATC operations and the necessary information pertaining to ATCO CDO-related decision making, the authors conducted a series of HITL simulations with the assistance of experienced former ATCOs. The results showed that since CDO is initiated with ATC approval, presenting information relevant to potential CDO-capable aircraft at the appropriate instant prior to TOD is effective for improving ATCO decision making. This can also expand the scope of CDO implementation, resulting in several benefits. Based on this result, we implemented controller support displays to aid the CDO-specific decision making, and evaluated them in further HITL experiments.

The experiments identified several influences faced by ATCOs pertaining to CDO, and we considered four issues underlying these influences. The issues include a wide variation in the CDO trajectories, difficulty in CDO trajectory prediction by ATCOs, the early approval required for CDO procedures, and the prioritization of CDO over conventional descents and other traffic to increase the success rate. We found that our support displays could be increasingly feasible if their information was sufficiently accurate. It is desirable to improve high accuracy trajectory prediction technology at the same time for its effective use as support information. It is also found necessary to provide such support displays to ATCOs to permit more proactive ATC measures for CDO execution, which are otherwise conventional reactive measures.

A review of the disadvantages of CDO implementation is also important to evaluate its overall effectiveness. Three trials were conducted in attempts to improve the CDO success rate. In each case, the constraints of speed adjustment, departure delay, and path stretching were imposed on the CDO aircraft and/or other competing aircraft. Among these constraints, speed adjustment appeared to be acceptable from the perspective of ATCOs. However, it is necessary to consider the aircraft operating efficiency to carry out speed adjustment to achieve overall effectiveness. The other constraints (departure delay and path stretching) need to be carefully examined, which will form the topic of our future works.

References

1. ICAO, in *Continuous Descent Operations (CDO) Manual*, ICAO Doc 9931 First edition (2010)
2. ICAO, in *Global Air Navigation Plan 2016–2030*, ICAO Doc 9750 Fifth edition (2016)
3. J.-P.B. Clarke, J. Brooks, G. Nagle, A. Scacchioli, W. White, S.R. Liu, Optimized profile descent arrivals at los angeles international airport. J. Aircraft **50**(2), 360–369 (2013)
4. FAA NextGen, in *Performance Based Navigation (PBN) Implementation and Usage*, https://www.faa.gov/nextgen/pbn/dashboard/. Referred Mar 2020
5. EUROCONTROL, in *Continuous Climb and Descent Operations*, https://www.eurocontrol.int/concept/continuous-climb-and-descent-operations. Referred Mar 2020
6. Japan Civil Aviation Bureau, in *eAIP Japan AD 2*, RJBB Kansai INTL, referred effective date 20 June 2019
7. Japan Civil Aviation Bureau, eAIP Japan "Operation Trial for Continuous Descent Operations (CDO) at Kagoshima AP/RJFK.", AIC 020/16, effective from 13 Oct 2016
8. Japan Civil Aviation Bureau, eAIP Japan "Operation Trial for Continuous Descent Operations (CDO) at Naha AP/ROAH.", AIC 010/20, effective from 26 Mar. 2020
9. H. Hirabayashi, S. Fukushima, M. Oka, N.K. Wickramasinghe, D. Toratani, in *55th Aircraft Symposium on Feasibility Study on the Expansion of Continuous Descent Operations (CDO) at Kansai International Airport with Track Data Analysis* (2017) (Japanese)
10. P.M.A. De Jong, F.J.L. Bussink, R.P.M. Verhoeven, N. De Gelder, M.M. Van Paassen, M. Mulder, Time and energy management during approach: a human-in-the-loop study. J. Aircraft **54**(1), 177–189 (2017)
11. Kansai Airports, in *Kansai airport seen by Numbers*, https://www.kansai-airports.co.jp/company-profile/about-airports/kix.html. Referred Mar 2020
12. H. Hirabayashi, N.K. Wickramasinghe, D. Toratani, Study of Requirements Necessary for CDO Operation expansion by Experienced Air Traffic Controllers, in *Proceeding of 19th Electronic Navigation Research Institute Research Workshop*, June 2019, pp. 63–69 (Japanese)

On the Use of Generative Adversarial Networks for Aircraft Trajectory Generation and Atypical Approach Detection

G. Jarry, N. Couellan, and D. Delahaye

Abstract Aircraft approach flight path safety management provides procedures that guide the aircraft to intercept the final approach axis and runway slope before landing. In order to detect atypical behavior, this paper explores the use of data generative models to learn real approach flight path probability distributions and identify flights that do not follow these distributions. Through the use of Generative Adversarial Networks (GAN), a GAN is first trained to learn real flight paths, generating new flights from learned distributions. Experiments show that the new generated flights follow realistic patterns. Unlike trajectories generated by physical models, the proposed technique, only based on past flight data, is able to account for external factors such as Air Traffic Control (ATC) orders, pilot behavior or meteorological phenomena. Next, the trained GAN is used to identify abnormal trajectories and compare the results with a clustering technique combined with a functional principal component analysis. The results show that reported non compliant trajectories are relevant.

Keywords Anomaly detection · Aircraft trajectory generation · Generative adversarial networks · Machine learning · Flight path safety management

G. Jarry (✉) · N. Couellan · D. Delahaye
Ecole Nationale de l'Aviation Civile, Université de Toulouse,
7 Avenue Edouard Belin, 31400 Toulouse, France
e-mail: jarry.gabriel@enac.fr

N. Couellan
e-mail: nicolas.couellan@enac.fr

D. Delahaye
e-mail: daniel.delahaye@enac.fr

N. Couellan
Institut de Mathématiques de Toulouse, UMR 5219, Université de Toulouse CNRS,
UPS, 31062 Toulouse Cedex 9, France

Air Traffic Management and Systems IV, Lecture Notes in Electrical Engineering 731,
https://doi.org/10.1007/978-981-33-4669-7_13

1 Introduction

Accidents that occur during initial, intermediate and final approach until landing represent every year 47% of the total accidents, and 40% of fatalities [1]. In nominal operations, approach flight path safety management consists in procedures which guide the aircraft to intercept the final approach axis, and the runway slope with an expected configuration in order to land. Some abnormal flights are observed with deviations from procedures and operational documentation.

The International Air Transportation Association (IATA) forecasts a growth of air passengers worldwide from around 4 billion today, up to 8.2 billion in 2037 [2]. Consequently, the number of non-standard procedures will also increase if nothing is done to mitigate them. This kind of trajectory generates difficulties for both crew and Air Traffic Control (ATC) and may induce undesirable events such as Non-Compliant Approach and Non-Stabilized Approaches that can drive to ultimate events like Runway Excursion, Control Flight Into Terrain, and Loss of Control In Flight. Analyzing and gaining a better understanding of these procedure deviations would be profitable for both air traffic managers and flight operators. Besides, generating realistic trajectories while data are not available can greatly benefit noise prediction simulation in the context of air traffic growth, and in many other applications.

Anomaly Detection is a well-known problem, which has been investigated for a long time. It consists in finding samples from a data set that do not comply with the overall behavior. Among the various methods available, the Multiple Kernel Anomaly Detection (MKAD) [3] technique is one of the most efficient algorithms. It was developed to detect anomalies in aircraft flight data records during approach.

It was developed to detect anomalies in heterogeneous data (i.e. discrete and continuous data), and has been used to detect anomalies in aircraft approach parameters from aircraft data.

Another kernel-based approach to study on-board aircraft parameters was detailed in [4]. Neural network auto-encoder reconstruction error can also be used to detect abnormal behavior [5, 6]. Other anomaly detection techniques using information geometry and functional representation have also proven to be efficient. In her thesis [7], the author presents different Outlier Detection in Space Telemetries. In [8, 9], functional principal component analysis is used to develop a local anomaly detection algorithm in aircraft landing trajectories.

This paper details the work conducted around the generation of trajectory and the detection of atypical trajectories using a novel machine learning technique called Generative Adversarial Networks (GAN). GAN are recent neural network techniques that have already provided successful results in various fields such as image or video generation [10, 11], image resolution enhancement [12], drug discovery [13], text-to-image synthesis [14] and many others. They enable learning the data distribution by solving a min-max optimization problem between a data generator and a data classifier. The data generator tries to generate realistic data while fooling the data classifier. The classifier tries to distinguish real data from generated data. Recently, GAN have also been applied to detect anomalies in imaging data [15].

In the specific field of trajectory generation with GAN, some work has already been conducted on learning and reproducing human motion behavior [16], on robot navigation [17], or on vehicle-to-vehicle-encounters [18]. GAN do not require prior knowledge on data to learn their distribution and are therefore well suited to applications where only physical model representation is available and little is known about responses to uncertainties or external factors such as aircraft approach trajectories analysis. Furthermore, to the best of the authors' knowledge, no investigation has been carried out on applying these techniques to aircraft trajectory generation or anomaly detection, which motivates the use of GAN. This article aims at conducting experiments with GAN to generate realistic aircraft trajectories based on airport approach and landing data. Classical trajectory generation is based on the physical aircraft model whereas here, the generation is data driven and does not use aircraft and flights physics. It can, therefore, account for external factors that impact real trajectories such as Air Traffic Control (ATC) orders, pilot behavior or meteorological phenomena. Further investigations on the use of the GAN to detect abnormal trajectory patterns were carried out and compared with the results of a prior information geometry based approach.

This paper only presents the first results of trajectory generation. Regarding the generation process, the comparison with other techniques is visual and focuses on obtaining a realistic aspect of the trajectories. In future works, more accurate metrics could be developed to compare two generated data sets. Regarding, the anomaly detection, the results of two different methods will be compared.

After introducing the principles of GAN, the application of GAN to generate approach trajectories is shown and results are compared with other methods such as geometric information techniques. The second part of the paper is dedicated to the detection of abnormal or atypical trajectories using the distribution of data learned by the network. The relevance of the results is discussed with operational criteria and the performance of our algorithm in real operations is detailed.

2 Generative Adversarial Networks (GAN)

GAN have recently attracted much interest in the machine learning community [10, 19]. These models have the ability to learn the distribution p_d of input data and generate new data according to the learned distribution. This is achieved through the use of a network that combines a generator G (usually a type of neural network) and a discriminator D (a classifier function). The generator G takes input noise vectors z from a low dimensional space so-called latent space, and generates new sample vectors in the data representation space. The discriminator D is trained on a given input data x to compute the probability of a sample being an input data rather than being generated by G. The process, that can be seen as a two player game is simultaneously repeated so that G minimizes $\log(1 - D(G(z))$ (generated data that could not fool the discriminator), and D maximizes $\log(D(x))$ (real data correctly

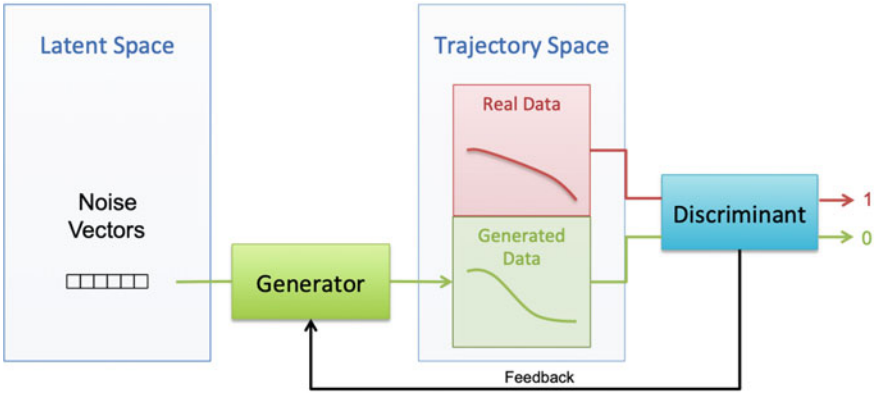

Fig. 1 GAN. It is composed of a generator G, that takes as input a noise vector from the latent space to compute a trajectory, and a discriminator D, that classifies trajectories between real and generated

classified). The process is initiated by drawing random noise vectors z. The two player game can be summarized in the following optimization problem:

$$\min_G \max_D \mathbb{E}_{x\sim p_d}\left[\log(D(x))\right] + \mathbb{E}_{z\sim p_z}\left[\log(1 - D(G(z))\right] \tag{1}$$

Figure 1 illustrates this principle in the specific case where x belongs to a space of trajectories. Initial vectors z are randomly generated in the latent space and mapped into the trajectory space via the Generator G. The discriminant function D returns a score value close to 1 if the generated trajectory belongs to the real trajectory data distribution or close to 0 otherwise. Next, the training phase of G receives the score feedback in order to generate a more realistic trajectory if the score is low. The process is repeated several times until an equilibrium of the min max game is found. The next section gives more details on the architecture of the generator and discriminator neural network maps used.

3 Trajectory Generation

The problem of trajectory generation is usually divided into two paradigms, model-driven generation, and data-driven generation. The approach with GAN is a data-driven generation. Since in model-driven generation, trajectories are generated with physical and dynamical models, they cannot take into consideration real-time constraints such as Air Traffic Control or even pilot behavior. Data-driven generation is supposed to provide more realistic generation considering all the parameters from real data. Model-driven generation can use real aircraft models directly, or the BADA (Base of Aircraft Data) model [20, 21] developed by Eurocontrol.

3.1 Aircraft Landing Trajectories

This section illustrates how GAN can be used to generate aircraft landing trajectories at Paris Orly (LFPO) airport. The dataset used is composed of 4401 A320 landing trajectories on runway 26 from Flight Data Monitoring Records. The parameters selected are the longitude, the latitude, the altitude and the ground speed for the last 25NM. The initial trajectory rate is one point every 4 seconds, but each trajectory is resampled to obtain 256 uniformly distributed points which fit a neural network structure. These parameters have been selected because they correspond to the basic parameters available in ADS-B or radar data. Thus, the results obtained can be reproduced with other data sources. Further experiments are in progress for models taking into account more parameters.

3.2 Neural Network Structures and Learning Process

In order to generate aircraft trajectories, specific neural network structures were built using 1D convolutional and transpose convolutional neural networks. The neural network of the discriminant consists of four convolution layers and one fully connected layer. The neural network of the generator is built by symmetry: one fully connected layer and four convolution transpose layers with upsampling. Additional details about the dimension of each layer are given on Fig. 2

A uniform distribution of the noise z was arbitrarily chosen in a 4-dimensional space since the output space considers 4 dimensions (longitude, latitude, altitude, ground speed). In addition to convolutional structure, each layer is followed by a batch normalization, max pooling, and dropout layers in order to regularize the network.

The learning task was made using Adam optimizer [22] with a decay. The learning rate starts from 10^{-3} and decreases to 10^{-7}. Networks were trained during 30 000 steps on a multi-GPU cluster. The cluster is composed of a dual ship Intel Xeon E5-2640 v4 - Deca-core (10 Core) 2.40GHz—Socket LGA 2011-v3 with 8 GPU GF GTX 1080 Ti 11 Go GDDR5X PCIe 3.0.

3.3 Generated Trajectories

After the learning phase, the generator was able to compute new trajectories from sampled noise distribution. However, the obtained trajectories were noisy with mainly high-frequency noise. Therefore, a smoothing filter was applied. In particular, a cubic smoothing spline interpolation was computed to remove the noise from the generated trajectories. Figure 3 illustrates filtered generated trajectories for all the parameters.

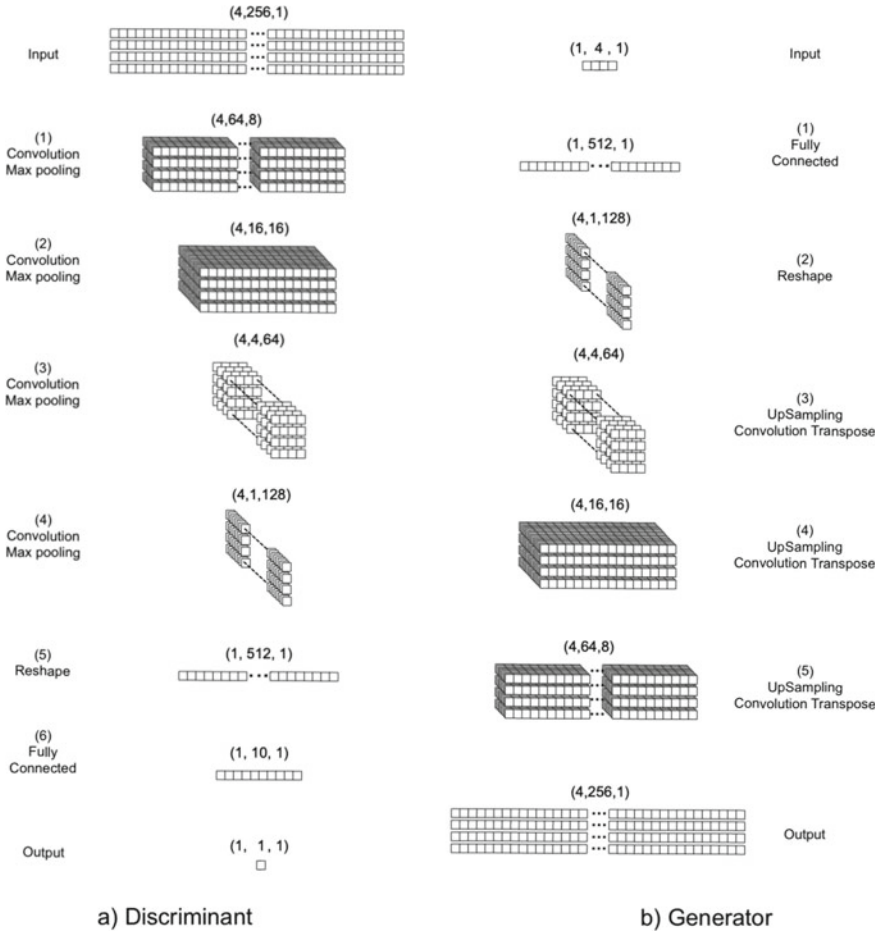

Fig. 2 Two network architectures; on the left **a** the discriminator structure, and on the right **b** the generator structure. Both structures use convolution or convolution transpose layers

The overall shape and distribution of the generated trajectories was satisfying since they followed the original distribution. Nevertheless, one can see that the generator was not able to capture some types of patterns. For the altitude profile, it is known that aircraft follow levelled-off path before descending on the glide path, but this was not captured by the generator. The same behavior was observed for the extended runway centre line which should be followed from 10NM to the threshold, but the generated trajectories barely followed the localizer path for the last nautical miles. This may be linked to the difficulty of convergence in GAN models. As a reminder, GAN models solve a min-max problem, which implies a very unstable optimal saddle point. The optimal solution in Eq. (1) may not be achieved, meaning that some information such as the levelled-off pattern might not be learned during the training phase.

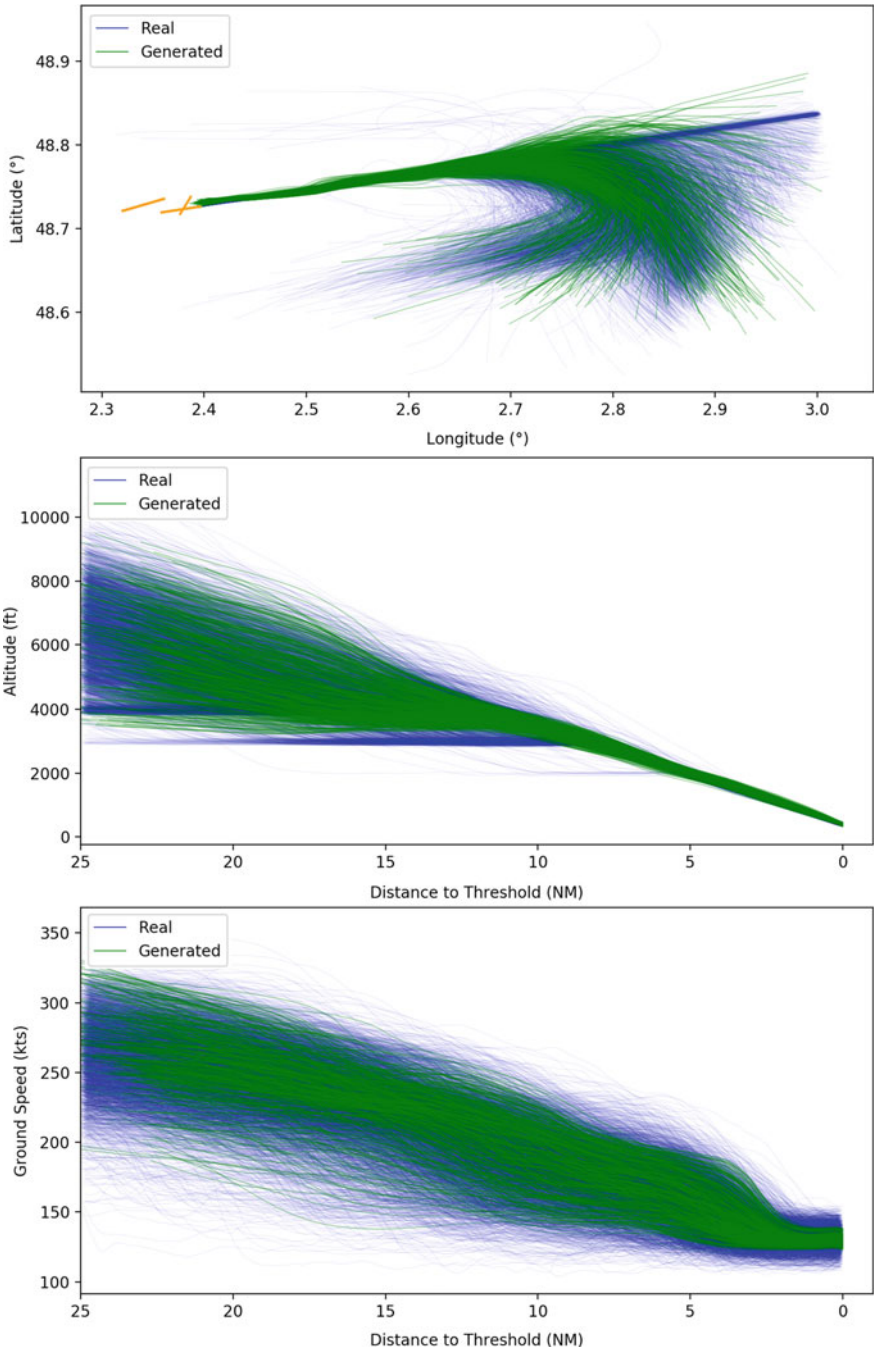

Fig. 3 1000 generated trajectories at Paris Orly Airport. In blue are represented the original trajectories and in green the generated trajectories. At the top, the longitudinal path is represented, in the center, the altitude profile, and at the bottom the ground speed profile

This effect is not problematic for anomaly detection. Even if the generator cannot reconstruct data with high levels of accuracy, it has still learned the general distribution of the data. Thus data that does not have characteristics similar to the learned data will have a large reconstruction error and will be detected as anomaly. Furthermore, anomaly detection using the discriminator is not affected at all.

3.4 Comparison with Information Geometry

Information geometry also enables the generation of new trajectories by estimating the Karhunen-Loève expansion [23] through the Functional Principal Component Analysis process [24]. It consists in considering each curve Γ as the weighted sum of a mean curve $\overline{\gamma}$ plus the principal components ϕ_j by defining the orthogonal basis that maximizes the explained variance in the first dimensions, as shown in the following equation:

$$\Gamma(t) = \overline{\gamma}(t) + \sum_{j=1}^{+\infty} b_j \phi_j(t)$$

Usually, the decomposition is truncated to retain a certain variance, which also enables dimensionality reduction. To generate new trajectories, one must first estimate the distribution of the principal coefficients b_j. Then, one is able to generate new trajectories using the decomposition basis. It is interesting to highlight that results from FPCA generation with dimensionality reduction are similar to those obtained with our GAN model. Indeed, applying dimensionality reduction in FPCA only preserves the largest variation mode around the mean curve. Therefore, the levelled-off flights are not captured with the truncated FPCA decomposition either.

4 Anomaly Detection

This section, illustrates how GAN provide solutions to the anomaly detection problem. As explained in Sect. 2, GAN combine a generator G, and a discriminator D. After the learning task, the discriminator has been trained to recognize real data from generated data. Consequently, the first approach to anomaly detection consists in using the score of D. Indeed, the closer the score is to 0 , the less realistic the data is supposed to be, or in other words, the less likely it is to belong to the original distribution.

Another way to perform anomaly detection with GAN is to build an encoder E (usually another neural network). The encoder embeds samples from the trajectory space to the latent space. The encoder is illustrated in Fig. 4. It can be automatically tuned during the GAN training (this setup is known as BIGAN), or after the training (Encoder). The anomaly detection can be applied to a dataset with the fol-

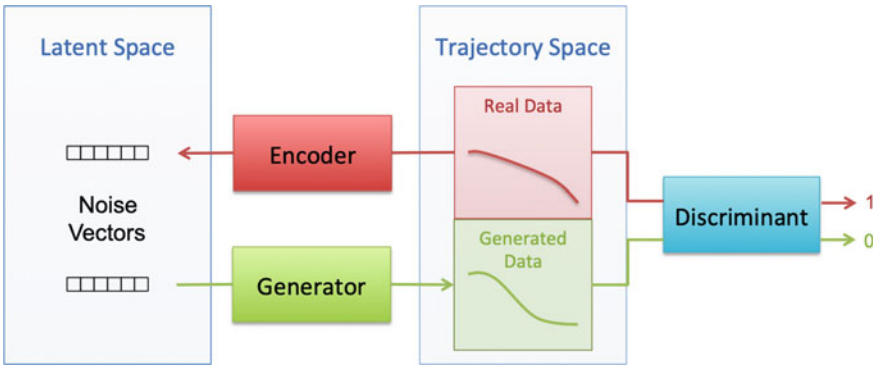

Fig. 4 This figure completes Fig. 1 with the encoder E. The encoder selects a trajectory and builds the corresponding noise vector in the latent space

lowing process : first, encode each trajectory in the latent space with the encoder E, next, rebuild the trajectories through the generator, and finally compute a distance between the original and reconstructed trajectories. The most distant trajectories can be considered as anomalies since the generator was not able to rebuild the trajectory properly. Indeed, if a trajectory does not belong to the trajectory distribution learned by the generator, the reconstruction error will be high. This approach is very similar to auto-encoder anomaly detection [5, 6]. Nevertheless, GAN are richer since they also provide trajectory generation. The encoder network structure is similar to the discriminant network detailed in Fig. 2. However, the last layer is sized to correspond to the latent space dimension.

4.1 Anomaly Detection Using the Discriminator

A first approach to performing anomaly detection is to use the discriminator. It is trained to distinguish real samples from the original data set and generates samples from the generator. Therefore, its natural behavior tends to give a score next to 1 for trajectories that are similar to the original data set and a score close to 0 for atypical trajectories.

This method of anomaly detection was applied to the original dataset of the Paris Orly Airport trajectories and the results are shown on Fig. 5. Red lines correspond to trajectories with the minimum discriminator score for the dataset, green lines to the maximum discriminant score, and orange lines to intermediate values.

The anomaly detection with the discriminator shows interesting results for the longitudinal trajectories and for the altitude profiles. The typical altitude profile (in green) follows a levelled-off path before descending on the glide path, which corresponds to the published procedure. On the other hand, the atypical profiles present high altitude or even Glide Interception From Above. 2D trajectories are

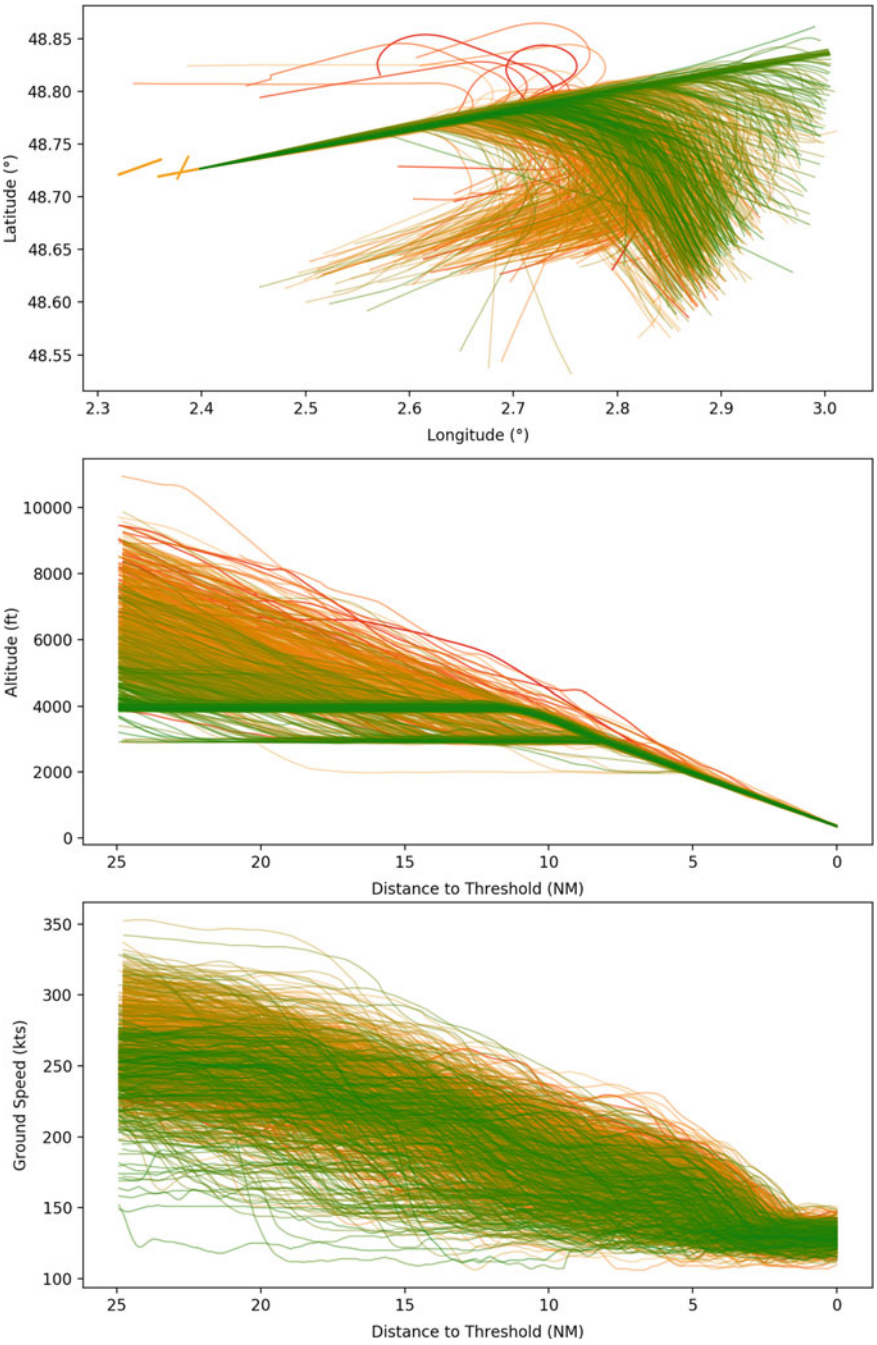

Fig. 5 Score given by the discriminator to the original dataset. The red lines correspond to the minimum discriminator score obtained for the dataset, and green lines to the maximum discriminator score (orange corresponds to intermediate scores). The longitudinal trajectories are illustrated at the top, the altitude profiles in the centre, and the speed profiles at the bottom

illustrated at the top of Fig. 5. It seems that typical 2D paths are approaches from the south and east, while less typical come from the west and very atypical from the north with holding patterns. The ground speed profiles, at the bottom of Figure 5, do not show any specific results.

4.2 Anomaly Detection Using the Encoder

This section illustrates the use of the encoder to detect anomalies. The encoder was tuned automatically after the GAN training phase. The encoder embedded the trajectory samples to the latent space. The anomaly detection was performed in three steps. First, each trajectory was embedded to the latent space with the encoder. Second, all trajectories were rebuilt through the generator. Third, the reconstruction error (L2 Norm) was computed between the original trajectories and the rebuilt trajectories. Finally, trajectory with high reconstruction errors were considered as atypical.

In order to be able to compare results with the functional principal component analysis method explained in [8], the anomaly detection was applied to specific total energy trajectories. The specific total energy is the sum of the potential energy and the specific kinetic energy per unit of mass. Since the mass is not available in radar data, the method developed in [8] considers an approximation of the total energy considering a mass constant over the last nautical miles. Considering specific total energy can be explained by the fact that safe approaches and landings are closely linked to good energy management. Therefore, one may assume that atypical energy management may induce safety events or incidents.

In this purpose, another network was trained to generate and encode specific total energy trajectories extracted from Paris Orly landing trajectories. Figure 6 illustrates the normalized distribution of reconstruction errors. The color variation is from green for small errors to red for large reconstruction errors. This corresponding color (and reconstruction error) is also used to represent the specific total energy trajectories in Fig. 7.

Two groups of anomalies can be found. The first group is composed of low energy profile trajectories, the second of high energy profile trajectories. However, the largest reconstruction errors correspond to high energy profiles (in red at the top of the figure). The flight with the highest reconstruction error was selected. The comparison with the atypical coefficient algorithm using FPCA [8, 9] is detailed below. Figure 8 illustrates the altitude profile and the speed profile of this flight. The colored dots correspond to atypical coefficients between 0 for typical and 1 for atypical. Between, 25 and 15 NM, one can observe a large atypical area due to high energy (high altitude and high speed). FPCA algorithm and GAN anomaly detection seem to be correlated. This result is also observed for the 10 highest reconstruction error flights from the GAN anomaly detection experiments.

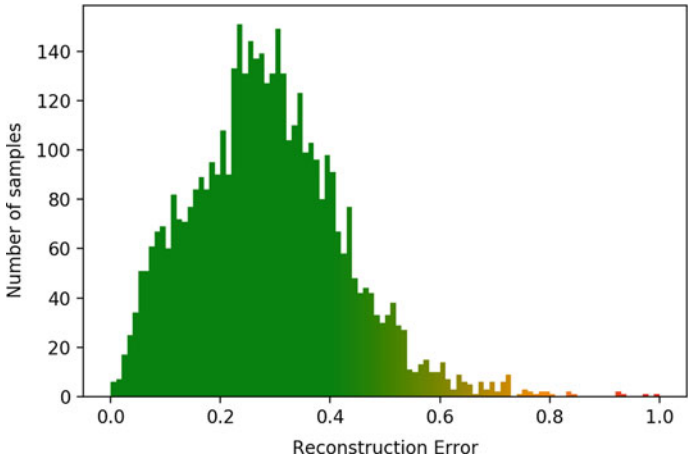

Fig. 6 Normalized distribution of the encoder-generator reconstruction errors for the specific total energy trajectories at Paris Orly Airport. The color green is attributed to small errors and goes from orange to red for larger errors. Trajectories corresponding to important reconstruction errors on the right of the plot are considered as atypical

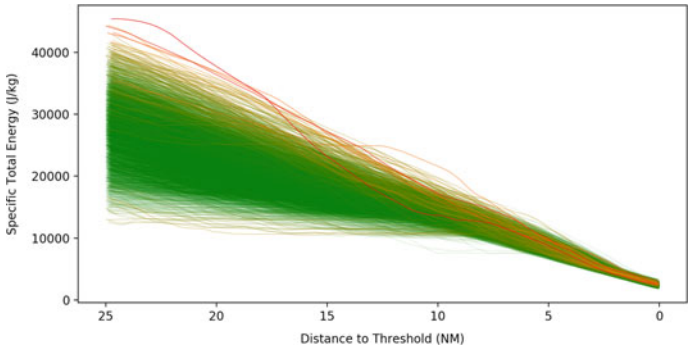

Fig. 7 Specific total energy trajectories at Paris Orly Airport. The color corresponds to the reconstruction error. Trajectories with a small reconstruction error are represented in green, and large errors in red

4.3 Latent Space Representation

The encoder enables the trajectories to be embedded in latent space. Each trajectory is then represented as a single point in a low dimensional space. Therefore, this enables a simpler representation of a group of samples with a dimensionality reduction. The embedding of the original trajectories in latent space is represented at the top of Fig. 9. The corresponding total energy trajectories are illustrated at the bottom. The embedded data of the two groups were clustered around the line $x + y = 0$. The first group in blue is above the line, and the second group in green is below the line.

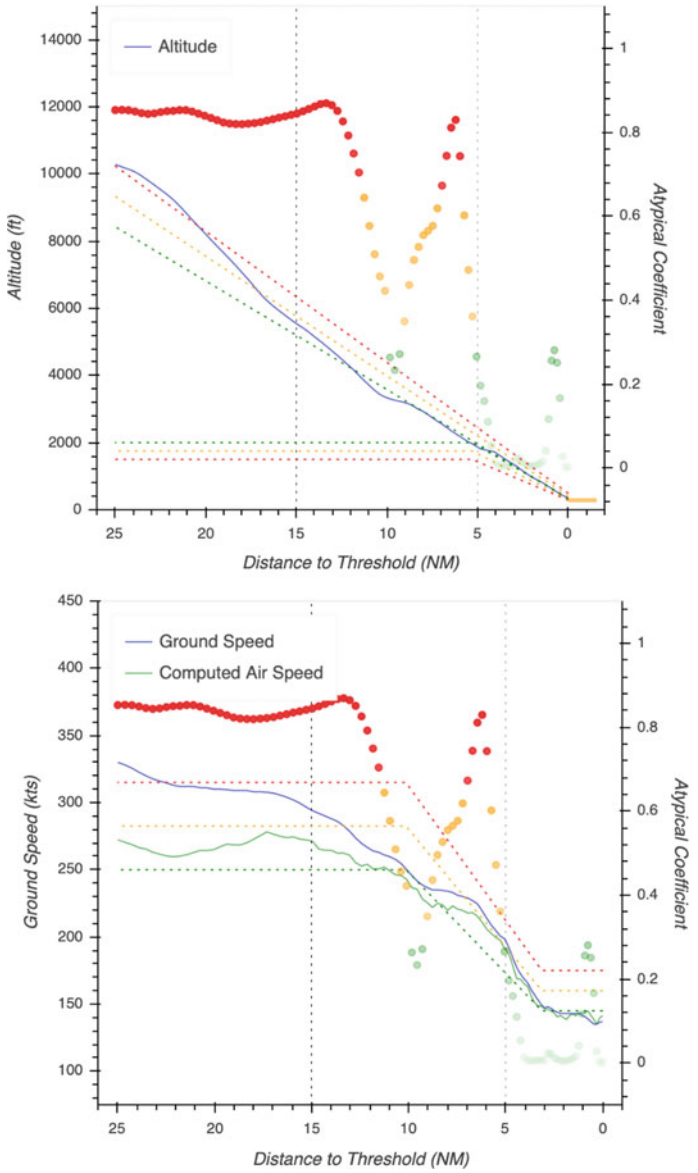

Fig. 8 Highest reconstruction score flight altitude profile (at the top), and speed profile (at the bottom). The flight presents a glide interception from above with high ground speed, and a little late power reduction. The colored dots correspond to the atypical FPCA coefficients of the total energy defined in [8]. The dashed colored lines correspond to operational limits: nominal (green), warning (orange), and critical (red). For more details see [8]

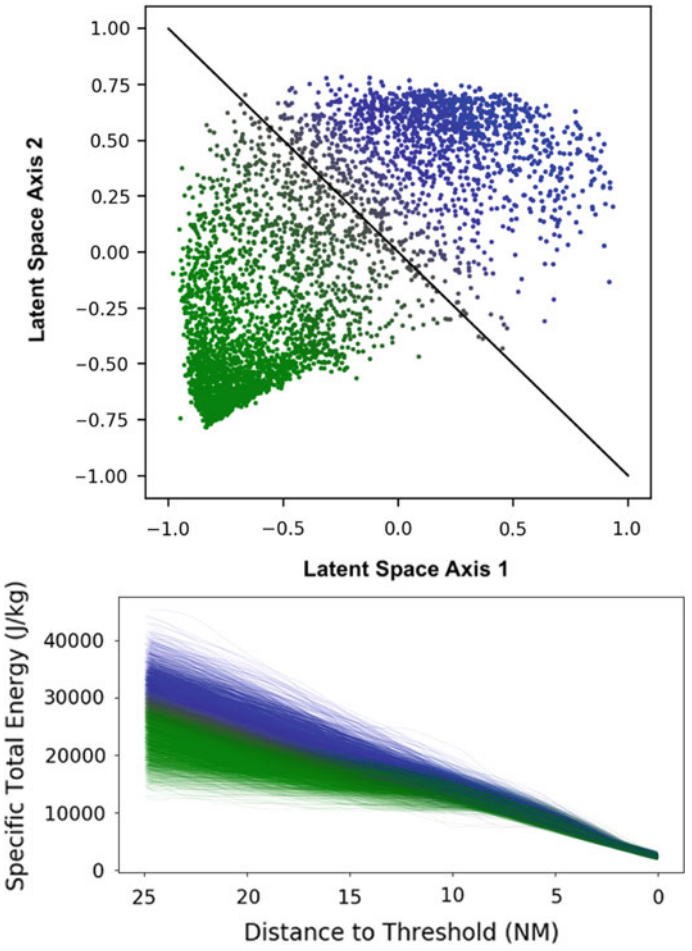

Fig. 9 At the top, the embedding of the original total specific energy trajectories into the latent space, and at the bottom the corresponding trajectories. Trajectories were clustered into two groups (green and blue) around the line $x + y = 0$

This representation enables different applications such as clustering, data analysis, or linear interpolation. For example, one may use this representation for approach procedure detection. Suppose we focus on a QFU approach with separate published procedures, a GNSS RNAV, a visual approach and a VOR/DME approach. These three types of procedures have a characteristic footprint. Approaches of the same type will be grouped together and will be easily discernible in the latent space.

By linear interpolation, we mean continuous deformation between two trajectories or objects of infinite dimension. It is a very complicated mathematical problem. The use of GAN makes it possible as the latent space is a low-dimensional normalized space. It would therefore consists in interpolating by a straight line the two points representing the trajectories in the latent space

4.4 Discussion

In this section, operational and scientific insights are provided for this research. There are several possible methodologies to detect anomalies on large dimensions elements. The GAN had not been used for the moment in this aeronautical safety framework. The operational objective is the analysis and identification of precursors to potential safety incidents or events. Atypical energy managements have shown a strong correlation with flight safety events [9], therefore GAN could be used post-operationally to analyse trajectories.

In addition, it is easy to understand the use of the total energy. Flying an aircraft consists in managing an altitude and a speed, and therefore its total energy. The final approach phase is a phase of decreasing energy. The plane goes from high speed at high altitude to landing where its potential energy and speed must cancel each other out. Energy transfers generally imply that a decrease in potential energy results in an increase in kinetic energy. On a standard 3° glide path, aircraft are facing the constraint of simultaneously reducing kinetic energy and potential energy. This constraint implies good energy management upstream, generally by configuring the flaps and landing gear to increase the drag and decrease the total energy, or by using a level-off deceleration flight to reduce the speed before descending on the glide path. Some aircraft have aerodynamic characteristics such that deceleration on final approach can be very difficult, especially in poor weather conditions such as tailwind. Therefore, there is a real operational interest in detecting atypical energy management that could lead to incidents or accidents such as the crash of Asiana flight 214 in San Fransisco (high energy then low energy) or more recently the Pegasus flight 2193 in Istanbul (high energy).

There are many similarities between GAN, auto-encoders and the FPCA methodology. The ultimate goal is to estimate a large dimension data distribution. GAN bring the generative aspect and the possibility to use both the discriminator and the generator for anomaly detection. However, like auto-encoders, they are subject to the convergence of the learning phase (even stronger for GAN). The FPCA methodology has the advantage of being deterministic. The use of GAN model on a sliding window as proposed in the FPCA methodology [8], seems much more complex and involves ensuring the convergence of each model resulting from a sliding window.

5 Conclusion

Generative adversarial networks have proven to be very effective in generating realistic scenes and objects in computer vision. This article investigates their use in the field of aircraft trajectory generation and abnormal or non-compliant trajectory detection. Preliminary experiments show that the generated trajectories follow realistic patterns. This confirms that GAN are promising alternatives to model-based trajectory simulators. The resulting generated trajectories are based on past historical data and therefore account for external factors that are often difficult to embed in physical models. Further experiments were also provided with GAN to detect non-compliant or atypical trajectories. A comparison with a technique based on functional principal component analysis also confirms that reported anomalies are relevant. To the best of our knowledge, this work is the first attempt to generate aircraft trajectories with such generative machine learning tools. There remains, therefore, much more to investigate in this domain. Further work should include the analysis of tailored network architectures and learning, or extensions to Wasserstein GAN [25] that can learn data from multimodal distributions.

Acknowledgements The authors would like to show their gratitude to Aigle-Azur airline company for providing Flight Data Monitoring Records.

References

1. F. Jackman, Nearly half of commercial jet accidents occur during final approach, landing (2014). [Online]. Available: https://flightsafety.org/asw-article/nearly-half-of-commercial-jet-accidents-occur-during-final-approach-landing/
2. IATA Forecast Predicts 8.2 billion Air Travelers in 2037, https://www.iata.org/en/pressroom/pr/2018-10-24-02/, library Catalog: www.iata.org
3. S. Das, B.L. Matthews, A.N. Srivastava, N.C. Oza, Multiple kernel learning for heterogeneous anomaly detection: algorithm and aviation safety case study, in *Proceedings of the 16th ACM SIGKDD International Conference on Knowledge Discovery and Data Mining* (ACM, 2010), pp. 47–56
4. N. Chrysanthos, in *Kernel Methods for Flight Data Monitoring* (Ph.D. dissertation, Troyes, 2014)
5. M. Sakurada and T. Yairi, "Anomaly detection using autoencoders with nonlinear dimensionality reduction," in *Proceedings of the MLSDA 2014 2nd Workshop on Machine Learning for Sensory Data Analysis* (ACM, 2014), p. 4
6. C. Zhou, R.C. Paffenroth, Anomaly detection with robust deep autoencoders, in *Proceedings of the 23rd ACM SIGKDD International Conference on Knowledge Discovery and Data Mining* (ACM, 2017), pp. 665–674
7. C. Barreyre, *Statistiques en grande dimension pour la détection d'anomalies dans les données fonctionnelles issues des satellites* (Ph.D. dissertation, INSA de Toulouse, 2018)
8. G. Jarry, D. Delahaye, F. Nicol, E. Feron, Aircraft atypical approach detection using functional principal component analysis. J. Air Transp. Manage. **84**, 101787 (2020)
9. G. Jarry, D. Delahaye, E.Féron, Trajectory approach analysiS: a post-operational aircraft approach analysis tool, in *SID 2019, 9th SESAR Innovation Days*, Athenes, Greece, Dec 2019. [Online]. Available: https://hal-enac.archives-ouvertes.fr/hal-02385671

10. I.J. Goodfellow, J. Pouget-Abadie, M. Mirza, B. Xu, D. Warde-Farley, S. Ozair, A. Courville, Y. Bengio, Generative adversarial nets, in *Proceedings of the 27th International Conference on Neural Information Processing Systems*, vol 2 (MIT Press, Cambridge, MA, USA, 2014), pp. 2672–2680. [Online]. Available: http://dl.acm.org/citation.cfm?id=2969033.2969125
11. C. Vondrick, H. Pirsiavash, A. Torralba, Generating videos with scene dynamics, in *Advances in Neural Information Processing Systems 29*, ed. D.D. Lee, M. Sugiyama, U.V. Luxburg, I. Guyon, R. Garnett (Curran Associates, Inc., 2016), pp. 613–621. [Online]. Available: http://papers.nips.cc/paper/6194-generating-videos-with-scene-dynamics.pdf
12. A. Brock, J. Donahue, K. Simonyan, Large scale GAN training for high fidelity natural image synthesis, in *International Conference on Learning Representations* (2019). [Online]. Available: https://openreview.net/forum?id=B1xsqj09Fm
13. E. Putin, A. Asadulaev, Q. Vanhaelen, Y. Ivanenkov, A.V. Aladinskaya, A. Aliper, A. Zhavoronkov, Adversarial threshold neural computer for molecular de novo design. Mol. Pharmaceutics **15**(10), 4386–4397 (2018). pMID: 29569445. [Online]. Available: https://doi.org/10.1021/acs.molpharmaceut.7b01137
14. S. Reed, Z. Akata, X. Yan, L. Logeswaran, B. Schiele, H. Lee, Generative adversarial text to image synthesis, in *Proceedings of The 33rd International Conference on Machine Learning*, ser. Proceedings of Machine Learning Research, ed. by M.F. Balcan, K.Q. Weinberger, vol. 48 (PMLR, New York, New York, USA, 2016), pp. 1060–1069. [Online]. Available: http://proceedings.mlr.press/v48/reed16.html
15. T. Schlegl, P. Seeböck, S.M. Waldstein, U. Schmidt-Erfurth, G. Langs, Unsupervised anomaly detection with generative adversarial networks to guide marker discovery. CoRR, abs/1703.05921 (2017). [Online]. Available: http://arxiv.org/abs/1703.05921
16. A. Gupta, J. Johnson, L. Fei-Fei, S. Savarese, A. Alahi, Social GAN: socially acceptable trajectories with generative adversarial networks, in *The IEEE Conference on Computer Vision and Pattern Recognition (CVPR)* (2018)
17. N. Hirose, A. Sadeghian, P. Goebel, S. Savarese, To go or not to go? a near unsupervised learning approach for robot navigation. CoRR, abs/1709.05439 (2017)
18. W. Ding, W. Wang, D. Zhao, Multi-vehicle trajectories generation for vehicle-to-vehicle encounters, in *2019 IEEE International Conference on Robotics and Automation (ICRA)* (2019)
19. I.J. Goodfellow, NIPS 2016 tutorial: Generative adversarial networks. CoRR, abs/1701.00160 (2017). [Online]. Available: http://arxiv.org/abs/1701.00160
20. D. Poles, A. Nuic, V. Mouillet, Advanced aircraft performance modeling for ATM: analysis of bada model capabilities, in *29th Digital Avionics Systems Conference*. IEEE (2010), p. 1-D
21. A. Nuic, D. Poles, V. Mouillet, Bada: An advanced aircraft performance model for present and future ATM systems. Int. J. Adapt. Control Signal Process. **24**(10), 850–866 (2010)
22. D.P. Kingma, J. Ba, Adam: A Method for Stochastic Optimization,arXiv:1412.6980 [cs] (2014). arXiv: 1412.6980. [Online]. Available: http://arxiv.org/abs/1412.6980
23. H. Stark, J. Woods, *Probability, Random Processes, and Estimation Theory for Engineers* (Prentice-Hall, Upper Saddle River, 1986). [Online]. Available: https://books.google.fr/books?id=2pFRAAAAMAAJ
24. C. Hurter, S. Puechmorel, F. Nicol, A. Telea, Functional decomposition for bundled simplification of trail sets. IEEE Trans. Visual. Comput. Graph. **24**(1), 500–510 (2018)
25. M. Arjovsky, S. Chintala, L. Bottou, Wasserstein gan. http://arxiv.org/abs/1701.07875. (2017)

RRT*-Based Algorithm for Trajectory Planning Considering Probabilistic Weather Forecasts

E. Andrés, M. Kamgarpour, M. Soler, M. Sanjurjo-Rivo, and D. González-Arribas

Abstract Convective weather and its inherent uncertainty constitute one of the major challenges in the air traffic management (ATM) system, entailing both safety hazards and economic losses. In the present work, we propose a stochastic algorithm for trajectory planning that ensures feasibility and safety of the path between two points while avoiding unsafe stormy regions. The uncertain zone to be flown is described by an ensemble of equally likely forecasts. We design a scenario-based optimal rapidly exploring random tree (SB-RRT*), and we able to dynamically allocate risk during its expansion so that a safety margin is not violated. The solution is a safe continuous trajectory that minimizes the distance covered. We present preliminary results assuming weather to be the only source of uncertainty. We consider an aircraft point-mass model at constant altitude and airspeed with manoeuvres being limited by a minimum turning radius.

1 Introduction

Weather uncertainties represent a major issue that the air traffic management (ATM) system needs to account for. In particular, areas of convective weather (also known as thunderstorms) constitute a potential safety hazard, being responsible of a quarter

E. Andrés (✉) · M. Soler · M. Sanjurjo-Rivo · D. González-Arribas
Department of Bioengineering and Aerospace Engineering, Universidad Carlos III de Madrid, Leganés, Spain
e-mail: eandres@ing.uc3m.es

M. Soler
e-mail: masolera@ing.uc3m.es

M. Sanjurjo-Rivo
e-mail: msanjurj@ing.uc3m.es

D. González-Arribas
e-mail: dangonza@ing.uc3m.es

M. Kamgarpour
Automatic Control Laboratory, ETH Zurich, Zurich, Switzerland
e-mail: mkamgar@control.ee.ethz.ch

Air Traffic Management and Systems IV, Lecture Notes in Electrical Engineering 731,
https://doi.org/10.1007/978-981-33-4669-7_14

of the en-route delays in Europe [1]. In order to enhance ATM's safety, efficiency and capacity, path planning techniques must take into consideration the inherent stochasticity of these phenomena. The aim of this work is to develop a methodology for safe aircraft trajectory planning considering the intrinsic uncertainties of the stormy environment.

The design of avoidance paths that prevent flying through risky areas is a problem of interest that has been covered in the literature using a wide spectrum of approaches with different applications. A first approach is based on geometric procedures, see e.g., [2]. They benefit from fast computing times at the cost of usually ignoring storm evolution and their uncertainty, aircraft dynamics or trajectory optimality. A second class of methods relies on robust optimal control [3]. The optimization problem considering aircraft dynamics and uncertain thunderstorm development can be solved using nonlinear programming. However, the solution of the robust optimal control problem is quite sensitive to the choice of the required initial guess. To this end, in [3], a randomized initialization is proposed, obtaining a wide range of local optima and identifying the best solution. A third possible approach is the so-called stochastic reach-avoid [4, 5], which is based on dynamic programming. These techniques are able to find optimal trajectories in uncertain and time-varying scenarios. Nonetheless, they are often computationally prohibitive, because there is a need to discretize and explore an entire state space. Therefore, the affordable dimension of the problem is limited due to the so-coined by Bellman "Curse of Dimensionality".

In this work, we opt for an incremental sampling-based algorithm, the rapidly exploring random tree (RRT) [6]. RRT-based algorithms are able to find feasible trajectories in high dimensional problems, including system kinematics, dynamics and constraints [7]. In addition, if the vehicle is moving in a constantly changing environment, they admit online planning, meaning that once a vehicle is following the planned trajectory they can incorporate new data and replan the route in almost real-time [8]. In the literature, there are different versions of RRT that have been applied to trajectory planning of autonomous driving cars [9–11] or UAV flights [12–14].

With regard to the stochasticity of the unsafe regions, previous works on RRT were built on chance constraint approaches with both linear [15] and nonlinear [16] dynamics. Chance constraints provide the probability of being above or below a safety margin for a particular state-space configuration [17], hence, these works only checked the safety of discrete points along the trajectory. To the best of authors' knowledge, RRT-based algorithms have not considered the safety of a continuous path. Moreover, RRT techniques have not been used for aircraft flight planning in areas of uncertain weather.

To assess safety during the flight, there is a need to develop models of thunderstorm evolution. Modelling thunderstorms for flight planning purposes are a challenging task, because it is difficult to forecast their birth and evolution in timescales close to flight departure. The main reason is that the atmospheric evolution is chaotic and extremely sensitive to perturbations, so any change might lead to huge errors in a prediction. In the numerical weather prediction (NWP) framework, the main trend is to characterize weather uncertainties with an ensemble forecast [18]. An ensemble

provides a number of realizations, typically between 10 and 50, that represent the atmosphere assuming slight variations during its evolution. By analysing the ratio of realizations that predict a storm, we can estimate how risky an area is.

Our main contribution and the purpose of this work are the design of a RRT-based algorithm for aircraft flight planning in stochastic weather regions ensuring the safety of a continuous trajectory. We propose a scenario-based rapidly exploring random tree (SB-RRT*) for general nonlinear systems able to grow in an uncertain environment which is described by an ensemble of discrete realizations. Unlike previous techniques that only considered the safety of a discrete set of points, our algorithm ensures that a whole continuous trajectory is safe. As the tree is expanding, it is able to dynamically allocate risk wherever is needed in order to never exceed a global safety margin.

The paper is structured as follows: we introduce RRT algorithms in Sect. 2. In Sect. 3, we propose the SB-RRT*, an optimal RRT able to expand in stochastic and hazardous regions. A case study and simulation results are included in Sect. 4. Finally, some conclusions are drawn in Sect. 5.

2 RRT: Rapidly Exploring Random Trees

RRT algorithms are path planning tools that look for a feasible trajectory between an initial and a final state configuration. From an initial state, RRTs are expanded, iteration by iteration, driving the system towards randomly selected targets. RRTs can deal with a static or dynamic environment made up of unsafe zones to be avoided. RRT planners are able to handle several degrees of freedom with constraints [6].

2.1 RRT Algorithm

Let $X \subset \mathbb{R}^{d_x}$ be the planning space in which the aircraft will manoeuvre. The constant d_x represents the dimension of the coordinate system, generally equal to 2 or 3. Let $X_{\text{storm}} \subset X$ be the unsafe zones that must be avoided, which in this case represent thunderstorms. The complementary set $X_{\text{safe}} = X \setminus X_{\text{storm}}$ represents the safe areas.

The RRT algorithm defines an iterative process that grows a tree $T = (A, E)$, where A is the set of randomly selected nodes (also known as vertices) and E represents the collection of edges connecting pairs of nodes in A. Individual nodes and edges are denoted by a_i and e_i, respectively, with the subscript i bounded by the maximum number of iterations. A fixed position $\mathbf{x}_i \in X$ obtained randomly defines a node a_i. An edge e_i represents a continuous trajectory between two nodes a_i and a_i'. Note that not every node or edge created by the algorithm is included in A or E, some of them are rejected if there is an intersection with X_{storm}. Let $\mathbf{x}_{\text{start}}, \mathbf{x}_{\text{goal}} \in X$ be the initial and goal state configurations, the nodes a_{start} and a_{goal} represent these positions respectively in T.

Let $S \subset \mathbb{R}^{d_s}$, with $d_s \geq d_x$, be the state space and let $U \subset \mathbb{R}^{d_u}$ be the control space. In general, the dynamics of our system will be represented by a state vector $\mathbf{s} \in S$ that evolves according to a transition equation,

$$\dot{\mathbf{s}} = f(\mathbf{s}, \mathbf{u}),$$

with $\mathbf{u} \in U$ the control input. Assuming the described setting, the RRT grows by following the set of procedures detailed hereafter:

- *RandomSample*: this function takes a random sample $\mathbf{x}_{rnd} \in X$ from the planning domain and creates its associated node a_{rnd}.
- *NearestNode*: it returns the closest node to a_{rnd}, $a_{nearest}$, according to a predefined metric, e.g. Euclidean distance, Dubins path length.
- *Steer*: this function drives the system from $a_{nearest}$ to a_{rnd} minimizing the distance covered or any other cost function, i.e. time and fuel consumption. The trajectory between both nodes is represented by an edge e_i.
- *Safe*: it checks if an edge goes through not allowed areas.
- *AddNode*, *AddEdge*: these functions include a node a_i or an edge e_i in the sets A and E, respectively.

By using the procedures here listed, the RRT pseudocode is summarized in Algorithm 1.

Algorithm 1 $T = (A, E) \leftarrow \text{RRT}(a_{start})$

```
T ← InitializeRRT();
T ← AddNode(a_start, T);
while i < MaxIter do
    a_rnd ← RandomSample();
    a_nearest ← NearestNode(a_rnd, T);
    e_i ← Steer(a_nearest, a_rnd);
    if Safe(e_i) then
        T ← AddNode(a_rnd);
        T ← AddEdge(e_i);
    end if
end while
return T
```

In order to grow a tree T, the RRT algorithm is initialized with the initial node a_{start}. For a predefined maximum number of iterations $MaxIter$, a random sample a_{rnd} is taken from X and there is an attempt to grow an edge and connect it to the closest node a_{nearest} in A. If the connection is successful and the edge does not go through X_{storm}, the sample and the edge are included in A and E, respectively. An example of RRT expansion is shown in Fig. 1. If the number of iterations is sufficiently large, almost every region in X can be connected with the initial position by a sequence of tree edges [19]. In trajectory planning problems, the main goal is to add the node a_{goal} to A so that it is connected to a_{start}.

Fig. 1 Example of RRT expansion with 200, 500 and 1000 iterations (from left to right)

2.2 *RRT* Algorithm*

Despite being able to obtain a feasible trajectory between two state configurations, the RRT does not ensure trajectory optimality. That means the solution will cover almost surely more distance than required, leading to a higher and unnecessary cost. An update for the RRT was introduced in [20], the optimal RRT, denoted RRT*. The RRT* is a path planning technique that ensures feasibility and asymptotic optimality of a trajectory between two given state configurations. The RRT* algorithm inherits the main core from the RRT including three additional features:

- *Near*: it obtains the set of nodes $A_{\text{near}} \subseteq A$ within a ball $B(a_{\text{rnd}}; k\frac{\log n}{n})$, with k a constant that depends on the RRT and n the number of nodes in T.
- *Parent*: among the set A_{near}, this function finds the node a_{min} that involves the smallest cost from a_{start} to a_{rnd} passing by a_{min}. The node a_{min} is selected as the parent of a_{rnd}.
- *Rewire*: the rewiring process checks if the cost from the initial node to each of the elements in A_{near} can be reduced going through a_{rnd}. It changes parent–child relations, establishing new edges.

These functions are included after line 7 in Algorithm 1. Once the safety of a possible edge has been ensured, the set of nodes A_{near} in the vicinity of a_{rnd} is obtained using the *Near* function. Given $a_{\text{near},i} \in A_{\text{near}}$, the cost c_i of the trajectory between a_{start} and a_{rnd} through $a_{\text{near},i}$ is calculated for each i. The node with the smallest value of c_i is chosen as the parent of a_{rnd} and denoted by a_{min}. The rewiring process takes place afterwards, removing non-optimal connections, so that each node is connected to the root of the tree with the smallest possible cost.

Parent–child relations are an important part of the algorithm, as one node can have many children, but each node only has one parent. Consequently, if we select an arbitrary node in A, we will be able to reach a_{start} just by following the sequence of parents. The aim of the RRT is then to find a parent for a_{goal} so that we can connect it to a_{start}. The RRT*, which is based on the RRT, goes further and removes redundant relations that involve longer trajectories between nodes.

3 Scenario Based RRT*

SB-RRT* is an extension of the RRT* algorithm in which the uncertain unsafe areas are provided as a set of possible scenarios. The tree growth is constrained in such a way that the solution is a safe continuous curve.

3.1 SB-RRT Expansion*

The SB-RRT* presented in this work is an update of the RRT* considering that X_{storm} is uncertain and described by a finite number of possible scenarios, all of which can be treated as deterministic. We assume, without loss of generality, that all the scenarios are equally weighted. However, the formulation can be extended to forecast members of different weights, if such information is available (see, e.g. [21]). In addition, we assume that, in each scenario, thunderstorms are objects described by closed curves.

Let the unsafe set X_{storm} be uncertain. In [15], the authors proposed a chance constrained RRT (CC-RRT), in which the probability of being inside X_{storm} was determined for each state configuration. In contrast to CC-RRT, we choose a scenario-based approach in which the environment is characterized by an ensemble forecast. The ensemble consists of different realizations, or scenarios, all of them possible. The set X_{storm} is composed of N_o different thunderstorms:

$$X_{\text{storm}} = \{C_1(\mathbf{p}_1), \ldots, C_{N_o}(\mathbf{p}_{N_o})\}, \tag{1}$$

$(\mathbf{p}_j)$ denotes a closed curve that describes the j-th thunderstorm and depends on an uncertain vector of parameters $\mathbf{p}_j \subset \mathbb{R}^{d_{p_j}}$, with $d_{p_j} \geq 1$. We assume that N_{sc} discrete realizations of X_{storm} are available, being all of them equally likely:

$$X^l_{\text{storm}} = \{C_1(\mathbf{p}^l_1), \ldots, C^l_{N_o}(\mathbf{p}^l_{N_o})\}, \quad \textit{with } l = 1, \ldots, N_{sc}, \tag{2}$$

where $C^l_j(\mathbf{p}^l_j)$ is a realization of the j-th thunderstorm obtained by sampling the uncertain vector $\mathbf{p}_j$. As each curve C^l_j can be treated as deterministic, we can determine whether a point lies inside it or a curve goes through it. In consequence, the SB-RRT* is able to work with a trajectory defined by a sequence of continuous curves (or edges) or by a sequence of discrete states (or nodes).

Once the environment is defined, the SB-RRT* expands according to the pseudocode in Algorithm 2. The proposed algorithm is essentially a RRT* as described in Sect. 2.2 that computes the safety of a sequence of edges and the following procedures that will be covered hereafter in Sect. ssec:safety (Fig. 2).

Algorithm 2 $T = (A, E) \leftarrow$ SB-RRT* (a_{start})

$T \leftarrow InitializeRRT()$;
$T \leftarrow AddNode(a_{start}, T)$;
while $i < MaxIter$ **do**
  $a_{rnd} \leftarrow RandomSample()$;
  $a_{nearest} \leftarrow NearestNode(a_{rnd}, T)$;
  $e_i \leftarrow Steer(a_{nearest}, a_{rnd})$;
  if $Safe(a_{rnd})$ **and** $Safe(e_i)$ **then**
    $A_{near} \leftarrow Near(a_{rnd}, A)$;
    $a_{min} \leftarrow Parent(a_{rnd}, a_{nearest}, A_{near})$;
    $T \leftarrow AddNode(a_{rnd})$;
    $T \leftarrow AddEdge(e_i)$;
    $T \leftarrow Rewire(a_{rnd}, a_{min}, A_{near})$;
  end if
end while
return T

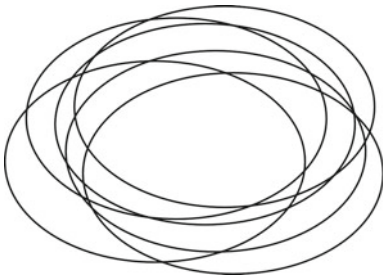

Fig. 2 Schematic representation of the different possible realizations of an unsafe region

3.2 Safety of a Trajectory

Algorithm 2 includes the function *Safe* that determines the safety of either nodes or edges. One of the key contributions of this work is the way the safety is computed so that the solution of the SB-RRT* can be considered safe as a whole continuous trajectory. In a planning in which the unsafe objects are described by deterministic parameters, a node is safe if it lies outside X_{storm} and an edge is safe if there is no intersection with any thunderstorm. If the environment is uncertain, we can only know that a node or an edge is safe up to a certain probability. In the present paper, given an event Z, the probability of Z being safe or not safe is represented by $(Z)^s$ and $(Z)^{ns}$, respectively. If $N_o > 1$, $(Z)^{ns,j}$ denotes the event of Z being not safe in the presence of the j-th thunderstorm. The different definitions of safety that are used in our work are listed down below.

Safety of a node: We say that a node a_i is safe if it is outside all the thunderstorms in X_{storm} with a probability of at least $1 - \epsilon_a$. In other words, it can only be inside at most $\lfloor \epsilon_a N_{sc} \rfloor$ deterministic realizations of unsafe object C_j^l. That is,

$$\Pr((a_i)^{ns}) = \Pr\left(\bigvee_{j=1}^{N_o}(a_i)^{ns,j}\right) \leq \epsilon_a \tag{3}$$

Safety of an edge: In a similar way, we say that an edge e_i is safe if the probability that it intersects with any of the thunderstorms in X_{storm} is less than a safety margin ϵ_e. It means that e_i only can interact with at most $\lfloor \epsilon_e N_{sc} \rfloor$ realizations of unsafe object C_j^l. That is,

$$\Pr((e_i)^{ns}) = \Pr\left(\bigvee_{j=1}^{N_o}(e_i)^{ns,j}\right) \leq \epsilon_e \tag{4}$$

Safety of a trajectory: Let $E^* = \{e_1^*, \ldots, e_{N^*}^*\}$ be the solution of the SB-RRT*, formed as a concatenation of safe edges e_i^*. Let N^* be the number of edges in E^*. The solution of the SB-RRT* will be safe, with a safety margin ϵ, if all the edges from E^* are safe at the same time [22]. That is,

$$\Pr((E^*)^s) = \Pr\left(\bigwedge_{i=1}^{N^*}(e_i^*)^s\right) \geq 1 - \epsilon. \tag{5}$$

By using De Morgan's law, which states that the negation of a conjunction is equal to the disjunction of negations, (5) can be rewritten as,

$$\Pr((E^*)^{ns}) = \Pr\left(\bigvee_{i=1}^{N^*}(e_i^*)^{ns}\right) \leq \epsilon. \tag{6}$$

With Boole's inequality, which states that for a finite number of events Z_i, we have $\Pr(\bigvee_i Z_i) \leq \sum_i \Pr(Z_i)$, and we can conservatively satisfy (6),

$$\Pr((E^*)^{ns}) \leq \sum_{i=1}^{N^*}\Pr((e_i^*)^{ns}) \leq \epsilon. \tag{7}$$

Using (4) and Boole's inequality, (7) is replaced by,

$$\Pr((E^*)^{ns}) \leq \sum_{i=1}^{N^*}\sum_{j=1}^{N_o}\Pr((e_i^*)^{ns,j}) \leq \epsilon. \tag{8}$$

Combining equations (5) and (8), the safety constraint for the solution E^* is,

$$\Pr((e_i^*)^{ns,j}) \leq \epsilon_{ij}, \tag{9}$$

which must be satisfied for $i = 1, \ldots, N^*$ and $j = 1, \ldots, N_o$. The elements ϵ_{ij} are individual safety margins for the i-th edge in the presence of the j-th thunderstorm.

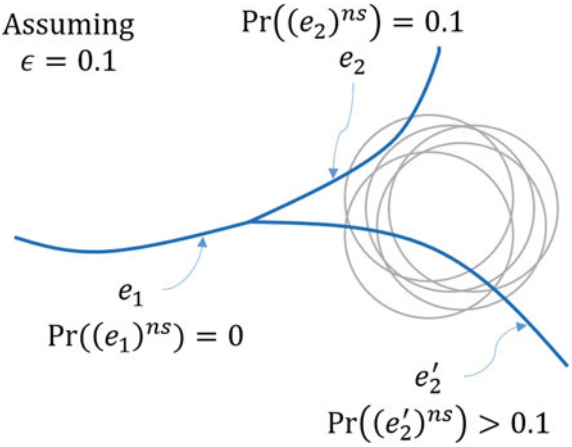

Fig. 3 Example of dynamic risk allocation

They must verify $0 \leq \epsilon_{ij} \leq 1$ and $\sum_{i=1}^{N^*} \sum_{j=1}^{N_o} \epsilon_{ij} \leq \epsilon$. In addition, the safety margin for the i-th edge considering the N_o thunderstorms is denoted by ϵ_i and verifies $\sum_{j=1}^{N_o} \epsilon_{ij} \leq \epsilon_i$. In order to allocate the risks ϵ_{ij}, it can be done in a uniform manner, so that $\epsilon_{ij} = \epsilon/(N^* N_o)$. This kind of allocation is overly conservative. Moreover, the value of N^* in any RRT is not known a priori as it is part of the solution and should be estimated. In reality, some parts of the trajectory will go through areas of no risk and as we get closer to the unsafe set the actual risk will increase.

This work proposes a *dynamic risk allocation* in which the risk is non-uniformly assigned to the different edges as the SB-RRT* is growing. This non-uniform risk allocation leads to a less conservative and more optimal solution in terms of distance. During the expansion, the probability of interaction with X_{storm} of any trajectory starting at $a_{start} \in A$ can be of, at most, ϵ. An example of the risk allocation with $\epsilon = 0.1$ is illustrated in Fig. 3. An arbitrary trajectory starts with an edge e_1, which is unsafe with probability 0. Then, the tree is able to grow in directions in which, according to (7), the total sum of probabilities of being unsafe is bounded by 0.1. Consequently, the edge e_2, which is unsafe with probability 0.1 is accepted:

$$\Pr\left(\bigvee_{i=1}^{2} (e_i)^{ns}\right) \leq \Pr((e_1)^{ns}) + \Pr((e_2)^{ns}) \leq 0.1.$$

On the contrary, e_2' is rejected, as the resulting sum of probabilities is higher than 0.1:

$$\Pr\left(\bigvee_{i=1}^{2} (e_i)^{ns}\right) \leq \Pr((e_1)^{ns}) + \Pr((e_2')^{ns}) > 0.1.$$

The tree could continue growing from e_2 provided that (7) is verified. The definitive mathematical formulation of the dynamic risk allocation is in progress and will be presented in future work

4 Case Study

In this section, the SB-RRT* is tested considering a simplified point-mass model of aircraft. We solve the problem in a simple environment formed by circular uncertain unsafe areas that represent possible stormy regions.

4.1 Aircraft Dynamics

We assume that it is flying at constant velocity V and constant altitude. Let $\mathbf{s} = (x, y, \lambda)$ be the state vector. The vector $\mathbf{x} = (x, y) \subset \mathbb{R}^2$ represents the aircraft position and $\lambda \in [-\pi, \pi]$ its heading angle. The manoeuvres are limited by the aircraft minimum turning radius $R_{\min}$ or equivalently, its maximum yaw rate $u_{\max} = V/R_{\min}$. For simplicity, only three control inputs are considered: no turn, right turn or left turn (with $u_{\max}$ or $R_{\min}$). The system dynamics is given by,

$$\dot{\mathbf{s}} = \begin{Bmatrix} \dot{x} \\ \dot{y} \\ \dot{\lambda} \end{Bmatrix} = \begin{Bmatrix} V\cos\lambda \\ V\sin\lambda \\ u \end{Bmatrix}, \tag{10}$$

with controls, $u \in \{-u_{\max}, 0, u_{\max}\}$. Each time we want to expand the SB-RRT* between two nodes and we must solve the system in (10) minimizing the distance covered. Given two states $\mathbf{s}_0 = (x_0, y_0, \lambda_0)$ and $\mathbf{s}_f = (x_f, y_f, \lambda_f)$, there exist an analytical solution for this optimization problem, the Dubins path [23]. Dubins paths are continuous and differentiable curves formed by one of the following:

- Three arcs of circle of radius $R_{\min}$.
- Two arcs of circle of radius $R_{\min}$ with one straight line in between.

Dubins paths are included in two functions from the SB-RRT* algorithm:

- *NearestNode*: they are used as the metric. When looking for the closest node to a_{rnd} from the tree T, it is appropriate to use the shortest Dubins path, as it considers the heading of the nodes and the minimum turning radius R_{min}. Using another metric, such as the Euclidean distance, could lead to manoeuvres that violate the turning constraint [10].
- *Steer*: this function drives the system from $a_{nearest}$ to a_{rnd} with a Dubins path.

4.2 Problem Setting

As a case study, the SB-RRT* is tested in a domain $X = [0, 200] \times [0, 160]$ (in km), with an aircraft flying between (0, 70) and (200, 80), and manoeuvering with $R_{\min} =$ 2 km. The unsafe set X_{storm} is formed by $N_o = 3$ circular and static thunderstorms

of known radii and uncertain centre positions sampled from a Gaussian distribution. Mean positions of the centres are (60, 60), (150, 70) and (110, 115), with radii of 20, 15 and 12 km, respectively. In this example, circles are used because they admit an analytical intersection with Dubins paths. The number of scenarios considered is $N_{sc} = 20$. A maximum risk of 10%, or $\epsilon = 0.1$, is allowed. In consequence, only $\lfloor \epsilon N_{sc} \rfloor = 2$ intersections with the unsafe set are permitted. They can occur with the same thunderstorm or be distributed between two. The algorithm is implemented in Python (basic Python and Numpy library). The computations are performed in a workstation equipped with an Intel Core i7-8550U CPU running at 1.8 GHz.

4.3 Results and Discussion

Figure 4 displays the SB-RRT* evolution and solution in two stages of its expansion, at the 500th and 1000th iterations. It can be seen that a higher number of iterations involve less distance covered by the solution trajectory. This fact results from the appropriate parent choice and the rewiring process, both of which keep optimizing the tree structure as it grows, removing redundant connections and ensuring that each point is connected to the root with the shortest possible trajectory. In addition, it can be observed that the tree is successfully avoiding the discrete realizations of uncertain thunderstorms. Each node, including the target, is connected to the starting point with a trajectory that involves at most two interactions with the unsafe regions. This fact guarantees that the flight would be safe in a 90% of the possible scenarios.

Figure 5 shows the solution after the 2000th iteration. As the number of iterations increase, the algorithm is able to find solutions through the corridor between the thunderstorms reducing the total distance that is required. In Table 1, the reduction in the distance covered with the number of iterations is shown. As a lower bound, the straight trajectory connecting the initial and target positions involved 200 km, but it is not valid as it assumes a high risk. With 2000 iterations, a 207 km trajectory

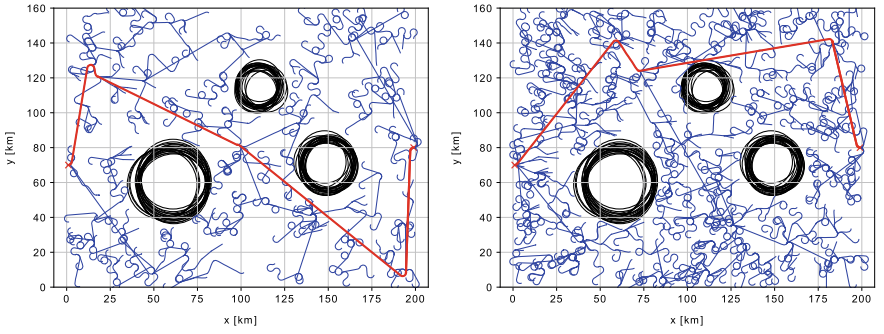

(a) 500 iterations (b) 1000 iterations

Fig. 4 SB-RRT* expansion and solution (in red) for different maximum number of iterations

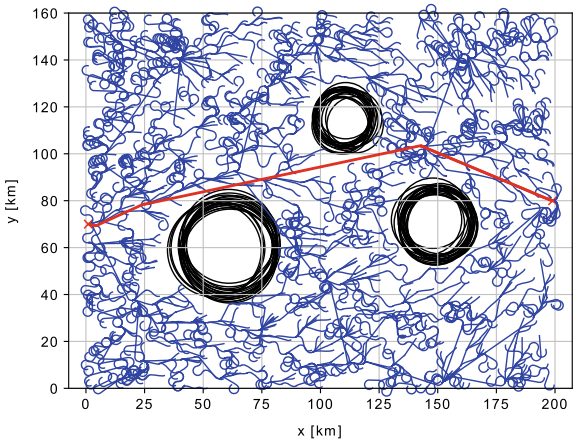

Fig. 5 SB-RRT* solution after 2000 iterations

Table 1 Length of the solution trajectory and execution time for the SB-RRT* with the number of iterations

Iterations	Solution length (km)	Execution time (s)
500	355	76
1000	291	283
2000	207	1160

was obtained, meeting the safety requirement. That is, a 3.5% increase in the total distance meant a 90% rise in the safety of the solution.

However, the main drawback of the SB-RRT* is the asymptotic convergence. That means there is no guarantee of optimality unless the number of iterations tends to infinity. In this example, increasing the number of iterations above 2000 was of little benefit, as it required an excessive computational time with no important shortening of the solution trajectory. As can be seen in Table 1, doubling the number of iterations means that the execution time grows by a factor of approximately 4. The main bottleneck in the SB-RRT* algorithm is *Safe* function, which checks if an edge is safe before being added to the tree or during the rewiring step. It must check if there is an interaction with any object in any scenario. The function is called in line 7 from Algorithm 2 and recursively inside *Parent* and *Rewire*. In particular, the safety checks from these two functions are what cause the exponential increase in CPU time. Both evaluate multiple connections during each iteration, one per node in the set A_{near}. As the iterations increase, the total number of nodes in A grows, and so does the possible nodes in A_{near}. Adding, for the total number of iterations, the CPU time associated with *Safe* function times the number of calls of the function leads to an exponential trend. Further research will be required to reduce the execution time of the algorithm, being able to work in timescales compatible with near-real-time modification of trajectories.

5 Conclusions and Future Work

We presented an incremental sampling-based algorithm for flight planning, the SB-RRT* able to obtain safe trajectories in an environment formed by stochastic unsafe regions. Provided that the uncertainties are characterized with an ensemble of discrete realizations, the algorithm ensures that the trajectory between two state configurations and never violates a predefined safety margin. The ability of the tree to grow, constrained by a maximum number of interactions with the unsafe set, is demonstrated. A RRT-based algorithm was chosen due to its versatility, and it can be easily modified and updated. For the moment, the algorithm has been tested assuming constant flight level, however, the extension to variable altitude considering 3D Dubins paths is immediate, e.g. in [24]. Moreover, no operational constraints have been considered, but RRT algorithms are compatible with speed or spatial limitations (see kinodynamic RRT algorithms, e.g. [25]). The main disadvantage of a RRT* is that theoretically, an infinite number of iterations are required for optimality. Nonetheless, the RRT*-smart extension presented in [26] can be incorporated, leading to an increase in the rate of convergence and significantly reducing the number of iterations required to approach the optimal trajectory. In future, data from real weather forecasts must be integrated in the algorithm. The thunderstorms to be avoided will not be described by analytical expressions, requiring a strategy to obtain intersections between tree edges and more general curves.

References

1. Eurocontrol, in *Performance Review Report. An Assessment of Air Traffic Management in Europe During the Calendar Year 2017*. Technical Report (2017)
2. H. Erzberger, T. Nikoleris, R.A. Paielli, Y.C. Chu, Algorithms for control of arrival and departure traffic in terminal airspace. Proc. Inst. Mech. Eng. Part G: J. Aerospace Eng. **230**(9), 1762–1779 (2016)
3. D. González-Arribas, M. Soler, M. Sanjurjo-Rivo, M-Kamgarpour, J. Simarro, Robust aircraft trajectory planning under uncertain convective environments with optimal control and rapidly developing thunderstorms. Aerospace Sci. Technol. **89**, 445–459 (2019)
4. S. Summers, M. Kamgarpour, J. Lygeros, C. Tomlin, A stochastic reach-avoid problem with random obstacles, in *Proceedings of the 14th International Conference on Hybrid Systems: Computation and Control (HSCC'11)* (ACM, New York, NY, USA, 2011), pp. 251–260
5. D. Hentzen, M. Kamgarpour, M. Soler, D. González-Arribas, On maximizing safety in stochastic aircraft trajectory planning with uncertain thunderstorm development. Aersopace Sci. Technol. **79**, 543–553 (2018)
6. S.M. LaValle, *Rapidly-Exploring Random Trees: A New Tool for Path Planning* (Iowa State University, Tech. Rep., 1998)
7. S.M. LaValle, J.J. Kuffner, Randomized kinodynamic planning, in *Proceedings 1999 IEEE International Conference on Robotics and Automation*, vol 1 (1999), pp. 473–479
8. S.R. Martin, S.E. Wright, J.W. Sheppard, Offline and online evolutionary bi-directional RRT algorithms for efficient re-planning in dynamic environments, in *IEEE International Conference on Automation Science and Engineering* (2007), pp. 1131–1136
9. P. Cheng, Z. Shen, S.M. LaValle, RRT-based trajectory design for autonomous automobiles and spacecraft. Arch. Control Sci. **11**(4), 167–194 (2001)

10. Y. Kuwata, J. Teo, G. Fiore, S. Karaman, E. Frazzoli, J.P. How, Real-time motion planning with applications to autonomous urban driving. IEEE Trans. Control Syst. Technol. **17**(5), 1105–1118 (2009)
11. C.E. Tuncali, G. Fainekos, *Rapidly-Exploring Random Trees-Based Test Generation for Autonomous Vehicles*. Arizona State University, Technical Report (2019)
12. J. Kim, J.P. Ostrowski, Motion planning a aerial robot using rapidly-exploring random trees with dynamic constraints, in *IEEE International Conference on Robotics and Automation*, vol 2 (2003), pp. 2200–2205
13. K. Yang, S. Sukkarieh, 3D smooth path planning for a UAV in cluttered natural environments, in *IEEE/RSJ. International Conference on Intelligent Robots and Systems* (2008), pp. 794–800 (2008)
14. Y. Bouzid, Y. Bestaoui, H. Siguerdidjane, Quadrotor-UAV optimal coverage path planning in cluttered environment with a limited onboard energy, in *IEEE 2017 IEEE/RSJ International Conference on Intelligent Robots and Systems (IROS)* (2017)
15. B.D. Luders, M. Kothari, J.P. How, Chance constrained RRT for probabilistic robustness to environmental uncertainty, in *AIAA Guidance, Navigation and Control Conference* (2010)
16. B.D. Luders, J.P. How, Probabilistic feasibility for nonlinear systems with non-gaussian uncertainty using RRT, in *AIAA Infotech@Aerospace Conference*, St. Louis, MO (2011)
17. L. Blackmore, A probabilistic particle control approach to optimal, robust predictive control, in *AIAA Guidance, Navigation, and Control Conference and Exhibit* (2006)
18. *Guidelines on Ensemble Prediction Systems and Forecasting*. World Meteorological Organization (2012)
19. S.M. LaValle (ed.), *Planning Algorithms* (Cambridge University Press, New York, NY, USA, 2006)
20. S. Karaman, E. Frazzoli, Sampling-based algorithms for optimal motion planning. Int. J. Robot. Res. **30**, 846–894 (2011)
21. Y. Matsuno, R. Kikuchi, N. Matayoshi, Robust optimal guidance algorithm for required time of arrival operations using probabilistic weather forecasts, in *AIAA SciTech Forum* (2019)
22. V. Lefkopoulos, M. Kamgarpour, *Using Uncertainty Data in Chance-Constrained Trajectory Planning* (2019). [Online]. Available: http://arxiv.org/abs/1904.12825
23. A.M. Shkel, V. Lumelsky, Classification of the Dubins set. Robot. Autonom. Syst. **34**, 179–202 (2001)
24. P. Pharpatara, B. Hérissé, Y. Bestaoui, 3-D trajectory planning of aerial vehicles using RRT*. IEEE Trans. Control Syst. Technol. **25**, 1116–1123 (2017)
25. S. Karaman, E. Frazzoli, Optimal kinodynamic motion planning using incremental sampling-based methods, in *49th IEEE Conference on Decision and Control (CDC)* (2010)
26. F. Islam, J. Nasir, U. Malik, Y. Ayaz, O. Hasan, "RRT*-smart: Rapid convergence implementation of RRT* towards optimal solution," in. IEEE International Conference on Mechatronics and Automation **2012**, 1651–1656 (2012)

Impact of Wind on the Predictability and Uncertainty Management of 4D-Trajectories

Á. Rodriguez-Sanz and M. Terradellas Canadell

Abstract The future Air Traffic Management (ATM) system will depend on Trajectory Based Operations (TBO) to accommodate the growing demand in air traffic. This system will expect aircraft to follow an assigned 4D-trajectory with high precision, meeting arrival times over established checkpoints with great accuracy. These time-constraints are called Target Windows (TWs). Wind is one of the greatest sources of uncertainty and, consequently, a key point for the improvement of predictability and, ultimately, the implementation of 4D-trajectories. The main aim of this paper is to develop a methodology to characterize these TWs and to assess the uncertainty on the evolution of 4D-trajectories due to the effect of wind. For such purpose, 4D-trajectories are modelled deterministically, using a point mass model and the BADA (Base of Aircraft Data) methodology of EUROCONTROL. In parallel, wind is modelled with a hybrid approach, where the stochastic component captures the error associated with weather forecasts. Through Monte Carlo Simulation, the variability of the trajectory´s parameters is evaluated under different atmospheric scenarios. Using these results, TWs are defined along the different stages of flight, quantifying the uncertainty associated with the aircraft´s position under the effect of wind.

Keywords ATM · Predictability · Uncertainty · 4D-trajectories · Time constraint · Target windows · Monte carlo simulation

1 Introduction and Justification

The recent rise in demand for air traffic poses challenging operational conditions for the existing Air Traffic Management (ATM) system [1]. While air traffic continues to grow, achieving reliable trajectory predictions is a critical prerequisite for the accurate identification and resolution of potential conflicts [2]. To ensure sustainable

Á. Rodriguez-Sanz (✉) · M. T. Canadell
Universidad Politécnica de Madrid (UPM), Madrid, Spain
e-mail: alvaro.rodriguez.sanz@upm.es

M. T. Canadell
e-mail: m.terradellas@alumnos.upm.es

Air Traffic Management and Systems IV, Lecture Notes in Electrical Engineering 731,
https://doi.org/10.1007/978-981-33-4669-7_15

support of airspace usage, SESAR (Single European Sky Air Traffic Management Research), CARATS (Collaborative Actions for Renovation of Air Traffic Systems) and NextGen (Next Generation Air Transportation System) are changing the ATM framework [3–5]. Enhanced predictability and reliability is one of the 11 objectives for the Global ATM Operational Concept as established in ICAO (International Civil Aviation Organization) Doc 9854 [6]. The optimization of trajectory synchronization and conflict detection/resolution is also one of the requirements of SESAR, NextGen and CARATS.

In this context, the upcoming ATM system is based on the Trajectory Based Operations (TBO) concept. TBO requires separating aircraft by defining a strategic (long-term) trajectory, instead of the tactical (short-term) conflict resolution traditionally practiced [6]. Under the TBO framework, airspace users (AUs) will negotiate a trajectory with Air Navigation Service Providers (ANSPs) and airport operators (AOs) [7]. Aircraft systems will exchange information with ground systems, revising the evolution of the trajectory and the planned airspace capacity to ensure that flights meet the assigned Controlled Time of Arrival (CTA) [4, 7, 8]. While this approach allows operators to choose a practically unrestricted, optimal trajectory (with the associated benefits in efficiency, reliability, sustainability and cost-effectiveness of aircraft operations [3, 9]), it also requires that aircraft do not deviate significantly from their agreed reference trajectory and therefore are kept within very small volumes around this trajectory [10]. The goal behind this condition is to ensure that safety separation standards are met. Consequently, a fundamental requirement to TBO operations is to achieve a greater precision on the real-time position of aircraft. To this purpose, SESAR, NextGen and CARATS support the 4D-trajectory operational concept. 4D-trajectories integrate time into the 3D aircraft trajectory, meaning that each point on the flight track is defined by position (latitude, longitude and flight level) and time. In exchange for a more optimal 3D flight path, the aircraft would be obliged to fulfil with great precision an arrival time or position over a specified four-dimensional checkpoint. Such time constraints or spatial constraints are called target windows (TWs) and require the ability to produce accurate and reliable predictions of trajectories [11]. Nevertheless, uncertainties such as the actual aircraft performance or atmospheric/weather conditions affecting the flight, have a great influence in this process [12, 13]. If not corrected, these uncertainties and its associated disruptions can result in the deterioration of the intended trajectory, a degradation that increases over time [14], directly impacting on the reliability and safety of operations. Thus, uncertainty management becomes a keypoint in the future air traffic operations, as adjustments in the trajectory need to be coordinated to ensure reliability. Meteorological circumstances (wind, temperature), aircraft performance (phase of flight, weight, speed), navigational constraints (holdings) and initial conditions are the factors with the largest impact on the evolution of trajectories [15]. Nonetheless, the effect of wind shear on optimum performance [16] has been identified as one of the most important uncertainties in path deviation [17, 18]. For this reason, the quantification of the uncertainty brought by wind constitutes the main focus of this paper.

Several studies have addressed the prediction of trajectories in different phases of flight [19–22]. Most of the methods used in the trajectory prediction (TP) problem

can be categorized as either deterministic or probabilistic [23, 24]. The traditional approach is deterministic and deals with TP as a mathematical problem that explains aircraft motion. This approach is heavily and fundamentally constrained by the accuracy of the models that describe the actual behavior of the aircraft and by the quality and consistency of the inputs [25]. In addition, the assumptions and hypotheses of the model might introduce potential inaccuracies or errors in the prediction, i.e. sources of uncertainty that are not considered explicitly by such deterministic methods. Where external factors or parameters (like aircraft performance, environmental conditions, accuracy of navigation systems or traffic regulations) are uncertain or cannot be reliably measured, the probabilistic approach turns the deterministic problem into a stochastic one [12, 13].

The CATS (Contract-Based Air Transportation) project developed the idea of 4D Target Windows (TWs), which the aircraft needs to reach during the flight execution phase, as a way of managing uncertainty [10]. The multiple stakeholders involved in the operation of a flight agree on the target windows definition and location, usually in the areas of transfer of responsibility [26]. Han et al. [27] confirmed that, by incorporating TWs at intermediate locations along a 4D-trajectory rather than just at sector boundaries, these TWs can help in the management of en-route punctuality and uncertainty. Additionally, TWs provide a useful balance between predictability and maneuverability of air traffic [12]. In terms of the TWs geometry, while some studies consider TWs to be circular cross-sections labelled with the expected times of arrival [27], others model them as rectangles with time or space characteristics [2, 28]. When considering the safety requirements associated to the 4D-trajectory operational framework, it is more reasonable and more practical to predict space intervals than exact aircraft positions [22]. This study focuses on TWs with a time control: times of arrival at certain points are fixed, stating the space intervals where the aircraft should be found when reaching these times (scheduled milestones). The idea for reducing uncertainty about the future evolution of a flight is therefore associated to the imposition of spatial constraints at various sections of the trajectory, i.e. TWs that each aircraft will have to meet. Therefore, these constraints or TWs will help to increase punctuality and safety during the flight [28]. Instead of precise and concrete 4D points, a TW is defined as a spatial window or interval, where the times of checkpoints are given as a series of constant values. Hence, uncertainty management is discussed in terms of spatial variability, and the analysis is approached as a spatial reachability problem.

When associated to TBO and RBTs (Reference Business Trajectories), TWs should be large enough to allow AUs and ANSPs to react flexibly to a variety of flight conditions but small enough to improve certainty and increase capacity [2, 7]. An experiment with an Airbus A320 test aircraft flying from Toulouse to Stockholm was performed by EUROCONTROL in 2012 and defined an achievable tolerance window of between -2 min and +3 min over the route and ±30 s for CTA [29]. Moreover, pilots were subjected to conditions where the aircraft deviated from the expected course. Results showed that compliance with 4D-trajectories (adherence to planned paths) in the cruise phase was feasible, whereas the TW for CTA was

more difficult to accomplish and needed additional cooperation between pilots and controllers [29].

The main goal of this paper is to design a methodology for characterizing TWs and for managing the uncertainty associated with the evolution of 4D-trajectories due to wind impact. The study uses a simplified flight path, which includes all phases (take off, climb, cruise, descent, final approach and landing). In this study, it is proposed to manage time-related uncertainty by setting multiple intermediate locations (checkpoints) along a trajectory, where TWs can constrain space variability. 4D-trajectories are modelled using a point mass approach and the Base of Aircraft Data (BADA) methodology of EUROCONTROL [30, 31]. The BADA aircraft model relies on a mass-varying, kinetic and kinematic view to aircraft performance modelling. Despite knowing the physics of the wind and its condition as one of the most influential agents in the degradation of the trajectory of an aircraft, many studies do not include it in the equations of motion. However, they do include other atmospheric variables such as temperature, pressure or density. This is due to the difficulty of modeling this phenomenon of changing nature. For this reason, it was decided to focus on the predictability implications of this less explored phenomenon, which is modelled as a stochastic variable while the rest of agents are modelled deterministically. Several wind models were developed with increasing complexity, culminating in a hybrid model in which the deterministic component is wind forecast data and the stochastic component captures the error associated with those weather forecasts. Through Monte Carlo simulation, the variability of the trajectory parameters in different atmospheric scenarios is evaluated. Based on the results of the simulation, TWs are defined for several checkpoints (time-milestones) along the trajectory to estimate and quantify the uncertainty associated with the position of an aircraft under the effect of the wind. Consequently, this will enable us to provide the probability of an aircraft achieving the TW constraint as a function of a space interval. Results are analyzed to draw lessons regarding 4D-trajectories predictability and uncertainty management.

The key contribution of this study is the provision of a model to address uncertainty in TP and improve predictability of flights, whilst offering a methodology to evaluate the robustness and reliability of 4D-trajectories, by quantifying one of its main perturbations (the impact of wind). The proposed methods may be applied in a predictive manner, hence being able to foresee and anticipate the degradation of the expected trajectory, in order to plan appropriate corrective actions. These models improve traffic synchronization and potentially ease conflict resolution in 4D-trajectories, which are cornerstones in future airspace operational environments.

This section presented the problem and its characteristics and reviewed how previous studies have approached this issue. The remainder of the paper is organized as follows. First, we develop a 4D-trajectory model for the specific scenario of study (problem statement). This model is validated using actual flight data, obtained from EUROCONTROL. Subsequently, we propose a model for the wind, as the objective of the study is to understand its impact on 4D-trajectory prediction. The wind model is calibrated with data obtained from the NOAA (National Oceanic and Atmospheric Administration). We then use a stochastic approach to simulate

4D-trajectories that allows us to evaluate variability in the control parameters (input variables that affect the model outputs). This conceptual framework is the basis for identifying TWs (space intervals) along different checkpoints (time constraints). It represents a methodology to characterize uncertainty in 4D-trajectories due to wind. Finally, results are reviewed, and novel insights related to 4D-trajectories predictability and management are proposed. Please see Annex I for the meaning of the acronyms presented throughout the paper.

2 Methodology

2.1 Scenario Characterization

The first assumption of this study is that the aircraft is flying a 4D-trajectory under the new SESAR operational concept and its associated systems and functionalities [2, 32]. This implies that the aircraft follows an optimized path, avoiding the complexity of traditional trajectories, which must use predefined airways, holding patterns and structured operational procedures for take-off and landing. In this framework, the trajectory consists on the following phases: take off, climb, cruise, descent and final approach, and landing. The take-off phase (1) is initiated with the aircraft cleared for take-off by the control tower, and the landing phase (11) finalizes after the aircraft has fully decelerated at the end of the runway. This is justified by the fact that, during the taxi phase, wind has little influence over uncertainty compared to other variables such as traffic congestion. As the climb and descent phases have 3 distinct sections (before passing the transition altitude and when changing to clean or non-clean configuration), they have been modelled taking into account the different performance equations under each of these conditions. The climb flight phase (2) starts at 35 ft and finishes when the aircraft reaches FL360. The cruise flight phase includes 4 stabilized horizontal flight sections (3, 5, 7, 9), an en-route climb section (4) and a descent section (6) that represent a flight level change between FL360 and FL380, and a levelled heading change at FL360 (8). The descent flight phase (10) starts at FL360 and initiates the landing phase (11) at a height of 50ft.

Sections 3, 7 and 9 have a length of 50km. Section 5 length is 100km. The length of the other sections is determined by the aircraft performance. Figure 1 and Table 1 schematize the described trajectory. Please note that the term “phase” refers to the 5 flight phases (take off, ascent, cruise, descent and landing), while the term “section” is used to describe the different segments of the trajectory model.

The aircraft selected to model and simulate the flight was the Boeing 737-900ER, as it is one of the most frequent aircraft used in short- medium range flights in Europe [33] (similar routes to the one modelled in the study).

The atmospheric variables are modelled in accordance to the International Standard Atmosphere (ISA) model [34]. Pressure and density are calculated as a function of the temperature, which is estimated from the flight altitude.

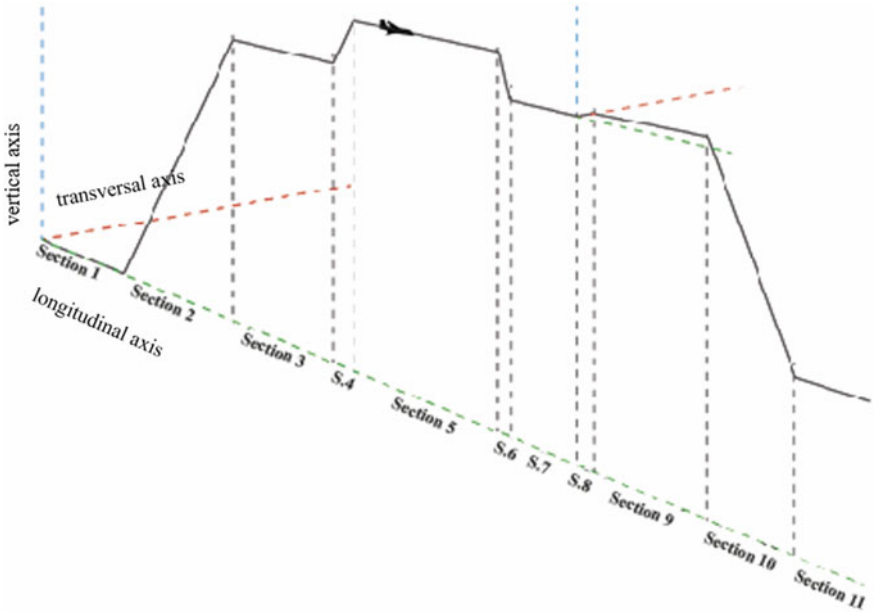

Fig. 1 Simulated flight profile

Table 1 Scenario of study

Flight phase	Section	Description
Take-off	1	Take-off run
Climb	2	35 ft → FL360
Cruise	3	Stabilized horizontal flight section
	4	En-route climb section (FL360 → FL380)
	5	Stabilized horizontal flight section
	6	En-route descent section (FL380 → FL360)
	7	Stabilized horizontal flight section
	8	Heading change
	9	Stabilized horizontal flight section
Descent and final approach	10	FL360 → 50 ft height (threshold)
Landing	11	Landing run

2.2 The 4D-Trajectory Model

The 4D-trajectory is modelled using EUROCONTROL's BADA 4.0 methodology [30], which is developed based on the aircraft´s kinetic and kinematic parameters.

BADA 4.0 employs the so-called Total Energy Model (TEM) to determine the performance of the aircraft. It applies the equations of classic flight mechanics with some coefficients which are specific to the aircraft type and to the flight envelope at each phase of the flight [2].

The BADA aircraft model is structured on a mass-varying, kinetic approach to aircraft performance modelling [35]. It can be considered as being a reduced point-mass model. TEM equates the rate of work done by forces acting on the aircraft to the rate of increase in potential and kinetic energy [30]. It is organized in three parts or blocks: (a) Aircraft Performance Model (APM), that provides complete information on the theoretical aircraft performance parameters for a number of different aircraft types; (b) Airline Procedure Model (ARPM), that provides nominal speeds for the climb, cruise and descent phases, assuming normal aircraft operations as provided in the aircraft manufacturers' documentation; and (c) Aircraft Characteristics Model (ACM), that provides a set of coefficients which represent characteristics that are intrinsic to the aircraft. These three elements, together with the Atmosphere model (AM), represent the Aircraft Dynamic Model (ADM), which determines the interdependencies between the modelling parameters. Therefore, each aircraft type in BADA 4.0 is characterized by a group of coefficients, called Aircraft Characteristics (included in ACM), which are used by the APM and ARPM [30]. These blocks allow us to estimate aerodynamic and propulsive variables from the input/control parameters (including mass) with the functional relationships shown in Table 2 (based on [2, 24, 30]).

The functional relationships and structural interdependencies between the parameters that shape the trajectory are directly obtained from the BADA manual [30]. A series of simplifications are performed to adapt the generic trajectory model to our scenario characteristics:

- The aircraft is considered as a point mass with three-degrees-of-freedom (3DoF) [12, 23, 36, 37]. Variation in mass is due to fuel consumption only. The flight is assumed to be symmetrical with all forces acting on the center of mass and included in the plane of symmetry, except during the heading change. The rotational equations are decoupled, the angular speeds are small, and the lifting surfaces do not affect the forces [24].
- We estimate that the aircraft's initial mass is 10% lower than the aircraft's MTOW (Maximum Take-Off Weight), following operational data and past studies [2].
- The maneuver in section (8) (levelled heading change) consists of two consecutive heading changes of 90° at a constant bank angle, μ, which is easily derived from the equations of motion of the aircraft:

$$\mu = \tan^{-1}\left(\frac{V_{\mathrm{TAS}}^2}{Rg}\right) \tag{1}$$

$$\boldsymbol{R} = \frac{\boldsymbol{V_{TAS}}}{\dot{\boldsymbol{\chi}}\,\frac{\pi}{180}} \tag{2}$$

Table 2 Modelling parameter

Block	Parameter	Dependencies	Description
Atmosphere Model (AM)	Pressure	$p = f[T(h), \rho(h)]$	T (temperature), ρ (density) and h (altitude)
	Speed of sound	$a_0 = f[k, R, T, M]$	M (flight Mach), R (universal gas constant) and k (adiabatic air coefficient)
	Wind	$w = f[\varphi, \lambda, h]$	φ (latitude) and λ (longitude)
Aerodynamic forces model (AFM)	Lift coefficient	$C_L = f[\delta, p_0, k, S, M, m, \varphi, g_0]$	δ (pressure ratio), p_0 (pressure at mean sea level), S (wing surface area), m (aircraft mass) and g_0 (acceleration of gravity at mean sea level)
	Lift	$L = f[\delta, p_0, k, S, M, C_L]$	–
	Drag coefficient	$C_D = f[C_L, \delta, d_1 \ldots d_{15}, M_{max}, p_0, k, S, M, m, \varphi, g_0]$	$d_1 \ldots d_{15}$ (characteristic parameters of aircraft)
	Drag	$D = f[\delta, p_0, k, S, M, C_D]$	–
Propulsive forces model (PFM)	Thrust coefficient	$C_T = f[t_{i1} \ldots t_{i12}, a_1 \ldots a_{36}, M, \delta, \delta_T]$	$t_{i1} \ldots \underline{t}_{i12}$ and $a_1 \ldots a_{36}$ (characteristic parameters of aircraft) and δ_T (throttle ratio)
	Thrust	$T_h = f[\delta, m_{ref}, \underline{W}_{mref}, C_T]$	m_{ref}, W_{mref} (aircraft reference mass and weight)
	Fuel consumption coefficient	$C_F = f[\delta, \theta, M, f_{i1} \ldots f_{i9}, C_T]$	$f_{i1} \ldots f_{i9}$ (characteristic parameters of aircraft) and θ (temperature ratio)
	Fuel consumption	$F = f[\delta, \theta, \underline{m}_{ref}, W_{mref}, a_0, L_{hv}, C_F]$	$f_{i1} \ldots f_{i9}$ (characteristic parameters of aircraft)

where V_{TAS} is the aircraft's true airspeed at the moment of calculation, R is the turn radius, $g = 9.81$ m/s^2 is the acceleration of gravity and $\dot{\chi} = 1.5$ °/s is the turn rate.

- The selected aircraft type (Boeing B737-900ER) uses a turbofan engine, with idle rating configuration for descent phase and non-idle rating for the rest of the flight. During climb phases, thrust is estimated with the *maximum available thrust in climb* (MCMB) while for the rest of the phases, *thrust for maximum cruise* is used (MCRZ).

- To determine the aerodynamic configuration of the aircraft at each stage of flight, as well as the speed regime in each of the phases, the Airline Procedure Model (ARPM) is used.
- The algorithm for trajectory prediction uses the ground speed of the aircraft (V_{gs}), which is the aircraft's horizontal speed relative to the ground. V_{gs} can be calculated, using vector addition, from wind speed (w), wind direction, heading angle ψ and the aircraft's true airspeed (V_{TAS}).

The model considers deviation control measures along the transversal axis. The automatic control will correct the lateral speed with the last measurement available of transversal wind. Similarly, during cruise phases, the vertical component of wind is compensated by the automatic pilot.

Considering these simplifications and operational adjustments, the 4D-trajectory model was generated using the MATLAB software [38], allowing us to compute theoretical 4D-trajectories. The model's accuracy, was checked by performing a validation test which compares the MATLAB simulated trajectory with real data flights extracted from the EUROCONTROL's database and scenario-based modelling tool DDR2–NEST (Demand Data Repository–Network Strategic Tool) [39, 40]. The convergence between the modelled trajectory and real flights is evaluated using different intra-European routes; particularly, the flights chosen for comparison were those that present similar characteristics to the studied scenario (flight level changes and rectilinear sections). The test error regarding time and position achieves an average value of 7%, reaching less than 5% during the stabilized flight level sections, which is in line with past studies [2, 24, 41]. As an example of the validation procedure, Fig. 2 presents a real trajectory that was flown by a Boeing B737-900ER between Madrid and Cologne; this trajectory is used to test and validate the model [39, 40]. The vertical profile of the trajectory and the section selected for validation are given in Fig. 3 [39, 40]. The vertical axis shows the altitude (FL) and the horizontal axis depicts the range (NM).

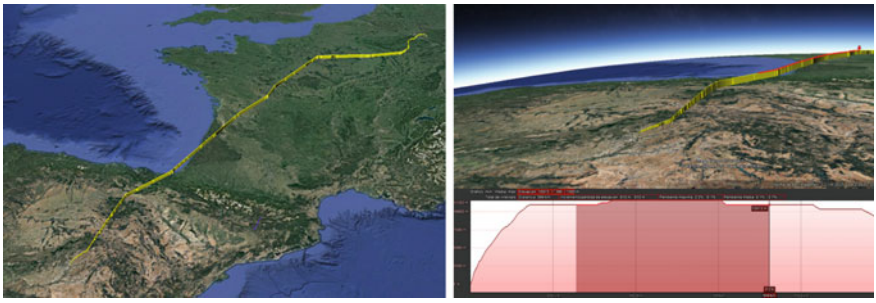

Fig. 2 Real flight between Madrid and Cologne by a Boeing B737-900ER used to validate the model

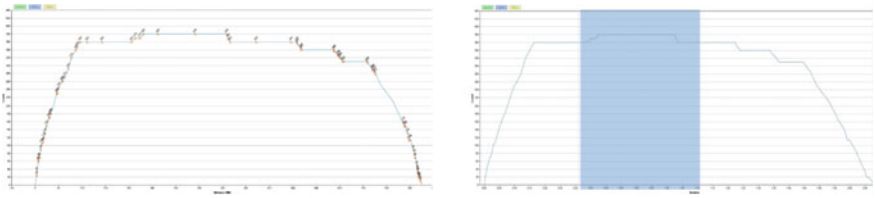

Fig. 3 Real trajectory (vertical profile) of a B737-900ER flight between Madrid and Cologne (left) and section of the trajectory used to validate the model (right)

2.3 The Wind Model

In this study, the wind has also been modelled in 4D. Space has been discretized in N layers of height, defining in each of these layers a grid in the horizontal plane composed of $C_x \times C_y$ cells. Time has also been discretized in order to capture the temporal variations of the wind in magnitude and direction. At any given time and position in space not corresponding to a grid note, the model linearly interpolates between the cells, layers and closest times to obtain the best wind approximation at the desired point. The result of this interpolation is a wind vector specific to the 4D-position of the aircraft in its trajectory.

To define the components of the wind vector, the model implements a hybrid approach, meaning that each vector component is the result of summing a deterministic and a stochastic wind value. The deterministic wind value is the weather forecast for the negotiated 4D-trajectory. Then, the intrinsic uncertainty associated with the wind is introduced by adding a stochastic variable that quantifies the expected error in the weather forecast.

The deterministic wind component is, as mentioned, the weather forecast for the negotiated 4D-trajectory. It is assumed that in the context of 4D-trajectory operation, weather forecast detailing the predicted en-route wind by region will be available during the trajectory planning phase, and it is reasonable to assume that this information will be used to choose the optimal flight path. Therefore, the model developed in this study uses real weather forecast data. In particular, wind data is obtained from the RAP (Rapid Refresh), the NOAA (National Oceanic and Atmospheric Administration) wind prediction tool for North America. This tool is selected because it stores wind data in a convenient format: it is updated every hour and generates a weather forecast stored in a 3D grid, with a resolution of 13 km and a vertical resolution of 50 mb. As the purpose of this study is exemplifying the potential methodology, the specific magnitude of the wind is not relevant and data for a random region and date is used.

In the wind model generated, the size of the grid and the cells adapts to that of the RAP, as well as the temporal variability, which adjusts to the frequency of updating of the aforementioned wind data tool. The code developed for this model loads the RAP results for 3 consecutive hours and stores the wind speeds corresponding to the heights of interest, between sea level and 14,000 m altitude, in a network formed

by grids at various heights. As the first layer of height available in RAP is at 12 m altitude, the hypothesis that this layer contains data at sea level has to be made. In addition, as the RAP does not consider vertical speeds, since it focuses on levelled flights, it has been decided to also take this approach and consider the vertical wind, ω_z, void [42].

The stochastic wind component is modelled as a random field, $\omega : \Re \times \Re^3 \rightarrow \Re^2$, where each value is calculated considering the correlation in space and in time of the forecast data [42]. If $\omega(t, P)$ is the wind at a point $P \in \Re^3$ at the time $t \in \Re$, we assume that $\omega(t, P) \in \Re^2$ is gaussian, with void mean and with covariance matrix defined by (3).

$$R\left(t, P, t', P'\right) \in \Re^{2x2} \tag{3}$$

The fact that the mean is zero reflects the hypothesis that all deterministic wind information is contained in the weather forecast. In addition, it is assumed that the wind field is isotropic (invariant to rotations) and that the north-south and east-west components of the wind are not correlated. Under these hypotheses, the covariance matrix R can be expressed by (4), with correlation given by (5).

$$R\left(t, P, t', P'\right) = E\left[\omega(t, P)\omega^T\left(t', P'\right)\right] = \begin{bmatrix} r\left(t, P, t', P'\right) & 0 \\ 0 & r\left(t, P, t', P'\right) \end{bmatrix} \tag{4}$$

$$r\left(t, P, t', P'\right) = \sigma(Z)\sigma\left(Z'\right) r_t\left(\left|t - t'\right|\right) r_{XY}\left(\left|\left|\begin{matrix} X - X' \\ Y - Y' \end{matrix}\right|\right) \cdot r_Z\left(\left|p(Z) - p\left(Z'\right)\right|\right) \tag{5}$$

$p(Z)$ is the atmospheric pressure at a height Z and $\sigma(Z)$ is the standard deviation of the wind in m/s at height Z. The functions $r_t(s)$, $r_{XY}(s)$ and $r_Z(s)$ can be obtained from the analysis developed by Cole et al. [43]. If $s \geq 0$, then:

$$r_t(s) = c_t + (1 - c_t - d_t)e^{-\frac{s}{G_t}} + d_t \cos\left(2\pi \frac{(s - e_t)}{g_t}\right) \tag{6}$$

$$r_{XY}(s) = c_{XY} + (1 - c_{XY})e^{-\frac{s}{G_{XY}}} \tag{7}$$

$$r_{Z(s)} = c_Z + (1 - c_Z)e^{-\frac{s}{G_Z}} \tag{8}$$

According to these equations, the correlation between points (t, P, t', P′) decreases exponentially with the horizontal distance and with the difference in height and time of the points. Cole et al. [43] defined the correlation parameters (c_t, d_t, G_t, g_t, e_t, c_{XY}, G_{XY}, b_{XY}, c_Z, G_Z) on Eqs. (6–8) as given by Tables 3, 4 and 5, where a distinction is made between the correlation on the longitudinal component of the wind (ω_x) and the transversal component of the wind (ω_y). The parameters of correlation in the horizontal plane are given in Table 3.

Table 3 Parameters of horizontal correlation

r_{XY}	ω_x	ω_y
c_{XY}	0.05	−0.06
G_{XY} [km]	311	363

Table 4 Parameters of vertical correlation

r_Z	ω_x	ω_y
c_Z	−0.016	−0.041
G_Z [mb]	153	273

Table 5 Parameters of temporal correlation

r_t	ω_x	ω_y
c_t	0.14	0.10
G_t [min]	141	254
g_t [min]	1275	935
e_t [min]	97	447
d_t	0.06	0.05

The parameters of correlation in the vertical plane are defined in Table 4.

The parameters of correlation for the time domain are defined in Table 5.

These parameters allowed us to adjust the RUC (Rapid Update Cycle) prediction tool properties to different functions: correlation data in horizontal and vertical planes is best fitted by an exponential curve (Eqs. 7 and 8 with parameters in Tables 3 and 4), while time correlation is best fitted by a sinusoidal function (Eq. 4 with parameters in Table 5).

Even though the parameters were calculated for RUC data (the predecessor to RAP), this resulted in an acceptable approximation given the nominal variations used in the simulation (of the order of seconds and less than 1km) versus the variations used in the correlation (of the order of thousands of seconds and hundreds of km). The value of the parameters suggests a strong correlation between the wind forecast error for points in the same horizontal plane, a very strong correlation in time and a weaker correlation between points at different heights. For variations in time of between 30 s and 1 h, it is acceptable to simplify the temporal correlation (6) as described by (9) [43].

$$r_t(s) = e^{-\frac{s}{G_t}} \tag{9}$$

With this approximation, the covariance matrix becomes constant over time, and then the wind matrices (W_x, W_y) can be expressed with a linear Gaussian model with the structure given by (10)–(11).

$$W_x(0) = \hat{Q} v_{X(0)} \quad W_X(k+1) = a \cdot W_x(k) + Q \cdot v_x(k) \tag{10}$$

$$W_y(0) = \hat{Q} v_{Y(0)} \; W_Y(k+1) = a \cdot W_Y(k) + Q \cdot v_Y(k) \tag{11}$$

In these equations, $v_x(k)$ and $v_y(k)$ are random, independent and standard Gaussian variables, meaning that they follow a normal distribution with zero mean and identity covariance matrix. These two random variables will be different in every simulation, making the variable stochastic. k is the current time step and a is a parameter given by (12). Q and $\hat{Q}$ are derived from Cholesky decomposition from the covariance matrix $\hat{R}$ [44].

$$a = e^{-\frac{d_t}{G_t}} \tag{12}$$

The stochastic component of the wind can now be calculated by implementing the previous equations in MATLAB. Figure 4 shows the evolution of the wind error between two samples.

Then, when this stochastic component is added to the meteorological forecast data (the deterministic component), the total wind that the model assumes is acting at each point is obtained. Figure 5 illustrates the calculated error of the wind in a given simulation -the stochastic component—(right) and the total corrected wind when this error is added to the forecast data -hybrid approach—(left).

The wind model here presented acts as an input for the remainder of the study. As the study deals with a prediction problem, weather forecasted data is used, since projected data is what would be available in the pre-tactical time horizon. The more accurate this weather forecast is, the more precise the model results will be. To validate the wind model, the forecasted wind values were compared with actual data and it was found that the maximum error is less than 10% in magnitude and direction. Therefore, the wind data used is accurate enough for the model to provide useful scenarios.

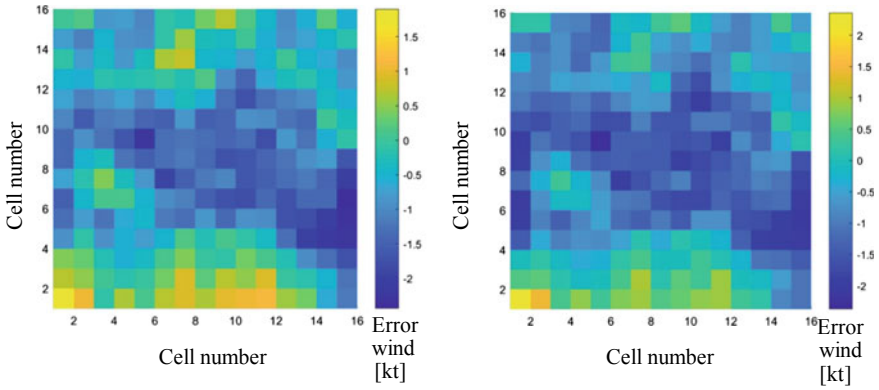

Fig. 4 Wind forecast error at the beginning (left) and at the end (right) of a one-hour period

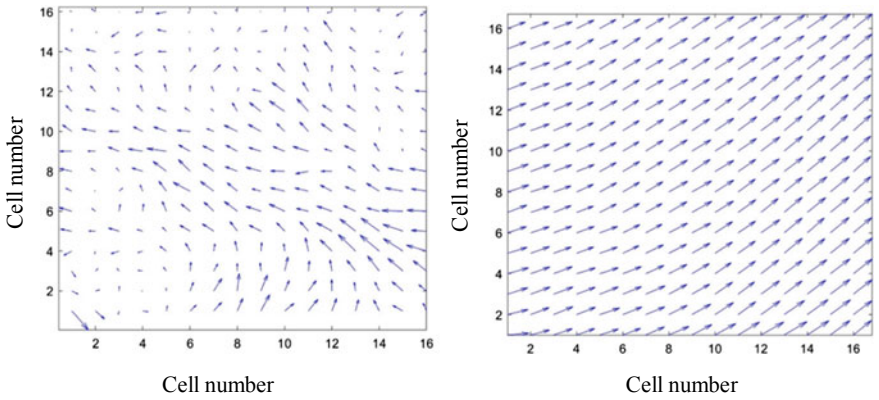

Fig. 5 Modeled error of the wind (left) and total corrected wind (right)

2.4 Monte Carlo Simulation

Monte Carlo simulation is a statistical technique to model the probability of a specific result, in non-deterministic processes where randomness intervenes [45]. This technique is based on the generation of a set of runs (simulations) which rely on the variability of probabilistic inputs. These inputs are randomly produced from a probability distribution that shapes the uncertainty associated with the defining parameters of the process (control variables) [2, 24]. For each set of inputs, the deterministic problem is solved, obtaining a bunch of outputs that are aggregated to obtain the stochastic solution [2]. This methodology can handle many random variables in a single model structure, several types of statistical distributions and non-linear dynamic models [2, 12]. Monte Carlo simulation completes a random sampling and eases the achievement of a large number of numerical experiments, which is essential in problems where extensive physical experimentation is not feasible [46]. The Monte Carlo technique has been widely used and proved effective in air traffic control for 4D-trajectories management [2, 24, 41], conflict resolution [47], safety verification [48], and to estimate the impact of wind uncertainty [49, 50].

In this specific study, we apply the Monte Carlo simulation technique to obtain a set of possible trajectories by varying the wind input in 1,000 consecutive simulations.

The first step of the Monte Carlo simulation consists on the determination of the statistical distribution of the input variable (the wind, in this case). In previous studies [13, 14, 25], a detailed analysis of the variables with the largest impact on 4D-trajectories (mass, temperature, pressure, wind and navigation systems precision) was carried out. Results indicated that wind is one of the parameters with the greatest influence. Therefore, in this study, to isolate the effect of the wind on the degradation of the negotiated trajectory, we consider a deterministic approach for all the other variables and modify the wind values. Therefore, aircraft positions are the parameters resulting in the use of different sets of weather forecast. As indicated previously, our

intention is to capture the wind disturbance on the motion of the aircraft with a stochastic dynamic model (aircraft positions are the output parameters resulting in the use of different sets of weather forecast). Specifically, the wind has been modeled as the sum of a nominal component that contains the weather forecast and a stochastic component that quantifies errors in the weather forecast. As described in Sect. 2.3 'The wind model', the stochastic part of the wind is modeled as the correlation between two 4D-points derived from the covariance matrix, multiplied by a random variable that follows a normal distribution of null mean and standard deviation 1; i.e. $N(0, 1)$. By means of this random variable, the wind input will take a different value in each simulation.

Figure 6 shows the wind acting along the entire trajectory for the 1000 simulations. Then, the mean of the wind acting on each simulation is calculated, and then this mean is approximated to a normal distribution, which expresses the mean wind parameters for the set of experiments. With this, it is obtained that the input variable of the model follows a normal distribution of mean $\mu = 9.34$ m/s and standard deviation $\sigma = 1.02$ m/s. This distribution is represented in Fig. 7.

The stochastic approach used to forecast the impact of wind on the trajectory introduces variability in the deterministic model. Figure 8 represents the set of trajectories resulting from the 1000 simulations. Because of the different wind scenario on each of the simulations, a dispersion is observed in the trajectory followed by the aircraft. In the following section, trajectory degradation is quantified through the estimation of TWs.

The variance of the variables estimated by the Monte Carlo technique converges to the inverse square root of the number of runs (N) [45]. Consequently, this method has an absolute error for the estimation that decreases like $1/\sqrt{N}$.

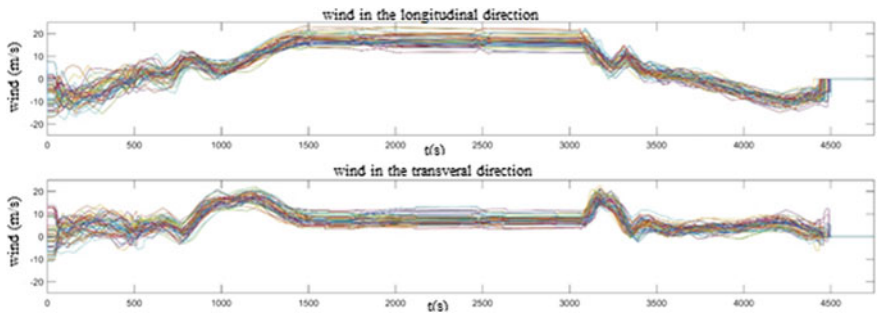

Fig. 6 Wind speed for the N simulations

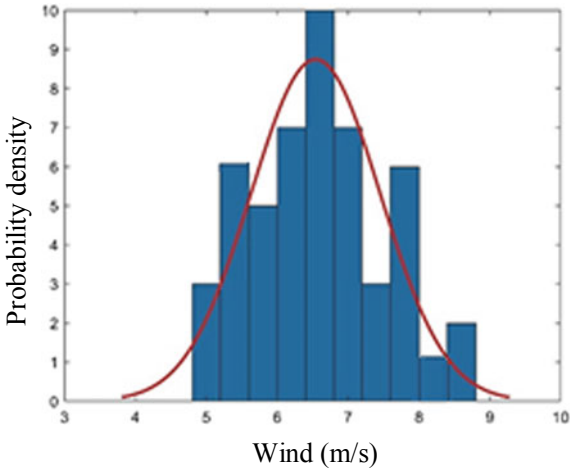

Fig. 7 Normal distribution of the mean wind speed for the *N* simulations

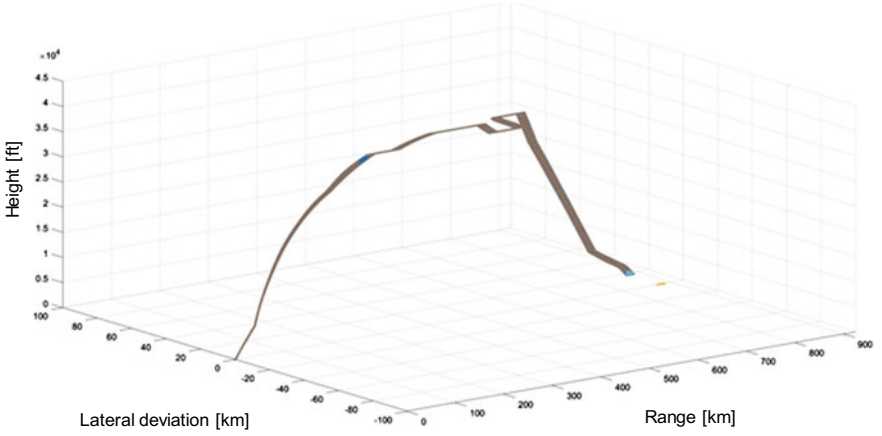

Fig. 8 Representation in 3D of the trajectories for *N* simulations

2.5 The Estimation of Target-Windows

The 4D-trajectory notion aims to ensure a practically unrestricted, optimum trajectory for a flight (if possible), in exchange for enforcing the aircraft to meet with great accuracy an arrival time over a designated control position (milestone) or checkpoint (CP). These time constraints are evaluated in this section by defining TWs or spatial limitations, where the aircraft is required to be found at specific flight times. The Monte Carlo methodology is applied, having as input variable the error in the weather forecast and as output variable the arrival position at each CP. Results reflect the stochastic and time-changing nature of the progress of the flight. Moreover, the variability in the output variable adds a more realistic approach to the deterministic

model by including actual uncertainties in trajectory prediction [2, 24]. The required TWs can be defined at all CPs of the agreed trajectory once the simulations are performed and the width of the spatial constraints is established; thereby, providing AUs, ANSPs and AOs with a framework for traffic synchronization and conflict detection and resolution. For the practical application of the TW concept, the size of these constraints on a RBT should at least represent the spatial interval within which any aircraft arriving at the checkpoint can avoid conflicts with other aircraft [27]. The first step to estimating the TW is setting the time (t) of the checkpoints (CP) which represent the CTAs. Each aircraft must hit them while holding a position versus the negotiated trajectory within the required precision [12]. Figure 9 shows the position of these CPs over the modelled trajectory.

Checkpoint 1 determines the deviation at the end of the take-off phase ($t = 41$ s). Similarly, Checkpoint 7 controls the deviation at the beginning of the landing phase ($t = 4441$ s). Checkpoints 2 and 6 aim to determine the deviation on the phases of climb ($t = 750$ s) and descent ($t = 3350$ s) respectively. Finally, checkpoints 3 ($t = 1640$ s), 4 ($t = 2240$ s) and 5 ($t = 2800$ s) will help us study the deviation from the negotiated trajectory during the course of the cruise phase.

After several simulations, these arrival intervals conform a histogram that can be fitted on a normal distribution for each checkpoint, given by the probability density function (13) which provides the probability of an aircraft achieving the

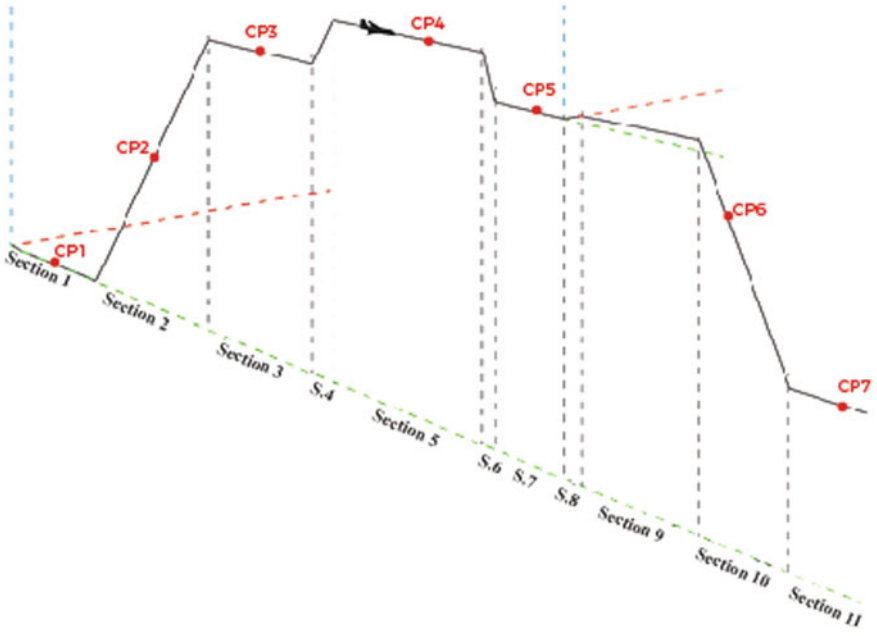

Fig. 9 Checkpoints over the vertical plane of a simulated trajectory

TW constraint as a function of a space interval centered at μ and the level of accuracy σ. Then, different TWs or intervals can be defined depending on the precision requirements established. The width of the TW is an indication of how predictable a flight is and how its progress can be managed. Setting longer space intervals increases predictability and reduces uncertainty, although this can lead to a less efficient time management. For this study, a sigma level of $\pm 2\sigma$ is used.

$$f_{\text{NORMAL}}(x, \mu, \sigma) = \frac{1}{\sqrt{2\pi} \cdot \sigma} \cdot e^{-\left(\frac{x-\mu}{2\sigma}\right)^2} \tag{13}$$

3 Results and Conclusions

The fitted probability curve for the longitudinal arrival position at checkpoints 2 and 6 is shown in Fig. 10.

The results for CP2 imply that there is a 95.44% ($\pm 2\sigma$) probability that an aircraft will be found at Checkpoint 2 (750s) within a TW of ±6km centered at 97km. Similarly, the arrival positions at Checkpoint 6 (3,350s) can be fitted to a normal distribution with mean $\mu = 729$ km and a standard deviation of $\sigma = 4.5$ km. There is a 95.44% ($\pm 2\sigma$) probability that an aircraft will reach CP6 within a TW of ±9 km. The values of σ and the Interquartile Range (IQR) are higher for CP6 than for CP2. This first result implies that, as the flight advances, the uncertainty and data dispersion are greater. The TWs calculated for the rest of these CPs can be found in Table 6.

The integration of time into the 3D trajectory becomes tangible by setting an instant of time and estimating the 3D position of the aircraft (Fig. 11 shows the aircraft's potential positions around the different control points, represented along the path followed in one of the simulations). However, it is necessary to note that, in each simulation, the aircraft will follow a unique trajectory, as shown in Fig. 8. In this context, the results of the work show that, for a time of 750 s, the aircraft will be found, with a 95.44% probability, within an ellipsoid defined by a longitudinal deviation of ±6000 m, a lateral deviation of ±4 m and a height range of ±276 m. Ultimately, the windows on the three axes define some ellipsoids around the aircraft. The volume of those ellipsoids may be used by ATM service providers to define security minimums, improve synchronization and anticipate the resolution of conflicts to the pre-tactical phase, increasing the predictability of the aircraft in its monitoring of the contracted trajectory.

In general, the trajectory will experience gradual nonlinear degradation over time. Results show a greater dispersion during the turn maneuver and the descent phase. On the other hand, the dispersion is very low at the end of the take-off stage, and at the beginning of the landing phase the dispersion is also reduced with respect to that presented in descent maneuver. Extending the estimation of TWs (space intervals) to several points of the trajectory shows that the relationship of the longitudinal position window with the flight time is monotonously increasing, implying that the aircraft

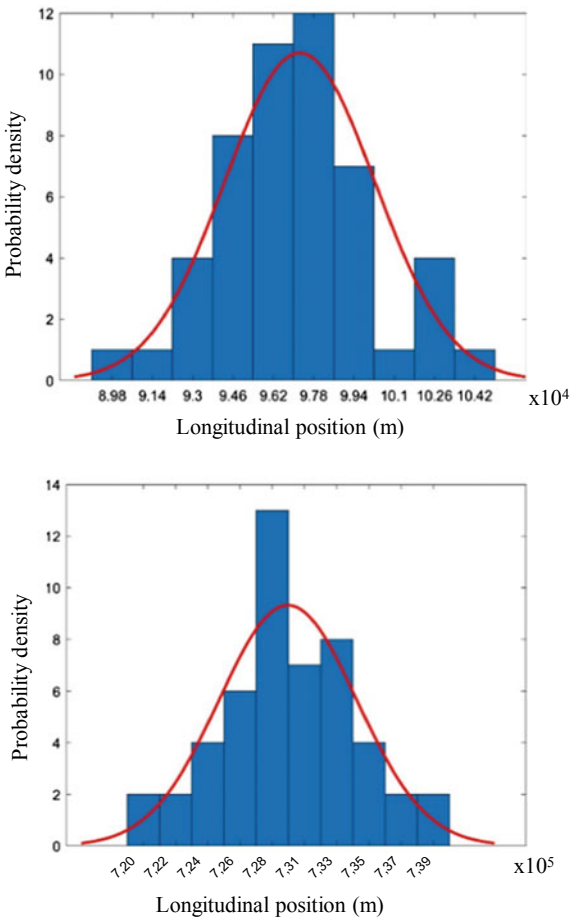

Fig. 10 Statistical distribution of the aircraft´s longitudinal position in m at CP2 (upper) and CP6 (lower)

suffers a gradual degradation of its ability to follow the contracted trajectory. This will have direct consequences on the operational procedures of the SESAR concept and a maximum amplitude of the position window will have to be specified in accordance with the requirements of the airspace. The dimension of the time window will then determine the maximum flight time before updating the flight data.

Other conclusions can be extracted by evaluating the sensitivity of the results to changes in the parameters that shape the case study (the modelled scenario). On the one hand, the lateral deviations are small in relation to the longitudinal deviation, since a simple control system that simulated the autopilot of the aircraft was applied in this dimension; this system compensated in each instant of time the wind measured in the immediately previous interval. However, even with this measure, the aircraft experiences lateral deviations of up to 50 m. Therefore, it is necessary to study the degradation of the trajectory, with the purpose of proposing the corrective measures that guarantee that the aircraft does not deviate excessively from the

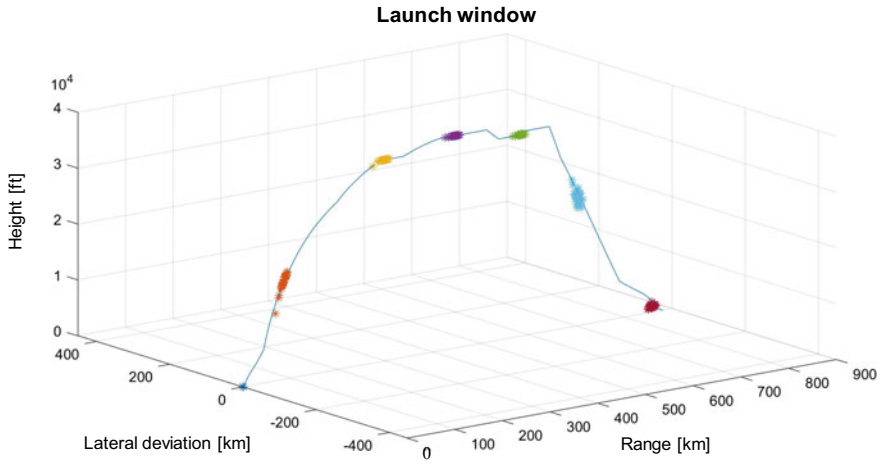

Fig. 11 3D Position of the aircraft in the time-constraint control points

planned trajectory. Finally, the deviations in altitude are smaller than those suffered in the longitudinal direction, although of similar relative magnitude when considering the distances travelled in the respective axes. From this observation, future works will conduct a sensitivity and causal relationships analysis, for example, through the application of Bayesian Networks [24], in order to quantify the dependence of the results obtained from the parameters defined in the model.

The presence of substantial uncertainties in the systems and models required for trajectory prediction represents a major challenge for the future TBO concept. Weather, and particularly wind, can be considered as one of the most relevant sources of trajectory degradation. Understanding and managing the impact of wind is hence necessary to increase the predictability of the ATM system. This study has presented preliminary results on trajectory prediction in which wind is assumed to be the unique source of uncertainty.

The main contribution of this paper regarding uncertainty management is the provision of a methodology to generate TWs (ellipsoids around the aircraft) at

Table 6 Results summary

	Window-x (km)	Window-y (km)	Window-z (km)
CP1	0.514	0.010	0.004
CP2	5.966	0.004	0.276
CP3	7.240	0.002	0.000
CP4	7.700	0.002	0.000
CP5	8.006	0.050	0.000
CP6	8.982	0.034	0.438
CP7	6.500	0.030	0.072

different checkpoints (time constraints) of the 4D-trajectory. These TWs are defined considering wind variations and allow us to determine, with a 95.44% probability, the position of the aircraft. Therefore, it increases the predictability of the aircraft flight and enhances the trajectory robustness when assessing its evolution.

Key findings of the paper are concrete values (Table 6) for space variability due to wind impact, which covers a gap in current literature and provides a rule of thumb for airspace users and network planners when evaluating 4D-trajectory potential deviations. The method also allowed us to appraise 4D-trajectories sensitivity to wind variations.

In the future TBO concept, the RBT is the trajectory which the AUs agree to fly and ANSPs and airports agree to facilitate (subject to separation provision) [3]. Therefore, an RBT is the representation of an AU's intention with respect to a given flight. This trajectory may be modified during the execution phase when constraints are to be changed due to separation of traffic or weather hazards, i.e. if the airspace's requirements regarding safety, regularity and efficiency are not achieved. The provision of TWs eases the definition of trajectory requirements when significant wind impacts are projected. The method can be practically applied in a predictive way to anticipate the trajectory degradation and determine potential corrective actions. This represents a move from reactionary (tactical) interventions to preventive (strategic) interventions.

Moreover, in a pre-tactical phase, this methodology could be used as an input for synchronization measures, and conflict detection and resolution algorithms. TWs offer pilots and air traffic controllers a better awareness of the positions that aircraft are projected to reach during the flight. It also provides intermediate objectives for a flight execution, while TWs were traditionally understood as boundary objects for coordinating timing between adjacent sectors in order to handle punctuality of aircraft as they transit between these sectors, we have extended this operational concept and presented a more flexible approach. We propose TWs distributed across the entire 4D-trajectory of an aircraft's flight, and not just at sector boundaries. However, this will demand additional procedures and tools to share the necessary information and enable smooth coordination between pilots and controllers, as a higher number of checkpoints and TWs will likely increase the amount of coordination required between them.

Our results suggest that the definition of TWs associated to 4D-trajectory management will offer a promising balance between predictability and maneuverability. It is concluded that uncertainty (in this case due to wind) can not only be quantified, but also managed and reduced by establishing TWs. The proposed methodology could prove useful for both airspace users and networks managers for the design of a more resilient and robust ATM system.

Acknowledgments This product/document has been created with or contains elements of Base of Aircraft Data (BADA) Family 4 Release 4.2 which has been made available by EUROCONTROL to UPM.

ANNEX I: List of Acronyms, Abbreviations and Parameters for Calculations and Equations

Acronym	Meaning
ACM	Aircraft characteristics model
ADM	Aircraft dynamic model
AFM	Aerodynamic forces model
AM	Atmosphere model
ANSPs	Air navigation service providers
AOs	Airport operators
APM	Aircraft performance model
ARPM	Airline procedure model
ATM	Air traffic management
AUs	Airspeed users
BADA	Base of aircraft data
C	Cells in the wind model
CARATS	Collaborative actions for renovation of air traffic systems
CATS	Contract-based air transportation
CP	Checkpoint
CTA	Controlled time of arrival
EUROCONTROL	European organisation for the safety of air navigation
FL	Flight level
g	Acceleration of gravity
ICAO	International Civil Aviation Organization
MCMB	Maximum thrust in climb available
MCRZ	Thrust for maximum cruise
MTOW	Maximum take-off weight
NextGen	Next generation air transportation system
NOAA	National Oceanic and Atmospheric Administration
P	Position
PFM	Propulsive forces model
R	Turn radius
RAP	Rapid refresh
RBTs	Reference business trajectories
RUC	Rapid update cycle
SESAR	Single European Sky Air Traffic Management Research
t	Time
TBO	Trajectory based operations

(continued)

(continued)

Acronym	Meaning
TEM	Total energy model
TP	Trajectory prediction
TWs	Target windows
V_{gs}	Aircraft's ground speed
w	Wind speed
V_{TAS}	Aircraft's true airspeed
$\dot{\chi}$	Turn rate
ψ	Heading angle
μ	Bank angle

References

1. SESAR, *European ATM Master Plan*, 2015th ed. (Publications Office of the European Union, Luxembourg, 2015)
2. Á. Rodríguez-Sanz, C. Claramunt Puchol, J.A. Pérez-Castán, F. Gómez Comendador, R.M. Arnaldo Valdés, Practical implementation of 4D-trajectories in air traffic management: system requirements and time windows monitoring. Aircr. Eng. Aerosp. Technol. (2020) https://doi.org/10.1108/AEAT-12-2019-0236
3. SESAR, *SESAR Concept of Operations Step 2*, 2014th ed (SESAR Joint Undertaking, Brussels, 2014) (Ed. 01.01.00)
4. NextGen, *Concept of Operations for the Next Generation Air Transportation System. Version 3.2*, (NextGen, Washington D.C., 2011)
5. CARATS, *Long Term Vision for the Future Air Traffic Systems Changes to Intelligent Air Traffic Systems—Changes to Intelligent Air Traffic Systems* (Ministry of Land, Infrastructure, Transport and Tourism Study Group for the Future Air Traffic Systems, Japan, 2010)
6. ICAO, *Doc 9854: Global Air Traffic Management Operational Concept* (International Aviation Civil Organization, Montreal, 2005)
7. A. Gardi, S. Ramasamy, R. Sabatini, K. de Ridder, 4-Dimensional Trajectory negotiation and validation system for the next generation air traffic management, in *AIAA Guidance, Navigation, and Control (GNC) Conference* (2016), p. 14. https://doi.org/10.2514/6.2013-4893
8. SESAR, *SESAR Concept of Operations Step 1*, 2012th ed. (SESAR Joint Undertaking, Brussels, 2012) (Ed. 01.00.00)
9. FAA, *The Future of the NAS* (U.S. Department of Transportation, Federal Aviation Administration, Office of NextGen, Washington, D.C., 2016)
10. CATS, *Contract-Based Air Transportation (CATS) Concept of Operation D1.2.2* (European Organisation for the Safety of Air Navigation, Brussels, 2010)
11. T. Rentas, S. Green, K. Cate, Characterization method for determination of trajectory prediction requirements, in *9th AIAA Aviation Technology, Integration, and Operations Conference (ATIO), Aviation Technology, Integration, and Operations (ATIO) Conferences* (2009). https://doi.org/10.2514/6.2009-6989
12. K. Margellos, J. Lygeros, Toward 4-D Trajectory management in air traffic control: a study based on Monte Carlo simulation and reachability analysis. IEEE Trans. Control Syst. Technol. **21**(5), 1820–1833 (2013). https://doi.org/10.1109/TCST.2012.2220773

13. E. Casado, C. Goodchild, M. Vilaplana, Identification and initial characterization of sources of uncertainty affecting the performance of future trajectory management automation systems, in *Proceedings of the 2nd International Conference on Application and Theory of Automation in Command and Control Systems (ATACCS'2012)* (2012), pp. 170–175
14. Á. Rodríguez-Sanz, D.Á. Álvarez, F.G. Comendador, R.A. Valdés, J. Pérez-Castán, M.N. Godoy, Air Traffic Management based on 4D trajectories: a reliability analysis using multi-state systems theory. Transp. Res. Procedia (2018). https://doi.org/10.1016/j.trpro.2018.11.001
15. P. Weitz, Determination and visualization of uncertainties in 4D-trajectory prediction, in *Integrated Communications, Navigation and Surveillance Conference (ICNS)* (2013). https://doi.org/10.1109/ICNSurv.2013.6548525
16. A. Valenzuela, D. Rivas, Analysis of wind-shear effects on optimal aircraft cruise, in *6th International Conference on Research in Air Transportation (ICRAT)* (2014)
17. D. De Smedt, J. Bronsvoort, G. McDonald, Model for longitudinal uncertainty during controlled time of arrival operations, in *10th USA/Europe Air Traffic Management Research and Development Seminar* (2015)
18. D. Gonzalez-Arribas, M. Soler, and M. Sanjurjo, Wind-based robust trajectory optimization using meteorological ensemble probabilistic forecasts, in *Proceedings of the 6th SESAR Innovation Days (SIDs)* (2016)
19. M. Hrastovec, F. Solina, Prediction of aircraft performances based on data collected by air traffic control centers. Transp. Res. Part C Emerg. Technol. **73**, 167–182 (2016). https://doi.org/10.1016/j.trc.2016.10.018
20. R. Alligier, D. Gianazza, N. Durand, Learning the aircraft mass and thrust to improve the ground-based trajectory prediction of climbing flights. Transp. Res. Part C Emerg. Technol. **36**, 45–60 (2013). https://doi.org/10.1016/j.trc.2013.08.006
21. A.W. Warren, Y.S. Ebrahimi, Vertical path trajectory prediction for next generation ATM, in *17th DASC. AIAA/IEEE/SAE. Digital Avionics Systems Conference*, vol 2 (1998). https://doi.org/10.1109/DASC.1998.739809
22. M. Ghasemi Hamed, D. Gianazza, M. Serrurier, N. Durand, Statistical prediction of aircraft trajectory: regression methods vs point-mass model, in *Proceedings of the 10th USA/Europe Air Traffic Management Research and Development Seminar* (2013)
23. Y. Matsuno, T. Tsuchiya, Stochastic 4D trajectory optimization for aircraft conflict resolution, in *IEEE Aerospace Conference Proceedings* (2014). https://doi.org/10.1109/AERO.2014.6836275
24. Á. Rodríguez-Sanz et al., 4D-trajectory time windows: definition and uncertainty management. Aircr. Eng. Aerosp. Technol. **91**(5), 761–782 (2019). https://doi.org/10.1108/AEAT-01-2018-0031
25. E. Casado, L. P. D'Alto, M. Vilaplana, Analysis of the impact of intent uncertainty on the accuracy of predicted trajectories for arrival management automation, in *6th International Conference on Research in Air Transportation (ICRAT)* (2014)
26. I. Berechet, F. Debouck, L. Castelli, A. Ranieri, C. Rihacek, A target windows model for managing 4-D trajectory-based operations, in *Proceedings of the 28th AIAA/IEEE Digital Avionics Systems Conference (DASC'09)* (2009). https://doi.org/10.1109/DASC.2009.5347513
27. F. Han, B.L.W. Wong, S. Gauhrodger, Improving future air traffic punctuality: 'pinch-and-pull' target windows. Aircr. Eng. Aerosp. Technol. **82**(4), 207–216 (2010). https://doi.org/10.1108/00022661011082687
28. K. Margellos, J. Lygeros, Air traffic management with target windows: an approach using reachability, in *Proceedings of Joint 48th IEEE Conference on Decision and Control and 28th Chinese Control Conference* (2009), pp. 145–150. https://doi.org/10.1109/CDC.2009.5400119
29. L.H. Mutuel, P. Neri, E. Paricaud, Initial 4D trajectory management concept evaluation, in *Tenth USA/Europe Air Traffic Management Research and Development Seminar* (2013)
30. EUROCONTROL, *User manual for the base of aircraft data (BADA) family 4. EEC Technical Scientific Report No. 12/11/22–58* (European Organisation for the Safety of Air Navigation, Brussels, 2014)

31. EUROCONTROL, *BADA technical documentation and datasets* (European Organisation for the Safety of Air Navigation, Brussels, 2017)
32. A. Gardi, R. Sabatini, T. Kistan, Y. Lim, S. Ramasamy, 4 Dimensional trajectory functionalities for air traffic management systems, in *ICNS 2015—Innovation in Operations, Implementation Benefits and Integration of the CNS Infrastructure, Conference Proceedings* (2015), pp. N31–N311. https://doi.org/10.1109/ICNSURV.2015.7121246
33. OAG, *OAG (Air Travel Intelligence) analyser* (2017)
34. ISO, *Standard Atmosphere, ISO 2533:1975*, Geneva, Switzerland (1975)
35. D. Poles, A. Nuic, V. Mouillet, Advanced aircraft performance modeling for atm: analysis of BADA model capabilities, in *AIAA/IEEE Digital Avionics Systems Conference—Proceedings* (2010). https://doi.org/10.1109/DASC.2010.5655518
36. W. Glover, J. Lygeros, A stochastic hybrid model for air traffic control simulation, in *Hybrid Systems: Computation and Control. HSCC 2004. Lecture Notes in Computer Science*, vol 2993, no. 2993, R. Alur, G.J. Pappas (Springer, Heidelberg, 2004), pp. 372–386
37. I. Lymperopoulos, J. Lygeros, Sequential Monte Carlo methods for multi-aircraft trajectory prediction in air traffic management. Int. J. Adapt. Control Signal Process. **24**(10), 830–849 (2010). https://doi.org/10.1002/acs.1174
38. MathWorks, *MATLAB - Mathworks—MATLAB & Simulink* (2019)
39. EUROCONTROL, *NEST Modelling Tool—Airspace Design & Capacity Planning* (2019)
40. EUROCONTROL, *EUROCONTROL Demand Data Repository DDR2* (2019)
41. Á. Rodríguez–Sanz et al., Air traffic management based on 4D-trajectories: requirements and practical implementation, in *MATEC Web of Conferences. 9th EASN International Conference on "Innovation in Aviation & Space*, vol 304 (2019). https://doi.org/10.1051/matecconf/201930405001
42. NOAA/ESRL, Rapid refresh pre-implementation performance assessment. Study Memorandum (2010)
43. R. E. Cole, C. Richard, S. Kim, D. Bailey, *An Assessment of the 60 km Rapid Update Cycle (RUC) with Near Real-Time Aircraft Reports* (1998)
44. S.S. Cherny, Cholesky secomposition, in *Wiley StatsRef: Statistics Reference Online* (2014)
45. N.T. Thomopoulos, *Essentials of Monte Carlo Simulation* (Springer, New York, 2013).
46. R.Y. Rubinstein, D.P. Kroese, *Simulation and the Monte Carlo Method* (Wiley, New York, 2016).
47. A.L. Visintini, W. Glover, J. Lygeros, J. Maciejowski, Monte Carlo optimization for conflict resolution in air traffic control. IEEE Trans. Intell. Transp. Syst. **7**(4), 470–482 (2006). https://doi.org/10.1109/TITS.2006.883108
48. H.A.P. Blom, J. Krystul, G.J. Bakker, A particle system for safety verification of free flight in air traffic, in *Proceedings of the 45th IEEE Conference on Decision and Control* (2006), pp. 1574–1579. https://doi.org/10.1109/CDC.2006.377796
49. R.A. Paielli, H. Erzberger, Conflict probability estimation for free flight. J. Guid. Control. Dyn. **20**(3), 588–596 (1997). https://doi.org/10.2514/2.4081
50. G. Chaloulos, J. Lygeros, Effect of wind correlation on aircraft conflict probability. J. Guid. Control. Dyn. **30**(6), 1742–1752 (2007). https://doi.org/10.2514/1.28858

Towards Automatic Trajectory Modification for Reducing Air Traffic Complexity Using an ATC Difficulty Index

S. Nagaoka, H. Hirabayashi, and M. Brown

Abstract Monitoring performance is an essential part of an air traffic management system and requires appropriate metrics such as complexity and safety corresponding to the monitoring objectives. We have proposed as a new metric an air traffic control (ATC) difficulty index that quantifies the 'difficulty' of an air traffic situation from an air traffic controller workload perspective. Once a traffic situation with a potentially high difficulty is predicted, it is desirable that an advisory should be provided to controllers to enable the trajectory modification of key aircraft to mitigate the difficulty. To investigate the feasibility of developing a controller decision support tool that can provide candidate trajectory modifications to mitigate high difficulty traffic situations, we have started a conceptual study based on simulations. This paper reports preliminary results of the study. We first describe the background of the study and briefly explain the proposed difficulty index. Then, we indicate the concept and algorithm for automatic trajectory modification and describe our approach for moving forward and challenges.

Keywords Air traffic management · Air traffic control difficulty index · Complexity · Trajectory

1 Introduction

Recent increases in air traffic demand have accelerated the modernization of air traffic management (ATM) systems worldwide. Aviation's shift towards 'performance-based' approaches, and 'trajectory-based operations' (TBO) [1] require appropriate

S. Nagaoka (✉) · H. Hirabayashi · M. Brown
ATM Department, Electronic Navigation Research Institute (ENRI), National Institute of Maritime, Port and Aviation Technology (MPAT), Tokyo, Japan
e-mail: nagaoka@mpat.go.jp

H. Hirabayashi
e-mail: h-hirabayashi@mpat.go.jp

M. Brown
e-mail: mark.brown@mpat.go.jp

Air Traffic Management and Systems IV, Lecture Notes in Electrical Engineering 731,
https://doi.org/10.1007/978-981-33-4669-7_16

indices for monitoring performance, such as safety and airspace/air traffic complexity. As air traffic control (ATC) shifts away from sector-based control with the introduction of TBO and 'free route' concepts, and with further automation and tool support, the tasks of air traffic controllers will change, and definitions of workload based on sector counts will no longer be appropriate for the future ATM environment. We therefore began investigating metrics such as the 'complexity' of an air traffic situation or the cognitive 'ATC difficulty' associated with air traffic controller workload and safety. Our aim is to predict 'hot spots' of airspace or air traffic based on trajectory information which will give a significant level of workload to air traffic controllers, and ultimately to allow alleviation of such hot spots before they arise through strategic trajectory modification.

Various metrics have been proposed for traffic complexity and difficulty. [2–6] Their methodologies vary from using only traffic data such as flight plan and trajectory data from radar or other surveillance sources, to those requiring judgements by air traffic controllers. Of the former approaches, most of these only evaluate the traffic situation at the present moment in time, and we have seen none that evaluate the spatial and temporal situations simultaneously. We have therefore proposed as a new metric an ATC difficulty index (which we call DI) that quantifies the difficulty of an air traffic situation [7–14] as it evolves into the future, taking into account projected proximity situations and the time to such events based on current and planned trajectory information. The metric is based on an aircraft pair-wise metric that can be transformed to an airspace-wise metric when evaluating the difficulty in volume of airspace.

The next step is to apply the metric. As ATM moves towards TBO in a collaborative framework, new tools will be required that will enable controllers to detect problems in the future traffic situation further ahead than mental projections allow, and in the case of a potential conflict or high difficulty traffic situation, to propose modifications to trajectories that will be shared electronically and possibly negotiated with pilots. We propose the application of the DI metric to create such a tool.

In this paper, we present the concept of a new controller assistance tool applicable to a future TBO environment and report preliminary results of a simulation-based study to investigate the feasibility of developing such a tool and the applicability of the DI metric. We first describe the background of the study and briefly explain the proposed difficulty index. Then, we indicate the concept and algorithm for automatic trajectory modification and describe our approach for moving forward and challenges.

2 Difficulty Index

2.1 Motivation for Constructing a Difficulty Index

The purpose of an air traffic control service is ensure the safe, orderly and expeditious flow of air traffic [15]. To prevent collisions, separation minima are designated for ATC operations in various types of airspace. Air traffic controllers (ATCo) monitor the traffic situation and intervene, where necessary to prevent proximity situations from arising. A significant part of their workload is detecting and preventing 'conflict' events, where two or more aircraft experience or are predicted to experience a loss of separation minima.

As trajectory-based and free route concepts are introduced, aircraft will fly less on airways and more direct point-to-point routes, increasing efficiency by reducing flight distance. This will result in less structured, more complex air traffic flows that could increase ATCo workload. In turn, this could reduce the volume of flights ATCos can handle—in other words, increased traffic complexity could reduce ATM capacity unless workload can be alleviated. A metric of ATCo workload in the future ATM environment, which could also be a surrogate for air traffic complexity, is therefore desirable.

When considering ATCo workload in dealing with conflicts for constructing a difficulty index of ATC, we came to recognize the importance of the remaining time to the closest point of approach (CPA) as well as the distance at CPA; in other words, the temporal as well as spatial aspects of potential proximity situations should be taken into account. We suppose that the subjective difficulty of a traffic situation increases as the time available to identify and resolve a conflict reduces. We have investigated the possibility of using temporal and spatial parameters to define a new index for evaluating ATC difficulty associated with proximity situations [7–14]. We have proposed a method for calculating the ATC difficulty for a pair of aircraft using trajectory information [8, 9] and expanded it from a pairwise index to multiple aircraft (airspace wise) index [9]. Then, the calculation methods for predicting future trajectory based on flight plan information were developed [13].

2.2 Pairwise Difficulty Index

ATCo decision-making is based not only on the current but also the predicted future traffic situation. A predicted proximity and perceived need for intervention may increase ATCo workload depending on the severity of the proximity event and the time remaining necessary for resolving it. We adopt such proximity situations as the basis of an ATC difficulty index (DI).

Let us consider a pair of aircraft A and B flying linearly at constant speeds at the observation time t_0 as shown in Fig. 1. The movement of trajectory can be described by relative vectors, $\overrightarrow{R_r}(t_0)$ and $\overrightarrow{V_r}(t_0)$. A future relative position vector at time t can

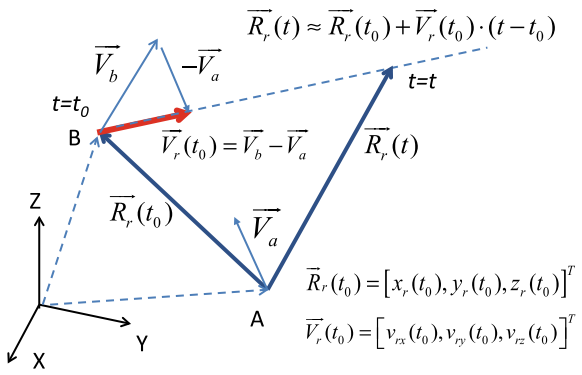

Fig. 1 Geometric configuration of relative motion

be estimated by linear extrapolation. The time duration from the observation time ($= t - t_0$) is called the look-ahead time, and T denotes transpose. We try to map the difficulty of proximity situations onto a real value between 0 and 1.

We define that the pairwise difficulty index value at time t_0 can be defined by

$$G(t_0) \equiv \max_{t \geq t_0} \exp[-C(t)] \tag{1}$$

where

$$C(t) = \left[x_r(t)^2 + y_r(t)^2 + k_z^2 z_r(t)^2 + k_t^2 (t - t_0)^2\right] / \lambda_H^2 \tag{2}$$

where λ_H, λ_z,λ_t are scale parameters for the horizontal, vertical and temporal dimensions.$x_r(t)$,$y_r(t)$,$z_r(t)$ are the relative positions between the pair at time t in the Cartesian X, Y and Z axes, respectively,

$$k_z \equiv \lambda_H / \lambda_z \tag{3}$$

and

$$k_t \equiv \lambda_H / \lambda_t \tag{4}$$

Our index Eq. (1) therefore looks at the maximum value of the function $\exp[-C(t)]$ which is a function of the current time t_0 and projected time t. Equation (2) is an objective function and a normalized four-dimensional (4D) distance measure. This equation assumes that the effect of spatial distance between a pair of aircraft at a given projected time on ATC difficulty can be dealt with equivalently as the length of the projected time from the observation (current) time. Equation (2) consists of the relative horizontal and vertical distances between the aircraft pair and the temporal 'distance' (the look-ahead time to the projected traffic situation). Table 1 summarizes the formula for calculating the difficulty value in terms of 4D

Table 1 Formula for pairwise difficulty value ($\vec{U}^2$ and $(\vec{U}\cdot\vec{V})$ stand for $\vec{U}^T\vec{U}$ and $\vec{U}^T\vec{V}$ respectively)

Pairwise difficulty value	$G(t_0) = \underset{t\geq t_0}{\text{Max}} \exp[-C(t)]$
$C(t) = \frac{(x_r(t)^2+y_r(t)^2)}{\lambda_H^2} + \frac{z_r(t)^2}{\lambda_z^2} + \frac{(t-t_0)^2}{\lambda_t^2} \equiv \vec{U}(t)^T\vec{U}(t)/\lambda_H^2$	
where $\vec{U}(t) \equiv \vec{U}_0 + \vec{V}_0(t-t_0)$	
$\vec{U}_0 \equiv [x_r(t_0), y_r(t_0), k_z z_r(t_0), 0]^T$	
$\vec{V}_0 \equiv [v_{rx}(t_0), v_{ry}(t_0), k_z v_{rz}(t_0), k_t]^T$	
$k_z \equiv \lambda_H/\lambda_z, k_t \equiv \lambda_H/\lambda_t$	
$G(t_0) = \begin{cases} \exp\left(-\vec{U}_0^T\vec{U}_0/\lambda_H^2\right) \text{ for } \vec{U}_0^T\vec{V}_0 > 0 \\ \exp\left\{-\left[\vec{U}_0^T\vec{U}_0 - \vec{U}_0^T\vec{V}_0{}^2/\vec{V}_0^T\vec{V}_0\right]/\lambda_H^2\right\} \text{ oterwise} \end{cases}$	

vector operations. The derivation of the explicit representation of $G(t_0)$ has been given in our previous paper [14].

2.3 Expansion to Routes with TCP

An aircraft's planned route can be modelled as a series of linear segments divided by waypoints at which the azimuth of the route segment changes. Smooth changes in flight path between the linear segments are ignored as transition time between segments is small compared to the segment time, and it is assumed that the speed is constant. The cruise portion of a flight usually has at least one such point (called a trajectory change point: TCP) at which the aircraft changes its heading or performs an altitude change manoeuvre (a transition between level flight and a constant rate climb or descent). In such a case, a simple linear extrapolation of the trajectory of the pair leads to improper estimate of the difficulty value if a TCP is encountered within the look-ahead time. Therefore, predicting the future trajectory using flight plan information is required. To address this issue, a method for calculating the difficulty index using information on TCPs has been considered [13].

2.4 Modification of Difficulty Functions

To calculate DI values, a maximum look-ahead time $\tau_{\max}$ is introduced. In Eq. (1), the domain of t, $[t_0, \infty)$ is not actually used for calculating the difficulty value. As reference [11] shows that Eq. (1) becomes less than 10^{-5} for the maximum look-ahead time $\tau_{\max} \approx 3.4\lambda_t$, and it can be negligible for larger $\tau_{\max}$ values. Scale parameters were determined taking into account ATCo cognitive thresholds (times before CPA at which a conflict is recognized, and at which a resolution intervention

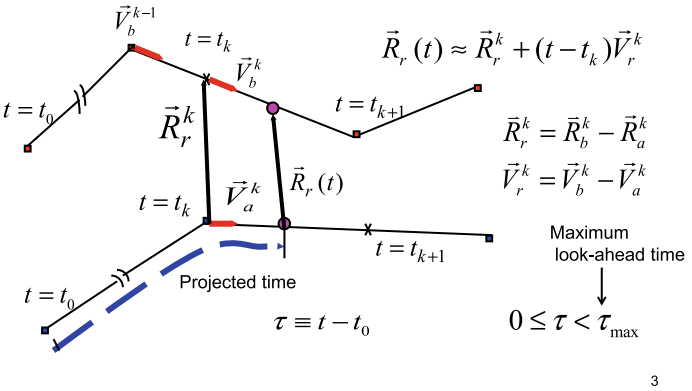

Fig. 2 Trajectory change point configuration

is made) for λ_t(= 6 min) [12] and separation minima for λ_H(= 6 NM) and λ_z(1200 ft).

Figure 2 shows the concept of calculating the difficulty value for trajectories with TCPs. The projection time range $[t_0,\ t_0 + \tau_{\max}]$ is divided into subintervals $[t_k,\ t_{k+1}]$, $(k = 1, 2, \ldots, N)$, in which the start or end time of at least one subinterval is the estimated time of arrival at a TCP. Herein, $t_1 = t_0$ is the current time and $t_{N+1} = t_1 + \tau_{\max}$. If each position and velocity vector corresponding to the subinterval is estimated, then the piecewise difficulty function for the subinterval can be expressed as

$$G_{\max}^k = \exp\left[-\min_{t_k \le t \le t_{k+1}} C^k(t)\right] \quad \text{for} \quad t \in \left[t_k, t_{k+1}\right] \tag{5}$$

where $C^k(t)$ is the evaluation function for the k-th subinterval. The modified difficulty value for an aircraft pair with TCP information at time t_0 is then given by

$$G_{\text{dif}}(t_0) = \max\left[G_{\max}^1, G_{\max}^2, \ldots, G_{\max}^N\right] \tag{6}$$

This metric provides a more accurate estimate of trajectory than simple linear extrapolation for aircraft flying a route with TCPs within the look-ahead time.

3 Concept of an Automatic Trajectory Modification Advisory System

3.1 Objectives

The main objective of this study on an ATC difficulty index is to predict 'hot spots' of ATC difficulty (high traffic complexity) based on trajectory information to assist in strategic traffic control and management. A secondary objective is to develop a tool for resolving the hot spots. Aiming at this, we have started a conceptual study based on simulations to investigate the suitability of the DI metric for this purpose.

In this section, we propose a concept of a controller decision support tool for a future TBO environment which automatically generates suggestions for trajectory modifications that will mitigate situations, where the airspace-wise DI value at a given time is predicted to exceed a prescribed threshold. The suggested trajectory modifications can then be shared with pilots via air-ground data link, allowing collaborative decision-making.

The proposed system assumes that real time trajectory data obtained from surveillance sources such as radar and flight plan information including TCPs are available for each flight in a volume of airspace. The system uses these to calculate the DI values for each aircraft pair and the airspace online.

3.2 Concept of Simulation System

Figure 3 shows the concept of a decision support system for trajectory modification to mitigate higher DI values (e.g. greater than 0.5). The difficulty metric maps a complex traffic situation in a volume of airspace onto a real number between [0, 1], where a value of 1 corresponds to the case of midair collision (separation distance at CPA = 0). The scale parameters of Eq. (2) are chosen such that a DI value of 0.5 is corresponds to a near-conflict case in which separation is close to being lost [12]. The conceptual system consists of the following processes:

(1) Difficulty index (DI) estimation,
(2) Threat detection and
(3) Trajectory modification.

The outputs of this system are proposed candidate trajectory modifications and their effects on each flight to the operator (ATCo).

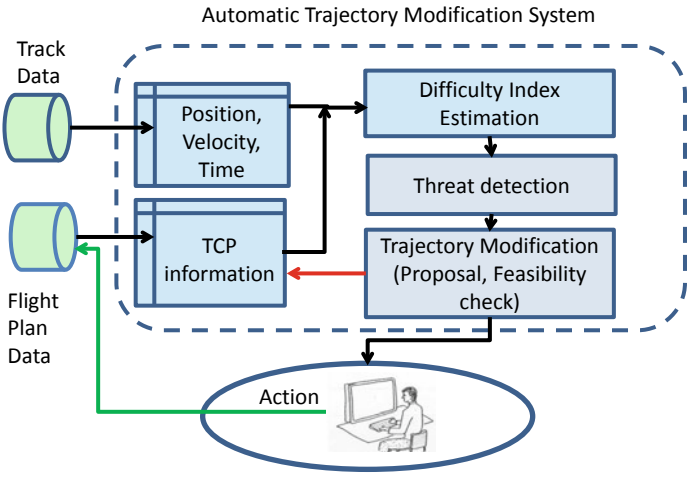

Fig. 3 Trajectory modification system configurations

3.3 DI Estimation Process

3.3.1 Data Pre-processing

Figure 4 shows the DI estimation process, which consists of data pre-processing and difficulty value estimation steps. Trajectory data (3D positions, velocities and time) are assumed to be extracted from radar data with a constant sampling period.

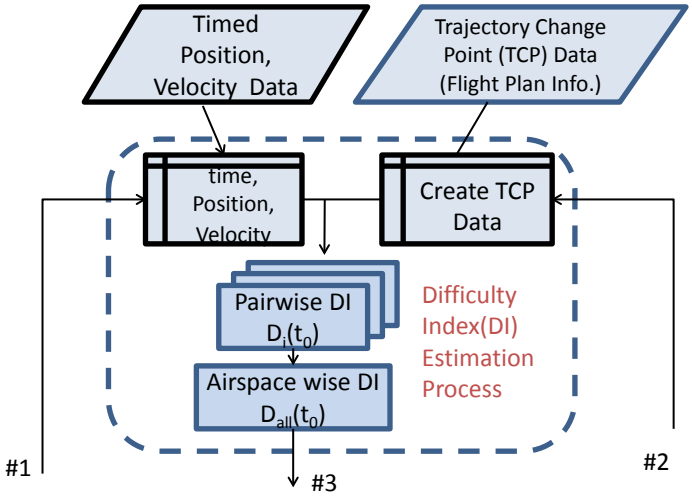

Fig. 4 Difficulty index estimation process

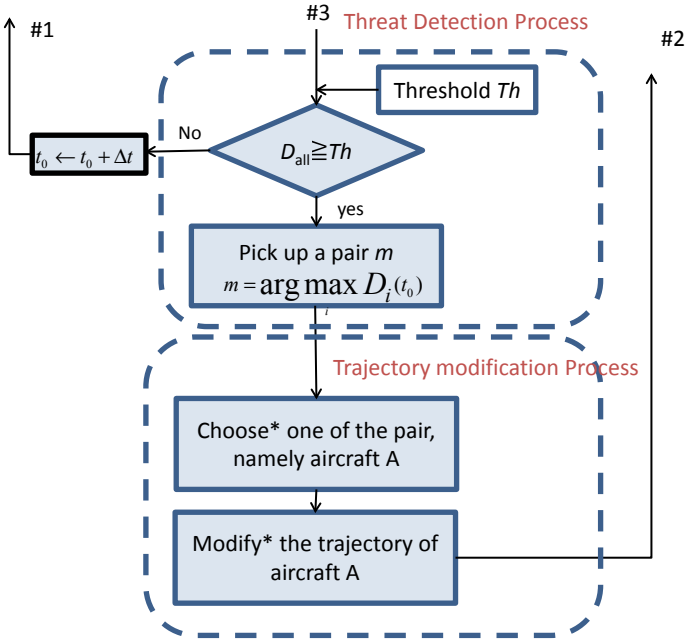

Fig. 5 Threat detection and trajectory modification processes

To simplify the calculation of the difficulty value, in the pre-processing step, the individual radar observations of each aircraft pair, which have different sample times, are adjusted to the same observation time. In addition, flight plan data on TCPs can be used to improve future trajectory estimation. Based on flight plan information, the spatial coordinates (latitude, longitude, altitude) of each TCP within the search time range $\tau_{\max}$ are created for each aircraft. For descending or climbing aircraft, altitudes can be determined by linearly interpolating between two given reference points [13].

The velocity vectors at each TCP and the elapsed time to the next TCP were estimated using a series of datasets on the coordinates of waypoints (TCPs) and the current ground speeds.

3.3.2 Estimation of Airspace Difficulty Values

Using the datasets of trajectory information and TCP data created in the pre-processing step, this process first estimates the pairwise difficulty values of each pair of aircraft in the airspace (or sector) of interest and then calculate the airspace-wise (or overall) difficulty value. The overall difficulty metric based on multiple aircraft pairs at time t_0 is calculated using each pairwise metric based on a reliability approach. Assuming that pairwise difficulty values are mutually independent, we

estimate the overall (or airspace wise) difficulty [9] of the system $D_{\text{all}}(t_0)$ by

$$D_{\text{all}}(t_0) = 1 - \prod_{i=1}^{N_{\text{pair}}} (1 - D_i((t_0)) \tag{7}$$

where $D_i(t_0)$ is the pairwise difficulty value ($= G_{\text{dif}}(t_0)$) of Eq. (6) for pair i, ($i = 1, \ldots, N_{\text{pair}}$). N_{pair} is the number of aircraft pairs in the airspace.

3.4 Threat Detection Process

Process 2) compares the estimated overall DI value with a prescribed threshold value Th (this may be set so as not to exceed 0.5, e.g. Th= 0.4). If the overall airspace DI value exceeds the threshold, then the pairwise difficulty values are reviewed to determine the dominant pair contributing to the proximity situation. After that, the trajectory modification proposal process is invoked on the identified pair (Fig. 5).

3.5 Trajectory Modification Process

Once the dominant aircraft pair has been detected, we create a candidate trajectory change for at least one of the pair from several possibilities of trajectory changes (altitude, heading or speed). Then, we recalculate the new overall difficulty value for the candidate trajectory modification and confirm that the value is lower than the threshold before proposing to the operator. Several candidates could be proposed ranked by DI reduction along with penalty information on each flight (e.g. flight time or fuel burn).

4 Current Status and Future Works

4.1 Sample Simulation Scenario

The threat detection process looks at the overall airspace DI value and each pairwise DI value. Figure 6 shows a simulation scenario of five trajectories over a 15-minute period. Two conflicts occur, one horizontally and the other vertically. Figure 7 plots the changes of calculated DI values over time. At each observation time t_0, the latest aircraft TCPs are obtained from flight plan data, and aircraft speeds and positions are obtained from track data, and DI values are calculated for each aircraft pair assuming that their speed will not change. Figure 7 indicates that the calculated DI values corresponding to the pairs with conflicts increase with elapsed time as their

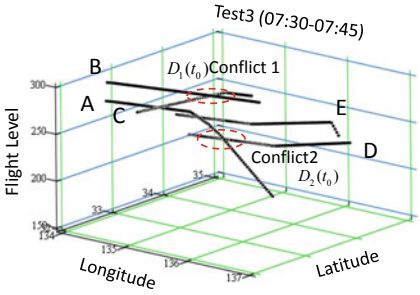

Fig. 6 Example of simulation scenario (Trajectories of five aircraft for 15 min)

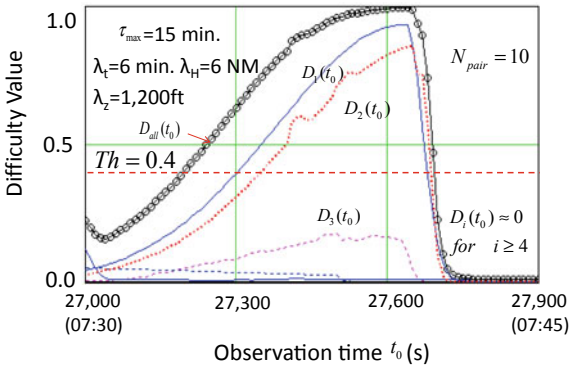

Fig. 7 Calculated difficulty values of ten pairs and overall difficulty value for the above scenario ($D_1(t_0)$ and $D_2(t_0)$ correspond to pairs with conflict 1 and conflict 2, respectively)

trajectories are predicted to converge. In this case, the pair with the largest value of pairwise difficulty value, $D_1(t_0)$, is chosen as a candidate for trajectory modification.

Figure 8 shows a PC screen shot of the sample simulation at observation time (t_0 = 27,220 s), when the overall DI value exceeds the threshold Th = 0.4. The threat detection process identifies the largest pairwise DI values and the corresponding aircraft. (This simulation programme does not include the trajectory modification process; that function is under development.) The graph in the screen shot indicates the distributions of predicted DI values.

In the above scenario and other scenarios, the DI metric successfully identified candidate aircraft pairs that will lead to high-complexity traffic situation in a suitably long look-ahead time that might allow trajectory management (seven minutes ahead in Fig. 7). Longer look-ahead times may be desirable and could be obtained by tuning the DI metric parameters; however, trajectory uncertainty also increases with look-ahead time, and too excessive a look-ahead time may therefore lead to unnecessary interventions.

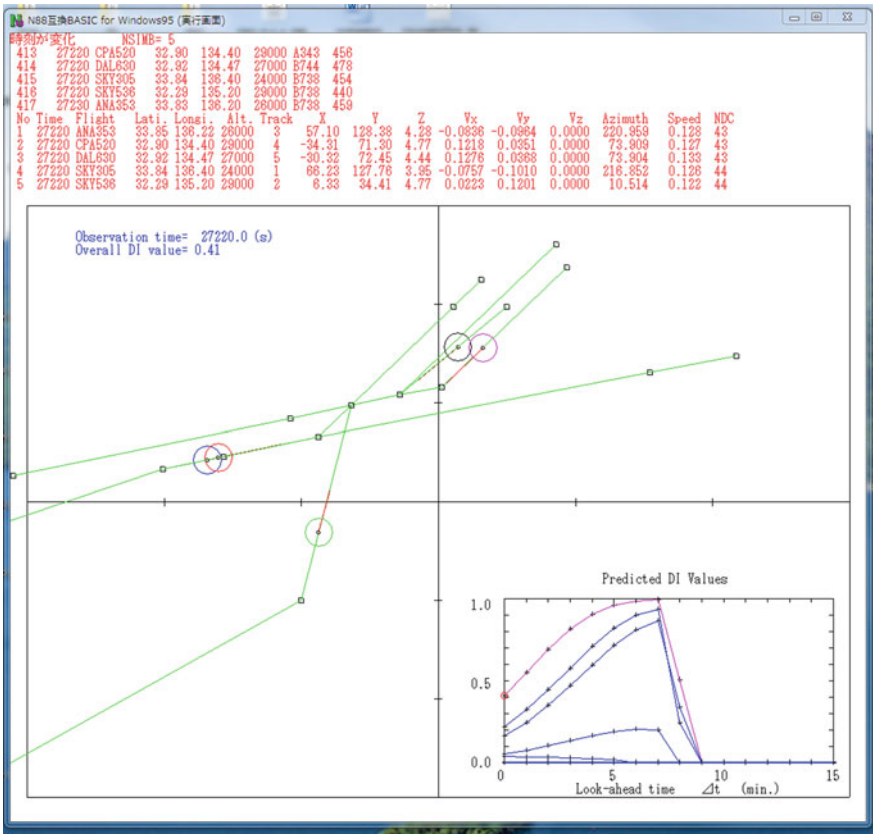

Fig. 8 A PC screen shot showing the scenario simulation when the overall DI first exceeded the threshold (Th = 0.4). DI values of each pair at present and future are plotted in the graph

4.2 Open Issues for Algorithms

In the above example scenario, the next step is to determine the criteria for the trajectory modification process. The main open questions are:

(i) which aircraft of the identified pair should be subjected to intervention?
(ii) what kind of trajectory change should be made?

Controller acceptability of proposed trajectory changes will be key as to whether this system will be practicable.

However, while studying airspace complexity, we found that ATCo reactions to a given traffic condition vary slightly from person to person [12]. These variations in strategies for handling traffic might depend on each ATCo's individual level of experience, personal preference or workload level; for example, a busy controller might wish to resolve potential conflicts early even though some of them may not actually

be conflicts, while a less busy controller may wait for a potential proximity situation to develop further before deciding whether to act in order to avoid unnecessary interventions. As a first step, we try to find an appropriate strategy for trajectory changes which will mitigate the difficulty index at a given instance for a few simple types of situation. Ultimately may be necessary to apply artificial intelligence techniques such as a rule base derived from ATCo knowledge, or machine learning to propose plausible candidates that controllers might themselves propose to resolve conflicts, e.g. if one of the pair is already close to top of descent and the other is in cruise, then initiating the descent of the arrival flight slightly early would be more operationally acceptable than adjusting the trajectory of the other aircraft.

A computer simulation programme is under development for a feasibility study. The scenarios will be based on the scenarios that were used for tuning the temporal scale parameter of Eq. (2), namely k_t [12]. The priory of selecting trajectory modification must be considered taking into account current ATC practices and suitability of computational logic for automatic assistance systems.

The development of the prioritization logic of trajectory modification and a simulation programme for demonstrating the feasibility of the concept are our future works.

5 Summary and Concluding Remarks

ATCo workload due to air traffic situation complexity may be a limiting factor of capacity of a future trajectory-based free routing ATM system. Furthermore, the new TBO environment will require new tools to enable ATCOs to strategically manage trajectories in an electronically linked collaborative environment.

To evaluate the complexity, we firstly developed the difficulty index (DI) metric for estimating air traffic control difficulty from aircraft trajectory data and flight plan information. As a next step, we propose a controller decision support tool that can provide candidate trajectory modifications to mitigate high-complexity traffic situations.

In this paper, we briefly reviewed our past works and newly propose a conceptual framework for such a tool. We then presented examples of simulations to investigate the feasibility of the DI metric for this application. As a result, it appears that the DI metric could be used to predict high traffic complexity sufficiently far ahead of time to allow strategic intervention, but on the other hand, trajectory uncertainty allows grows with time, so a trade-off is necessary to reduce unnecessary interventions.

For the other components of the tool, there are still many open issues such as detailed criteria for creating and selecting candidate trajectory modifications. To resolve these open issues are our future works.

References

1. M. Brown et al, *Full 4D Trajectory Based Operation Concept Study*. in Proceedings of APISAT (Asia Pacific International Symposium on Aerospace Technology) 2013, 04-05-02 (Takamatsu, 2013)
2. B. Hilburn, *Cognitive Complexity in Air Traffic Control- A Literature Review*. EEC Note No.04/04, EUROCONTROL (2004)
3. M. Prandini et al., Toward air traffic complexity assessment in new generation air traffic management systems. IEEE Trans. Intel. Transp. Syst. **12**(3), 809–818 (2011)
4. D. Delahaye, S. Puechmorel, *Air Traffic Complexity: Towards Intrinsic Metrics*. in The 3rd ATM Seminar (Napoli, 2000)
5. S.R. Kinnersly, I. Wilson, *INTEGRA Metrics & Methodologies Safety Metrics Technical Definitions*. EUROCONTROL (2000)
6. R. Gingell, C. Strachan, A. Taylor, S. Kinnersly, S. Fox, *INTEGRA Metrics & Methodologies Execution Phase-Final Report*. 1.0 edn. EUROCONTROL (2004)
7. S. Nagaoka, M. Brown, A review of safety indices for trajectory-based operation in air traffic management. Trans. JSASS Aerospace Tech. Japan **12**(APISAT-2013), a43–a49 (2014)
8. S. Nagaoka, M. Brown, Constructing an index of difficulty for air traffic control using proximity parameters. Procedia Eng. **99**(2015), 253–258 (2015)
9. S. Nagaoka, M. Brown, *Integrating Pairwise Proximity-based Air Traffic Control Difficulty Indices into an Airspace Index*. in The 7th Asia-Pacific International Symposium on Aerospace Technology (APISAT 2015) (Cairns, 2015)
10. H. Hirabayashi, M. Brown, S. Nagaoka, *Visualization of Airspace Complexity based on Air Traffic Control Difficulty*. in Proceedings of the 30th Congress of the International Council of the Aeronautical Sciences, ICAS 2016-0160, ICAS2016 (Daejeon, 2016)
11. S. Nagaoka, H. Hirabayashi, M. Brown, *Method for Scale Parameter Determination of Air Traffic Control Difficulty Index Based on Survey Results of Controller's Recognition for Aircraft Proximities*. in 8th APISAT 2016 (Toyama, 2016)
12. S. Nagaoka, M. Brown, *Tuning the Temporal Parameter of ATC Difficulty Metrics Using Controller's Cognitive Thresholds and Trajectory Change Point Information*. in 9th APISAT 2017 (Seoul, Korea, 2017)
13. S. Nagaoka, M. Brown, *Predicting Trajectories with Course Change points for Calculating Proximity-based Air Traffic Control Difficulty Indices*. IEICE Technical Report, SANE2017-79 (2017)
14. S. Nagaoka, H. Hirabayashi, M. Brown, *A Concept of Automatic Trajectory Modification for Mitigating Complex Air Traffic Situations with a High Difficulty Index Value*. IECE Technical report, SANE18-80 (2018)
15. V.D. Hopkin, *Human Factors in Air Traffic Control*. AGARDograph No.275, AGARD (1982). https://apps.dtic.mil/dtic/tr/fulltext/u2/a116394.pdf

Communication, Navigation and Surveillance

Air/Ground SWIM Integration to Achieve Information Collaborative Environment

X. D. Lu, K. Morioka, S. Egami, T. Koga, Y. Sumiya, J. Naganawa, and N. Yonemoto

Abstract The current ground-based collaboration environment is not sufficient to enable the full range of benefits defined in the ICAO Global Air Navigation Plan (GANP). In order to achieve a safe, secure, high-performing, and sustainable global air traffic management, the collaborative information exchange should be achieved for not only ground operational systems but also connected aircrafts. However, it is difficult for the current command-and-control Air-to-Ground (A/G) communication approaches to satisfy different and extensive information exchanges between the aircraft and the air navigation service providers. To promote the implementation of information collaborative environment in pre-departure phase and improve operational awareness and Collaborative Decision Making (CDM) through information exchange, the Electronic Navigation Research Institute (ENRI) has developed a test system. Several practical experiments have been deployed based on the integration of these systems to show the benefit of A/G SWIM (System-Wide Information Management) integration. In this paper, the concept and the technical framework of A/G SWIM integration are introduced. To provide timely, relevant, accurate, authorized, and quality-assured information for high-assurance operation,

X. D. Lu (✉) · K. Morioka · S. Egami · T. Koga · Y. Sumiya · J. Naganawa · N. Yonemoto
Surveillance and Communications Department, Electronic Navigation Research Institute (ENRI), National Institute of Maritime, Port and Aviation Technology (MPAT), Tokyo, Japan
e-mail: luxd@mpat.go.jp

K. Morioka
e-mail: morioka@mpat.go.jp

S. Egami
e-mail: s-egami@mpat.go.jp

T. Koga
e-mail: koga@mpat.go.jp

Y. Sumiya
e-mail: sumiya@mpat.go.jp

J. Naganawa
e-mail: naganawa@mpat.go.jp

N. Yonemoto
e-mail: yonemoto@mpat.go.jp

Air Traffic Management and Systems IV, Lecture Notes in Electrical Engineering 731,
https://doi.org/10.1007/978-981-33-4669-7_17

the multi-layered system architecture and the collaborative information exchange technology are proposed. Moreover, the development of practical validation system for ground taxiing experiment is presented. Finally, the definition and comparison of communication quality, information quality, and service quality for constructing the collaborative operating environment to include interactions of A/G stakeholders, systems, and services through the A/G SWIM integration are discussed.

Keywords System-Wide Information Management (SWIM) · Air Traffic Management (ATM) · Collaborative information exchange · Communication network

1 Introduction

With the rapid increase in local and global air traffic, the system-wide operational information exchange and life cycle management technologies are required to improve the capacity, safety, and efficiency of global Air Traffic Management (ATM). The System-Wide Information Management (SWIM) concept is to change the conventional ATM information architecture from point-to-point data exchanges to system-wide interoperability and to achieve life cycle management of data, information, and service [1]. The main objective of SWIM is to achieve interoperability and harmonization of global ATM operations through seamless information sharing among the multiple stakeholders.

In addition, the Flight and Flow Information for a Collaborative Environment (FF-ICE) is a SWIM concept-oriented operation. It has been developed by International Civil Aviation Organization (ICAO) to illustrate information for flight planning, air traffic flow, and trajectory management associated with ATM operational components [2].

The current collaboration environment focuses on the ground-based ATM service providers and Flight Operations Centers (FOC) with little opportunity for flight deck involvement in the collaboration process. The processes used to collaborate with airspace users, especially those without dispatch operations, are not sufficient to enable the full range of benefits defined in the ICAO Global Air Navigation Plan (GANP) [3].

In order to achieve a safe, secure, high-performing, and sustainable global ATM, the collaborative information exchange should be achieved for not only ground operational systems but also connected aircrafts. Therefore, the concept of A/G SWIM has been proposed to provide an environment for collaborative information exchange between the aircraft and the air navigation service providers. Through A/G data connectivity and aircraft on-board systems, the operational awareness and Collaborative Decision Making (CDM) can be improved [1].

However, current A/G communication approaches, such as A/G voice, Controller-Pilot Data Link Communications (CPDLC), and Automatic Dependence Surveillance-Contract (ADS-C) data link, are mainly used for command-and-control

information. These approaches are difficult to fully support the collaborative information exchange between the aircraft and the air navigation service providers. Moreover, because of the limitations of traditional data link mechanisms, such as communication methods, message formats, and associated avionics, it is difficult to satisfy the requirement of the aircraft for real-time and rich information exchanges. Due to these observed limitations, flight crews may not be available to access the ground SWIM information sharing platform and get their required information in pre-departure and post-departure phases. The difficulty for flight crews to obtain the required information in real time prevents them from sharing information with related stakeholders to make correct decisions [1, 4]. Therefore, it is difficult to satisfy the requirements of CDM without the seamless A/G information sharing.

In this paper, the architecture of an A/G SWIM integration system and the collaborative information exchange technology to achieve interoperability is presented. Moreover, the development of practical validation system for ground taxiing experiments conducted by Electronic Navigation Research Institute (ENRI) is reported. Finally, the communication, information, and service quality analysis and definition for constructing the collaborative operating environment to include interactions of A/G stakeholders, systems, and services through the A/G SWIM integration are discussed.

The paper is structured as follows. In the Sect. 2, the A/G SWIM concept is introduced. In Sect. 3, the proposed system architecture and the collaborative information exchange technology are presented. In Sect. 4, the development and analysis of practical validation system for ground taxiing experiments at Sendai airport are presented. The paper presents the conclusions in Sect. 5.

2 A/G SWIM Concept

2.1 Overview

The availability of low-cost data link capabilities significantly improves the uptake of the aircraft and its automation to become a SWIM participant and obtain information supporting air traffic management and advisory information exchange. A/G SWIM will enable enhanced information exchanges, such as for advisory and trajectory information, between Airspace Users (AUs) and ATM Service Providers (ASPs). As a result of access to shared information, both AUs and ASPs can make improved decisions. Information available on A/G SWIM is applicable to all flight phases, including pre-departure, departure, airborne, arrival, and post-arrival phases.

The A/G SWIM concept envisions two separate phases, as shown in Fig. 1. Phase 1 focuses on non-safety-critical information, while phase 2 will extend the concept to include safety-critical information [1].

The current document is focused on phase 1 of the A/G SWIM concept, which is intended to be utilized for non-safety-critical information or command-and-control

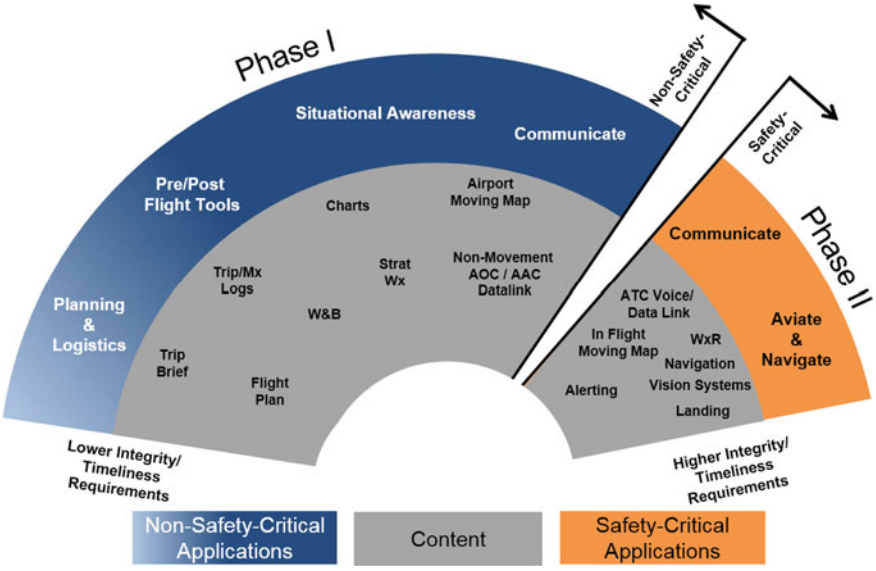

Fig. 1 Phases of A/G SWIM

functions, but rather to increase situational awareness. The use of A/G SWIM will support FF-ICE by providing a mechanism for the flight crew to exchange flight and flow information and become an integral part of the CDM and 4 Dimension Trajectory (4DT) management processes.

2.2 Technical Framework

To ensure the various operational scenarios relative to the differing configurations, the technical framework is organized based on the level of A/G SWIM connectivity available to the airborne platform as well as the level of connectivity between the flight deck application and the avionics on the airborne platform.

Figure 2 is a table showing various levels of A/G SWIM connectivity and avionics interface [1]. There are three SWIM connection levels defined:

1. No connection to A/G SWIM
2. Connection to A/G SWIM uplink only (airborne platform can receive A/G SWIM information)
3. Connection to/from A/G SWIM uplink/downlink (airborne platform can receive/send A/G SWIM information)

There are three avionics connection levels defined:

A. No connection to avionics

		Avionics Connection Level		
	Avionics Connection / SWIM Connection	A. No Connection to Avionics	B. Connection from Avionics Only	C. Connection to/from Avionics
SWIM Connection Level	1. No Connection to A/G SWIM	1A. No Connection to A/G SWIM, No Connection to Avionics	1B. No Connection to A/G SWIM, Connection from Avionics Only	1C. No Connection to A/G SWIM, Connection to/from Avionics
	2. Connection to A/G SWIM Uplink Only	2A. Connection to A/G SWIM Uplink Only, No Connection to Avionics	2B. Connection to A/G SWIM Uplink Only, Connection from Avionics Only	2C. Connection to A/G SWIM Uplink Only, Connection to/from Avionics
	3. Connection to/from A/G SWIM Uplink/Downlink	3A. Connection to/from A/G SWIM Uplink/Downlink, No Connection to Avionics	3B. Connection to/from A/G SWIM Uplink/Downlink, Connection from Avionics Only	3C. Connection to/from A/G SWIM Uplink/Downlink, Connection to/from Avionics

Fig. 2 Technical framework of A/G SWIM

B. Connection from avionics only
C. Connection to/from avionics

The table represents progressively more sophisticated connectivity/equipage down and to the right. It is not intended that this is the only equipage set in which these operations can be completed, but different connection levels are available during the transition period.

Interoperability is critical to widespread adoption of A/G SWIM. Applications and the infrastructure on

A/G SWIM should be able to operate across Flight Information Regions (FIRs), through the region, and as practicable, globally, without major modification. This will reduce the AU requirements to equip and train, especially for AUs that operate globally.

3 A/G Swim Integration

3.1 System Architecture

The A/G SWIM integration provides a collaborative environment that supports fully connected aircrafts to exchange different and extensive information with air and

ground systems. It requires two major communication network infrastructures to support A/G SWIM integration (Fig. 3). One is the G/G communication network to support ground SWIM for information exchange among ground stakeholders. The other is the A/G communication network to provide data link functions for information exchange with aircrafts [4].

It is expected that open Internet Protocol (IP) will provide the connectivity for both networks. Many open standards for communications exist, and the use of proprietary networks should be transparent. On-board wi-fi systems, non-safety satellite communications accessed using passenger networks, global system for mobile, etc. would all allow IP-based access to information nodes.

According to different communication environments and capabilities, several data link technologies have been developed and applied for A/G communications. However, most of them are applied for special on-board devices without interoperability. As the in-flight wi-fi service has been available for most airlines, the concept of Data Link as a Service (DLaS) is proposed to achieve Aircraft Access to SWIM (AAtS) for providing not only non-safety-critical information sharing but also safety-critical information exchange according to the available communication capabilities and qualities [4].

The A/G data layer provides the functionality of interoperable information exchange to deliver right information to a right aircraft at right time via the connection of G/G and A/G communication network infrastructures. The aircraft connects to Data Management Service (DMS) not only for accessing the required information

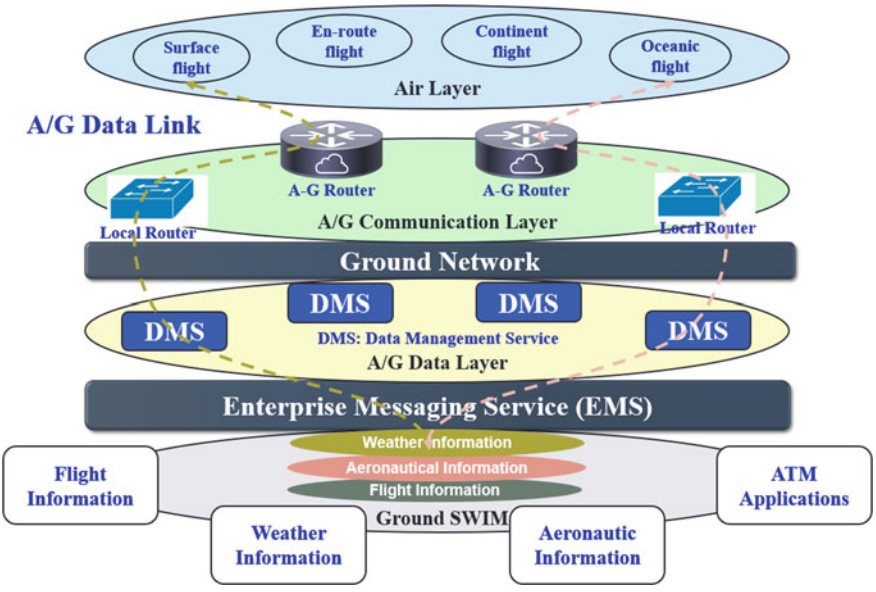

Fig. 3 System architecture

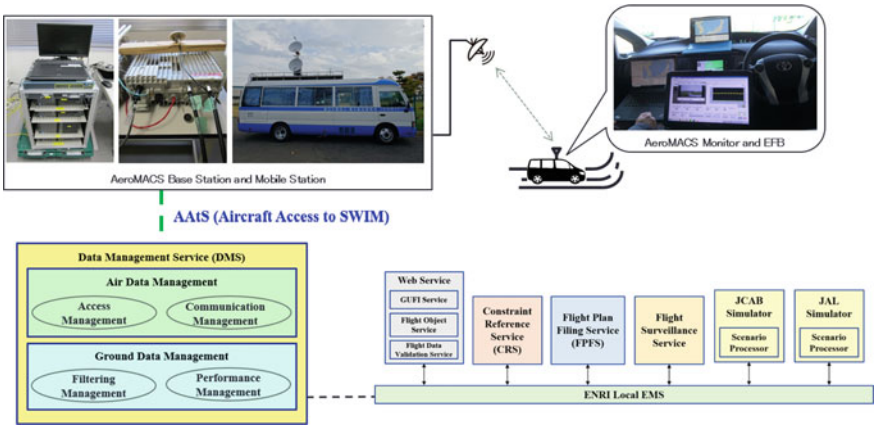

Fig. 4 Validation system for A/G SWIM integration

from the ground SWIM but also providing the on-board information to related stakeholders. The DMS is a main component of A/G data layer, and its functionalities are to store, manage, filter, and deliver ground and air information. As SWIM implementation is based on the concept of Service Oriented Architecture (SOA), it is more appropriate to consider the DMS as a SWIM-enabled service. To provide continuous accessing service for the aircraft in different phases, the autonomy of each DMS is required to control itself and coordinate with others. As shown in Fig. 4, the air data management and ground data management are main functions of a DMS to enable information exchange not only between aircraft and ground systems but also between DMSs within A/G data layer [5].

3.2 Information Exchange

The SWIM is a loosely coupled architecture, in which each system should collaborate with other systems for information exchange. Therefore, it requires a common messaging infrastructure to support collaborative information exchange between different systems. As a core service of SWIM technical infrastructure, the Enterprise Messaging Service (EMS) is able to assure that a message is transported from its source to its destination by using the appropriate message format, communication protocol, security policy, and business rule [6].

One operation needs heterogeneous information with different types, volumes and real-time scales to be seamlessly exchanged between different systems and dynamically converted according to different applications. By considering different conditions and specific operational requirements, three communication approaches are developed to achieve collaborative information exchange between G/G and A/G applications [4].

- Publish/subscribe (pub/sub) approach for dynamic and real-time information;
- Request/reply approach for static and non-real-time information;
- Push/pull approach for emergency information.

To assure required information quality for different applications, the data with different time scales are divided into different logical layers, and the life cycle management is applied. This approach is able to avoid the trouble of one application affecting other applications and the data with low real-time priority interfering with the applications in high real-time level. Moreover, in order to achieve the system expandability, the EMS is configured in autonomous architecture to associate with application systems according to their different information level requirements [4].

4 Practical Validation

4.1 Test System

To validate the services and functions of A/G SWIM integration system, the ground taxiing experiments have been deployed in the Sendai airport (Fig. 4). The vehicle used the Electronic Flight Bag (EFB) simulator to achieve information exchange with SWIM. The EFB simulator was developed to subscribe related flight information, aeronautical information, and weather information for a certain aircraft; show related information and documents on the map; generate takeoff and landing report according to the on-board and ground information and submit it to the DMS; request Notice to Airman (NOTAM), Meteorological Aerodrome Report (METAR), and Terminal Aerodrome Forecast (TAF) information from the ground SWIM services.

The Aeronautical Mobile Airport Communications System (AeroMACS) has been standardized by the ICAO to achieve information sharing on airport surface [7]. Moreover, the prototype of AeroMACS has been developed by our research group at the Sendai airport [8]. Therefore, the AeroMACS is applied as a media for A/G communication to achieve effective information exchange between the vehicle and the ground facilities. Different with current aeronautical communication systems, the AeroMACS is an IP-based communication system to provide high-capacity data transmission and higher communication link security with low system introduction and application development costs. It can be effectively used to share a large and varied amount of information among air traffic controllers, pilots, airline companies, airport operators on both the airport surface and during takeoff and landing [4].

In the practical validation, ENRI local EMS facilitates data sharing between a variety of services and applications. It provides the message routing and management functions to different SWIM services and ATM applications for seamless information exchange by using the standard aeronautical, flight, and weather information exchange models (AIXM, FIXM, and IWXXM) defined message formats.

To achieve secure communication, the network connection between AeroMACS and SWIM system is established on the Virtual Private Network (VPN) over Internet.

In addition, the Secure Sockets Layer (SSL) is applied for the communication between EFB and DMS. The communication standard of Advanced Messaging Queuing Protocol (AMQP 1.0) is used for publish/subscribe messaging approach.

The simulators of Japan Civil Aviation Bureau (JCAB) and Japan Airlines (JCAB) are serve as an ASP system and an AU system, respectively, to support the scenario-based validation and demonstration. There is a set of services and applications developed that support both SWIM-based information sharing and FF-ICE-based message exchange [4].

- The Globally Unique Flight Identifier (GUFI) is a single reference for flight information exchange. The GUFI service provides the generation, update, and lookup functions to users and applications.
- The flight object service maintains all flight data of one operation with same GUFI into a flight object. In addition, these data can be updated and queried by FIXM-based messages.
- The data validation service provides validation and reporting on FIXM, AIXM, and IWXXM messages conformance to schema and set of business rules.
- The Constraint Reference Service (CRS) provides aeronautical and weather information in AIXM and IWXXM format to support continuous monitoring for FF-ICE flight plans.
- The Flight Plan Filing Service (FPFS) evaluates the flight plan messages and checks the constraints affecting the route. It provides continuous monitoring functions for filed flight plans according to the updates of constraints.
- The flight surveillance service transforms airport surface and en route surveillance data to FIXM format and publishes to other SWIM services.
- The JCAB simulator is an application to manage subscribed FIXM messages from AUs and show trajectories on the map. It is also able to publish AIXM and IWXXM messages included constraints to AUs.
- The JAL simulators is a graphical user interface to generate and publish FF-ICE messages and submit new requests and updates according to subscribed responses and constraints from ASPs.

4.2 Validation

To evaluate the information sharing via Pub/Sub among related stakeholders, the FF-ICE messages defined in the pre-departure phase were exchanged between JAL and JCAB. The flight plan process in the FF-ICE pre-departure operation includes preliminary phase and filed phase. In each phase, ASPs should reply to the AU regarding the operational acceptability of their flight plans [9]. The preliminary and filed flight plans for JAL5 from Sendai airport (RJSS) to Inchon international airport (RKSI) were submitted by the JAL that contains additional information including 4DT, aircraft dynamics, weight, etc. According to the evaluation of format and constraint, the FPFS replied CONCUR and ACCEPTABLE for planning status and filing status to the JAL [10, 11]. As a subscriber of the information of JAL5, when the EFB

connected to the DMS with JAL5 account, all published messages related to JAL5 were received automatically (Fig. 5). Moreover, when the vehicle started to move, the track messages in FIXM format provided by the flight surveillance service were subscribed by the EFB in real time (Fig. 6).

The latest weather information of the airport is required to generate the takeoff report of the flight before departure. The EFB is able to send the request to the SWIM service and get the reply of the latest METAR and TAF information from CRS (Fig. 7). Other constraints registered on the CRS are also available for Request/Reply access via the EFB.

Each ASP is able to publish constraints, such as aeronautical information, traffic flow management data, and severe weather conditions. For some emergency information and constraints, the ASP is able to send a notification to a certain flight using push/pull approach. It not only assists the flight in making decision by identifying the operational environment and ATM constraints, but also enables the flight to obtain an earlier, more detailed and more accurate assessment of the anticipated traffic demand. As shown in Fig. 7, the limited air space information near the Sendai airport was pushed from JCAB to JAL5 in AIXM message and automatically shown on the map of EFB.

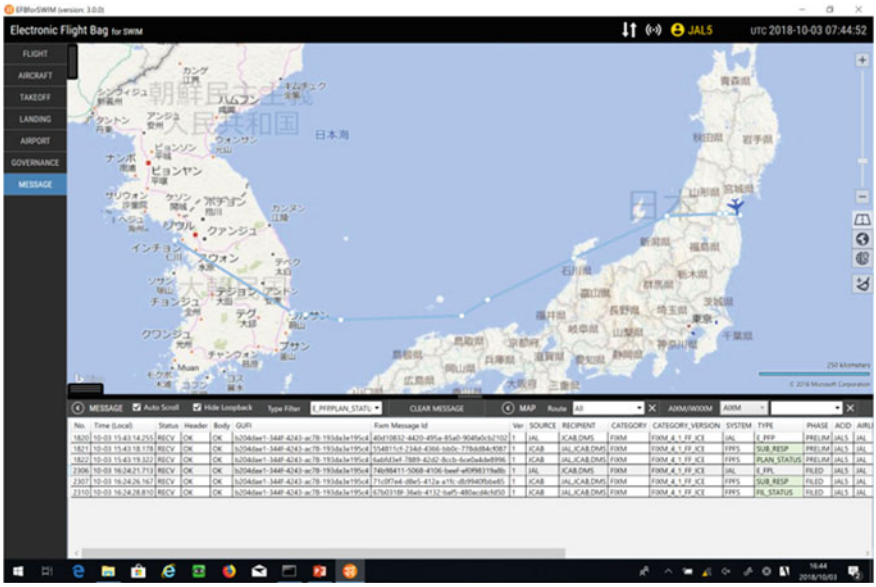

Fig. 5 Pub/sub for flight plan messages

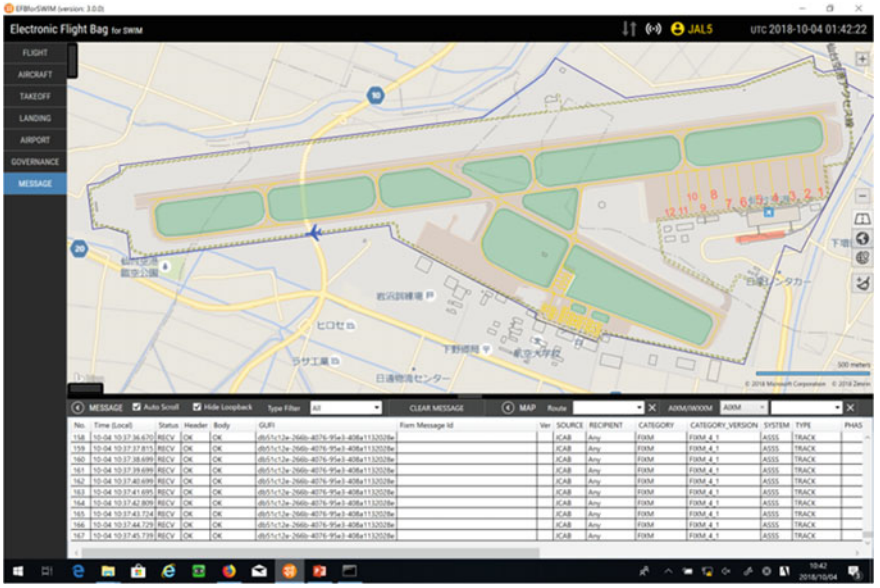

Fig. 6 Pub/sub for track messages

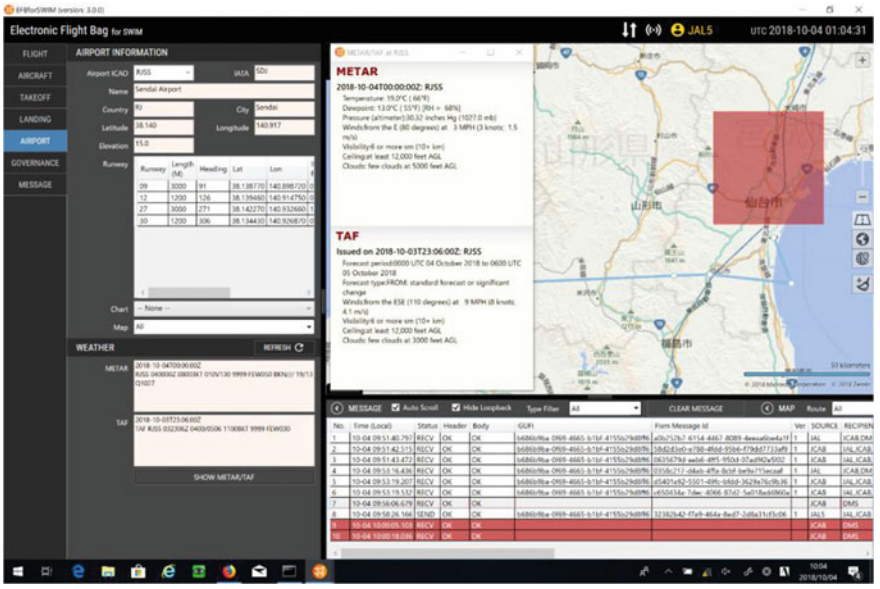

Fig. 7 Test of request/reply and push/pull

4.3 Analysis

Due to the fact that A/G SWIM integration includes several different systems, it is difficult to evaluate its performance just with the Quality of Service (QoS). To evaluate the performance of A/G SWIM integration, we divided the QoS into three important dimensions: communication quality, information quality, and service quality. The main objective of A/G SWIM integration is to improve the quality of communication, information, and service for meeting the information requirements of A/G stakeholders.

The A/G communication has the critical role to assure information exchange between air and ground systems and applications. The communication quality consists of three factors: latency, packet loss ratio, and throughput. One of the advantages of AeroMACS over other existing aeronautical radio system is the QoS control, which enables high priority for critical information transmission.

The communication quality of AeroMACS was evaluated by transmitting messages with high priority while downloading a large volume of non-critical files via File Transfer Protocol (FTP). The results in Table 1 show that AeroMACS with QoS control can not only improve the communication quality but also assure the stable communication under dynamic changing environments [12].

The information that is transmitted to the consumer plays a critical role in the service encounter. When information is incomplete or incorrect, severe inconsistencies can arise and affect the service quality perceptions. To improve the information quality that consists of accuracy, timeliness, and integrity, the message exchange in XML format based on the standard information exchange models is applied. Table 2 shows the comparison of information quality between text-based information exchange and SWIM-based information exchange.

Table 1 Comparison of communication quality

Communication quality	Without QoS control	With QoS control
Latency	622 ms	244 ms
Packet loss ratio	49.4%	0%
Throughput	2.80 Mbps	4.58 Mbps

Table 2 Comparison of information quality

Information quality	Current approach	SWIM approach
Accuracy	Low (difficult to check)	High (easy to validate)
Timeliness	Low (difficult to share)	High (easy to process)
Integrity	Low (difficult to assure)	High (easy to manage)

The satisfaction level of a SWIM service encounter is a result of discrepancies between the operational expectations and the actual performance. Due to the SWIM governance and business rules that manage the interactions between service providers and consumers, a "delicate balance between flexibility and safety" is required. In regards to achieving collaborative decision making between ASPs and AUs, the importance of service quality has been widely recognized. From the technical point of view, the service quality deals with availability, response time, and reliability. In the validation test, the calculations for these parameters of service quality are as follows:

$$\mathrm{Av}(s) = 1 - (\text{Disable Time})/(\text{Total Time}) \tag{1}$$

$$\mathrm{Rt}(s) = \text{Receipt Time} - \text{Request Time} \tag{2}$$

$$\mathrm{Re}(s) = \text{Sucess Request}/\text{Total Request} \tag{3}$$

where Av(s) is availability, Rt(s) is response time, and Re(s) is reliability for service s. In here, the service is the utilization of data management service.

Due to the unstable connection of A/G wireless communication, disconnection and package loss might occur in the real conditions according to the different network conditions. In the validation test, the unstable network communication is the main reason for the disable time of service utilization and the package loss of message exchange. To solve this problem, the A/G synchronization technology by setting the timestamps in the metadata of message header has been proposed and applied in the test system. The efficiency of the proposal was proved in the ground taxiing experiments by recovering the lost messages after the EFB reconnected to the DMS via synchronization process. As shown in Table 3, the system with proposed A/G synchronization technology can not only assure the service quality but also improve the satisfaction of users' requests.

Moreover, the A/G SWIM integration can enhance security from communication, information, and service levels by using appropriate and standard technical protocols. Therefore, the A/G SWIM integration is able to provide not only higher performance but also more flexible and less costly for achieving information exchange and interoperability at global, regional, and local levels.

Table 3 Comparison of service quality

Service quality	Without A/G synchronization	With A/G synchronization
Availability	98%	100%
Response time	325 ms	325 ms
Reliability	98%	100%

5 Conclusion

In this paper, the A/G SWIM concept for achieving FF-ICE and Trajectory-Based Operation (TBO) is introduced. Then, based on this concept, the architecture and the collaborative information exchange technology of an A/G SWIM integration system are presented. Moreover, the development of a practical validation system for ground taxiing experiments by using AeroMACS as a A/G data link is reported. Finally, to evaluate the performance of the proposed system architecture and technology, the communication quality, information quality, and service quality are defined and analyzed by comparison with or without A/G SWIM integration for constructing a collaborative operating environment. The results and analysis of practical validation show the efficiency of proposed system architecture and technology. In future, flight trials enabling the quantitative evaluation of the A/G SWIM integration will be conducted.

References

1. Manual on System Wide Information Management (SWIM) Concept, ICAO Doc 10039, ICAO, 2015
2. Manual on Flight and Flow—Information for a Collaborative Environment, ICAO Doc. 9965, ICAO, 2012
3. 2016-2030 Global Air Navigation Plan, ICAO Doc 9750, 5th ed., ICAO, 2016
4. X.D. Lu, K. Morioka, T. Koga, Y. Sumiya, *Air-Ground System Wide Information Management to Achieve Safe Flight Operation.* IEEE HASE2019, 2019
5. X.D. Lu, T. Koga and Y. Sumiya, *SOA-based Air-Ground Information Exchange for High-assurance Operation.* IEEE GCCE2018, 2018
6. X.D. Lu and T. Koga, *System Wide Information Management for Heterogeneous Information Sharing and Interoperability.* IEEE ISADS2017, 2017
7. ICAO Annex 10—Volume 3, Aeronautical Telecommunications Chapter 7, ICAO, 2016
8. K. Morioka, X.D. Lu, N. Kanada, S. Futatsumori, N. Yonemoto, Y. Sumiya, A. Kohmura, *Field-taxiing experiments of aircraft access to SWIM over AeroMACS.* in IEEE International Conference on Antenna Measurement and Applications (CAMA) (2018)
9. X.D. Lu, T. Koga, Y. Sumiya, *Coordinated Validation for SWIM Concept-Oriented Operation to Achieve Interoperability.* in ENRI International Workshop on ATM/CNS (2017)
10. ENRI, Lab Exercise for FF-ICE/1 and A/G SWIM Validation, SWIM-TF/2-IP/06, ICAO, April 2018
11. X.D. Lu, K. Morioka, T. Koga, Y. Sumiya, *Collaborative Flight and Flow Information Exchange to Achieve Seamless Air Traffic Management Operation.* IEEE ISADS2019, 2019
12. K. Morioka, J. Naganawa, X.D. Lu, N. Miyazaki, A. Kohmura, N. Yonemoto, Y. Sumiya, *QoS Validation Tests for Aircraft Access to SWIM by Ground Taxiing Experiments.* IEEE ISADS2019, 2019

A Simple Note on Shadowing Effects and Multipath Propagation for CNS

R. Geise, J. Klinger, and B. Neubauer

Abstract This contribution discusses shadowing effects of large objects with respect to navigation and communication systems. Since the current practice for assessing the impact of scattering objects on those systems is based on mainly quasi-optical wave propagation, a simplified, but yet improved analysis of possible disturbances is proposed. Based on scattering theory, a simple analytic formula is derived applying fundamentals of the radar cross section concept. As for at least canonical objects, such as metal plates or cylinders, for which an accurate analytic description for the radar cross section is well known, simple shadowing examples are discussed. With the derived formula a more sophisticated sensitive area layout can be developed than it is currently recommended with an overall layout, i.e. typically a circular area with a fixed radius. Finally, measurement results in a miniaturized anechoic chamber are presented that give additional insight into the shadowing phenomena discussed in this contribution. Further, measurement results are shown as examples for travelling waves and shadowing effects.

Keywords Navigation systems · Communication systems · Radar cross section · Shadowing

1 Introduction

Multipath propagation or shadowing effects can affect the integrity of navigation and communication systems such as radar, the VHF omnidirectional radio range (VOR) or other directional communication links, e.g. the 'link 16' standard [1]. Multipath propagation phenomena are present, if additional propagation paths due to reflections

R. Geise (✉) · J. Klinger
University of Applied Science for Telecommunication, Leipzig, Germany
e-mail: geise@hft-leipzig.de

R. Geise · B. Neubauer
Institute for Electromagnetic Compatibility, Technische Universität Braunschweig, Brunswick, Germany

Air Traffic Management and Systems IV, Lecture Notes in Electrical Engineering 731,
https://doi.org/10.1007/978-981-33-4669-7_18

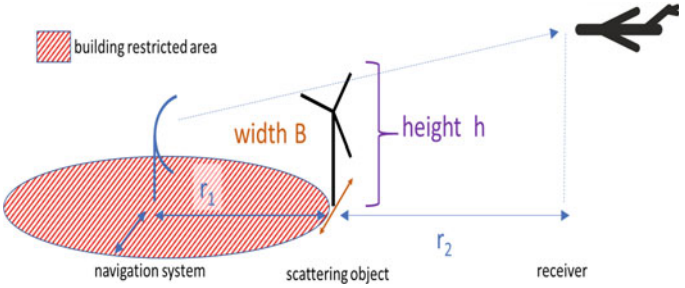

Fig. 1. Sketch of shadowing scenario

on existing objects occur. Since this always is associated with a performance degradation of the respective navigation or communication system, building restricted areas are introduced to prevent disturbances. Actually, from academic point of view, reflection properties of larger objects, such as buildings and wind turbines, can well be described in terms of radar cross section (RCS). Though, guidance material on the restricted area sizes, as, for example, provided by the ICAO, for practical reasons only recommend a rough and overall layout according to the respective communication or navigation system [2]. Such recommendations are mainly based on a solely optical propagation behaviour and are actually not based on scattering theory. This contribution develops practical guidance material for initial and individual dimensions of building restricted areas as derived from scattering theory fundamentals.

Figure 1 is a simple sketch of a shadowing scenario and introduces relevant geometrical measures. In fact, as scattering scenario a wind turbine is chosen. In Germany, there are more than 4000 MW of installable wind power investments not realized due to assumed, but not yet proven incompatibilities between wind turbines and navigation systems, communication systems, respectively, [3].

In Sect. 2, fundamentals of shadowing effects and radar cross sections are discussed, and Sect. 3 focuses on the relevance of shadowing effects in terms of probabilities. Sections 4 and 5 present measurement examples to visualize the mechanism of shadowing effects and to present quantitative examples. Finally, a conclusion is given in Sect. 6.

2 Shadowing and RCS

Usually, the scattering properties of an object are described by its radar cross section [4], which can be calculated nowadays with a lot of commercially available simulation tools, e.g. [5]. In particular, the calculation of complex multipath propagation with such a numerical tool is time consuming and usually not done individually for an object, applying a simple concept of building restricted areas of a given size. As, for example, stated in [2] considerations of tolerable blockage are simply done by an

optical test, if a ray reaches the wings of a wind turbine as it exceeds a certain height. Such quasi-optical ways of testing are a priori neglecting edge diffraction effects and systematically lead to an overestimation of the blockage attenuation. However, those diffraction effects are part of an angular-dependent radar cross section description. Consequently, in the following, the concept of radar cross section is used to derive a simple blockage description by already known formulas that can be found in the standard literature.

For a line of sight propagation in free space, the known Friis transmission equation

$$\begin{aligned} P_{r,\text{direct}} &= \frac{P_s \cdot G_s}{4\pi \cdot (r_1 + r_2)^2} \cdot \frac{\lambda^2}{4\pi} \cdot G_e \\ &= \frac{E^2_{\text{direct}}}{377\,\Omega} \cdot \frac{\lambda^2}{4\pi} \cdot G_e \end{aligned} \tag{1}$$

applies, where G_s and G_e are the gains of the emitting and the receiving antenna; P_s is the emitted power; and $P_{r\text{direct}}$ is the received power. E_{direct} denotes the field strength as measurable at the observer's location. The distances r_1 and r_2 are explained in Fig. 1, and λ is the wavelength.

Likewise, the received power and field strength of a scattered path with an object, $P_{r,\text{indirect}}$ and E_{indirect} are given applying the object's radar cross section RCS as:

$$\begin{aligned} P_{r,\text{indirect}} &= \frac{P_s \cdot G_s}{4\pi \cdot (r_1)^2} \cdot \frac{RCS}{4\pi \cdot (r_2)^2} \cdot \frac{\lambda^2}{4\pi} \cdot G_e \\ &= \frac{E_{\text{indirect}}}{377\,\Omega} \cdot \frac{\lambda^2}{4\pi} \cdot G_e \end{aligned} \tag{2}$$

The radar cross section relates the electric field strengths of a wave impinging on an object $E_{\text{at object}}$ and the scattered field strength at the receiver's location E_{indirect} and is defined as

$$RCS = \lim_{r_2 \to \infty} 4\pi \cdot r_2^2 \cdot \frac{E^2_{\text{indirect}}}{E^2_{\text{at object}}} \tag{3}$$

The electric field strength at the object can be calculated applying Eq. (1) with:

$$\frac{E^2_{\text{at object}}}{377\,\Omega} = \frac{P_s \cdot G_s}{4\pi \cdot (r_1)^2} \tag{4}$$

Of course, these simple equations have to meet several conditions for their applicability, such as fulfilling far field conditions both for the antennas and the scattering object. Moreover, it is noted that ground reflections are currently not taken into account. This might be feasible with image theory. However, the aim of these considerations is not to develop an exact and complete method, but to improve the current overall building restriction area layout concept substantially using the quantity of

RCS, which describes the scattering properties of an object. Applying Eqs. (1)–(4), a simple attenuation measure a is derived in the following. In the fundamentals of scattering theory, the measurable field strength at receiver's location is the superposition of the field strengths of the incident plane wave E_{direct} and the scattered field strength E_{indirect} (with negative sign due to the 180° phase shift). For the field strength in the shadowing scenario $E_{\text{shadow,}}$ following expression is obtained:

$$\begin{aligned} E_{\text{shadow}} &= E_{\text{direct}} - E_{\text{indirect}} \\ &= \sqrt{\frac{P_s \cdot G_s \cdot 377\,\Omega}{4\pi \cdot (r_1 + r_2)^2}} - \sqrt{\frac{\text{RCS} \cdot E^e_{\text{at object}}}{4\pi \cdot (r_2)^2}} \end{aligned} \tag{5}$$

Finally, applying Eq. (4) again the attenuation measure a is given by:

$$\alpha = 1 - \sqrt{\frac{\text{RCS}}{4\pi}} \cdot \frac{(r_1 + r_2)}{r_1 \cdot r_2} \tag{6}$$

Two special cases for r_1 and r_2 are discussed here. For example, if the receiver is very far away, thus $r_2 \gg r_1$, a complete blockage for $a = 0$ requires that $\text{RCS} = 4\pi \cdot r_1^2$, corresponding to a sphere with radius r_1 completely enclosing the emitter. It is quite obvious that such an object is hardly realizable. On the other hand, it is a good example that the quasi-optical evaluation, that, if a single ray hits an object, then a high blockage is achieved, is in contradiction to the concept of the radar cross section. Further examples are given in Sect. 4 with measurements in a miniaturized anechoic chamber. Before, in the following section, further scattering properties are discussed.

3 Edge Diffraction and Blockage Probability

In the previous section, so far only the magnitude of the radar cross section is considered, in particular its maximum in a certain direction. However, a fundamental principle of scattering theory should be considered here with respect to a sophisticated compliance analysis, i.e. the distribution of the scattered fields in space, and associated with that, the probability of significant shadowing effects. In order to show this fundamental principle, the scattering of a rectangular plate of given width and height at a frequency of 1 GHz is discussed in the following. For non-grazing incidence and an electrically large object, where the object's dimensions are large compared to the wavelength, the scattering properties can well be described with the method of physical optics (PO) [4]. The maximum of the radar cross section in specular reflection and shadowing direction can be calculated with:

$$\mathrm{RCS} = 4\pi \frac{(\mathrm{width} \cdot \mathrm{height})^2}{\lambda^2} \tag{7}$$

Figure 2 describes the example scenario, where a metal plate is illuminated under an incidence angle ϕ_{in}, and the scattering is described with the angle-dependent (ϕ_{scat}) radar cross section. Additionally, Fig. 2 denotes the specular reflection direction and the shadowing region.

In this simple example, an incidence angle ϕ_{in} of 20° is chosen. The angle-dependent RCS is plotted against ϕ_{scat} in Fig. 3.

The maxima of scattered fields are in the specular reflection direction and in the shadow region. Of course, the larger the object's surface is, the larger its RCS is as well in mentioned directions. However, with increasing size the main lobe of

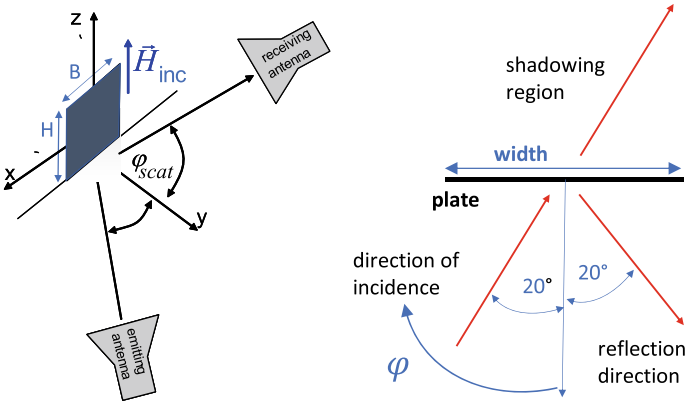

Fig. 2. Sketch of a scattering scenario with a metallic plate as reference object

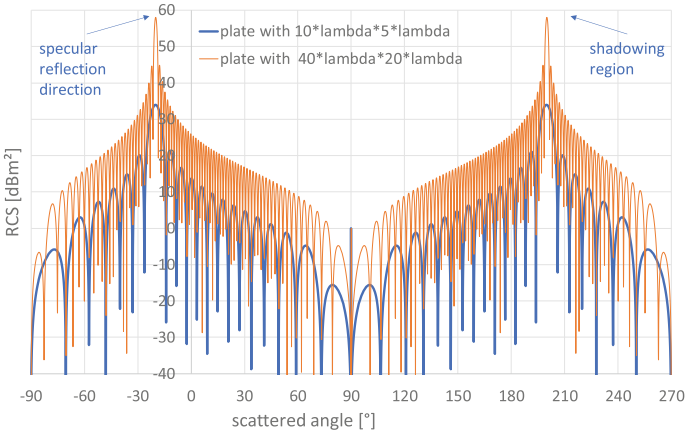

Fig. 3. Radar cross section of a metallic plate as calculated with the PO method

Table 1. Summary of a metal plate's scattering properties

Structure	Max. RCS in shadowing direction logarithmic	Max RCS in shadowing direction linear	Shadowed angular range (10 dB width)	Transfer coefficient a for $r_2 = r_1 = r =$ 4 km
Plate (40 λ * 20 λ)	58 dBm^2	6.3e5 m^2	3,4°	0.88
Plate (10 λ *5 λ)	34 dBm^2	2500 m^2	9°	0.99

scattered pattern always gets narrower, thus covers a smaller angular area. Thus, for any shadowing scenario, especially for large objects, the probability of maximum shadowing decreases. Following Table 1 summarizes major properties of these two examples. Table 1 also shows the transfer coefficient a into the shadowing direction as calculated with Eq. (6).

It is noted that though an optical propagation path would be considered to be fully blocked, the transfer coefficient hardly decreases. For the larger metal plate, the loss due to shadowing only is about 10%. The table also shows that large shadowing effects only occur within a small angular range behind the object. This angular range decreases with the size of the object.

In the following, a practical and easily reproducible academic measurement example are presented to further confirm that shadowing effects are highly overestimated if solely considering optical wave propagation.

4 Example Measurements of Shadowing

To measure the attenuation due to shadowing, an object (DUT) is placed in between a linear polarized horn antenna (Horn) and a receiving dipole antenna as Figs. 4

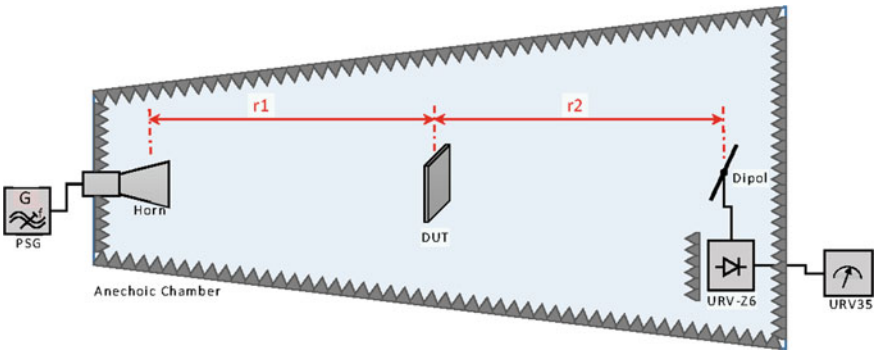

Fig. 4. Sketch of measurement setup within a miniaturized anechoic chamber

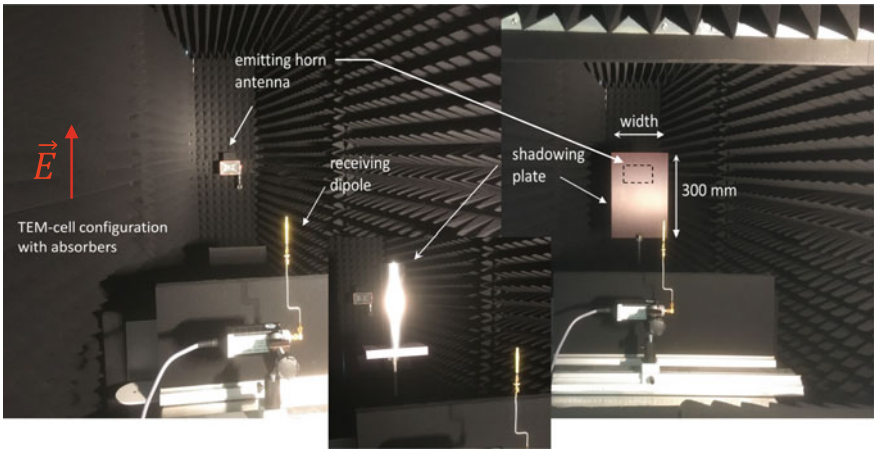

Fig. 5. Photograph of measurement setup within the anechoic chamber, (left) without shadowing object (right) with shadowing object

and 5 show. Measurements were done in a self-built miniaturized anechoic chamber as shown in Fig. 5.

A continuous wave signal at 9.45 GHz provided by a RF signal generator (PSG) positioned outside the anechoic chamber is fed into a horn antenna. An output power of 14 dBm is used. Since these measurements only deal with shadowing attenuation as a relative measure, cable losses and antenna gains do not need to be taken into the account. The transmit power level just provides sufficient dynamic level to have the attenuated signal at least 20 dB above the noise floor.

A combination of a linear antenna, a semiconductor detector (URV-Z6) connected to the millivolt metre (URV35) acts as the measurement receiver as Fig. 4 shows. All shadowing measurements results are related to a reference measurement without DUT; thus, all measurement results state the relative attenuation measure due to the object's shadowing.

Two reference objects are exemplarily measured. On the one hand, alumina coated cylinders with different diameters and constant height and on the other hand rectangular shaped copper plates of different width and constant height are chosen. The variable sizes, i.e. diameter for the cylinder and width for the thin plate, are shown in Table 2 together with the measurement results. The fix geometric dimension is the height of 300 mm. The DUT is always placed in direct line-of-sight, where the distance between the objects to the respective antennas is equal, i.e. 80 cm. Measurements are done in vertical polarization as indicated in Fig. 5. From Fig. 5, it can be seen that the large metallic plate completely blocks the line-of-sight; thus, a ray of light would have a total blockage. However, the measured attenuation of those large objects in direct line of sight has a maximum of 16 dB only. For a communication scenario, this can still be considered not critical, provided; there is a reasonable margin for a dynamic range. As previously explained in Sect. 3, because of the

Table 2. Measurement results

Diameter or width in [mm]	Diameter or width in wavelengths	RCS of plate [m^2]	Measured attenuation by plate [dB]	Measured attenuation by cylinder [dB]
50	1.6	2.8	−2.58	−3.54
80	2.5	7.2	−2.93	−4.61
100	3.2	11.3	−3.71	−5.02
120	3.8	16.3	−4.14	−6.13
150	4.7	25.4	−6.01	−7.29
200	6.3	45.2	−10.28	n.a.
224	7.1	56.7	−16.18	n.a.

phenomenon of edge diffraction, induced current on the edges contribute to measurable, only partially shadowed field strengths. It can be seen that both for the cylinder and the plate the shadow attenuation is comparable.

The attenuation behind the cylinders is about 1.5 times higher than shadowed by metalized plates as Fig. 6 shows. Also, doubling the area leads to about twice the attenuation. This is consistent considering Eqs. (6) and (7), because usually, the RCS is a function squaring the geometrical area.

Figure 6 summarizes the measurement results and provides a least error fitting function shown with Eqs. (8) and (9). For larger areas, that effect might change as the graphs let expect. In the graph, the standard deviation between the optimized functions and the measurement results are given as well.

$$\frac{L_{\text{cylinder}}}{[dB]} \approx 2.3 + 129.5 \cdot A, (\sigma = 0.17) \tag{8}$$

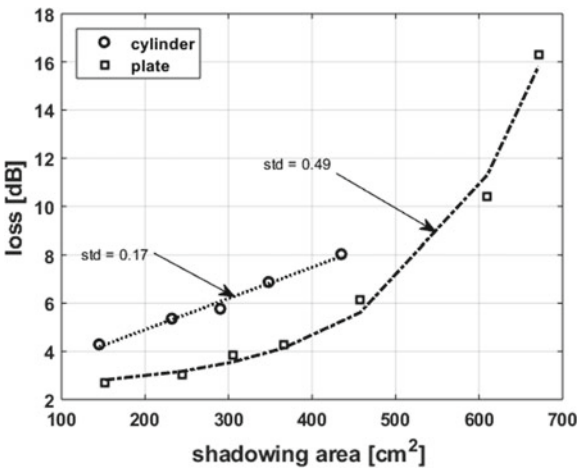

Fig. 6. Measured losses due to shadowing by area A in [m^2]

$$\frac{L_{\text{plate}}}{[\text{dB}]} \approx 2.4 + 0.15 \exp(67 \cdot A), (\sigma = 0.49) \tag{9}$$

The shape of shadowing objects relates to the slope of the function. Based on the measured value, Eqs. (8) and (9) are first approximations with $\boldsymbol{a}$ as the geometric area, in squared metre.

Decreasing the shadowing area down to zero, which means no shadow appears, the attenuation of course has to become to zero value as well. Equations (8) and (9) do not follow this constraint. So the range of validity of these both equations has to be considered as narrow, for larger values of the area A as well. The distance between object and receiver (r_2) is around 25 times of the wavelength, and the object dimensions are up to ten times the wavelength.

It has to be stated that these functions are not meant to be directly applicable for predicting shadowing scenarios. However, they show that defining, for example, a strict height limit for structures according to optical wave propagation does neither cope with the theoretical analysis nor with the measurement examples shown in this contribution. In fact, the aim of defining height limits as proposed in international guidance material [2] is to provide scenarios, where definitely no further testing is necessary. Thus, if an object does not block the line-of-sight between emitter and receiver, then no further testing is required at all. The reverse conclusion—often applied by responsible authorities in Germany—if an object just slightly blocks the line-of-sight, then there is a significant shadow effect, is both fundamentally wrong, as exemplarily discussed in this contribution and not originally intended by the ICAO itself.

5 Travelling Waves and Shadowing Examples

As explained in the previous section, the phenomenon of travelling waves, thus induced currents flowing along objects, causes electromagnetic fields also radiated behind the object's shadowing region. As a simple example for illustrating this in a similar context, measurement results are presented as performed in [6] investigating wave propagation in a miniaturized scaled measurement setup.

Figure 7 shows the measurement setup at the open area test site at the national metrology institute in Braunschweig, Germany.

A modular terrain topology is constructed and made conductive with a lacquer coating. The manufacturing process and the material characterization is explained in [6].

An emitting antenna is located in front of the hill structure, and receiving antennas are placed directly behind it as indicated in the photograph for two different positions at a distance of 3.2 and 5 m. Transfer functions between two antennas are measured with a network analyzer ZVA24 in the frequency range from 1 GHz up to 24 GHz using broadband horn antennas from Q–par Angus Ltd.

Fig. 7. Wave propagation measurements along larger structures

In this case, it is obvious that the direct line-of-sight between emitting and receiving antenna is blocked by the conductive hill structure. Following figures present measured transfer functions both in frequency domain as obtained with the network analyzer and in time domain after an inverse Fourier transform of the measured data.

Figure 8 shows that the presence of the hill structure leads to an additional shadowing attenuation of about 20 dB. Of course, this scenario can be understood as an example only for a demonstration of how larger objects or structures shadow wave propagation. It cannot directly be adopted to shadowing effect of terrains with probably different conductivity. A deeper insight into the shadowing process becomes obvious from the impulse response derived from the frequency measurement data by applying inverse Fourier transform. These impulse responses are shown in Figs. 9 and 10.

The impulse response without the hill structure (blue line) shows a runtime of the signal of 72 ns, which is the direct line-of-sight distance divided by the speed of light (including runtime through the connecting cables). The presence of the hill blocks the line-of-sight, and consequently, this propagation path does not occur in the impulse response with the hill structure (red line). However, the induced currents obviously form a travelling wave along the surface of the hill, so the time of arrival slightly

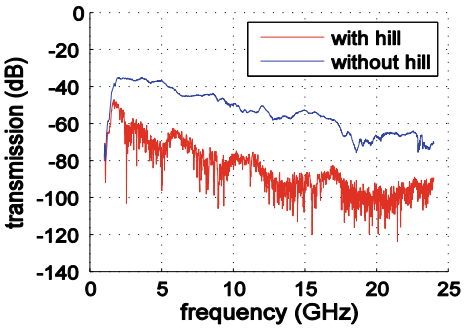

Fig. 8. Measured transfer function in frequency domain with receiving antenna at position 1

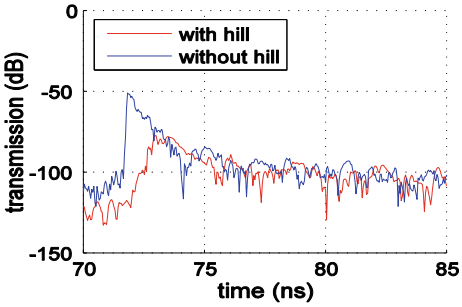

Fig. 9. Impulse response in time domain after Fourier transform with receiving antenna at position 1

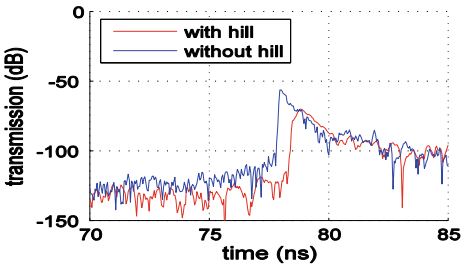

Fig. 10. Impulse response in time domain after Fourier transform with receiving antenna at position 2

increases by the additional propagation way along the hill's surface. Of course, this travelling wave is attenuated as already visible in the frequency domain, but a total blockage definitely does not occur. Corresponding observations can be made for the other position of the receiver as shown in Fig. 10.

Figure 10 also shows the same effect of travelling waves, but for larger runtimes due to the shifted antenna position. The relative shift in runtime becomes slightly lower as clearly visible due to the changed geometric dimensions.

Presented shadowing scenarios with the hill structure are another example that a detailed analysis is mandatory to quantitatively investigate shadowing effects. In addition, the optical wave propagation as currently often applied does not comply with presented measurement results presented in Sects. 4 and 5.

6 Conclusion

This contribution discusses shadowing effects of large objects in the context of navigation and communication systems. A simple formula is derived from fundamentals of scattering theory, which can be applied individually to scattering objects, rather than defining an overall layout of building restriction areas. Moreover, example measurements of shadowing effects are performed to demonstrate that shadowing effects are currently overestimated, if solely optical wave propagation is considered.

Whereas in current recommendations [2] only the height of an object is taken into account, a more sophisticated but simple practice is recommended by applying the real scattering properties, i.e. the radar cross section of an object that either can be calculated numerically by nowadays software simulation tools or at least by approximated canonical shapes of similar geometric size. The proposed method can also be used by governmental authorities, which probably do not have access to nowadays high-end numerical simulation tools.

These new method of estimating shadowing effects in the context of navigation and communication systems will very likely lead to shrinking restricted areas around CNS radio systems and reduce building height restrictions.

References

1. R. Geise, B. Neubauer, G. Zimmer, *Analysis of Navigation Signal Disturbances by Multipath Propagation—Scaled Measurements with a Universal Channel Sounder Architecture*, Frequenz. (2015) Band 69, Heft 11–12, pp. 527–542, ISSN (Online) 2191-6349, ISSN (Print) 0016-1136. https://doi.org/10.1515/freq-2015-0080
2. *The European and North Atlantic office of ICAO, European Guidance Material on Managing Building Restricted Areas.* Tech. Report, Available [Online]: https://www.icao.int/EURNAT/EUR%20and%20NAT%20Documents/EUR%20Documents/EUR%20Documents/015%20-%20Building%20Restricted%20Areas/ICAO%20EUR%20Doc%20015%20Third%20Edition%20Nov2015.pdf, looked up 30.07.2019
3. *Bundesverband WindEnergie (BWE)* [Online], https://www.wind-energie.de/sites/default/files/attachments/page/arbeitskreis-luftverkehr-und-radar/20150907-ergebnisse-2-radarumfrage-bwe-final_0.pdf, looked up 30.03.2018
4. F. Knott, *Radar Cross Section*, 2nd edn. (SciTech Publishing Inc, Raleigh, NC, 2004). ISBN 978-0-89006-174-9
5. *CST MICROWAVE STUDIO®*. User Manual Version 2016, Sep. 2016, CST GmbH, Darmstadt, Germany [Online], www.cst.com, looked up 30.07.2019
6. B. Neubauer, R. Geise, G. Zimmer, O. Kerfin, A. Andree, N. Ueffing, *Modular Terrain Modeling with Flexible Conductive Materials in a Scaled Measurement Environment*. In European Conference on Antennas and Propagation (March, Paris, France 2016), pp. 1–5, 19–24. . Reprinted, with permission from IEEE ©2017

ADS-B Coverage Design in Mountainous Terrain

K. Wangchuk, Sangay, J. Naganawa, D. Adhikari, and K. Gayley

Abstract This paper describes an approach to the ADS-B coverage design being undertaken for the mountainous terrains of Bhutan. Existing ADS-B implementation studies have mostly focused on coverage design based on interference criteria. There is a lack of ADS-B coverage design studies in challenging terrain like in the Himalayan kingdom, where about 98% of the land cover is mountains. To account for the unique environment, a physical optics-based deterministic channel modeling methodology is adopted. A radio siting algorithm developed to determine the best location of additional ADS-B receivers is outlined. The effectiveness of the algorithm is demonstrated by applying it to determine the location of additional ADS-B receiver at PARO control zone to improve coverage in areas critical to flight operations. This study will be augmented by analysis of opportunistic ADS-B signal measurements being carried out before the ADS-B receiver network is implemented for use in air traffic management purpose.

Keywords Surveillance · ADS-B · Mountainous terrain · Coverage design · ATM · Physical optics

K. Wangchuk (✉) · K. Gayley
Air Navigation Services Section, Bhutan Civil Aviation Authority (BCAA), Paro, Bhutan
e-mail: kwangchuk@bcaa.gov.bt

K. Gayley
e-mail: kgaley@bcaa.gov.bt

Sangay
Department of Air Transport (DoAT), Communication Navigation Surveillance Section, Paro, Bhutan
e-mail: sangay@doat.gov.bt

J. Naganawa
Surveillance and Communications Department, Electronic Navigation Research Institute (ENRI), National Institute of Maritime, Port and Aviation Technology (MPAT), Tokyo, Japan
e-mail: naganawa@mpat.go.jp

D. Adhikari
Department of Communication Engineering, Vellore Institute of Technology, Vellore, India
e-mail: dadhikari@doat.gov.bt

Air Traffic Management and Systems IV, Lecture Notes in Electrical Engineering 731,
https://doi.org/10.1007/978-981-33-4669-7_19

1 Introduction

More than 98% of Bhutan is mountains [1]. With elevation ranging from 97 meters to 7570 m and average elevation of 3280 m above sea level—located in the eastern end of the Himalayan mountain range—it is one of the most mountainous country in the world. Figure 1 is the obstacles chart showing the contour lines of high terrain on approach to runway 33 of Paro International Aerodrome. Due to the terrain, implementation of conventional radar-based surveillance system is only feasible for the en route phase, but not cost-effective given the low density of traffic in the airspace. On the other hand, ADS-B is an attractive and a viable solution for both En –route and Terminal Area (TMA) surveillance. The representative cost of implementing ADS-B in a TMA is lower by a factor of almost 16 compared to implementing Mode S radar for the same purpose [2]. Existing ADS-B implementation studies have mostly focused on coverage design based on interference criteria. Studies have shown that the main factor to be considered in coverage design and conversely the siting of terrestrial ADS-B receivers is interference from existing systems using the 1090 MHz frequency [3]. As such, there were no publicly available studies conducted on ADS-B coverage design in areas, where there are no existing 1090 MHz terrestrial systems, and coverage is affected primarily by the location of the receivers. In such areas, the existing 1090 MHz propagation models used are not suitable. A more robust propagation modeling methodology using terrain information for prediction of the coverage area is necessary.

This study presents an approach to ADS-B coverage design using 1090 MHz propagation channels simulated with Physical Optics (PO) based method and a radio siting algorithm developed for the purpose. Using existing communication and navigation aid station locations as initial state, the radio siting algorithm determines the best location of additional ADS-B receivers to improve coverage in the required coverage area.

The rest of the paper is organized as follows; Sect. 2 describes the coverage design requirements, and Sect. 3 discusses PO-based simulation results. The radio siting algorithm is outlined in Sect. 5, and the results of application of the algorithm is discussed in Sect. 6. The summary and future work are presented in Sect. 7.

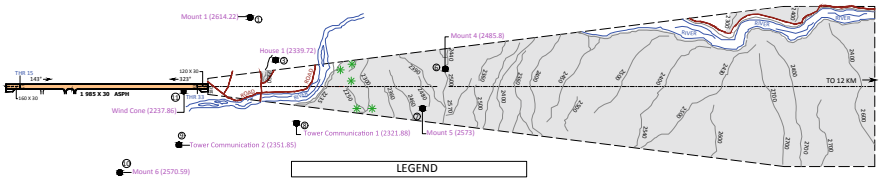

Fig. 1. Part of aerodrome obstacle chart—ICAO Type A, for areas within the PARO CTR (Reproduced with permission from department of air transport—Bhutan)

2 Coverage Design Requirements

It will take an impractically large number of ADS-B receiver stations, on the ground, to provide coverage in all the valleys in the country. This study will only target to design ADS-B coverage on the published Air Traffic Services (ATS) routes, both domestic and international, and around the aerodromes; containing the final approach phase of a flight. Figure 2 shows the Control Zones (CTR) around the four aerodromes in the country. Paro (ICAO: VQPR, PARO CTR) is the only international aerodrome. Bumthang (ICAO: VQBT, BUMT CTR), Yongphula (ICAO: VQTY, YONG CTR) and Gelephu (ICAO: VQGP, GELP CTR) are the three domestic aerodromes. Currently, the CTRs are not formally designated; it is proposed to be established soon. For this study, a volume of cylindrical airspace with a 10 NM radius from the Aerodrome Reference Point (ARP) and extending till 16,000 feet Above Ground level (AGL) is defined as the CTR. The ARP of each aerodrome is also indicated in the figure. Of the four CTRs, the ARP of three CTRs; PARO, BUMT, and YONG are at an altitude of 2580.2 m (8465.2 ft) Mean Sea Level (MSL), 2244.5 m (7363.8 ft) MSL, 2562 m (8405 ft) MSL respectively, and only GELP CTR is at 300.9 m (987.2 ft) MSL. The figure also shows the published ATS routes [4]. Bhutan has only two international routes connecting to the PRO VOR waypoint from BOGOP and SUBSU designated as routes R598 and G348, respectively. There are six RNAV 5 domestic routes (Y_1, Y_2, Y_3, Y_4, Y_5, and Y_6) connecting the various aerodromes within the country. The upper and lower limits on the international routes are 16,000 feet till Flight Level (FL) 460. For domestic routes, the upper and lower limits are defined from 18,000 feet till FL 290.

For coverage design, we set out the following requirements:

i. All areas in the CTRs containing final approach and departure path should have 100% coverage;

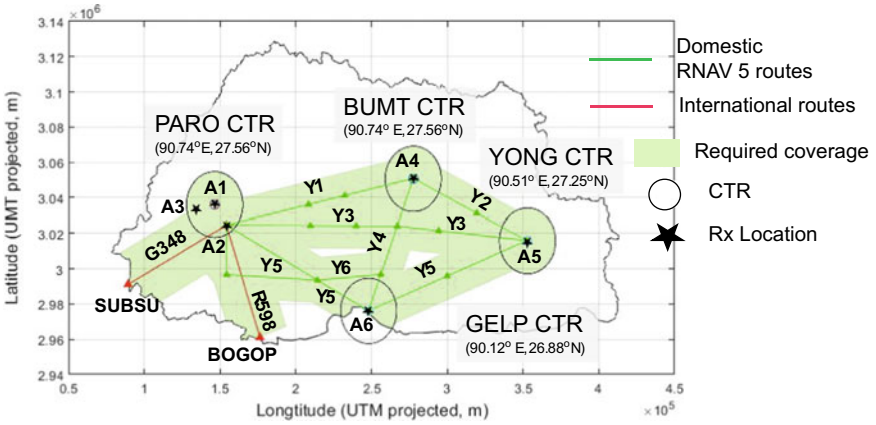

Fig. 2. Required coverage area (shaded) and ADS-B receiver locations

ii. International routes should have coverage from 16,000 feet MSL till FL 460 vertically and 10 NM on either side from the center line of the ATS track;
iii. Domestic routes should have coverage from 18,000 feet MSL till FL 290 vertically and 7 NM on either side from the center line of the ATS track.

The design problem can therefore be stated as maximizing coverage within the required coverage areas, indicated by the shaded region in Fig. 2, utilizing minimum number of receivers.

3 Physical Optics-Based Simulation

A stochastic channel model is generally preferred for use in designing mobile systems; as it captures all possible channel states. However, for a fixed terrestrial ADS-B receiver network, a deterministic channel modeling methodology that utilizes the terrain information will be more accurate. In this study, the 1090 MHz ADS-B signal propagation channel is simulated using a Physical Optics (PO) based method utilizing a 90 m resolution NASA Shuttle Radar Topographic Mission (SRTM) Digital Elevation Model (DEM).

Installing ADS-B receiver (Rx) ground stations at the existing Communication and Navigation (Com/Nav) system stations is most practical and cost-effective from implementation point of view. As an initial state, seven receiver locations coinciding with existing communication and navigation aid stations and aerodrome control towers are chosen. These Rx locations are labeled as A_1 to A_7 in Fig. 2. The coordinates of these locations are obtained from the current Aeronautical Information Publication (AIP) of Bhutan [4]. For receivers co-located with VHF radio antennas at the aerodrome control tower, an antenna height of 15 m is used. For receivers that are located at remote Com/Nav stations, antenna height of 10 m is used in the simulation. A model of a 1090 MHz vertically polarized, 9 dBi gain, omnidirectional antenna is used for simulation.

The infovista mentum planet wireless access network planning and optimization software [5], a popular simulation platform with mobile RF planners, is used to carry out the simulations. The simulator supports various access technologies and wireless propagations models; however, the most suitable propagation model supported for our purpose is the predict air model [6] that is based on physical optics and therefore deterministic in nature. It is highly dependent on the terrain information or the DEM. The simulator environment and simulation parameters used are summarized in Table 1.

In the actual simulation, the reciprocity of propagation channels is exploited. Simulation is carried out by positioning transmitter antennas at the Rx locations and calculating the received signal strength at gridded locations, of 50 m resolution. According to ICAO Annex 10 volume IV chapter 5, Table 5-1 [7], the minimum power at antenna feed for an airborne system should be 51 dBm; however, in this study, only 40 dBm power at antenna feed is used mainly to account for losses in

Table 1 Simulation environment and parameters

Simulator	Infovista mentum planet 6.3.0
Propagation model	Physical optics-based predict air
Receiver antenna coordinates	Co-located with Com/Nav antenna as per AIP Bhutan, second edition
Antenna height	10 m (Com/Nav stations), 15 m (Aerodrome control tower)
Antenna	9 dBi Omni antenna (Vertically Polarized)
Output power at antenna feed	40 dBm
Com/Nav system site coordinate and altitude	A_1 = (27.40 N, 89.42 E, 2590 m) A_2 = (27.30 N, 89.51 E, 3469 m) A_3 = (27.38 N, 89.33 E, 4095 m) A_4 = (27.57 N, 90.78 E, 3447 m) A_5 = (27.25 N, 91.51 E, 2528 m) A_6 = (26.88 N, 90.46 E, 310 m) A_7 = (27.56 N, 90.74 E, 2595 m)

signal path leading to the antenna feed. This is a very pessimistic but a practical assumption given that we expect the ADS-B antennas to be positioned at significant distances from the stations—for optimal coverage.

4 Simulation Results and Discussion

From an altitude of 16,000 feet to FL 490 on the international routes and from 18,000 feet till FL 290 on the domestic routes, the seven ADS-B receivers located at existing Com/Nav stations and aerodrome control towers provide adequate coverage on these routes. No additional ADS-B receivers are required. However, with only the seven receivers, coverage at lower altitudes is patchy and not adequate; does not cover whole of approach and departure paths. This is particularly severe within PARO CTR, where areas along the published RNP-AR approach paths does not have ADS-B coverage.

For determining coverage in the lower altitude areas in the CTR, areas with terrain higher than the altitude at which the coverage is being determined should be excluded from the coverage calculation. For instance, Fig. 1 shows the terrain on the approach path to runway 33 at Paro International Airport, within the PARO CTR. It is clear that even at an altitude of 8500 feet (2591 m) MSL, there are many areas where terrain is higher than this altitude. Therefore, for determining the area over which coverage is required at a particular altitude, areas with terrain higher than that altitude should be excluded. At 8500 feet, these areas in all the CTRs are indicated by black shaded region in Fig. 3.

From Fig. 3, we see that in PARO CTR and BUMT CTR, majority of the terrain in the CTR are above 8500 feet. The figure also shows the signal strength of the

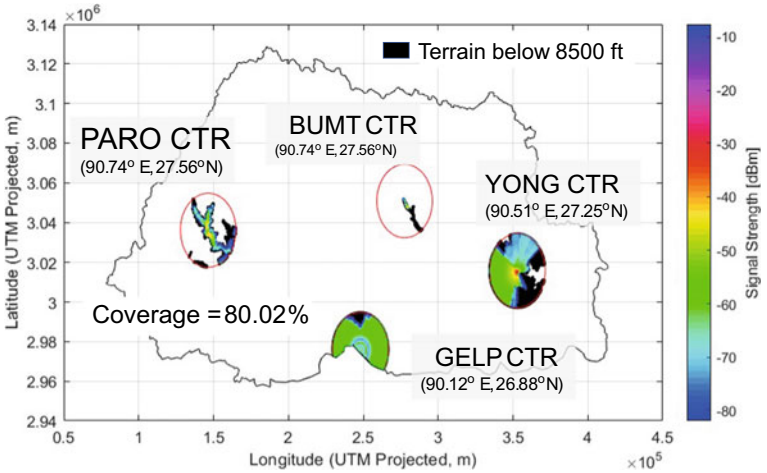

Fig. 3. Simulated signal strength within the CTRs superimposed on coverage required areas

received signal, for transmitters located at various points in the coverage area and receivers located at A_1–A_7, super imposed over the areas that require coverage. The areas appearing shaded in black in the figure are areas that require coverage but does not have coverage.

Coverage percentage P, taking into account the terrain can therefore be expressed as:

$$P = \left[1 - \frac{R}{(A - A')}\right] \times 100 \tag{1}$$

where A is the area in which coverage is required without considering the terrain; A' is the area for which the terrain is higher than the altitude at which the coverage is being determined; and R is the area within the required coverage region for which signal strength value is higher than the threshold value. For this study, -82 dBm is used as the threshold value, which is within the minimum receiver trigger threshold level defined in Annex 10 Volume IV, chapter 5, Table 5-3 [7].

Using the expression in (1), the coverage percentage at 8500 feet in Fig. 3 is found to be only 80.2%. More stations strategically located are required to fill in this coverage gap. Coverage at higher altitudes is much better, with more than 90% coverage at altitudes above 11,000 feet. It is clear that at lower altitudes within CTRs, more strategically located receivers are required to satisfy the coverage requirements.

5 Radio Siting Algorithm

A simple radio siting algorithm to determine the best location of additional ADS-B receivers to improve coverage in the required coverage area is developed. The main component of the algorithm is a ray tracer, where the number of reflections is set to zero, and strength of each rays is weighted not by the total path loss, as in conventional radio propagation ray tracing algorithms, but set to one. The algorithm finds the number of unobstructed rays, unobstructed by triangulated (using Delaunay triangulation) faces obtained from DEM point clouds, originating from the point in space, where coverage is required and directed toward the centroid of triangulated terrain faces. We then determine the centroid of the triangulated terrain face that receives the maximum power. This centroid location is, therefore, the best location for the additional receiver as it has line-of-sight to maximum number of points, where coverage is required. For simplicity of implementation, other propagation mechanisms such as reflection and diffraction are not considered in the algorithm.

Figure 4 (Left) shows the outline of the receiver siting algorithm. The most computationally intensive part of the algorithm is to determine if a ray is obstructed by the triangulated terrain faces. In order to reduce the number of triangulated terrain faces considered for the determination, only the triangulated faces whose centroids are within the cylindrical Region of Interest (RoI) of radius $\boldsymbol{r}$, and with its axis aligned along with the ray is considered. In this study, $r = 80$ m is chosen since the longest distance from vertices of the triangulated faces to their centroid is found to be 78 m.

The overall runtime of the algorithm is directly proportional to the number of rays being considered. On carefully observing the location of approach paths and departure paths from each aerodrome, particularly PARO CTR and BUMT CTR, it is seen that flights approach and departs from the aerodrome along the valley in which the runway is located. At lower altitudes coverage in valleys other than that in which the runway is located, even if the valley is situated within the CTR, is not necessary. For these aerodromes, we assume that only those triangulated terrain faces that are facing toward the valley could be the next ADS-B receiver location. In Fig. 4 (Middle and Right), the curved line segment LM is the trace of the floor of the valley, where the runway is located. Only those triangulate faces are retained, whose face

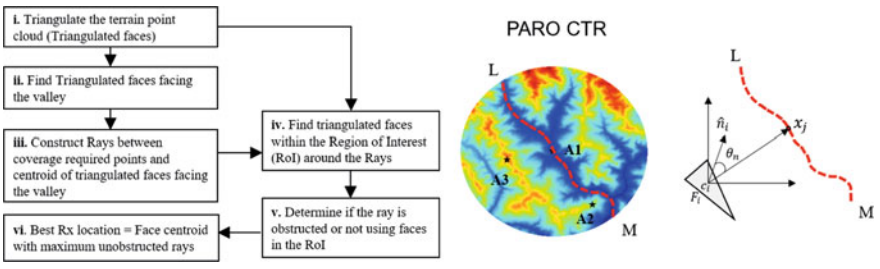

Fig. 4. (Left) Outline of the radio siting algorithm developed. (Middle) Trace of the valley in which the runway is located. (Right) Illustration of a triangulated face facing the valley

normal projected on to the XY-plane (Longitude—Latitude plane) makes an angle $\theta_n < \theta_{\min}$ with the all the vectors originating at the centroid and terminating at any point on the curved line segment LM. For instance, in Fig. 4 (Right), the triangulated terrain face F_i will be retained if the angle θ_n between the vectors $\hat{\boldsymbol{n}}_i$ and $\overrightarrow{\boldsymbol{c_i x_j}}$ is less than $\theta_{\min}$ $\forall j$ and x_j located on LM; where $\boldsymbol{c_i}$ is the face centroid, $\hat{\boldsymbol{n}}_i$ is the face normal vector projected onto *XY*- plane, and x_j is a point on LM. This is a reasonably safe assumption as the triangulated faces with face normal facing away from the valley are located on the other side of the ridges. $\theta_{\min} = 60^{\circ}$ is heuristically chosen.

To determine if the rays are obstructed by the triangular faces, whose centroid are located within the RoI, the Möller–Trumbore algorithm [8] is implemented in Matlab™. To make the algorithm runtime practical for running on a desktop computer, the number of rays is further reduced by resampling the coverage required points in space and also removing adjacent triangulated faces. The algorithm is then run separately for each CTR.

6 Coverage Improvement with Additional ADS-B Receiver Locations

For PARO CTR, additional ADS-B receiver location is necessary to cover the final phase of approach path on both ends of the runway; RWY 15 and RWY 33. These regions are marked as R1 and R2 in Fig. 5. This is also observed in the test measure-

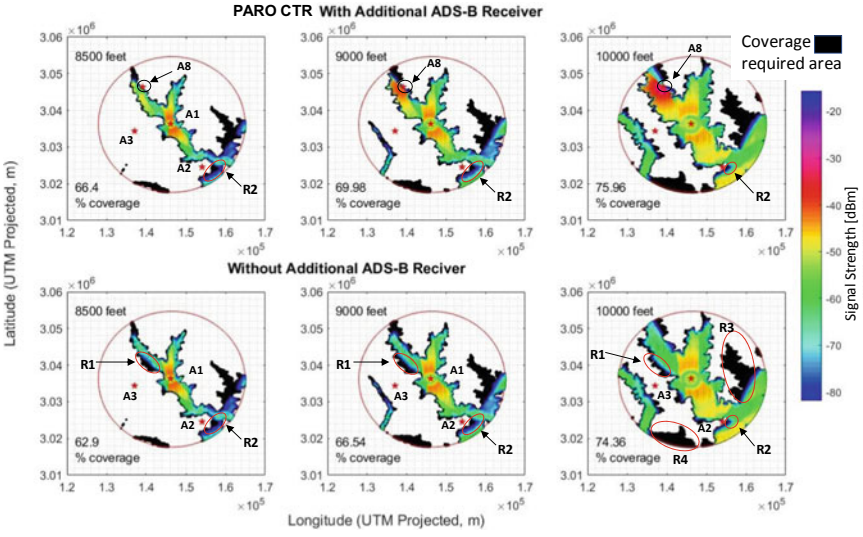

Fig. 5. Comparison of ADS-B coverage with and without additional ADS-B receiver (additional receiver location obtained from radio siting algorithm)

ments taken with ADS-B receivers implemented on a software-defined radio platform and with antennas located at A_1 and A_2 [9].

Applying the radio siting algorithm described above to PARO CTR, site A_8 was determined to be the best location for an additional ADS-B receiver in terms of line-of-sight to areas, where coverage is required. As described in Sect. 5, for simplicity of implementation, the algorithm does not take into account other propagation mechanisms such as reflection and diffraction. Figure 5 shows the improvement in coverage with the added ADS-B receiver location at various altitude for PARO CTR. At 8500 feet, there is a 3.5% improvement in coverage, 3.4% improvement at 9000 feet, and 1.6% improvement at 10,000 feet. At altitudes higher than 10,000 feet, the coverage without the additional ADS-B receiver is already more than 90%, the additional receiver improved the coverage by less than 1%. Although the percentage improvement is not significant, with the additional receiver the critical region, marked R_1 in Fig. 5, which contains the final approach phase of the flight toward runway 15 at Paro International Aerodrome, is now covered. However, there is no improvement in another critical region, marked R_2 and containing the final approach phase of flight toward runway 33 at the aerodrome. Repositioning the antenna at receiver location A_2 might be able to improve coverage in region R_2. Although the regions R_3 and R_4 contain large areas without coverage, they are not critical for actual flight operations to and from Paro International Aerodrome as these regions are located on the other side of the ridges that form the valley within which the aerodrome is located.

For BUMT and YONG CTRs, additional ADS-B receiver location is not warranted given the low number of flights currently handled and forecasted in the future. The coverage with receivers located at existing Com/Nav stations is adequate. There are also no set approach procedures for these aerodromes. Locally repositioning the antennas could be explored to improve coverage, if needed. GELP CTR will not require any additional ADS-B receiver locations; the coverage with the receiver located on the aerodrome control tower is adequate.

7 Summary and Future Work

In this paper, an approach to ADS-B coverage design using physical optics-based simulation of the 1090 MHz ADS-B frequency, and a radio siting algorithm that uses the local terrain information was presented. The approach has been developed specifically for ADS-B coverage design in the mountainous terrains of Bhutan. Using simulated 1090 MHz propagation channel and the developed radio siting algorithm, improved coverage in critical regions of flight operation has been demonstrated.

As future work, the results from this study will be compared with the results from analysis of opportunistic ADS-B measurements to improve and validate the simulated coverage. The measurement campaign using ADS-B receivers implemented on an SDR platform is already underway. The improved coverage prediction thus obtained will be used for implementation of ADS-B network in the Bhutanese airspace for ATM purposes

Acknowledgements The authors would like to acknowledge the generous support received from the Ministry of Land, Infrastructure, Transport, and Tourism—Japan to conduct a part of this study at the ENRI.

This work is also supported by JSPS KAKENHI Grant (No. 17K14688).

References

1. L. Semernya A. Ramola, B. Alfthan, Giacovelli, Waste management outlook for mountain regions: Sources and solutions. Waste Manage. Res. **35**(9), 935–939
2. ICAO, *Guidance Material on Comparison of Surveillance Technologies (GMST)*, 1st edn (ICAO 2007)
3. E. Boci, *RF Coverage Analysis Methodology as Applied to ADS-B design.* in 2009 IEEE Aerospace conference (Big Sky, MT, 2009), pp. 1–7
4. DoAT, *Aeronautical Information Publication of Bhutan*, 2nd edn (2018)
5. InfoVista Mentum Planet, https://www.infovista.com/planet/rf-planning-software
6. J.H. Whitteker, Physical optics and field-strength prediction for wireless systems. IEEE J. Selected Areas Commun. **20**(3) (2002)
7. ICAO, *Aeronautical Telecommunications Volume IV Surveillance and Collision Avoidance System,* 4th edn (2007)
8. T. Moller, B. Trumbore, fast, minimum storage ray/triangle intersection. J. Graphics Tools (1998)
9. J. Naganawa et. al., *Measurement of Opportunistic Aircraft Signals and Verification of a Propagation Prediction Tool in Mountainous Region*, submitted to EUCAP 2020

Nearfield Inspection of Navigation Systems with UAVs—First Results from the NAVANT Project

R. Geise, A. Weiss, B. Neubauer, T. Fritzel, R. Strauß, H. Steiner, F. Faul, T. Eibert, and J. Honda

Abstract Regular flight inspection of navigation systems, such as instrument landing system (ILS) and the VHF omnidirectional radio range (VOR), is an important part of maintenance to ensure safe flight operations. Usually, this is done with aircraft flying and measuring at trajectories according to international recommendations from the ICAO. With the arising technology of unmanned aerial vehicles (UAVs), such flight inspections could be performed in a much more economic and efficient manner, in particular, if combined with nearfield measurement technology, allowing farfield predictions anywhere in space without limitations to particular flight trajectories. This contribution discusses an innovative approach for such nearfield inspections with UAV as research focus of the navigation aid antenna characterization—next generation (NAVANT-NG) project with corresponding requirements and first measurement results. In this contribution, both the dynamic range and the accuracy of phase measurements and stability are investigated. In particular, the accuracy and stability of phase measurements are a crucial part in such nearfield measurements. First measurement results with a test antenna and a UAV demonstrate the feasibility of proposed nearfield measurements.

Keywords Navigation systems · Instrument landing system · VHF omnidirectional radio range · Nearfield measurements · Unmanned aerial vehicle

R. Geise (✉) · A. Weiss · B. Neubauer
University of Braunschweig, Institute for Electromagnetic Compatibility, Brunswick, Germany
e-mail: r.geise@tu-braunschweig.de

T. Fritzel · R. Strauß · H. Steiner
Aeroxess UG, Munich, Germany
e-mail: torsten.fritzel@aeroxess.com

F. Faul · T. Eibert
Department of Electrical and Computer Engineering, Technical University of Munich, Munich, Germany
e-mail: fabian.faul@tum.de

J. Honda
Electronic Navigation Research Institute (ENRI), National Institute of Maritime, Port and Aviation Technology (MPAT), Tokyo, Japan
e-mail: j-honda@mpat.go.jp

Air Traffic Management and Systems IV, Lecture Notes in Electrical Engineering 731,
https://doi.org/10.1007/978-981-33-4669-7_20

1 Introduction

With the recent development in the field of unmanned aerial vehicles (UAVs), new possibilities of radio wave measurements can be realized. With such UAVs a large spatial area to measure electromagnetic fields can be covered very fast and accurately, enabling new approaches of flight inspection, that are performed by real aircraft with demanding flight trajectories so far. However, a decisive issue is the motion of the UAV in flight, which may have influence on the measurement quantities, in particular on the phase that must be measured as well, if nearfield to farfield (NFFF) transforms are to be applied. This contribution focuses on the navigation aids instrument landing system (ILS), VHF omnidirectional radio range (VOR), and Doppler VOR (DVOR) [1], which both operate at VHF frequencies at about 110 MHz. Because the mentioned navigation systems are large antenna arrays, a large spatial area needs to be covered by the UAV incorporating a long measurement time, which is beyond the available flight time of state-of-the-art battery-driven UAVs. Consequently, the proposed measurement system uses a tethered UAV with theoretically unlimited flight time. A preceding EMI compliance analysis has been carried out in [2]. With the tethered setup, a fiber optical system is used both in order to anticipate propagation losses in long cables and phase measurement errors due to the motion of the cables.

This contribution presents first measurement results, which show the feasibility of the proposed setup in general. It is organized as follows. In Sect. 2, fundamental properties of navigation systems are highlighted, which are not yet conform with the current state of the art of antenna nearfield measurements with continuous wave. Section 3 discusses the measurement architecture, and Sect. 4 focusses on measurement requirements and corresponding features of the UAV. Section 5 presents the validating measurement setup and its results, and finally, Sects. 6 gives a conclusion.

2 Nearfield Measurement of Navigation Systems

Whereas antenna characterization in the nearfield is well established in the scientific community, nearfield characterization of navigation systems bears two fundamental difficulties to be addressed. On the one hand, such installed navigation systems are not accessible and cannot be fed individually for an inspection setup. On the other hand, the mentioned navigation systems cannot be characterized by means of continuous wave only, because the spatially varying navigation information is provided by modulation properties that need to be measured as well. Basically, the fundamental functional principle of most navigation systems is that the modulation properties vary in space. Consequently, spectra must be measured and transformed into the farfield. Another issue, when measuring navigation systems in the nearfield is that, due to the required phase resolution of a minimum of 1/50 of a wavelength, there are high demands on the frequency stability of the system. For the normal operation, the navigation information is obtained within a few milliseconds by demodulation

in the receiver, but the measurement time is much longer for the case of measuring the nearfield pattern within several minutes or even hours. In this case, even small frequency drifts in the navigation system can cause phase measurement errors. Consequently, a measurement system architecture is needed to cope with phase drifts, that only depend on the motion of the receiving UAV, but not on the frequency drift of the system itself.

Finally, it is quite clear that the measurement locations will not be located on regular scanning surfaces like spheres, planes or cylinders due to the motion of the UAV itself. The UAV itself will never reach a positioning accuracy as known from sophisticated nearfield measurement ranges.

To cope with this, the UAV-position is measured by a laser tracker with submillimeter accuracy. The measured nearfield data are transformed to the farfield by the fast irregular antenna field transformation algorithm (FIAFTA) [3]. FIAFTA includes features, which are very suitable for in situ measurements like treating arbitrary measurement locations and considering dielectric ground [4].

The following figures exemplarily show the contents of the instrument landing system to be measured with the UAV. Since most navigation systems operate with such modulations (AM and FM) that vary in space, it serves as a representative example for the VOR as well. The presented examples have been synthesized by the exciting amplitudes of a large aperture 24 antenna array ILS. Figure 1 shows the carrier itself with a very small beam width of only a few degrees with the main direction into the middle of the runway. Very close to the ILS at a distance of 50 m the amplitude taper of antenna elements can be identified. Figure 2 shows ILS spectra that vary with the horizontal observation angle relative to the middle of the runway. According to the high directivity of the ILS array, the carrier signal strength decreases to higher azimuth angles as well as the sidebands of the amplitude modulation. These

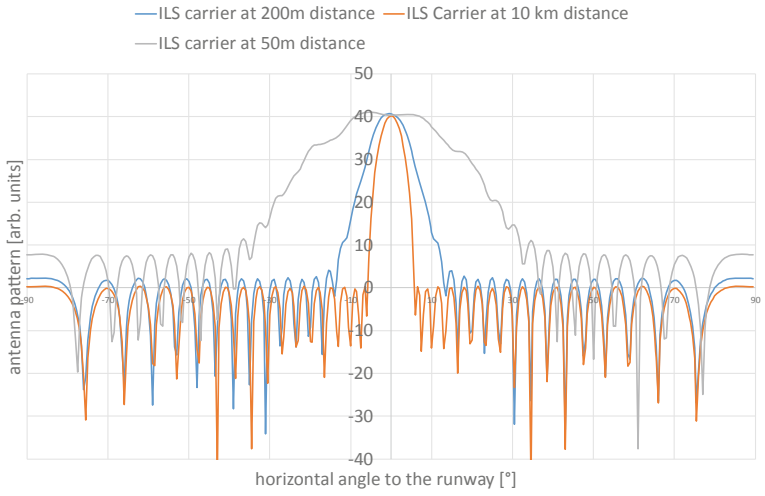

Fig. 1. Carrier example of the instrument landing system

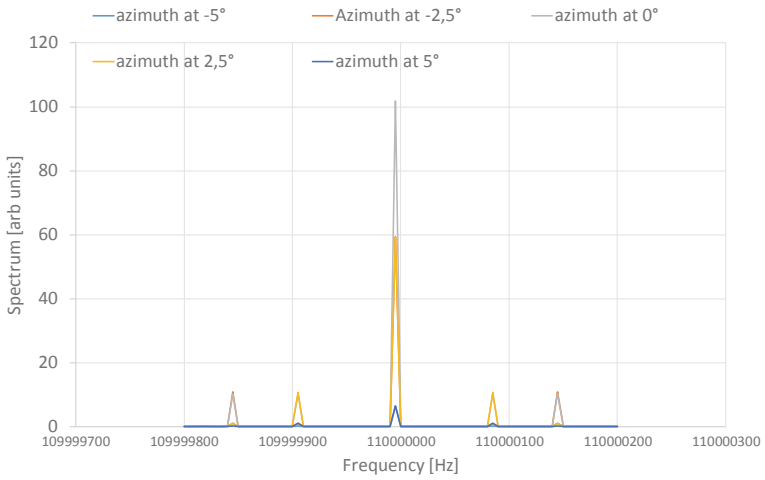

Fig. 2. Spectra examples of the instrument landing system

sidebands bear the navigation information and vary with the azimuth angle. In fact, the difference in degree of modulation (ddm) is the navigation information. It becomes obvious that the whole spectrum of the navigation system needs to be measured within nearfield inspection.

3 System Architecture

Figure 3 presents a sketch of the measurement principle, e.g., for the instrument landing system. The ILS radiates amplitude modulated signals, while the degree of modulation varies with the horizontal angle to the middle of the runway. The inset graph in Fig. 3 shows a spectrum example of the ILS as measured at different angles φ to the middle of the runway. The sideband intensities according to the degree of modulation at 90 and 150 Hz change. It is noted that these modulation frequencies are quite low and require a corresponding long measurement time to be resolvable in the frequency domain. In order to measure phase shifts, only dependent on the measurement location of the UAV, a stationary monitor is used, which serves as phase reference. Thus, only phase changes are measured that occur due to the motion of the UAV, which is compensated for phase drifts of the navigation system or the measurement receiver. Flight tracks of the UAV are automatically flown. The position of the UAV is recorded with a laser tracker system that is synchronized with the measured field data. The data is recorded in the intermediate frequency band to allow real-time streaming of the data without any losses or synchronization failures.

The RF is linked from the UAV with a fiber optic to the ground station, where the down mixing and recording are performed. The detailed hardware concept is

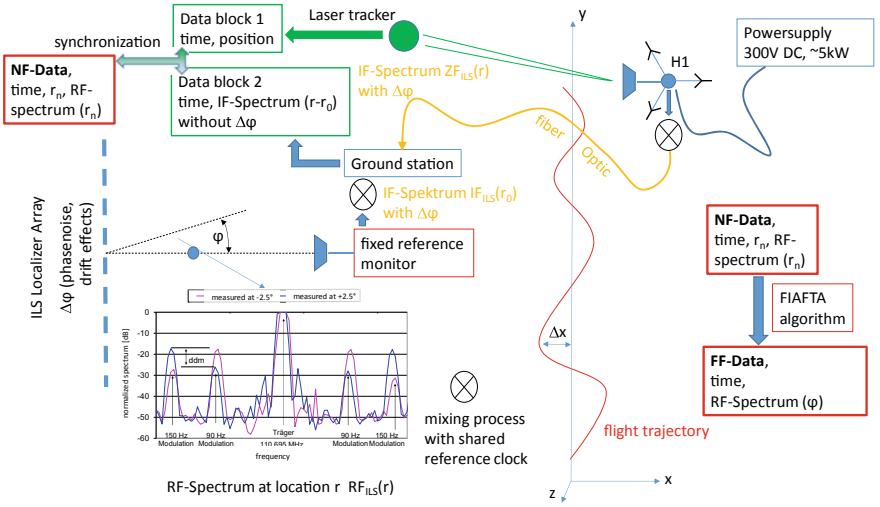

Fig. 3. Measurement setup for nearfield measurements of navigation systems

not presented in this contribution. In this study, fundamental investigations are done on the phase measurement accuracy. Thus, proof-of-concept measurements are conducted with a network analyzer. Measurement requirements and corresponding features of the UAV are described in the following section.

4 Measurement Requirements and Features of the UAV

For the described RF-field measurements, the same UAV is used as the one planned for the nearfield measurements of the ILS and DVOR installations at a next step within the NAVANT-NG project.

The UAV is called Hercules-One (H1) [5], which is designed and operated by Aeroxess Company in Munich/Germany. Since the H1-UAV is especially designed for large-scale and complex RF-field characterization, it is also fully compliant with the mission requirements of NAVANT-NG.

The described RF-measurements form the basis for nearfield measurements of a DVOR installation and an ILS installation. In addition to classical nearfield antenna measurements, two other major goals are set:

1. Transformation of modulated navigation signals of a DVOR/ILS installation anywhere into the far-field, respectively, anywhere into the airspace based on measured modulated signals in the close vicinity (nearfield) of the DVOR/ILS installation.

2. Localization of interferers from airport or surrounding of an ILS installation in the region where aircraft touch the runway or at locations along the runway, where signal deviations have to be reported, e.g., by flight inspections.

Since the DVOR operates over 360 degrees in azimuth by its rotating beams, the nearfield data collection shall be captured along a vertical and cylindrical measurement contour around the DVOR. In order to comply with the transformation needs and the aimed farfield coverage, the planned measurement diameter of the cylinder shall be 40 m and the height 50 m, as shown in Fig. 4 (left side). Considering a sample density of nearfield measurement points of $\lambda/2$ the number of measurement points results in 7600. Assuming an average continuous flight speed of the H1-UAV of, e.g., 1.0 m/s the total measurement time results in about 1.5 h at a minimum. For the RF-field characterization of the ILS installation, it is planned to sample the radiating ILS RF-field along a vertical and planar measurement surface of 300 m in width and 50 m in height as shown in Fig. 4 (right side) resulting in a total flight time of about 3.1 h without any flight interruptions of the UAV.

Since the H1-UAV is a tethered UAV, the transmission of electrical energy, RF-measurement signals, and control data occurs either by copper wire or fiber optic cables and such providing sufficient scan dimensions and flight durations required for DVOR and ILS RF-field measurements.

Further features of the H1-UAV promoting RF-field measurements are listed below:

- Payload capacity: 8.0 kg
- Flight time: unlimited
- Large flexibility for integration of a wide range of different payloads
- Fully closed and EMC-shielded airframe accommodating all UAV and payload equipment and components
- Compact dimensions with outer diameter of 2.1 m by tri-copter geometry and use of coaxial 4-bladed rotors

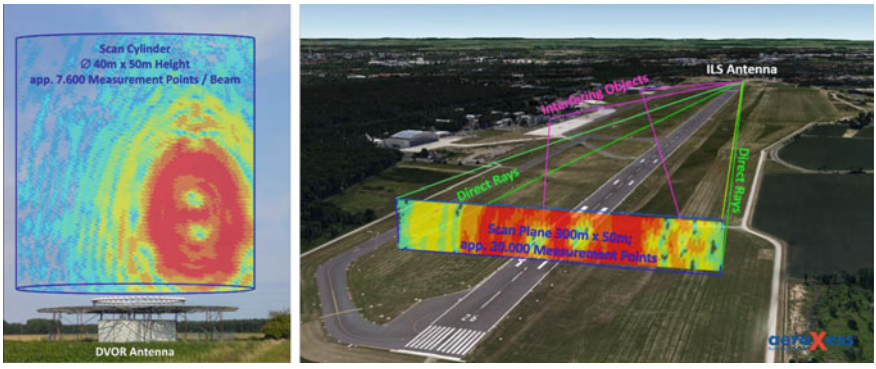

Fig. 4. Proposed RF-measurement contours of DVOR (left) and ILS (right)

Fig. 5. H1-UAV equipped with L-band probe antenna and 6D-RTK equipment

- Extreme agile flight dynamics allowing measurements also at rough weather conditions
- Optionally a 2-axes gimbal unit can be provided to enlarge field of views of laser targets when UAV positions shall be measured with laser tracker equipment.
- Optionally, a 6D-RTK system can be integrated providing up to 2.0 mm 3D-position measurement accuracy and 0.2 degree 3D-orientation measurement accuracy relative to the antenna under test within a test volume of 10 km.
- Back-up battery on-board in case of absence of line power ensuring safe landing.
- In case of failure of one of the 6 rotors, the H1-UAV remains fully operational.

Figure 5 shows the H1-UAV equipped with the 6D-RTK system. The system comprises of three GPS antennas installed above the non-rotating centers of the three coaxial rotor heads. Further, a dual-polarized L-band nearfield probe antenna is integrated at the front of the UAV as an example antenna.

The H1-UAV is prepared for RF-field measurements up to 20 GHz and above, but also for any other applications requiring large-scale operations, extreme long flight durations and precise 6D information of the UAV or of the sensors mounted at the UAV.

5 Measurement Setup and Results

Figure 6 shows a reference measurement setup as a feasibility study if, despite the UAV motion, phase measurements are accurate enough for a NFFFT.

As antenna under test (AUT) a biconical VHF antenna is used and a self-built VHF folded dipole is mounted on the UAV serving as probe antenna. A network analyzer measures the complex transfer functions from the AUT to the probe antenna,

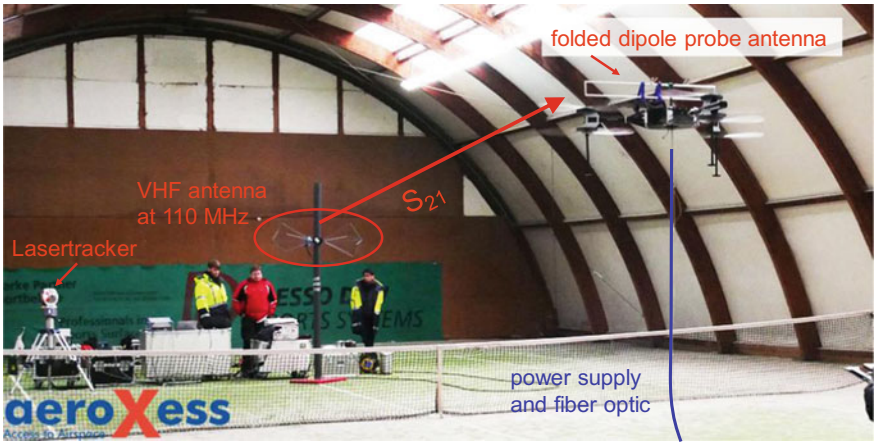

Fig. 6. Measurement setup with a reference antenna

which is connected to a fiber optic conversion module. The fiber optic signal is converted into RF again on the ground and fed into the receiving port of the network analyzer. The network analyzer is operated in zero span mode at a continuous wave frequency of 110 MHz with a measurement bandwidth of 100 kHz. Measurements are, respectively, done within a time span of 10 s.

In the following, measurements are presented to assess the measurement accuracy of the phase. The UAV is flown manually toward the antenna and away from the antenna as presented in Sect. 5.1. In order to assess the influence of the flight performance with respect to the phase a hover flight is done, the results of which are presented in Sect. 5.2. The synchronization with the data acquisition and the laser tracker is presented in Sect. 5.3. Finally, a gearing flight test is performed to measure the probe radiation pattern.

5.1 Phase Variations

In order to assess the function principle of measuring the phase, flights are performed toward the antenna and away from the antenna as presented in Figs. 7 and 8. Both the magnitude and the phase are plotted. The flight toward the antenna shows a slightly increasing amplitude over the flight time toward the antenna. Clearly identified is the increasing phase that follows the product of wavenumber and distance. At this stage, it is not yet synchronized with the laser tracker and the position of the UAV, but the phase measurement results indicate, that both the measurement dynamics and the conversion over the fiber optic yield reasonable results for a linearly increasing and wrapping phase.

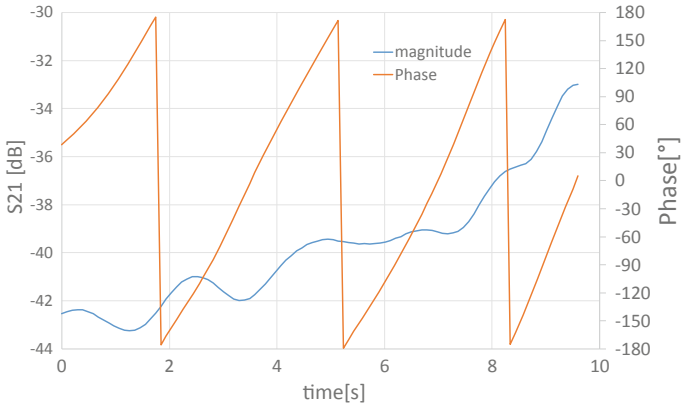

Fig. 7. Measurement results with flight toward the antenna

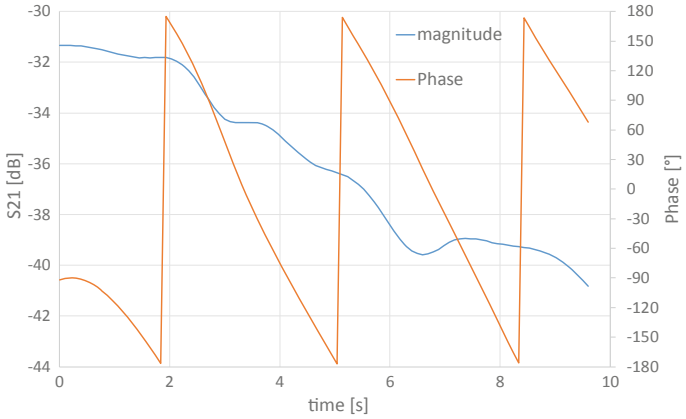

Fig. 8. Measurement results with flight away from the antenna

In the same manner, it can be seen that the phase decreases with increasing distance to the antenna under test. Both measurements demonstrate that the UAV can well be controlled in the indoor environment slightly above ground. The measurement power of the network analyzer was +10 dBm. Since the output power of navigation systems is several 10 W, these measurements are a lower estimate for the dynamic range, which clearly seems to be sufficient for the later application. The optical fiber cable has a length of 50 m, and the phase information does not seem to be distorted by the movement of the fiber with the UAV. These measurements demonstrate the feasibility of measuring the phase via optical fiber conversion in a zero span mode.

5.2 *Hovering Flights of the UAV*

Since measurement data is recorded with a UAV in motion the fundamental question is, how the motion affects the phase stability. For example, in order to measure the modulation content of the navigation system, for VORs with modulation frequencies of 30 Hz the minimum measurement time is 33 ms. Thus, within such a time the motion of the UAV should have negligible influence, especially on the phase. In order to assess these properties, a hovering flight is conducted, the measurement results of which are presented in Fig. 9.

On the time scale of 10 s amplitude variations of 6 dB and phase variations of 150° can be observed. This is due to the motion of the UAV, which slightly varies both its distances to the antenna under test and its height above ground. However, the timescale for measurements of navigation systems as stated above is much smaller, i.e., roughly up to 100 ms only. In order to evaluate the phase stability on that timescale, Fig. 10 shows the derivative of the phase with respect to time. This derivative has its maximum at a time of 5 s with slightly above 60° per second. Consequently, with a measurement time of 100 ms the maximum phase uncertainty is only 6°, which is suitable for nearfield measurements.

So far the ability to measure the phase of a transfer path from an antenna under test with an optical fiber in the dynamic state of an UAV in motion has been presented. In the following section, a measurement example is shown including the synchronization with a laser tracker as localization system.

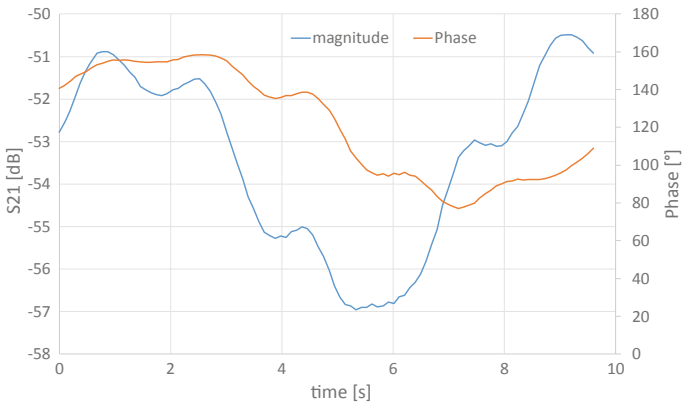

Fig. 9. Hovering flight at a distance of 10 m

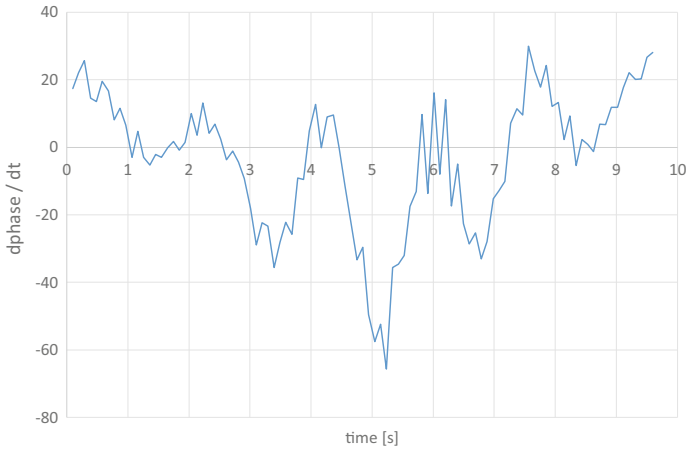

Fig. 10. Analysis of phase deviations due to the motion of the UAV, derivative with respect to time

5.3 Planar Scan Example

Figures 11, 12 and 13 show measurement results as recorded in front of the antenna under test at a distance of about 12 m. Figure 11 shows the 3D-localization data as recorded with the laser tracker system with the parameters distance, elevation, and azimuth angle. Figure 12 plots the measured data in magnitude and phase that are mapped to the same time stamp on the *x*-axis.

For better readability, the recorded data is post processed to show a planar plot in front of the antenna under test. These results are shown in Fig. 13.

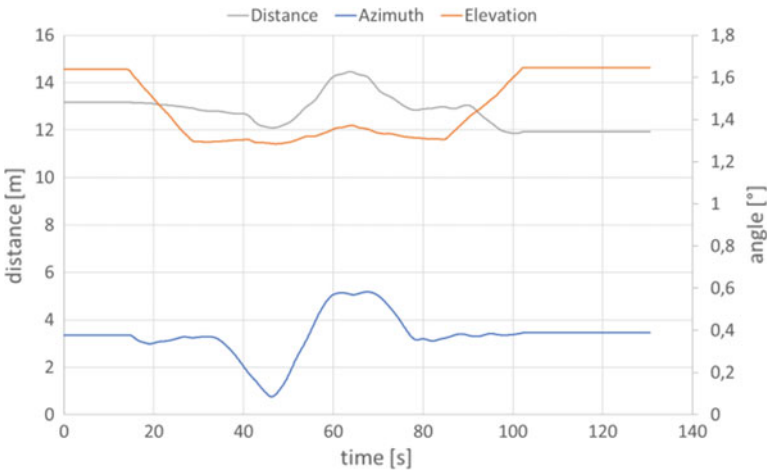

Fig. 11. Localization data of the UAV as recorded with the laser tracker system

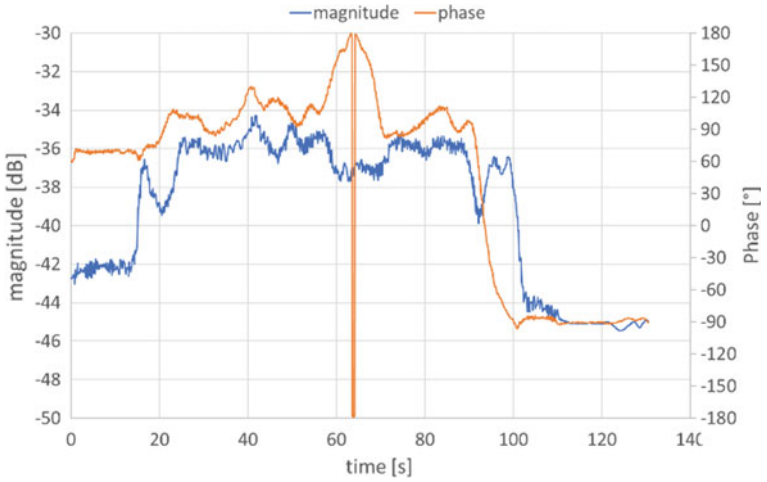

Fig. 12. Measured transfer functions in magnitude and phase

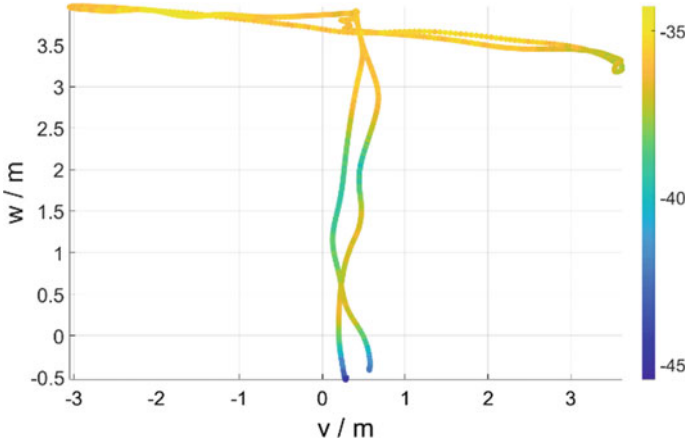

Fig. 13. Planar scan example with synchronization between network analyzer and laser tracker

The local coordinate system is described with w as the height above the laser tracker level and v as coordinate tangential to the antenna under test, where $v = 0$ is the main lobe direction of the antenna.

The antenna under test has a large beam width; thus, nearly a constant transfer function is observed with respect to the v coordinate. The height scan with the w-coordinate shows that ground reflections are present, which lead to variations of around 10 dB. This is a successful demonstration of dynamic antenna nearfield measurements including the phase with a corresponding synchronization of the UAV and the localization system.

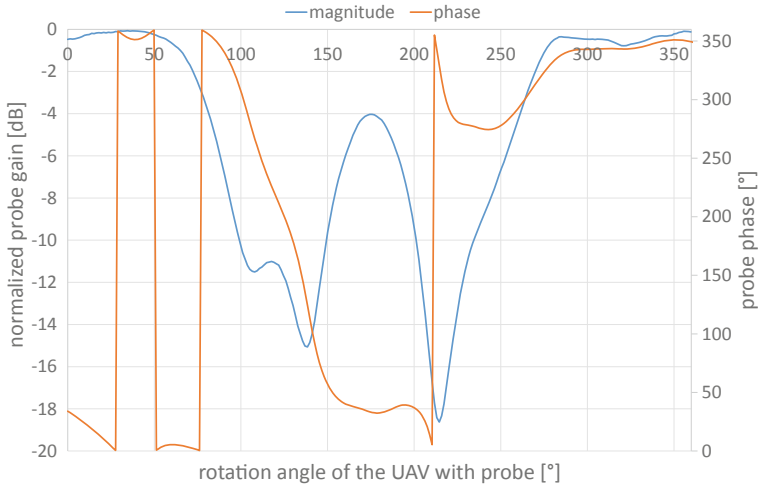

Fig. 14. Measured probe antenna pattern by gearing the UAV

5.4 Assessment of the Mounted Probe Performance

Finally, dealing with nearfield to farfield transformations, it is essential to have a probe antenna with a very broad radiation beam, because the navigation systems to be measured in the NAVANT project have very large dimensions, i.e., for the ILS more the 30 m. Consequently, during a flight of the UAV not only the dynamic position itself might affect the measurement quantities but also the gearing of the UAV.

Thus, in the following Fig. 14 measurement results are presented for a gearing test of the UAV turning 360° around its own axis. Ideally, the pattern of the folded dipole is obtained during this procedure.

Since at the current stage of the measurement setup the information of the heading is not yet taken into account, the gearing angular information is obtained by the nearly constant angular gearing speed. Figure 14 shows the folded dipole antenna pattern with a maximum at around 40°, because the starting angle has not been adjusted. Two minima of the dipole pattern are measured at angles around 90° and 180°. The measured probe antenna pattern also shows that the presence of the UAV does not significantly change the dipole characteristic of the antenna mounted on the UAV. Anyhow, future measurements will also take into account a probe antenna correction.

6 Conclusion

Fundamentals of nearfield measurements for navigation systems with an unmanned aerial vehicle have been addressed. Two key issues have been discussed, i.e., the

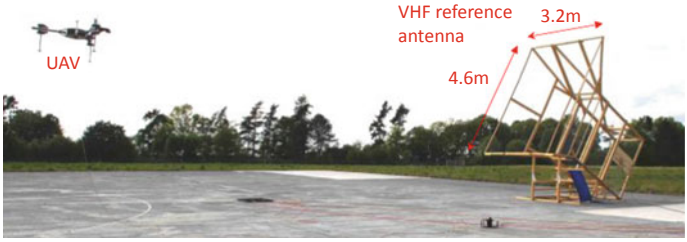

Fig. 15. Measurement setup with the VHF reference antenna for future measurements

necessity of measuring a spectrum of modulated signals, which vary in space as well as the accuracy of phase measurements that needs to be better than 1/50 of a wavelength. With first measurements of a VHF biconical antenna, a proof of principle is given that UAV-based nearfield inspection of navigation systems is possible, since the measured phase accuracy is satisfying the 1/50 wavelength condition, despite the UAV motion and signal transmission over an optical fiber link. In ongoing work [6], the authors in detail present the self-developed hardware that is capable of continuously streaming the intermediate frequency band of both the mobile probe on the UAV and the fixed reference monitor.

Future work will also show results of the nearfield measurement transformation of a large self-built VHF horn antenna as shown in Fig. 15. This VHF standard gain horn antenna is an ideal reference antenna for evaluation purpose of the overall measurement system and the corresponding post-processing. The manufacturing process and the measurement results with an electro-optical nearfield probe in the aperture are presented in [7]. Figure 15 shows a photograph of the reference VHF horn antenna at the open area test site of the national metrology institute of Germany in Braunschweig. The aperture of this horn antenna is 4.6 m $\times$ 3.2 m.

In the final stage of the NAVANT-NG project, nearfield measurements of the ILS and the VOR are performed and compared to nowadays flight inspection results. Ongoing work will also deal on the frequency expansion up to higher frequencies, where the phase accuracy becomes even much more relevant.

Acknowledgements This work is funded by the German ministry of economic affairs and energy under the project NAVANT-NG, grant number 20E1711B.

References

1. W. Mansfeld, *Funkortungs- und Funknavigationsanlagen* (Hüthig Verlag, Heidelberg, 1994). ISBN 3-7785-2202-7
2. R. Geise, A. Weiß, T. Fritzel, R. Strauß, F. Faul, T. Eibert, *Interference Measurements of a High Power Cable-Bound Unmanned Aerial Vehicle.* in European Conference on Antennas and Propagation (Krakau, Polen, 2019)

3. T.F. Eibert, E. Kilic, C. Lopez, R.A.M. Mauermayer, O. Neitz, G. Schnattinger, Electromagnetic field transformations for measurements and simulations (invited paper). Progress Electromag. Res. **151**, 127–150 (2015). https://doi.org/10.2528/PIER14121105
4. T.F. Eibert, R.A.M. Mauermayer, *Equivalent Sources Based Near-field Far-field Transformation Above Dielectric Half Space*. in Proceedings 40th Annual Meeting and Symposium of the Antenna Measurement Techniques Association (AMTA) (Williamsburg, VA, 2018)
5. T. Fritzel, R. Strauß, H. Steiner, C. Eisner, T.F. Eibert, *Introduction into an UAV-based Near-field System for In-Situ and Large-Scale Antenna Measurements (invited paper).* in Proceedings of IEEE 50 Conference on Antenna Measurements Applications (CAMA) (Syracuse, NY, 2016). https://doi.org/10.1109/CAMA.2016.7815762
6. A. Weiß, R. Geise, B. Neubauer, F. Faul, T. Eibert, T. Fritzel, H. Steiner, R. Strauß, *RF-Signal Receiver for UAV-Based Characterization of Aeronautical Navigation Systems.* in European Conference on Antennas and Propagation (Kopenhagen, Denmark, 2020)
7. A. Akar, *Realisierung einer Hornantenne zur Bereitstellung von VHF-Referenzfeldstärken (Realisation of a horn antenna for providing VHF reference field strengths).* Bachelor thesis, Institute for EMC at university of Braunschweig, Germany (2017)